# Tumour microenvironment shapes eosinophil plasticity in murine models of breast cancer

Zofia Varyova


University of Oxford
Linacre College

**Supervisors**
Professor Kim Midwood
Professor Adrian Harris

Thesis submitted for the degree of
Doctor of Philosophy

October 2025

*Pre Mamu a Tata*

## Table of Contents

## Acknowledgments

First, I would like to thank my supervisory team. I am deeply grateful to Kim for the opportunity to work in her lab, along with her time, patience, and supervision over the past four years. I would also like to thank Adrian for his insights, consistent enthusiasm, and overarching support, even in difficult times. I am thankful to Audrey Gérard for her guidance and for helping me to find a direction when I needed it the most; this thesis and the last year of my PhD would have looked very different without the many discussions and her advice, for which I am truly grateful. Last but not least, I would like to thank Mathilde Pohin, who twice a year found all the gaps in this project and then helped me to fill them up. This work was supported by the generous funding from CRUK that allowed me to grow as a scientist.

I am grateful for the support and advice of past and present Midwood members, as well as many scientists at the Kennedy Institute who helped me along the way. I am thankful to my fellow PhD students Libby, JB, Linda, Caroline, and Luca, for sharing the many exciting and disappointing (non)scientific moments over the years, for spreading the coconut mall fever, for the many laughs over coffee and pints of Jubel, and ultimately for never refusing to proofread my emails. I am also grateful to the Midwood post-docs Anja Schwenzer and Valeria Da Costa for their supervision and guidance in and out of the lab. Thank you to many scientists who helped me shape my scientific curiosity; my thesis committee, Ilaria Malanchi, Hannah Garner, Isabelle Arnold; and Vicky Bridgeman, who always found time to discuss this project. I am also very thankful to Franze Progatzky, Helen Byrne, Philip Maini, Joe Pitt-Francis and Vedang Narain for their trust and support when setting up the microscopy collaboration. I would also like to extend my gratitude to Katarína Mikušová and Priyanka Tibarewal for their lasting and thoughtful mentorship.

I am grateful for the support of many friends I had a chance to meet during my time in Oxford. Thank you to Xime and Dušan, who provided me with a home away from home; to my London support group, Evka, Andrew, and Klara, who kept my mind off work when necessary; and to my two Graces, Tama and Anči, who were with me ever since my early undergraduate days and stayed close even when we all ended up in different places.

Finally, none of this would be possible without the unwavering support of my family. I am grateful for the unconditional love of my parents, Barbora and Maroš, who despite many personal sacrifices supported my studies and always reminded me of what truly matters. I am also thankful that our family *karass* has brought us Mirka and Lucas. Lastly, I am greatly indebted to my brother Šimon, whose encouragement, constant guidance and compassion through the most difficult times provided me with the confidence to follow my goals.

## Statement of originality

I declare that all data, words, figures, and results included herein are my own work and have not been submitted for another award, degree, or diploma at any other university or learning institution. I certify that this thesis is the result of my own work and all collaborations and use of published public data have been acknowledged at the appropriate locations within the text.

This project was completed at the Kennedy Institute of Rheumatology, Nuffield Department of Orthopaedics, Rheumatology and Musculoskeletal Sciences, University of Oxford.

## Abbreviations

| | |
|---|---|
| **A-eos** | Active eosinophils |
| **AF** | Alexa Fluor |
| **APC** | Allophycocyanin |
| **APCs** | Antigen presenting cells |
| **ATX** | Autotaxin |
| **B-eos** | Basal eosinophils |
| **Balb/c** | Balb/cAnNCrl strain |
| **Bl6** | C57BL/6J strain |
| **BM** | Bone marrow |
| **BMDMs** | Bone marrow-derived macrophages |
| **bulkRNA-seq** | bulk RNA sequencing |
| **BUV** | Brilliant Ultra Violet |
| **BV** | Brilliant Violet |
| **BVI** | Blood vessel invasion |
| **CAF** | Cancer-associated fibroblast |
| **CCL** | Chemokine ligands |
| **CCR** | CC chemokine receptors |
| **CD** | Cluster of Differentiation |
| **cDNA** | Complementary DNA |
| **CHX** | Cycloheximide |
| **CLO** | Clodronate liposomes |
| **$CO_2$** | Carbon dioxide |
| **CRC** | Colorectal cancer |
| **CTL** | Control |
| **CXCL** | Chemokine (C-X-C motif) ligand |
| **DC** | Dendritic cells |
| **DC-** | Diffusion map components |
| **DEGs** | Differentially expressed genes |
| **DESeq2** | Differential gene expression analysis |
| **dFBG** | Heat-denatured FBG |
| **DMEM** | Dulbecco's Modified Eagle Medium |
| **DoRothEA** | Discriminant Regulon Expression Analysis |
| **DPP4** | Dipeptidyl peptidase |
| **DTC** | Disseminated tumour cells |
| **E2** | Estrogen |
| **Ear** | Eosinophil-associated ribonuclease |
| **ECM** | Extracellular matrix |
| **ECP** | Eosinophil cationic protein |
| **EDN** | Eosinophil-derived neurotoxin |
| **EDTA** | Ethylenediaminetetraacetic acid |
| **EdU** | 5-ethynyl-2'-deoxyuridine |

| | |
|---|---|
| **EEtosis** | Eosinophil extracellular trap formation |
| **ELISA** | Enzyme-Linked Immunosorbent Assay |
| **Epx** | Eosinophil peroxidase |
| **ER** | Estrogen receptor |
| **FACS** | Fluorescence-activated cell sorting |
| **FBG** | Fibrinogen-like globe domain |
| **FBS** | Fetal bovine serum |
| **FC** | Fold change |
| **FITC** | Fluorescein isothiocyanate |
| **Fltl3** | FMS-related tyrosine kinase 3 ligand |
| **FMO** | Fluorescence minus one |
| **GATA-1** | GATA-binding factor 1 |
| **GEMMs** | Genetically engineered mouse models |
| **GEO** | Gene Expression Omnibus |
| **GFP** | Green Fluorescent Protein |
| **GI** | Gastrointestinal |
| **GO** | Gene Ontology |
| **GPI** | Glycosylphosphatidylinositol |
| **GSEA** | Gene set enrichment analysis |
| **H&E** | Haemoxylin and Eosin |
| **HEPES** | 4-(2-hydroxyethyl)-1-piperazineethanesulfonic acid |
| **HER2** | Human epidermal growth factor-2 |
| **HRP** | Horse radish peroxidase |
| **ICB** | Immune Checkpoint Blockade |
| **iEos** | Inflammatory eosinophils |
| **IF** | Immunofluorescent |
| **IFN** | Interferon |
| **IFNAR1** | Interferon alpha receptor 1 |
| **IFNGR2** | Interferon gamma receptor 2 |
| **IHC** | Immunohistochemistry |
| **IL** | Interleukin |
| **Il5-tg** | IL-5 transgenic mouse model |
| ***Il5ra*** | IL-5 receptor-a |
| **KRT** | Cytokeratin |
| **LIAR** | Local Immunity And/or Remodelling/Repair hypothesis |
| **LPA** | Lysophosphatidic acid |
| **Ly6** | Lymphocyte antigen-6 family |
| **Mac** | Macrophage clusters |
| **MACS** | Magnetic cell separation |
| **MAREMO** | MAtrix REgulating Motif-mimicking peptide |
| **MBP** | Major basic protein |
| **MDSC** | Myeloid-derived suppressor cells |
| **MFI** | Median fluorescent intensity |

| | |
|---|---|
| **MFP** | Mammary fat pad |
| **MHC** | Major histocompatibility complex |
| **MMPs** | Matrix metalloproteinases |
| **MMTV** | Mouse mammary tumour virus |
| **mSCF** | Murine stem cell factor |
| **NES** | Normalised enrichment scores |
| **OP-Puro** | *O*-propargyl-puromycin |
| **p-adj** | Adjusted p-value |
| **P/S** | Penicillin-Streptomycin |
| **PARP** | Poly ADP-ribose polymerase |
| **PBS** | Phosphate Buffered Saline |
| **PC** | Principal component |
| **PCA** | Principal component analysis |
| **pCR** | Pathological complete response |
| **PD-L1** | Programmed death-ligand 1 |
| **PDAC** | Pancreatic Ductal Adenocarcinoma |
| **PE** | Phycoerythrin |
| **PR** | Progesterone receptor |
| **PyMT** | Polyomavirus middle T |
| **$R^2$** | Squared correlation coefficient |
| **REC** | Research Ethics Committee |
| **rEos** | Resident eosinophils |
| **RLT** | RNeasy lysis buffer |
| **ROS** | Reactive Oxygen Species |
| **RPMI** | Roswell Park Memorial Institute 1640 medium |
| **RT** | Radiotherapy |
| **RT-qPCR** | Real-time quantitative PCR |
| **scRNA-seq** | Single cell RNA sequencing |
| **shRNA** | Short hairpin RNA |
| **sLP** | Lipid-soluble vector |
| **SSC-A** | Side scatter area |
| **ST2** | IL-33 receptor |
| **SUnSET** | SUrface SEnsing of Translation |
| **t-SNE** | t-Distributed Stochastic Neighbour Embedding |
| **TAE** | Tumour-associated eosinophils |
| **TAM** | Tumour-associated macrophages |
| **TAN** | Tumour-associated neutrophils |
| **TBS** | Tris Buffer Saline |
| **TCGA** | The Cancer Genome Atlas |
| **TDLU** | Terminal duct lobular units |
| **TEBs** | Terminal end buds |
| **TF** | Transcription factor |
| **TGF** | Transforming growth factor |

| | |
|---|---|
| **Th** | T helper |
| **TIL** | Tumour-infiltrating lymphocytes |
| **TLR** | Toll-like receptor |
| **TLS** | Tertiary lymphoid structure |
| **TMA** | Tumour microarrays |
| **TME** | Tumour microenvironment |
| **TNBC** | Triple-Negative Breast Cancer |
| **TNC** | Tenascin-C |
| **TNF** | Tumor Necrosis Factor |
| **$T_{reg}$** | Regulatory T cell |
| **TUNEL** | Terminal deoxynucleotidyl transferase dUTP Nick End Labelling |
| **UMAP** | Uniform Manifold Approximation and Projection |
| **VIPER** | Virtual Inference of Protein-activity by Enriched Regulon analysis |
| **VST** | Variance-stabilising transformation |

## Abstract

Eosinophils have emerged as important mediators of successful response to immune checkpoint blockade (ICB) treatment in breast cancer. However, in contrast to colorectal or lung tumours, depletion of eosinophils or induction of eosinophilia in murine models of breast cancer did not alter tumour growth. This indicates that the breast tumour microenvironment (TME) can evade eosinophil cytotoxicity by shaping their phenotypic and functional plasticity.

Using NT193, 4T1, and E0771 murine models of breast cancer, the heterogeneity of eosinophils in the TME was explored by spectral flow cytometry. This analysis identified two novel subsets of tumour-associated eosinophils. While eosinophils express relatively high levels of the Ly6C glycoprotein in healthy tissues, such as bone marrow, blood and mammary fat pad, they gradually lose Ly6C expression in the TME during tumour progression, resulting in Ly6C+ and Ly6C- eosinophil populations. Further experiments revealed that Ly6C+ eosinophils represent a long-lived population that naturally transitions into a Ly6C- state with reduced cytotoxic potential.

To understand the underlying differences between these two eosinophil subsets, both Ly6C+ and Ly6C- populations were analysed by bulk mRNA sequencing. Ly6C+ eosinophils were more responsive to IFNγ and IFNβ, and upregulated pathways associated with cytotoxicity. Indeed, stimulation of both eosinophil subsets with IFNs enhanced their cytotoxic abilities ex vivo. Because of the proposed role of eosinophils in mediating ICB responses and the role of IFN in regulating eosinophil cytotoxicity, the impact of ICB and anti-IFN treatment on eosinophil subset regulation was examined in NT193 tumours. ICB treatment led Ly6C+ eosinophils to a more activated phenotype, while blocking IFN signalling resulted in defective degranulation.

These data provide new evidence that eosinophils are a highly plastic population shaped into a less active state by the progressing breast TME. While IFNs are potent activators of eosinophil cytotoxicity, further identification of factors driving the eosinophil transition into the Ly6C- state might help with preventing the loss of anti-tumorigenic functions and improve immunotherapy outcomes.

# Chapter 1 | Introduction

## 1.1 The role of the tumour microenvironment in cancer progression

### 1.1.1 Introduction to cancer biology

Cancer is a set of complex diseases of diverse genotypic and phenotypic origin that share common biological features – the hallmarks of cancer. First proposed in 2000, the hallmarks of cancer represent a set of core principles explaining how tumours grow, survive, and spread. The initial hallmarks emphasised cancer cell-intrinsic traits, such as sustained proliferative signalling, resistance to cell death, and evasion of growth suppressors; all tightly connected to genetic alterations of the cancer cell[1]. Because cancer incidence correlates with increasing age[2], cancer was for a long time considered a genetic disease that is a result of accumulating oncogenic mutations. Even though important, it is now recognised that the somatic mutation theory cannot alone explain the initiation and progression of the tumours.

A combination of cancer-intrinsic and cancer-extrinsic factors is necessary for the tumour growth. This was first demonstrated by an experiment in which injection of Rous sarcoma oncovirus into adult chicken results in tumour growth exclusively at the site of the injection. No additional tumours were observed unless the tissue underwent another insult in the form of wounding, with the wounding process unlocking the tumorigenic potential of other infected cells[3]. The role of the host tissue environment in cancer progression can also be demonstrated by an experiment using the two-stage skin carcinogenesis model, in which mice lacking proinflammatory cytokine TNF$\alpha$ fail to develop tumours, despite acquiring the same mutational burden as their wild type counterparts[4,5]. These studies demonstrated that while acquisition of oncogenic mutations is an essential first step, tumour outgrowth depends on additional cellular and non-cellular factors that dictate the fate of the cancer cell. Consequently, the original set of cancer hallmarks was expanded to reflect this increasing appreciation of cancer complexity, with the emerging hallmarks of cancer including “avoiding immune destruction” and “tumour-promoting inflammation”[6].

As this thesis is mainly focused on understanding the role of the breast tumour microenvironment (TME) with emphasis on the altered function of the immune system, this introduction will first briefly discuss the main players shared across diverse TMEs, before moving towards the specifics of breast cancer, eosinophil biology, and the role of the extracellular matrix in cancer.

### 1.1.2 Tumour microenvironment – composition and dynamics

Tumours are highly organised ecosystems that consist of cancer cells and neighbouring non-malignant cells, all embedded in extracellular matrix (ECM) and collectively forming the TME. The cellular components of the TME include stromal cells and diverse immune cell populations, all engaging in a complex crosstalk that dictates how the tumour cells grow, invade other tissues and respond to therapies. These interactions can play pleiotropic roles; while certain cell types within the TME can produce an anti-tumour response that restrains the tumour growth, tumours are often successful in establishing a supportive niche that promotes their immune escape and metastasis. This dynamic interplay between the host and tumour cells makes the TME establishment an essential bottleneck that determines tumour growth[7]. The heterogeneity of cellular and non-cellular TME components was recently reviewed in depth[8], and is briefly discussed within this section.

The adaptive immune system, consisting of T cell and B cell subsets, plays an important role in anti-tumorigenic responses, with the abundance of specific subsets being associated with different clinical outcomes. CD8+ cytotoxic T cells are an effector cell type that can recognise and directly kill cancer cells that present tumour antigens. Higher intratumoral CD8+ T cell density is broadly associated with improved overall survival across different cancers[9,10]; however, tumours are capable of escaping the cytotoxic T cells by driving them into an exhausted phenotype and by downregulating the MHC class I antigen presentation[11]. Effective CD8+ T cell activation often depends on signals from CD4+ Th1 T cells that activate antigen-presenting cells and provide cytokines, IFNγ and TNF$\alpha$, that sustain cytotoxic priming, and

are also capable of direct anti-tumorigenic effects[12]. On the other hand, CD4+ Th2 T cells provide the TME with anti-inflammatory cytokines – IL-4 and IL-13 – supporting the immune escape and pro-tumoral myeloid polarisation[13]. As discussed in the breast tumour immune microenvironment section below, regulatory T cells ($T_{reg}$) are the most immunosuppressive cell type, with higher intratumoral $T_{reg}$ abundance or decreased CD8/$T_{reg}$ ratios often associated with poor outcomes and therapy resistance[14,15]. $T_{regs}$ are essential for regulating T cell responses during homeostasis and preventing autoimmunity, however, during cancer progression, they suppress the anti-tumour innate and T cell-mediated immunity[14]. Because of the anti-tumorigenic potential of the T cell-mediated response and their suppression through engagement of checkpoint receptors, multiple immunotherapies aiming to reactivate CD8+ T cells have been developed[16].

B cells represent the other arm of adaptive immunity and are commonly present in the TMEs in the form of tertiary lymphoid structures (TLSs), where they help to prime and support T cell responses through antigen presentation[17]. B lymphocytes have a dual role in the TME; B cells can differentiate into plasma cells that produce tumour-specific antibodies and present antigens to T cells, therefore contributing to tumour reduction. On the other hand, a subset of regulatory B cells can present with pro-tumorigenic effects by producing immunosuppressive cytokines[18].

Tumours are simultaneously infiltrated by a variety of innate immune cells of myeloid lineage that through their phenotypical plasticity exert dual roles in cancer progression. Tumour-associated macrophages (TAMs) are the most abundant myeloid cell type in the TME. Macrophages can originate from bone marrow-derived precursors and differentiate from recruited monocytes, or can arise from tissue-resident yolk sac-derived population[19]; both exhibiting a large functional heterogeneity. The advances of single-cell RNA sequencing technologies have explored the whole spectrum of macrophage activation in cancer[20], however, for simplicity, macrophages are commonly categorised into M1 classically activated

pro-inflammatory and M2 anti-inflammatory phenotypes[21]. M1-like macrophages produce inflammatory cytokines, such as IL-6 and TNFα, exert a higher phagocytic and antigen-presenting activity, and are capable of activating CD8+ T cells. Conversely, M2-like macrophages secrete immunosuppressive cytokines, such as IL-10 and TFGβ, present with higher levels of CD206 receptor and are associated with tissue remodelling and repair[21]. On the spectrum of M1/M2 polarisation, TAMs are more closely related to the M2 phenotype that develops under the immunosuppressive TME through IL-4/IL-13 and TGFβ signalling. TAMs, exert pro-tumorigenic functions through promoting tumour angiogenesis, T cell inhibition, and promote cancer metastasis by enhancing cancer cell motility[22]. Clinically, higher densities of TAMs are often associated with poor patient prognosis[23], and preclinical studies point to the potential of TAMs repolarisation or depletion to improve cancer resolution[24]. This shows that while TAMs usually orchestrate pro-tumorigenic cancer cross-talk, macrophages can be used to activate T cell responses or directly kill cancer cells, if placed within the right context.

Another myeloid cell type presenting with phenotypical and functional plasticity under the influence of the TME is monocytes. Monocytes are recruited to the tumours from the bloodstream via the CCR2-CCL2 axis[25] and then differentiate according to local cues. Once the monocytes infiltrate the TME, they can give rise to macrophages, monocyte-derived dendritic cells, or myeloid-derived suppressor cells[26]. While differentiation into inflammatory dendritic cells links monocytes with anti-tumorigenic functions, under the influence of the TME, monocytes often acquire an immunosuppressive phenotype that further hinders T cell activation, and leads to ECM remodelling and cancer-associated angiogenesis[26].

Additionally, tumours are also infiltrated by granulocytes, such as neutrophils and eosinophils. Because eosinophils are described in more detail within section 1.3, only the role of neutrophils in cancer is briefly discussed here. Neutrophils are the most abundant cell type in the bloodstream and an increased neutrophil-to-lymphocyte ratio is associated with worse patient outcomes in many solid tumours[27]. Within primary tumours, neutrophils get recruited

mainly through the CXCR2-CXCL1/CXCL2/CXCL5 axis and can exert a direct cytotoxicity through degranulation or reactive oxygen species (ROS) production; however, they are frequently reprogrammed by immunosuppressive signalling, such as TFGβ, into a tumour-promoting phenotype that suppresses T cells, remodels the ECM and promotes cancer-related angiogenesis[28]. Similar to macrophages, although less commonly used, this neutrophil polarisation can be simplified into N1 antitumour- and N2 protumour- phenotypes[29]. Furthermore, neutrophils are an important component of (pre)metastatic niches that they establish through promoting systemic inflammation[30,31] , or through neutrophil extracellular trap formation, trapping circulating tumour cells and promote metastasis[32]. Targeting recruitment of neutrophils through CXCR2 blockade results in improved CD8+ T cell responses[33], and depletion of neutrophils can reduce the metastatic dissemination in pre-clinical models[31]; therefore, blockade of neutrophil recruitment through CXCR2 is currently under investigation in clinical studies[34].

Lastly, the TME also comprises structural cells – cancer-associated fibroblasts, pericytes and endothelial cells – that actively shape the physical scaffold and immune context in which tumours grow. Cancer-associated fibroblasts (CAFs) are a key stromal cell type that have many phenotypically and functionally distinct subtypes. CAFs are potent remodellers of the ECM, and shape immune responses through secretion and sequestration of chemokines and cytokines, or as discussed later, by forming physical barriers through ECM deposition that exclude cytotoxic T cells and sustain immunosuppression[35]. Despite CAFs being mainly associated with tumour protective roles, paradoxically, certain subsets of myofibroblasts can also be associated with better patient prognosis, as shown in pancreatic cancer patients and a murine model of this disease[36].

Tumour growth is also dependent on abnormal angiogenesis. In healthy tissues, blood vessels have a continuous layer of endothelial lining, supported by surrounding pericytes and form an intact basement membrane which collectively supports blood flow and regulates immune

responses[37]. This structural order is disrupted during tumour growth as new vessels form rapidly, and therefore display a leaky phenotype and poor perfusion of the tissue. These changes cause uneven oxygen and nutrient delivery, formation of hypoxic regions, and an immunosuppressive environment through the common upregulation of immune checkpoint molecules[38]. Furthermore, the tumour-associated vasculature contributes to reduced drug delivery and treatment resistance, and therapies that induce vascular normalisation have been shown to improve patient outcomes[39].

Resident stromal and immune cells are uniquely imprinted into their organ-specific microenvironment at the baseline homeostatic state. Local cues, represented by diverse ECM composition, oxygen levels, metabolites, microbiome, or hormonal influence, alter gene expression and phenotypic profiles of cells long before the tumour onset. Therefore, it is not surprising that tumours originating from different organs establish the immunosuppressive TME through different mechanisms and present with different treatment resistance strategies. Because this thesis is mainly centred around breast cancer and murine models of this disease, the origin, treatment options, and breast cancer-specific immune microenvironment are introduced along with the commonly used preclinical models that enable a more mechanistic understanding of the dynamic TME interplay.

## 1.2 Breast Cancer: subtypes, treatment, and immune context

Breast cancer is consistently the most commonly diagnosed cancer in women, in part owing to the advances in screening programmes and improved diagnostic tools[40,41]. Despite the advancements in diagnosis, the disease heterogeneity, together with the associated therapy resistance, makes breast cancer the fourth leading cause of cancer-related deaths[41]. Because breast cancer carcinogenesis is driven by numerous molecular alterations, a number of classification systems based on histology, morphology and genetic composition have been established. Within the next sections, the broad breast cancer classifications, the current treatment strategies addressing the disease heterogeneity, the advances in understanding the role of immune infiltration of the tumours and the mouse models used to study breast cancer are briefly described.

### 1.2.1 Clinical classification and intrinsic molecular subtypes

The healthy breast structure is organised into branching ducts that terminate in terminal duct lobular units (TDLUs). TDLUs are composed of a luminal epithelial layer and a basal/myoepithelial layer, both supported by an outer basal membrane[42] (Figure 1.1A). During malignant transformation, epithelial neoplastic proliferation commonly arises within the luminal cells of the TDLUs and may progress from non-malignant hyperplasia to carcinoma *in situ* and ultimately invasive carcinoma[43] (Figure 1.1B). The further steps of progression to invasion are summarised in Figure 1.1C.

While histological and morphological classification remains an essential part of the diagnostic process, it does not capture the biological diversity that drives prognosis and treatment response. Using genome-wide transcriptional profiling with early cDNA microarray assays, seminal work from Perou and Sørlie identified the intrinsic gene set – a set of genes that were stable within paired samples of the same patient but largely variable across breast cancer patients[44,45]. Using this set of genes, unsupervised hierarchical clustering revealed 4 intrinsic

breast cancer subtypes defined by their molecular portraits – Luminal A, Luminal B, human epidermal growth factor-2 (HER2)-enriched and Basal-like subtype. Each of these subtypes was defined by a different expression program: Luminal A strongly overexpresses estrogen receptor (ER) signalling and luminal cytokeratins (KRT8/18/19) together with progesterone receptor (PR) expression and is characterised by a low Ki67 proliferation index. Luminal B retains the ER-signalling, but exhibits a lower luminal gene signature, presents with a higher proliferation index and can be further split based on HER2 expression. HER2-enriched subtype is characterised by strong overexpression of *Erbb2* (gene encoding for HER2) and usually presents with low expression of both ER and PR. Finally, Basal-like subtype expresses basal epithelial cytokeratins (KRT5/6/14), is often associated with TP53 mutations and germline BRCA-induced disease, high proliferation and commonly lacks expression of all three hormone receptors, therefore it largely overlaps with a triple negative phenotype.

As these subtypes were reproducible across multiple breast cancer cohorts and helped with predicting prognosis[46–49], they were transformed to a more routine immunohistochemistry (IHC) testing, based on staining of hormone receptors and Ki67. This resulted in 5 surrogate intrinsic subtypes commonly used at the point of diagnosis[50]: triple negative (TNBC)/basal-like (ER-, PR-, HER2-, high Ki67), HER-2 enriched (ER-, PR-, HER2+, high Ki67), Luminal B HER2+ and HER2-(ER+, HER2+/-, mid-Ki67), and Luminal A (ER+, PR+, HER2-, low Ki67) (Figure 1.1D).

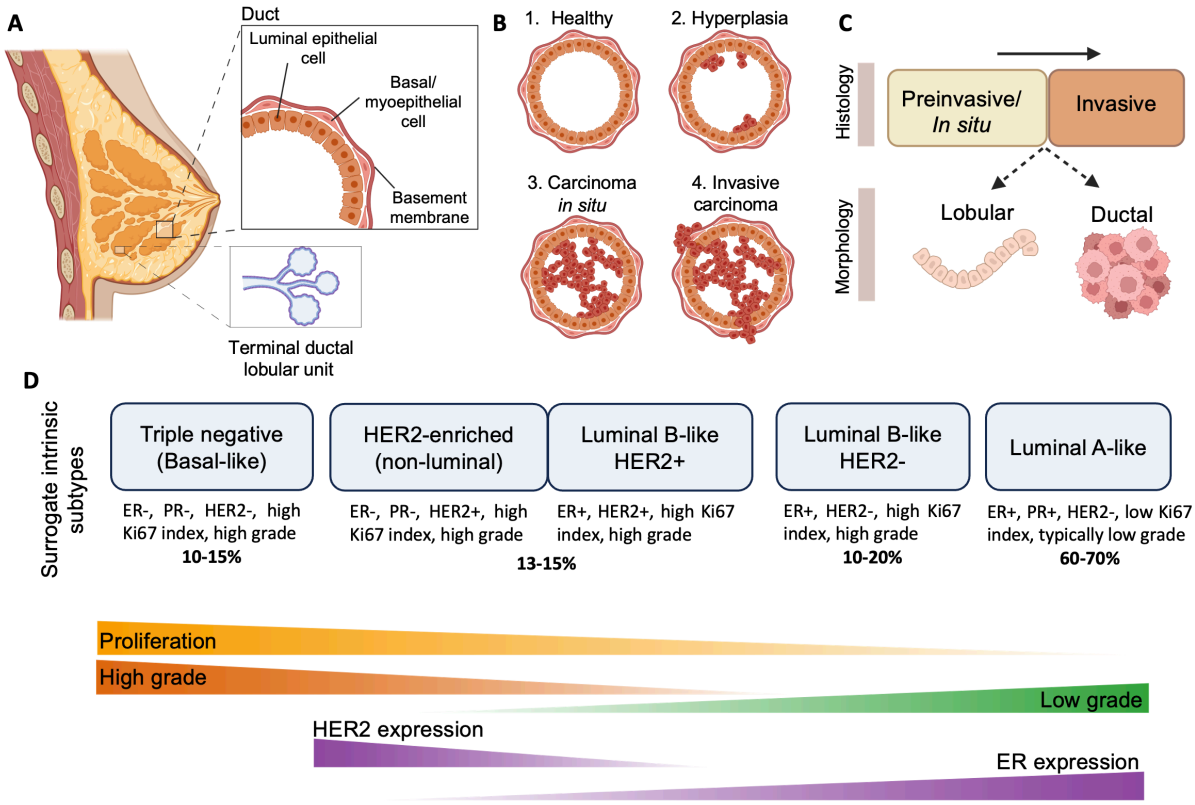


**Figure 1.1. Overview of breast structure and breast cancer classification. (A)** Representation of healthy breast structure showing branching ducts terminating in terminal ductal lobular units and a cross-sectional view of a morphological architecture of the duct. (B) Brief overview of breast carcinogenesis starting with healthy duct structure and progressing through hyperplasia, carcinoma *in situ* and resulting in invasive carcinoma overgrowing through the basal membrane. (C) Overview of histological (preinvasive/*in situ* vs invasive carcinoma) and morphological (lobular versus ductal) classification used at the point of diagnosis. Both *in situ* and invasive carcinomas are further classified based on morphology as ductal or lobular. The main difference stems from the adhesive phenotype of the cancer cells. Lobular carcinomas present with functional loss of E-cadherin that results in a discohesive phenotype characterised by diffuse single layer growth, in contrast, ductal carcinomas, retain expression of E-cadherin and form tumour nests that present as a tumour mass. (D) Brief summary of immunohistochemistry-based surrogate intrinsic subtypes, distinguished by expression of hormonal receptors and Ki67 proliferation index. Estrogen receptor (ER), progesterone receptor (PR), human epidermal growth factor receptor 2 (HER2), proliferation index (Ki67), percentages below individual subtypes show prevalence of disease of invasive carcinomas, gradient bars below summarise overall trends across subtypes. Adapted from Nolan E., Lindeman G. J, and Visvader J. E (2023)[43] and Harbeck et. al (2019)[51]. Created with BioRender.com.

### 1.2.2 Disease heterogeneity informs the treatment selection

Currently, surgery and radiotherapy remain key components of treatment for all breast cancer patients, while the tumour classification by intrinsic subtypes enabled the development of more targeted systemic therapies[14,15]. Briefly, endocrine therapy, such as tamoxifen, which blocks the estrogen receptor, is used for ER+ (luminal) disease[52]; monoclonal antibodies targeting HER2 receptor, such as trastuzumab, are effective in HER2-enriched tumours[53]; and

cytotoxic/cytostatic-based chemotherapies remain the backbone of the treatment strategy for TNBC patients lacking expression of hormone receptors[54] (Figure 1.2). Besides these examples, a wide range of systemic therapies are licensed for breast cancer, including anthracyclines (doxorubicin), alkylating agents (cyclophosphamide) and antimetabolites (methotrexate, gemcitabine)[51]. In addition, targeted therapies informed by the molecular profiles of the subtypes have emerged, such as poly ADP-ribose polymerase (PARP) inhibitors, for patients with BRCA1/BRCA2 mutations associated mainly with TNBC[55]. Moreover, many new therapies have been developed, including CDK4/6 inhibitors for ER+ disease[56], and PI3K inhibitors for PIK3CA-mutant ER+ breast cancer patients[57]; however, these are beyond the scope of this chapter.

Because TNBC is typically considered the most aggressive breast cancer subtype and lacks the targetable ER, PR, and HER2 receptor expression, different combinations of platinum- and taxane-based chemotherapy treatments broadly targeting cell division are being used to improve the pathological complete response (pCR), disease-free and overall survival rates, as reviewed by Poggio and colleagues[54]. Despite these advances in patient stratification for treatment management, recurrence and treatment failure remain common, with TNBC patients that do not achieve pCR following the neoadjuvant chemotherapy having a significantly worse long-term prognosis[58]. These challenges motivated the development of treatments reactivating the adaptive immune system through immune checkpoint blockade (ICB).

T cell-mediated immunity is regulated by inhibitory checkpoint receptors, such as CTLA-4 and PD-1, that upon engagement with ligand restrain T cell activation. During cancer progression, chronic antigen exposure and inflammatory cues drive overexpression of these receptors, leading to T cell exhaustion[59]. Complementary to the antigen-driven T cell exhaustion, tumour and myeloid cells create PD-L1-rich niches that further contribute to T cell deactivation[22,23]. Therefore, blocking these interactions with antibody-based therapies is an attractive therapeutic option for cancers as melanoma and non-small-cell lung cancer, successfully

responding to anti-PD-1 treatment (pembrolizumab)[61,62]. Pre-existing immunogenicity in the form of higher tumour mutational burden, PD-L1 expression, or higher levels of tumour-infiltrating lymphocytes (TILs) are predictors of better response to ICB therapies, as shown across many solid tumours[63]. Even though breast cancer is overall less immunogenic compared to melanoma or lung cancer[64], the TNBC subgroup presents with a higher mutational burden and PD-L1 expression compared to other breast cancer subtypes[65,66]. For patients with metastatic TNBC disease that expresses PD-L1, the combination of pembrolizumab with chemotherapy improved overall survival from 16.1 to 23 months in the latest follow-up of the phase-3 KEYNOTE-355 trial[67]. Usage of pembrolizumab was recently also approved for early high-risk TNBC patients and significantly improved overall survival at 60-month cut-off by 5%[68]. These results encouraged testing of ICBs in other breast cancer subtypes that also present with higher mutational burden and express PD-L1, however, they have not yet resulted in improved patient outcomes in HER2+ breast cancer patients[69], which had already been greatly improved by anti-HER2 therapies.

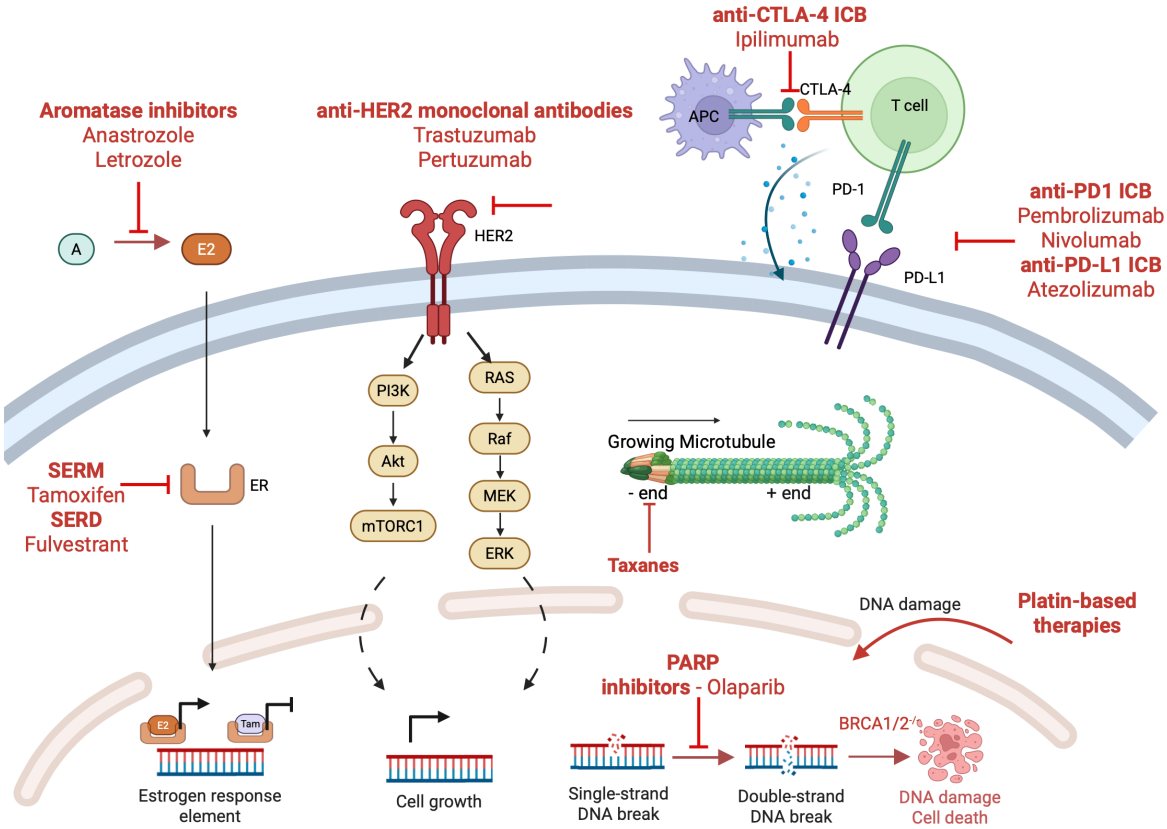


**Figure 1.2. Overview of antibody and small molecule treatment options for breast cancer patients.** Schematic overview of major drug classes used in breast cancer. Endocrine therapies are

targeting 1) estrogen (E2) synthesis – aromatase inhibitors, 2) binding of estrogen receptor to estrogen-response elements – SERM, or 3) estrogen receptor degradation – SERD. The most common HER2-targeted therapies are monoclonal antibodies against HER2 receptor that prevent HER2 dimerisation and downstream activation of PI3K/mTOR pathway or Ras/Raf/MEK/ERK pathways. Cytotoxic/cytostatic modulators used for TNBC patients are mostly based around taxane treatments that block microtubule degradation and inhibit mitosis, or platinum-based therapies that induce DNA cross-linking and DNA damage. PARP inhibitors are approved for patients with germline BRCA1/BRCA2 mutations unable to repair double-strand DNA breaks, leading to cell death. Lastly, three common types of ICB therapies are used: 1) inhibition of PD-1, 2) inhibition of PD-L1, both supporting T cell reactivation or 3) CTLA-4 blockade to enhance T cell priming. A – androgens, SERM - Selective Estrogen Receptor Modulators, SERD - Selective Estrogen Receptor Degraders, Tam - Tamoxifen, PARP - Poly(ADP-ribose) polymerase, ICB – Immune checkpoint blockade, APC – antigen-presenting cell. Adapted from Nolan E., Lindeman G. J, and Visvader J. E (2023)[43]. Created with BioRender.com.

### 1.2.3 Breast tumour immune microenvironment

Although defining the intrinsic subtypes adds granularity to the breast cancer classification at the point of diagnosis, prognosis and treatment response still vary within the individual groups. As discussed above, immunogenicity and overall TIL infiltration improve prediction of treatment response, yet general immune infiltration does not guarantee benefit from immunotherapies. The initial studies addressing the inter-patient heterogeneity focused on profiling large cohorts of patients with a multi-omics approach analysing DNA, RNA, and protein composition of bulk tumour samples, resulting in the creation of The Cancer Genome Atlas (TCGA) database[70]. Pan-cancer analysis using the TCGA database broadly defined 6 main immune subtypes based on main immune expression signatures – 1) wound healing, 2) IFNγ dominant, 3) inflammatory, 4) lymphocyte depleted, 5) immunologically quiet, and 6) TGFβ dominant – all distributed among the 5 main breast cancer subtypes and correlating with different survival prognosis; with the inflammatory phenotype corresponding with increased overall survival compared to other signatures[33]. Furthermore, CIBERSORT analysis predicting infiltration of 22-immune cell types in almost 11 000 tumours, linked infiltration of $T_{regs}$ and M2-like macrophages with poor patient outcomes across all breast cancer subtypes[72]. These studies started to reveal the complexity of the immune microenvironment beyond the general TIL count measurement and linked patients' prognosis with different immune compositions. However, the main limitation of these studies was the bulk nature of these experiments that did not allow for deeper deconvolution of cell-cell interactions.

Single-cell profiling of breast tumours has revealed a phenotypical heterogeneity associated with the TME on both transcriptomic and proteomic levels[20,73], for example, opposing the traditional polarisation of macrophages to M1/M2 phenotypes and revealing a whole spectrum of T cell activation[20]. This TME-related phenotypic plasticity likely mirrors the heterogeneity of niches within the tumours that are regulated by different local cues and allow tumours to adapt and resist therapies. These initial studies prompted the generation of larger datasets that could better determine the association of diverse immune microenvironments with disease progression.

Over the past 5 years, multiple large cohort studies building on single cell datasets defined novel breast cancer subtypes[73–76], based on a) the diverse cellular frequencies found in tumours, often termed "ecosystems"/"ecotypes"[73,75] or b) on recurrent spatial stromal and immune structures[74,76]; each of these classifications is associated with predictive or prognostic role of disease heterogeneity and survival outcomes. Despite each study defining its own new classification of breast cancer subtypes, several patterns can be recognised, such as subsets of macrophages overexpressing PD-L1 and tumours dominated by an overall immunosuppressive phenotype being associated with worse prognosis. Macrophages overexpressing PD-L1/PD-L2 were associated with worse survival when deconvolved into METABRIC ecotypes and negatively correlated with CD8+ and CD4+ T cells in a spatial transcriptomic analysis[75]. Moreover, of the 3 defined ecosystems based on immune composition of tumours, the ecosystem dominated by PD-L1+ macrophages also positively correlated with a higher frequency of $T_{reg}$, exhausted T cells and was linked with more aggressive disease[73]. Adding to the evidence of how immunosuppressed breast TME is predictive of poor clinical outcomes, imaging mass cytometry-based niche analysis defined 10 distinct recurrent TME structures by detecting repeating cell–cell neighbourhoods. While immunosuppressed T cells and macrophages were not detected within the same structural archetype, both "suppressed expansion" and "APC-enriched" TME structures, driven by T cell

expansion and macrophage prevalence, respectively, were independently associated with worse prognosis in ER+ but not ER- patients[76].

In contrast to the well-defined immunosuppressive phenotypes, two TNBC studies show how the spatially distinct neighbourhoods can predict favourable ICB response. In a randomised neoadjuvant ICB clinical trial, the expansion of stem cell-like CD8+TCF1+ T cells and the cancer-B cell interactions were the strongest predictive factors of positive ICB response[77]. Moreover, an in-depth spatial transcriptomic analysis of 92 TNBC patients allowed the generation of a 30-gene tertiary lymphoid structures (TLS) signature that predicted better pCR response in a cohort of breast cancer patients treated with neoadjuvant ICB [78]. This is particularly important as TLS appearance was predicted to have a role in responses to ICB treatment[17]. However, because TLSs are lymphoid-like structures that require spatial identification, a spatial transcriptomic assay is essential for generating their gene signature which cannot be generated by RNA-seq assays missing the spatial context. Furthermore, higher expression levels of the TLS-specific signature correlated with improved progression-free survival of metastatic melanoma and pancreatic cancer patients receiving ICB[78].

Collectively, these studies indicate that variation in prognosis and response to immune-checkpoint blockade is shaped by both the tumour microenvironment composition and spatial architecture, and that capturing this cross-subtype heterogeneity more in-depth than overall TIL densities may improve patient stratification.

### 1.2.4 Mouse models of breast cancer

To reflect the clinical diversity of breast cancer patients, a number of in vivo systems are used to address different aspects of tumour progression and therapy resistance. Patient-derived xenografts preserve the intrinsic genomic and histological features of the human disease[79] and are a valuable tool for drug screening and understanding mechanisms behind treatment

resistance driven by genetic mutations[80]. However, to avoid tumour rejection, the patient-derived xenografts have to be engrafted into immunodeficient hosts, therefore, their main limitation is the lack of anti- and pro-tumorigenic modulation by the adaptive immune system. Therefore, murine studies investigating responses to immunomodulating agents are based on either a) genetically engineered mouse models (GEMMs) that develop spontaneous tumours or b) syngeneic allografts of murine cancer cell lines.

The recent technological advances expanded the repertoire of breast cancer GEMMs that closely recapitulate the tumour development and progression. This can be demonstrated on the panel of 16 breast GEMMs, all generated on an FVB background and differing only in tissue-specific driver mutations, mimicking the inter-patient heterogeneity[81]. Screening of circulating leukocytes in this panel of GEMMs revealed that the neutrophil expansion, clinically associated with poor outcomes[82] and linked with higher metastatic potential in murine studies[30,31], is specifically associated with a loss of p53 in cancer cells when comparing all 16 tumour types. This observation then led to elucidation of a full cascade connecting the loss of p53 expression by cancer cells to overexpression of Wnt ligands, causing downstream induction of IL-1β in tumour-associated macrophages and ultimately contributing to the systemic inflammation marked by emergent granulopoiesis[81]. Furthermore, these models were then used to elucidate the molecular mechanism behind IL-1β induced emergent granulopoiesis with an immunosuppressive phenotype, potentially revealing a clinically relevant target that might help with reducing metastasis[83].

While GEMMs better recapitulate the stepwise tumour progression and the long-term co-evolution of the tumour with the host immune system, these models are often time-consuming and expensive for routine experiments. Syngeneic models, based on engraftment of murine-derived breast cancer cell lines into an immunocompetent host, are therefore a more accessible option for studying breast cancer. Similar to GEMMs, both the host and the genetic make-up of the cancer cell line dictate the tumour immune composition and response to

therapies. While albino mice (Balb/c and FVB) are often skewed towards Th2 immune responses, mice on C57/Bl6 background present with a stronger Th1-like response[84,85]. However, within a single strain, the immune response still differs depending on the cancer cell line used. Both EMT6 and 4T1 cancer cell lines are derived from mammary tumours isolated from the Balb/c strain, their primary growth patterns are similar, yet their metastatic potential differs[86]. Interestingly, despite both models having similar rates of early disseminated tumour cells (DTCs), the EMT6 tumour model induces a strong anti-tumour immunity early during tumour development that protects the tumour-bearing mice from metastatic colonisation. However, this can be reversed either in $Rag2^{-/-}$ mice with a defective adaptive immune system, or by transfer of granulocytic myeloid-derived suppressor cells from 4T1 tumour-bearing mice, both experiments restoring the ability of EMT6 DTCs to form lung metastasis[86]. This underscores the importance of understanding the local and systemic responses of hosts to different tumour models when selecting and interpreting preclinical models.

In this thesis, the main mouse model used is based on an NT193 cancer cell line that originated from a spontaneous MMTV-NeuNT model. The MMTV-NeuNT model utilises the mouse mammary tumour virus (MMTV) promoter that is hormonally responsive[87] and links the onset of carcinogenesis to hormonal cues in the gland[88]. In the transgenic MMTV-NeuNT model, the rat homologue of HER2 (*neu*/*ErbB2*) bears a mutation that leads to constitutive activation of the receptor NeuNT[89], placed under the MMTV-promoter, leading to an early tumorigenesis specifically in the mammary gland[90]. Overexpression through the MMTV-promoter strategy is also used in the commonly studied MMTV-PyMT model that depends on the overexpression of polyomavirus middle T (PyMT) oncoprotein, also leading to spontaneous primary and metastatic breast cancer[91]. In this thesis, the orthotopic NT193 model was picked due to the already set-up genetic modification of tenascin-C (TNC) that leads to different extracellular matrix formation, chemokine expression profile, and ultimately establishment of more immunosuppressive (TNC+) and immunopermissive (TNC-) TME[92,93].

## 1.3 The role of eosinophils in tissue biology

Eosinophils are bone marrow-derived granulocytes, commonly studied in the context of allergy and parasite infection. However, their role in the TME is being increasingly recognised[94], with the role of the TME in shaping eosinophil plasticity being a key topic of this thesis. Therefore, within this section, the eosinophil ontogeny, their main phenotypical and functional characteristics, together with their role in health and disease, are briefly discussed.

### 1.3.1 Overview of eosinophil biology

Because of the granulocytic nature of eosinophils, their functions and ontogeny were for a long time intuitively linked to neutrophils. However, despite being granulocytes, their ontogeny is strongly coupled with GATA-binding factor 1 (GATA-1) expressing lineages such as basophils, erythrocytes, and megakaryocytes; while neutrophils arise from a distinct arm of myelopoiesis shared also with monocytes and macrophages (Figure 1.3A)[95–97]. Recent study shows that eosinophils develop through a common eosinophil/basophil/mast cell progenitor, and upregulate IL-5 receptor-$\alpha$ (*Il5ra*) only after the lineage commitment step, with *IL5ra* expression marking the presence of the first recognised eosinophil progenitor[98]. The finding of *Il5ra* expression in the first committed eosinophil progenitor and the consecutive maturation stages, but not in the developmental stages before the lineage commitment, fits with observations that IL-5$^{-/-}$ mice fail to develop eosinophilia upon stimulation[99,100], however, they do not lack any of the recently described eosinophil maturation stages[98]. Eosinophil maturation was recently resolved to occur in 4 sequential stages[98]; stages I and II are enriched for surface expression of cKit and upregulating pathways associated with ribosome enrichment and proliferation, stage III is defined by downregulation of the cell proliferation gene signatures but upregulation of genes associated with eosinophil innate immune response (*Ear1*, *Ear2*), and stage IV is defined by the highest surface expression of CCR3, upregulation of genes associated with myeloid cell activation and chemotaxis, but also downregulation of eosinophil peroxidase on gene level (*Epx*).

Because IL-5 is a common target of antibody-based therapies against severe asthma[101], it is crucial to understand how it affects the survival and expansion of eosinophils, while not affecting the eosinophil commitment step, as permanent depletion of eosinophils might lead to defective anti-tumour immunity[102]. Furthermore, expression of GATA-1, IL-5, and IL-5Rα is used for the generation of GEMMs that help elucidate the role of eosinophils in health and disease, through ablation, overexpression or tracking of their development (Table 1.1).

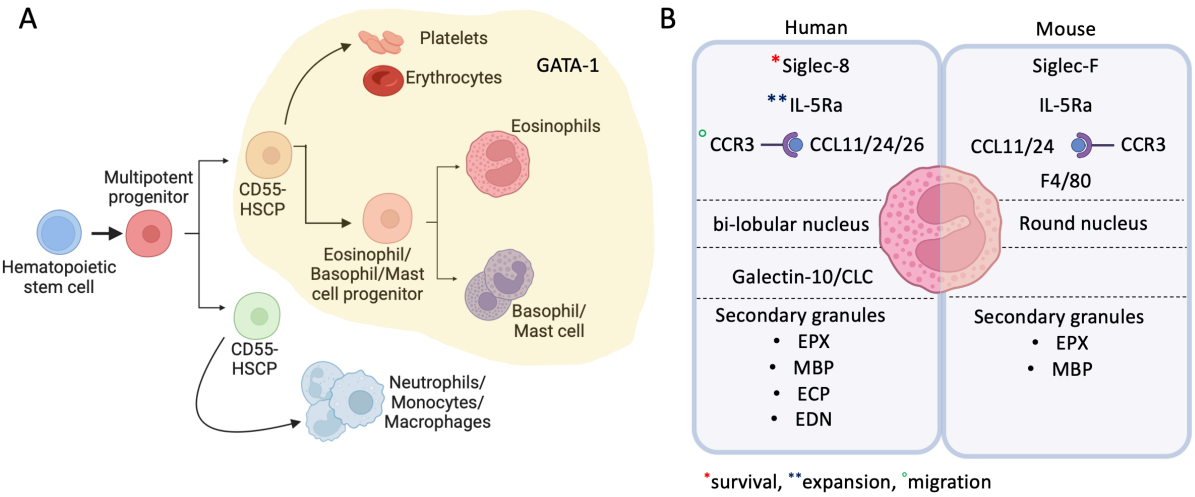


**Figure 1.3. Eosinophil ontogeny and characteristics**. **(A)** Simplification of the haematopoietic tree. Eosinophils develop along GATA-1 expressing lineages, separately from neutrophils. **(B)** Overview of the main eosinophilic features in human and murine eosinophils. Figure A adapted from Jorssen et al[98]. Created with BioRender.com.

At steady state, eosinophils preferentially reside in mucosal barrier organs, such as the gut, uterus, and lung, but are also present in the thymus, adipose tissue, lymph nodes, skin, and the mammary gland[94,103]. Mature eosinophils can be distinguished by a combination of surface receptors of growth factors, cytokines, adhesion, and migration. Murine eosinophil markers include CD11b, F4/80, Siglec-F, CCR3, and IL-5Rα. Similarly, human eosinophils can be identified based on expression of CD11b, Siglec-8, CCR3, IL-5Rα and CD15[104] (Figure 1.3B). A combination of these markers is needed for conclusive eosinophil identification, as these markers are not eosinophil exclusive, such as Siglec-F expression on both murine eosinophils and alveolar macrophages[105], or CCR3 expressed on human basophils[106]. CCR3 is an eotaxin (CCL11, CCL24, CCL26) receptor essential for eosinophil recruitment and migration[107]. While

eosinophils can migrate towards CXCL1, CCL4, CCL13, and CCL17 in vitro[108], the eotaxin-CCR3 axis is considered the prime mode of trafficking in vivo.

**Table 1.1 Overview of the main eosinophil GEMMs**

| | Genetic modification | Mouse strain | Biological effect | Reference |
|---|---|---|---|---|
| **ΔdblGATA** | Deletes the high-affinity "double GATA" binding site in the Gata1 hematopoietic promoter | C57BL/6J or BALB/c | Specific eosinophil lineage ablation | 109 |
| **PHIL** | Diphtheria toxin A expression under EPX promoter | C57BL/6J or BALB/c | Specific eosinophil lineage ablation | 110 |
| **iPHIL** | Knock-in of human diphtheria toxin receptor into the endogenous EPX locus | C57BL/6J | Conditional eosinophil ablation | 111 |
| **IL5-/-** | Germline deletion of *Il5* | C57BL/6J | Loss of IL-5 signalling, reduced eosinophil numbers in type 2 inflammation | 100 |
| **IL5Ra-/-** | Null allele; premature stop in exon 5 of *Il5ra* | C57BL/6J | IL-5 unresponsiveness, decreased numbers of eosinophils during disease onset | 112 |
| **CCR3-/-** | Knockout of CCR3 (eotaxin receptor) | BALB/c | CCL11 and CCL24 unresponsiveness, defective trafficking | 113 |
| **IL5tg** | Ligation of *Il5* to the dominant control region of human CD2 | C57BL/6J | Systemic expression of IL-5 leading to eosinophilia | 114 |
| **EPX-Cre** | Knock-in of Cre recombinase into the endogenous Epx locus by homologous recombination | C57BL/6J | Cre-lox conditional deletion or fate mapping if crossed with reporter mice | 103,115 |

Both human and murine eosinophils carry eosinophil-specific secondary granules containing highly cationic proteins, such as EPX or major basic protein (MBP), but also different cytokines and chemokines (IFNγ, IL-4, IL-13, TGFβ, CCL3, CCL5, CXCL10)[116]. Secretion of the highly cationic proteins into the extracellular space has an anti-tumorigenic and anti-parasitic effect, while secretion of the cytokines has the potential to broadly contribute to immune regulation[117].

For a long time, eosinophils were considered to be a short-lived and terminally differentiated cell type. However, it is becoming clear that despite their short half-life in circulation (approx.

18 hours)[118], eosinophils can be long-lived and plastic cells adapting to their local niche and contributing to many physiological processes[94].

### 1.3.2 Eosinophils in tissue homeostasis

Because eosinophils often infiltrate tissues at high rates during parasite infections or allergy, this initially formed an opinion that eosinophils are a terminally differentiated proinflammatory cell type involved in host defence and tissue damage through active degranulation. However, even at steady state, eosinophils present a significant resident population in tissues such as the gut, uterus or bone marrow[94]. This observation led to the formation of the LIAR (Local Immunity And/or Remodelling/Repair) hypothesis[119]. Building on the fact that eosinophils are often found in niches with high epithelial turnover and stem cell activity, James Lee and colleagues hypothesised that eosinophils might act as regulators of local immune homeostasis and tissue repair. Indeed, over the past decade, a number of studies provided evidence that eosinophils contribute to the tissue homeostasis, regeneration and regulation of immune responses and are capable of more than just degranulating, as recently reviewed by Arnold and colleagues[94].

Within the gastrointestinal tract (GI), eosinophil distribution is highly organised. Eosinophils are sparse in the oesophagus, and their densities start to increase distally from the stomach towards the colon, with the largest tissue resident population found in the small intestine[120]. GI resident eosinophils are essential for maintaining mucosal barrier immunity[121], epithelial architecture[122], villi structure upon microbial colonization[123], and nutrient uptake[123,124]. These functions are aligned with their distribution along the crypt-villus axis. In the healthy GI tract, eosinophils infiltrate the small intestine within the crypt niche and then migrate towards the tips of the villi for at least 18 days, as proven by BrdU pulse-chase approach[124]. This experiment also demonstrates that eosinophils are a long-lived resident population and explains the recently observed phenotypical and functional adaptation described on a single cell transcriptomic level. By using an IL-5 transgenic mouse model (Il5-tg) with expanded

eosinophil compartment, Gurtner and colleagues were the first to robustly profile bone marrow, circulating, splenic, and GI (stomach, small intestine and colon) eosinophils[125]. Transcriptomic analysis revealed a developmental trajectory consisting of precursor and immature eosinophil subsets emerging from the bone marrow, altering their transcriptomic signature in circulation and then adapting to GI organs by acquiring basal (B-eos) and active (A-eos) phenotypes. Most importantly, while B-eos upregulated genes related to matrix regulation and tissue development, A-eos arose from B-eos and were exclusively present in the colon and small intestine where they expressed immunomodulatory molecules PD-L1 and CD80[125]. This study was pivotal in understanding the plastic potential of eosinophils and led to the recent development of a protocol for eosinophil single-cell sequencing in other tissues[126], which might help with understanding eosinophil adaptation to different disease states in the future.

In comparison to gut, the phenotypical, functional and spatial adaptation of eosinophils in the lung is yet to be explored on a single cell transcriptomic level. Nevertheless, eosinophils play an important role in healthy lung homeostasis. During postnatal development, eosinophils appear in the lung on postnatal day 7 (P7) and their peak recruitment around P10-P14 temporally corresponds with the primary septation phase and extracellular matrix (ECM) remodelling[127]. While eosinophils are likely not essential for lung development, as indicated by the viability of ΔdblGATA or PHIL mice lacking eosinophils[128], their absence causes mild ECM alterations, such as incomplete gene switch towards mesenchymal phenotype in lungs of adult mice[127]. Furthermore, eosinophils were observed to be patrolling around the vasculature in healthy lungs, supporting their potential contribution to immune surveillance at baseline level[103]. These lung resident eosinophils (rEos; SiglecF$^{int}$, CD62L$^{+}$, CD101$^{low}$) are functionally and phenotypically distant from inflammatory eosinophils (iEos; SiglecF$^{high}$, CD62L$^{+}$, CD101$^{high}$) infiltrating lungs during house dust mite–induced airway allergy. Functionally, rEos restrain allergic sensitisation by limiting maturation of allergen-pulsed dendritic cells and indirectly reducing Th2 priming following allergen exposure[129]. While it was proposed that rEos reside in lungs independently of IL-5, these results were later challenged

by experiments showing that anti-IL-5 treatment reduced Siglec-F expression and depleted all lung-associated eosinophil subsets[130]

Although often overlooked, eosinophils co-localise with macrophages around the tips of the terminal end buds (TEBs) of a developing murine mammary gland, where they contribute to branching and formation of TEBs[131]. Interestingly, this resident population of eosinophils is recruited to the mammary fat pads (MFP) based on the CCL11 gradient, with $Ccl11^{-/-}$ mice lacking eosinophils, and therefore confirming that MFP-resident eosinophils are bone-marrow derived and recruited from circulation[131]. Furthermore, it is becoming increasingly recognised that eosinophils are highly regulated by estrogen levels. Administration of estrogen almost completely abolished eosinophil levels in blood and MFP of healthy mice, while ovariectomy or administration of fulvestrant (ER antagonist) led to expansion of resident MFP eosinophils almost 4-fold[132]. Of note, despite the long-discussed macrophage-eosinophil crosstalk in healthy MFPs[133], macrophage levels were fluctuating the opposite way, with ovariectomy and fulvestrant treatment reducing the macrophage proportions, compared to the increased eosinophil levels during these estrogen-modulating treatments[132]. Despite the role of eosinophils in the development of healthy human breast tissue being unclear, eosinophils are present in human milk[134], their levels are regulated during endocrine treatment of breast cancer patients, and the estrogen treatment that results in eosinophil depletion leads to a significant increase in tumour growth of murine tumours[135].

### 1.3.3 Eosinophil effector functions and role in inflammation

Eosinophils contribute broadly to host-defence and allergic inflammation, with the effector functions being dependent on the nature of the stimuli. The key effector functions of eosinophils are organised around the three types of degranulation: a) piecemeal degranulation, b) exocytosis and c) cytolytic degranulation; each of these represents a mechanism that leads to the release of the eosinophilic granular content into the extracellular space[136]. The main differences between these 3 degranulation processes stem from the initial

trigger, the mechanism of granule trafficking, the granule-plasma membrane fusion step prior to secretion, and the kinetics of the granule release (Figure 1.4A).

Piecemeal degranulation is a gradual release of selective granule proteins by secretion of small vesicles without causing any major ruptures of the cell wall. It is typically activated by immunomodulatory cytokines, for example, IFNγ, TNFα, platelet-activating factor or eotaxin-1 (CCL11)[137,138]. Exocytosis, a less common degranulation mechanism, occurs after direct fusion of granules with the plasma membrane, with either a) individual granules (classical exocytosis) or b) multiple granules fused together before the secretion (compound exocytosis)[139]. It is important to notice that piecemeal degranulation and compound exocytosis are not mutually exclusive processes and can occur within the same cell, as was reported for eosinophils infiltrating a human gastric tumour[140]. In contrast, cytolytic degranulation causes rupture of the plasma membrane and release of intact granules, resulting in a non-apoptotic cell death[139]. This process is commonly associated with eosinophil extracellular trap formation (EEtosis), however, eosinophils can also produce extracellular DNA traps by rapid release of mitochondrial DNA while remaining viable[141]. During EEtosis, eosinophils release their chromatin into the extracellular space, creating net-like structures together with the intact granules, serving as a non-phagocytic defence against helminths that get trapped in the nets[142]. Which type of degranulation dominates the eosinophil response is shaped by the activation state of eosinophils, stimulus, and involvement of intracellular protein machinery accommodating the fusion step; as shown in Figure 4A and reviewed in[94,136]. Even though less efficient than macrophages or neutrophils, eosinophils are also capable of phagocytosis in vitro[143], with case studies reporting their phagocytic activity even in human blood eosinophils[144].

Because eosinophil granule proteins are highly cytotoxic and cationic, degranulation is the primary route of anti-microbial, viral and fungal activity. These activities are dependent on the secreted proteins that are capable of a) membrane disruption (MBP, eosinophil cationic protein

(ECP), eosinophil-derived neurotoxin (EDN)), b) degradation of viral ssRNA (EDN, ECP), c) causing oxidative tissue damage through peroxidase mediated halogenation (EPX), or d) through the cytotoxic properties of extracellular trap formation (Figure 1.4B)[136]. Furthermore, eosinophil granules store a wide array of cytokines that are secreted upon stimulation and shape both Th1 and Th2 immune responses[145]. Because eosinophils do not rely on de novo synthesis of cytokines upon stimulation, they are one of the first IL-4 producing cells in response to helminth infection[146] and allergic challenges[147]. Moreover, eosinophils also possess cytokines related to Th1 immune responses, such as IFNγ, IL-2, and TNFα, or tissue remodelling, such as TGFβ[145].

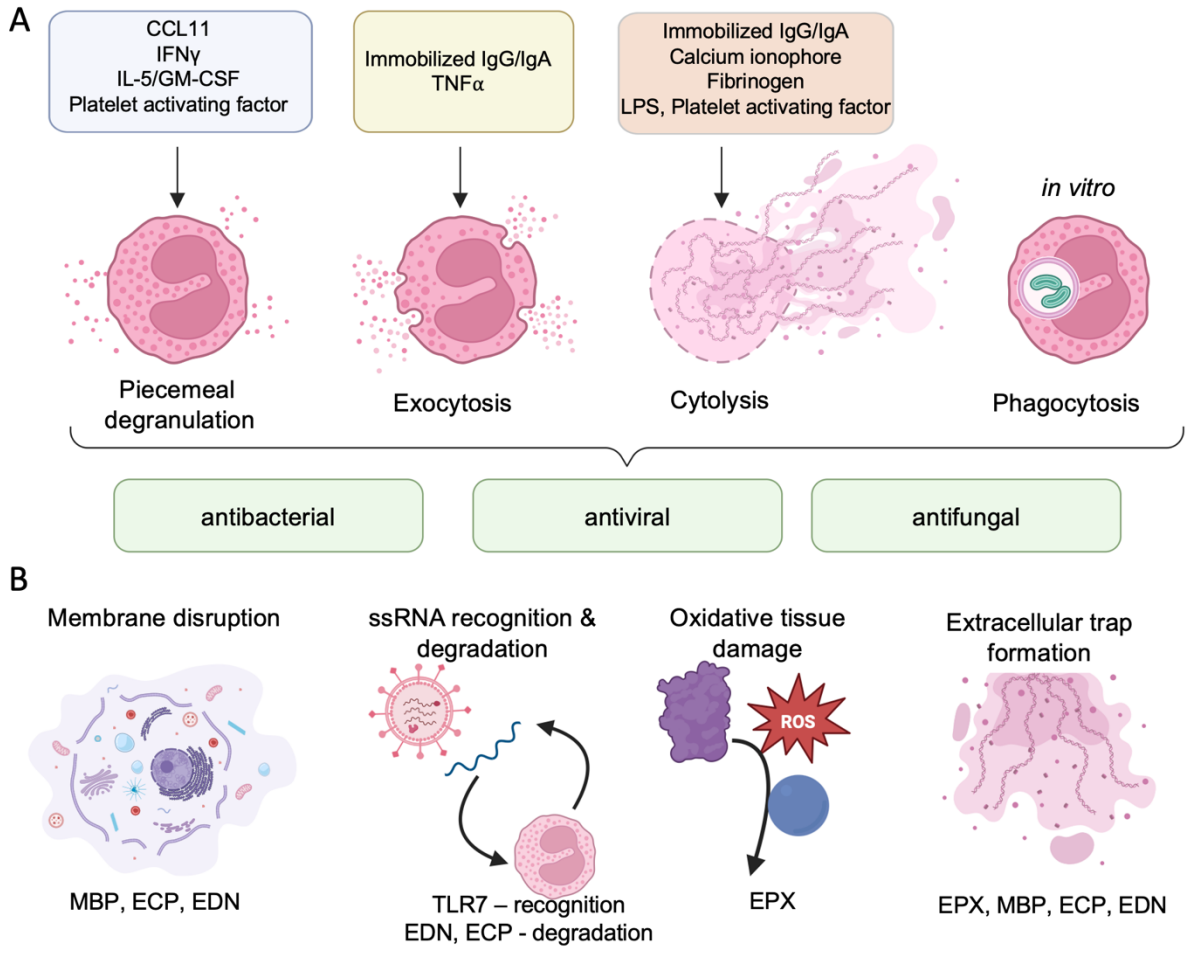


**Figure 1.4. Overview of eosinophil cytotoxic properties. (A)** Different stimuli lead to different types of degranulation. Eosinophils mediated their antibacterial, antiviral, and antifungal activity through 3 different types of degranulation – gradual piecemeal degranulation, classical and compound exocytosis releasing granule/s through fusion with plasma membrane during secretion and cytolytic degranulation leading to cell death and formation of eosinophil extracellular traps (EEtosis). Additionally, eosinophils are also known to be phagocytic in vitro. **(B)** Overview of the main cytotoxic mechanisms employed by eosinophils and matched cationic/peroxidase proteins to the function. MBP – major basic protein, ECP

– eosinophil cationic protein, EDN- eosinophil-derived neurotoxin, ROS – reactive oxygen species, EPX – eosinophil peroxidase. Figure A adapted from Fettrelet et al. (2021)[136]. Created with BioRender.com.

During helminth infection, eosinophils are actively recruited by eotaxins and type-2 cytokines (IL-5 and GM-CSF) and as mentioned above, can reduce the bacterial load through degranulation. However, their role in the tissue is highly context- and infection-dependent. In vivo, IL-5 transgenic mice, with constantly elevated eosinophil levels, presented with enhanced resistance to *Nippostrongylus brasiliensis* infection, however, this effect did not repeat when infected with *Toxocara canis*; showcasing how eosinophils can promote anti-helminth immunity in the context of one but not another pathogen[148]. The observation that eosinophils may not always be anti-parasitic was further validated in a study using eosinophil-deficient PHIL and ΔdblGATA mouse models infected by *Trichinella spiralis* affecting muscles during the final stage of the parasite's life-cycle[149]. Eosinophil-deficient mice presented with fewer muscle larvae and increased IFNγ and iNOS production, suggesting that eosinophils in certain scenarios are promoting parasite persistence by restraining Th1 immunity.

The dual role of eosinophils in bacterially driven GI inflammation, through both, restraining Th1 immune response but also promoting bactericidal activity through EETosis and degranulation, was confirmed in *Helicobacter pylori* and *Citrobacter rodentium* infection models[120]. Furthermore, in this study, eosinophils upregulated PD-L1 in an IFNγ-dependent manner, and their depletion improved bacterial clearance by Th1/Th17 immune response. Conditional loss of IFNγ receptor in eosinophil lineage phenocopied this bacterial protection, suggesting that upstream IFNγ signalling in eosinophils is limiting Th1 response in certain contexts[120]. Therefore, eosinophils contribute to the immune response by more than degranulation.

Although eosinophils are not considered the main antigen-presenting cell type, some of the eosinophil effector functions are potentially linked to antigen presentation. Interestingly, while both murine and human eosinophils were found to express MHC-II in the context of allergen

challenge[150], in vitro assays with bone marrow-derived eosinophils testing eosinophil antigen-presenting abilities in co-culture with OT-I CD8+ T cells and OT-II CD4+ T cells, suggested that eosinophils sufficiently present antigens to T cells only through the MHC-I complex[125]. Opposite to T cell activation, eosinophils presenting with A-eos phenotype and increased expression of PD-L1 were capable of attenuating CD4+ T cell activation[125], supporting the immunoregulatory role of eosinophils during tissue inflammation[120].

Finally, as previously mentioned, eosinophils are extensively studied in the context of allergy and asthma. Asthma is a chronic inflammatory disease of the airways characterised by a number of symptoms, including airway hyperresponsiveness and inflammation, mucus hypersecretion, and tissue remodelling; with eosinophils being linked to each of these heterogeneous symptoms[151]. Eosinophil counts in peripheral blood and bronchoalveolar lavage fluid of asthmatic patients are elevated compared to healthy controls[152,153], with higher eosinophil counts correlating with disease severity[154]. The essential role of eosinophils in asthma was first revealed in murine pre-clinical models, with eosinophil deficient PHIL mice being protected from mucus accumulation upon allergen stimulation[110] and ΔdblGATA mice did not present with increased collagen deposition and airway smooth muscle thickness when challenged with allergens[155]. These data collectively pointed to the role of eosinophils in the structural but also functional remodelling of the airways. Even though the role of eosinophils in asthma severity and tissue damage is closely associated with the release of their cationic granule proteins, eosinophils were also proposed to be a source of TGFβ. Eosinophils presented with high levels of TGFβ in bronchial biopsies of asthmatic patients[156], pointing to their role in tissue remodelling. In summary, eosinophils are central effector cells that couple the airway hyperresponsiveness, mucus secretion, tissue damage, and airway remodelling through diverse mechanisms. Therefore, treatment strategies reducing eosinophil numbers, such as antibodies targeting IL-5 or IL-5Rα leading to a rapid eosinophil depletion[157,158], help reduce exacerbations of patients with severe asthma.

### 1.3.4 Role of eosinophils in the tumour microenvironment

Eosinophils also have pleiotropic roles in the tumour microenvironment, as recently reviewed[159], with human studies suggesting both pro- and anti-tumorigenic function, dependent on the cancer type[160,161]. An immune histochemistry (IHC) eosinophil staining ($EPX^+$ cells) of 2890 mucosal (colon, lung, oesophageal, and cervical) and non-mucosal (breast, and ovarian) tumours confirmed that eosinophils are more abundant in tumours arising from mucosal tissues[162] (Figure 1.5A). Although breast tumours were the least eosinophil-infiltrated, eosinophils were more abundant in tumour nests than in stroma, contrary to all other tumour types investigated[162]. However, in direct opposition to the reports linking increased peripheral or intratumoral eosinophils to better prognosis of breast cancer patients[72,160,163–165], increased eosinophil infiltration positively correlated with clinical stage and tumour size exclusively in breast tumours compared to the other mucosal tumour types[162]. It is therefore possible that eosinophils display a different prognosis based on the type of identification (IHC vs bulkRNA-seq prediction), age, menopausal status of patients, and the type of baseline therapy used in the studied cohort of patients.

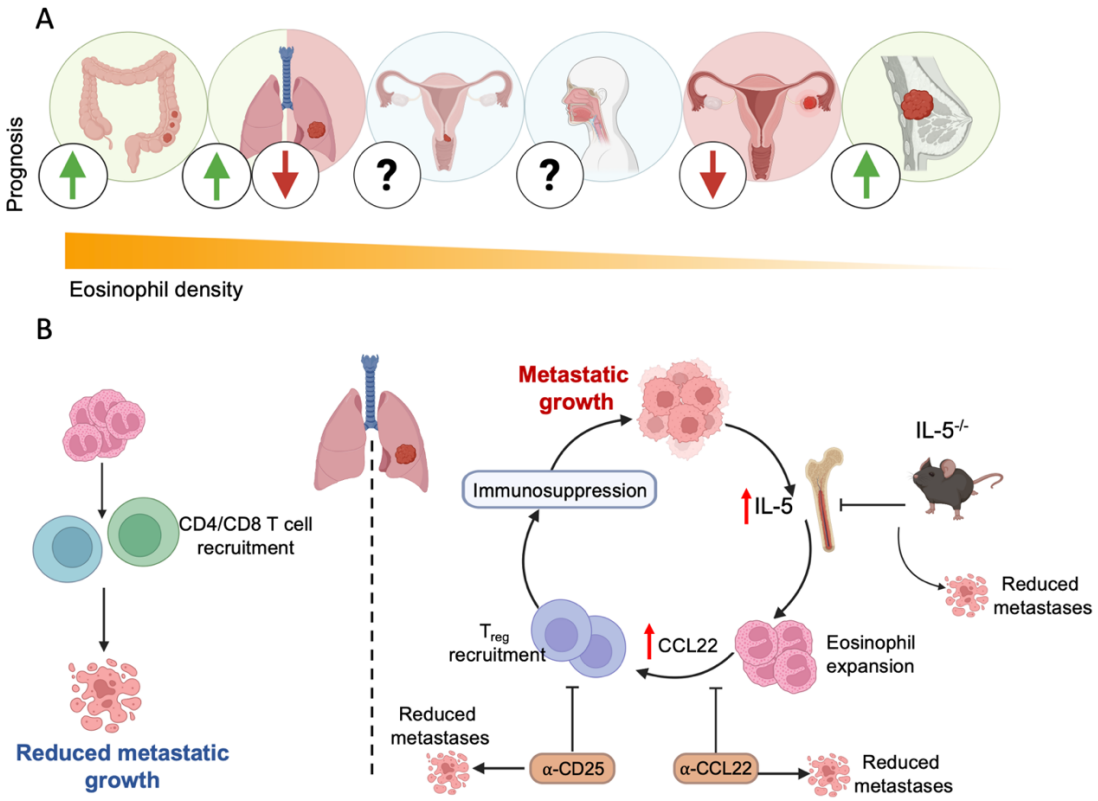


**Figure 1.5. Dual role of eosinophils in the tumour microenvironment. (A)** Eosinophil density in mucosal and non-mucosal organs organised in descending order (gradient bar) – gut, lung, cervical,

esophageal, ovarian, and breast cancer. Green colour indicates eosinophil correlation with good prognosis, red colour indicates worse prognosis, blue/question mark labels cancers with no known association of eosinophils to cancer prognosis. **(B)** Overview of eosinophil anti-tumorigenic and pro-tumorigenic roles in metastatic disease. Higher infiltration of eosinophils leads to CD4+ and CD8+ T cell recruitment and reduced metastatic growth, opposite to this cancer cancer-induced eosinophil expansion, CCL22 eosinophil expression and $T_{reg}$ recruitment support immunosuppression and metastatic growth. Treatments/mouse models that can inhibit this eosinophil-driven immunosuppression are indicated. Created with BioRender.com.

The dual functionality of eosinophils is highly dependent on the TME composition, as can be best exemplified by a range of studies exploring the role of eosinophils in lung metastasis (Figure 1.5B). Eosinophils exert anti-tumorigenic effects during metastatic colonisation of lungs in murine models of breast cancer, with eosinophil-deficient ΔdblGATA mice or mice treated with eosinophil-depleting anti-Siglec-F antibody being more permissive to lung metastasis in both E0771 and PyMT breast cancer models[166,167]. In agreement with these results, Il5tg mice with constant eosinophilia were to a large extent protected against breast cancer metastasis[166,167], suggesting an antitumorigenic role of eosinophils. However, in contrast to these findings, eosinophils were also found to promote lung and bone metastasis[168,169]. IL-$5^{-/-}$ mice with deficient eosinophil expansion did not develop metastasis for 28 days post intravenous Lewis lung carcinoma cell line injection, compared to WT mice[169]. Administration of eosinophils increased the number of metastases in both WT and IL-$5^{-/-}$ mice, with eosinophils being linked to the establishment of early immunosuppressive TME through CCL22 – $T_{reg}$ axis[169]. Collectively, these studies demonstrate that the pro- and anti-tumorigenic roles of eosinophils are highly dependent on the different TME established by the cancer cells (Figure 1.5B). It would be interesting to know which cancer-derived factors drive the immunosuppressive phenotype that ultimately leads to the CCL22 expression dependent on eosinophil presence, and whether the same set of cytokines would be capable of establishing a more $T_{reg}$-dominant breast TME in the different cancer models.

The TME exploits the intrinsic plasticity of infiltrating immune cells and actively shapes their phenotype and function to its advantage[8]. While eosinophil heterogeneity is well described in non-malignant settings; active vs basal subset in GI[125] or resident vs inflammatory eosinophils

in lungs[129]; less is known about how the TME shapes eosinophil heterogeneity. In murine models of breast cancer-induced lung metastasis, two eosinophil populations were observed in metastasis-bearing mice, Siglec-F$^{int}$ and Siglec-F$^{hi}$, with the Siglec-F$^{int}$ subset also present in healthy mice[166]. Although further transcriptomic and proteomic analysis revealed major differences between healthy and disease-associated eosinophils, no significant phenotypical change was observed between the Siglec-F$^{int}$ and Siglec-F$^{hi}$ eosinophil subsets in metastatic lungs[166]. Similarly to these findings, only one type of tumour-associated eosinophils was found on a scRNA-seq level, in an orthotopic colon model of adenocarcinoma[170]. Interestingly, all of the adenocarcinoma infiltrating eosinophils resembled the A-eos phenotype associated with increased IFNγ responsiveness and immunomodulatory function[125], agreeing with the STAT1 overexpression and IFNγ activation of their metastatic-entrained counterparts[166]. Future research is needed to explore if eosinophils can be polarised/transition to a tumour-specific discrete subset or are adapting along a continuum of activation states.

The anti-tumorigenic role of eosinophils can be observed as both – direct cytotoxic effect on tumour cells and indirect cytotoxicity through cross-talk of eosinophils with other TME infiltrating cells. There is a number of studies proving a negative correlation between eosinophils and primary or metastatic tumour growth in murine models of colorectal cancer[102,171], metastatic breast cancer[166,167], melanoma[172], fibrosarcoma[173], and hepatocellular carcinoma[174], however, only few of these reports explore the mechanism behind eosinophil-mediated cytotoxicity. The evidence that eosinophils can directly mediate antitumorigenic effects comes mainly from in vitro studies in which eosinophils induce apoptosis or reduce tumour growth of cancer cell lines in direct co-cultures[171]. The tumorigenic potential of eosinophils can be further enhanced by cytokines such as IL-33, IFNγ, TNF$\alpha$, or CCL11[171,175–178]. For example, stimulation of IFNγ leads to active degranulation of eosinophils ex vivo[125], has a profound effect on eosinophil transcriptome[179,180], and promotes eosinophil cytotoxicity in direct co-culture with tumour cells[171], yet a direct mechanism of how IFNγ facilitates this cytotoxicity in co-cultures with tumour cells is still unclear.

In a mechanistic study, eosinophils gained cytotoxic activity in a contact-dependent manner upon stimulation with IL-33. Eosinophils incubated with IL-33 upregulated adhesion receptors CD11b/CD18, formed stable conjugates with tumour cells and polarised their secondary granules towards the junction with tumour cells, resulting in increased cytotoxicity (Figure 1.6A)[177]. This cytotoxic effect was lost if a) eosinophils were stimulated with IL-33 in a Transwell assay that reduced their contact with the tumour cells, or b) by blocking the CD18 adhesion receptor with a monoclonal antibody, proving that eosinophils don't just passively degranulate after stimulation but need the physical contact to drive the cancer cell lysis[177]. Eosinophil adhesion ability seems to be a crucial determinant of their in vitro cytotoxicity, as stimulation of eosinophils by IL-18 also leads to overexpression of ICAM-1, LFA-1, and mild upregulation of CD18 and correlates with enhanced apoptosis of colorectal cancer cell line(Figure 1.6B)[181]. Furthermore, IL-33 administration led to overexpression of eotaxins and reduced tumour growth in an eosinophil-dependent manner in models of colorectal cancer and metastatic melanoma[178,182], making IL-33 a potent activator of eosinophil migration (Figure 1.6C)[183,184] and anti-tumorigenic potential. Future research will help with understanding how exactly eosinophils recognise tumour cells. At the moment, the only evidence of eosinophil specificity against cancer cell lines comes from eosinophils not being cytotoxic against a population of human fibroblasts[185].

Eosinophil direct cytotoxicity in vivo is dependent on their abundant presence in the TME, as shown by the tumour growth in the eosinophil-depleted or IL5tg eosinophil-enriched mouse models[102,167,171]. Because eosinophil infiltration of the TME is often dependent on the CCR3-CCL11/CCL24 gradient, tumours commonly hijack this axis to restrain eosinophils from entering the tissue by a) transcriptionally supressing *Ccl11* expression through autotaxin (ATX) - lysophosphatidic acid (LPA) axis in pancreatic cancer models (PDAC) (Figure 1.6D)[186], b) through enzymatic cleavage of CCL11 by dipeptidyl peptidase (DPP4) (Figure 1.6E)[187], or c) through immunosuppressive $T_{reg}$ activities (Figure 1.6F)[188]. Conversely, inhibiting the ATX or DPP4 activity genetically or by small molecule inhibitors restored the *Ccl11* expression and

led to an increase in intratumoral eosinophil infiltration and tumour reduction[186,187]. The tumour reduction upon the ATX- and DPP4-inhibition was directly linked to eosinophil infiltration in the PDAC, hepatocellular carcinoma, and breast tumour models with a proposed direct cytotoxicity of eosinophils[186,187]. However, the tumour reduction following $T_{reg}$ depletion in melanoma models was associated with increased eosinophil infiltration that led to eosinophil-dependent CD8+ T cell infiltration and vessel normalization[188]. Eosinophils contributed to the expression of T cell chemoattractants *Cxcl9* and *Cxcl10* in vivo, and IFNγ and TNF stimulation of eosinophils in vitro led to their direct overexpression of *Cxcl9* and *Cxcl10* and enhanced migration of CD8+ T cells in Transwell migration assays[188]. Collectively, these studies show that eosinophils are capable of direct anti-tumorigenic activity, however, also orchestrate the anti-tumorigenic response by contributing to T cell recruitment and activation, presenting a novel connection between the Th1 and Th2-mediated immune responses.

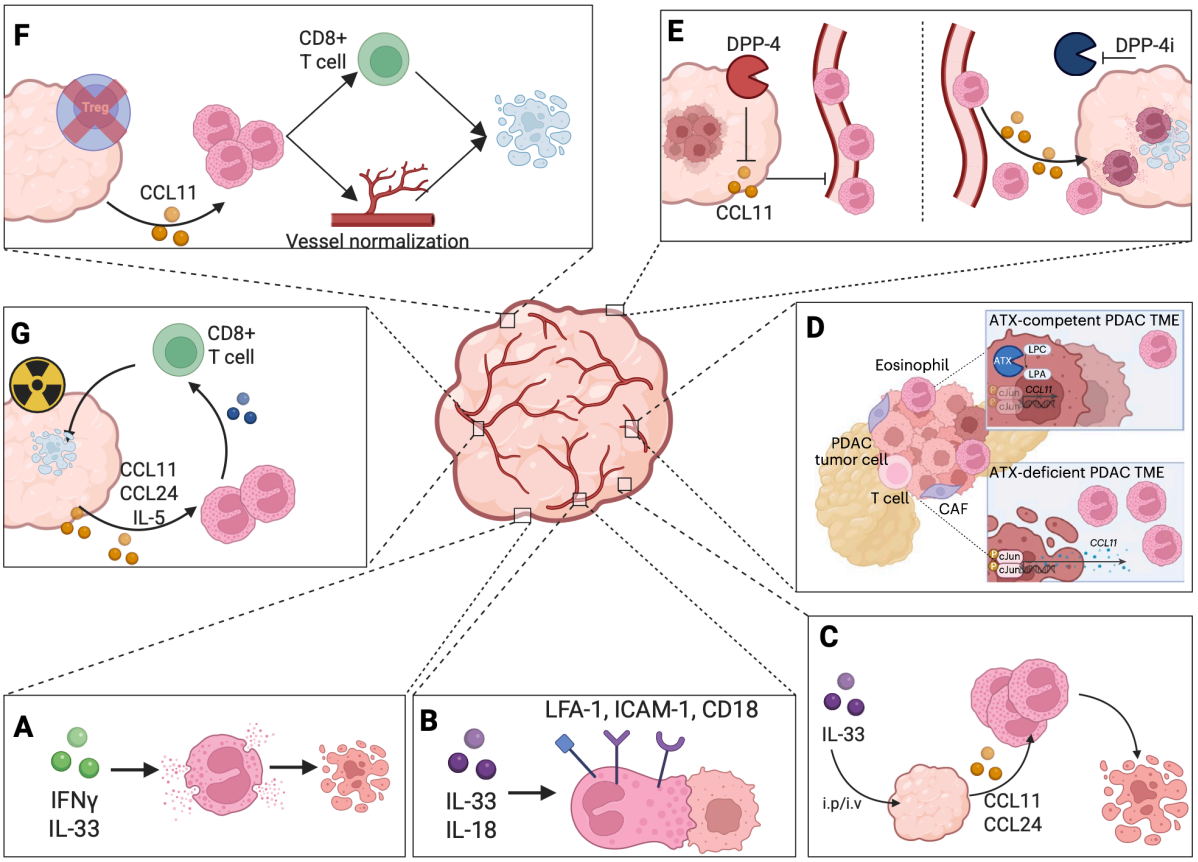


**Figure 1.6. Overview of anti-tumorigenic eosinophil activities. (A)** Stimulation of eosinophils ex vivo with IFNγ and IL-33 leads to increased cytotoxicity towards cancer cell lines. **(B)** Stimulation of eosinophils with IL-33 or IL-18 leads to overexpression of adhesion receptors and increased anti-tumorigenic properties. **(C)** administration of IL-33 through intraperitoneal (i.p) or intravenous (i.v) injection leads to eosinophil infiltration through CCL11/CCL24-CCR3 axis and reduction of tumour

burden. **(D)** Adapted from Bhattacharyya et. al 2024[186]. Cancer-derived autotaxin (ATX) leads to cleavage of lysophosphatidylcholine (LPC) into lysophosphatidic acid (LPA) that suppresses production of CCL11 and eosinophil infiltration. Deletion of *Atx* in cancer cells restores CCL11-CCR3 eosinophil infiltration and leads to tumour reduction. **(E)** Inhibition of dipeptidyl peptidase (DPP4) that cleaves CCL11 leads to eosinophil infiltration and inhibition of tumour growth. **(F)** Eosinophils mediate the anti-tumorigenic effect of $T_{reg}$ depletion through vessel normalisation and CD8+ cytotoxic T cell recruitment. **(G)** Radiation-induced eotaxin (CCL11, CCL24) and IL-5 production leads to eosinophil recruitment, that is essential for infiltration of CD8+ T cells that regulate anti-tumorigenic response. Created with BioRender.com.

In line with the studies pointing to eosinophil-mediated T cell infiltration, radiotherapy (RT) treatment of the melanoma murine model resulted in decreased tumour growth associated with increased infiltration of eosinophils and CD8+ T cells, and overexpression of CCL5, CXCL9, and CXCL10, compared to non-treated tumours (Figure 1.6G)[189]. Depletion of eosinophils by anti-Siglec-F treatment diminished the anti-tumorigenic effect of RT and reduced CD8+ T cell infiltration and IFNγ-related signature. Furthermore, eosinophils regulated activation of CD8+ T cells even in murine models of treatment-naïve colorectal cancer; eosinophil-deficient models presented with increased tumour growth and reduced T cell activation; in agreement with this, IL5tg mice presented with a tumour reduction[102]. This effect was further explained through the GM-CSF-IRF5 activation axis, in which loss of GM-CSF receptor or a downstream transcription factor IRF5 specifically in the eosinophil lineage, reproduced the eosinophil depletion phenotype and led to increased tumour growth and defective T cell activation[102]. Collectively, these data position eosinophils as important mediators of T cell immunity in tumour settings.

### 1.3.5 Role of eosinophils in ICB response

Building on the recognised eosinophil-mediated T cell cytotoxicity, the early increase of circulating eosinophils following the anti-CTLA4 (ipilimumab) ICB treatment was associated with improved survival of melanoma patients[190]. Following these results, elevated baseline levels of eosinophils, assessed even before drug administration, were predictive of better treatment response to ipilimumab[191,192]. Eosinophil role in response to ICB also became more apparent with the growing body of clinical trials associating higher levels of peripheral eosinophils with increased overall survival in non-small cell lung cancer[193], renal cell carcinoma[194], urothelial carcinoma[195], and triple-negative breast cancer patients[184,196]. It is

important to notice that recently, a higher eosinophil count was predictive of worse response to ICB in head and neck squamous cell carcinoma[197], likely to be related to higher eosinophil counts being predictive of severe immune-related adverse events associated with ICB[198]. However, the main body of evidence supports a role for eosinophils in a successful response to ICB.

The finding of higher peripheral eosinophil counts correlating with better responses in the majority of ICB-treated patients prompted the question of whether eosinophils are actively involved in tumour rejection or have a role of just predictive bystanders. In murine models of breast cancer, eosinophils were necessary for mediating vessel normalisation and CD8+ T cell infiltration following CTLA-4 blockade[199]. Furthermore, eosinophils also had a role in mediating the anti-tumorigenic effect achieved by a combination of anti-PD1 and anti-CTLA-4 treatment[187], with both treatment effects being diminished by eosinophil depletion.

How ICB stimulates the eosinophil expansion/accumulation and anti-tumorigenic activity was only recently uncovered in a combined study of metastatic TNBC patients undergoing cisplatin and anti-PD1 treatment and a matched mouse model of the disease[184]. In TNBC patients, both peripheral and intratumoral eosinophils correlated with better treatment response and elevated levels of IFNγ-signature that is predictive of T cell activation. Furthermore, comparison of a) isotype, b) ICB, c) cisplatin, or d) a combination of ICB and cisplatin treatments of mice with established mammary tumours, revealed that only the combination of ICB and cisplatin prolonged the overall survival of the mice; with this effect being associated with almost a 5-fold increase in peripheral and intratumoral eosinophils. In the absence of eosinophils, this effect was diminished and led to inefficient activation of CD8+ T cells. Further mechanistic experiments revealed that while ICB is necessary to induce IL-5 expression of CD4+ T cells in bone marrow and leads to eosinophil expansion, cisplatin treatment enhances eosinophil infiltration of the tumours in IL-33 dependent manner[184]. This work mechanistically links eosinophils with ICB response, however, how eosinophils contribute to CD8+ T cell activation remains an open question.

## 1.4 The role of extracellular matrix in cancer with focus on tenascin-C

### 1.4.1 Overview of extracellular matrix properties in cancer

Even though the majority of cancer research is centred around the cellular composition of tumours, a growing body of work highlights the importance of remodelled ECM for cancer progression and treatment resistance[200]. The ECM is a dynamic network that embeds all tissue resident cells and actively shapes tissue structure and function through a set of ECM-associated proteins and modifiers – collectively forming the matrisome. The matrisome represents a complete list of ECM-related proteins and consists of 1) core structural proteins – collagens, glycoproteins and proteoglycans, 2) ECM-modifiers and regulators – proteases and cross-linkers, and 3) matrisome-associated secreted factors – growth factors, cytokines and others[201,202]. In homeostasis, ECM provides a structural support, mediates cell-cell/cell-matrix communication and spatially regulates extracellular signalling, together leading to a control of cell adhesion, polarity, survival, and migration[203]. Following tissue injury, ECM composition and spatial organisation are rapidly remodelled through altered deposition, degradation, and cross-linking of matrix proteins to restore the tissue architecture. However, if the ECM gets dysregulated, this leads to an expansion of fibrotic stroma and fibrosis[204]. Fibrotic composition prolongs injury resolution and causes chronic inflammation. Because cancer is often referred to as a “wound that never heals”[205], analogous processes guide the persistent wound-repair programmes that result in quantitative and qualitative changes of ECM associated with disease progression.

Within the TME, all cellular components – tumour, stromal and immune cells – actively remodel and interact with the ECM. These interactions are dependent on families of adhesion and matrix receptors, most notably integrins, collagen-binding receptor tyrosine kinases DDR1/DDR2, and glycosaminoglycan receptors such as hyaluronic acid receptor CD44[206]. Together, these receptors couple matrix binding and mechanical properties with cytoskeletal and transcriptional reprogramming of TME resident cell behaviour. In parallel, resident cells

regulate the ECM by both deposition and degradation of matrix, with CAFs being the main producers of the ECM, myeloid cells remodelling the ECM network through secretion of matrix metalloproteinases (MMPs) and cross-linkers, and tumour cells also modifying the matrix composition through deposition and remodelling depending on their epithelial-to-mesenchymal transition status[207]. Together, these reciprocal processes continuously shape TME mechanical properties (stiffness, fibre alignments), cytokine composition (growth factors, chemokines), and vascularisation to establish a more pro-tumorigenic niche with altered immune composition (Figure 1.7A, B).

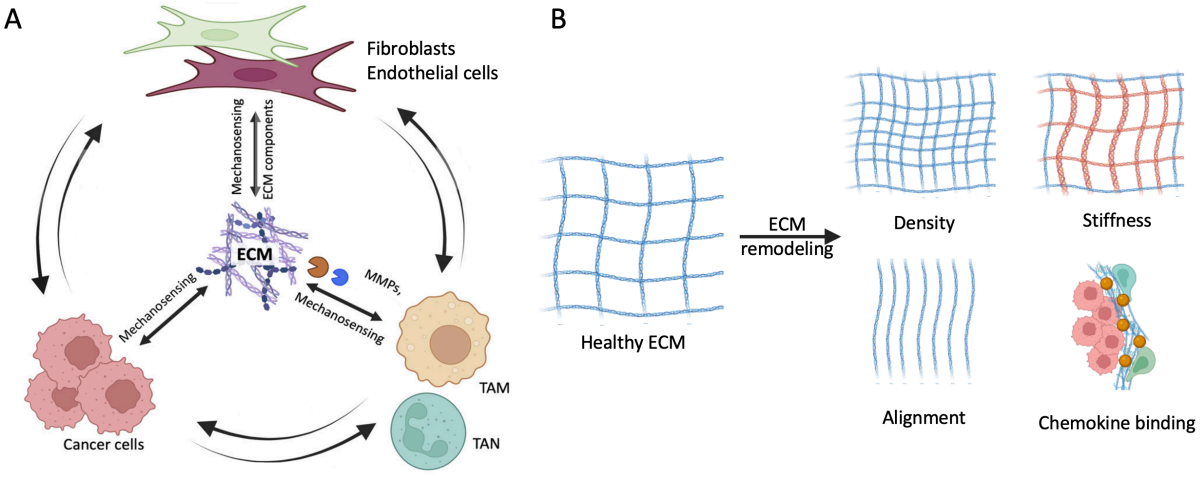


**Figure 1.7. Overview of ECM changes during tumour progression. (A)** Reciprocal relationships between ECM deposition and degradation by stromal, immune and cancer cells. Remodelled ECM further mediates the altered crosstalk of the TME resident cells. **(B)** Overview of TME altered ECM, increased density, stiffness, and fibre alignment further contribute to disease progression with altered ECM-chemokine binding mediating immune exclusion. Figure A adapted from Prakash and Shaked, 2024[208]. Created with BioRender.com.

In inflamed tissues, distinct ECM architectures guide migration and differentiation of immune cells through mechanical and biochemical cues, directing leukocytes towards the site of tissue damage or infection[209]. In tumours, the abnormal ECM composition and density can serve as both a permissive or restrictive barrier for leukocyte infiltration and activity. An increase in tumour stiffness caused by the build-up of excess collagen and hyaluronan causes vascular compression leading to tumour hypoxia, however, this can be reversed through targeting collagen deposition that restores the vessel perfusion and drug delivery[210]. The increased stiffness observed in tumours is also caused by collagen stabilisation through cross-linking. Collagen cross-linking was successfully targeted, for example, through inhibition of LOX2

enzyme in murine models of lung cancer; LOX2 inhibition led to restored anti-PD-L1 treatment activity, increased CD8+ T cell infiltration and reduction of the T cell exhausted phenotype[211]. This study is particularly interesting as an increase of collagen deposition and cross-linking is often induced by different treatments, such as ICB or chemotherapy[211,212], therefore ECM remodelling presents a potent mechanism that helps tumours escape the immune reactivation. Furthermore, structural alignment of collagen fibres is as important as their density; cancer cells that can align collagen fibres through DDR1 receptor-dependent mechanism produce a physical barrier by creating longer aligned fibres and restrict T cell infiltration[213]. Lastly, the ECM composition regulates the activation status of infiltrating immune cells, either through engagement with ECM-related receptors or through modulating the availability and composition of tumour secreted factors[209,214]. Taken together, the ECM changes determine not only whether immune cells reach tumour nests but also whether they arrive activated or exhausted. Although these interactions were successfully targeted in vivo, less success is seen in clinical practice[200].

Tumour stiffness and ECM deposition correlate with disease aggressiveness, invasiveness and metastatic potential; accordingly, tumour stiffness is also associated with worse patient prognosis in breast cancer, hepatocellular carcinoma and pancreatic cancer, with elevated stiffness linked to worse disease-free survival and early recurrence post-surgery[212,215–218]. Furthermore, overexpression of 9 core matrisome genes across all cancer types was strongly associated with worse prognosis in all studied adenocarcinomas[219]. Remodelling of ECM also leads to resistance to chemo- and radio-therapy, either by inducing stemness of cancer cells or by providing a physical protection against drug delivery[208]. Moreover, as discussed above, ECM-mediated lymphocyte restriction is a common mechanism of ICB resistance. Therefore, ECM presents an attractive therapeutic target, with ongoing trials likely to provide more information on the success of the novel anti-ECM therapies[208].

### 1.4.2 Role of tenascin-C in the TME

One of the ECM proteins that is commonly expressed in the context of tissue remodelling – wound healing, chronic inflammation, and cancer – but mostly absent in majority of healthy adult tissues, is tenascin-C (TNC)[220]. Tenascin-C is a large multifunctional glycoprotein with a complex structure consisting of EGF-like repeats, fibronectin type III domains, and a C-terminal fibrinogen-like globe (FBG) domain, mediating interactions with other stromal and immune cells through different classes of surface receptors. These interactions allow TNC to regulate cell adhesion, migration, and immune activation, moreover, in the context of cancer, TNC contributes to increased proliferation and survival of cancer cells[221]. TNC is predominantly produced by stromal cells, such as fibroblasts, endothelial cells, and pericytes however, its expression can also be harnessed by cancer cells to promote the establishment of an early metastatic niche[222].

Increased expression of TNC is associated with worse patient outcomes, as can be demonstrated by lower lung metastasis-free survival[222] and increased recurrence rates[223] in breast cancer patients, and lower overall survival of patients with esophageal squamous cell carcinoma, colorectal cancer, or lung carcinoma[224–227]. Functionally, TNC supports tumorigenesis through multiple mechanisms, including promotion of cell migration and survival, aberrant vessel formation in metastatic disease and immunosuppression. In primary breast cancer models, TNC-rich matrix binds CXCL12 and restrains CD8+ T cells infiltration of the tumour nests leading to an immunosuppressive phenotype, however, inhibition of CXCR4 (CXCL12 receptor) can release CD8+ T cells and macrophages from the CXCL12-bound stroma and reduce tumour burden[92]. Cancer-derived TNC was linked by some studies to increased primary tumour growth[228,229], however, this phenotype was not confirmed in the same murine breast cancer model[92,93,230] or by other studies showing a pro-tumorigenic role of TNC in metastatic formation but not primary tumour growth[222,231,232]. Therefore, the exact pro-tumorigenic role of TNC in primary breast tumours is yet to be fully understood.

The contribution of tenascin-C to the formation of the metastatic TME has been more explored. TNC was recognised among the 12 genes that are consistently upregulated by stromal cells in both early and late metastatic niches in breast cancer-derived lung metastasis[233]. The host-derived TNC was shown to promote metastatic colonisation of lungs in a murine model of breast cancer, with this effect being independent of cancer-derived TNC[231]. In this study, host-derived TNC was essential for blood vessel invasion (BVI), with mice lacking *Tnc* expression developing smaller metastatic lesions correlating with smaller BVIs and increased apoptotic rates within the metastatic nests. In agreement with these findings, the ability of cancer cells to express *Tnc* during the metastatic colonisation was essential for the establishment of the early TME, however, at the later stages the stromal-derived TNC was capable of substituting the cancer-derived TNC and supporting the tumour growth and proliferation through the Notch and Wnt signalling[222]. Furthermore, TNC mechanistically induced cancer stemness through TGFβ signalling, explaining the increased proliferation of tumour cells in mice with wild type *Tnc* expression compared to TNC-KO mice[231]. The importance of TNC in metastatic vasculature formation was further observed in a mechanistic study where deposition of perivascular TNC triggered macrophage activation through TLR4 signalling and consequently led to inflammatory response of endothelial cells and promotion of cancer stemness, with blocking the TNC-TLR4 interaction interrupting this pro-metastatic loop[232].

TNC is a potent regulator of myeloid cells in diverse disease settings. It can serve as an endogenous macrophage activator by engaging TLR4 through its FBG domain and sustaining chronic inflammation in murine models of rheumatoid arthritis[234]. Beyond TLR4 activation, TNC also activates macrophage adhesion and migration through integrin signalling[235]. Furthermore, TNC regulates myeloid cell infiltration and migration by chemokine binding, such as TNC-bound CXCL12, CCL2, or CCL26[92,229,236]. In this thesis, TNC interaction with tumour-associated macrophages was mostly studied in the context of macrophage polarisation. In this regard, TNC-TLR4 interaction is essential for regulating the M1/M2 phenotype; bulk RNAseq comparative analysis of naïve, TNC-stimulated, and TLR4 inhibited TNC stimulated bone

marrow-derived macrophages confirmed the proinflammatory macrophage phenotype induced through the TLR4 activation that is associated with production of TNFα, IL-6 and other pro-inflammatory cytokines[232,234,237]. Furthermore, macrophage presence in the TNC-rich perivascular niche correlated with increased levels of TNF and pro-inflammatory cytokine milieu during late stages of breast cancer metastasis, with the TNF signalling being proposed as the main trigger for endothelial cell remodelling[232]. Contrary to these findings, TNC was found to polarise macrophages towards a more M2-like immunosuppressed phenotype in murine breast TME, with this effect being specific for cancer-derived TNC[228].

Therefore, inhibition of TNC-macrophage interaction to restore anti-tumorigenic immune response is an attractive therapeutic target. Blocking of FBG by monoclonal antibodies reduced primary tumour burden and improved response to anti-PD-L1 treatment through macrophage repolarisation to a more pro-inflammatory M1-like phenotype[228]. A recent study showed that blocking of TNC by a MAtrix REgulating Motif-mimicking peptide (MAREMO) also resulted in reduced primary tumour growth, an effect that was caused by vessel normalisation, restored IFNγ response, and release of stromal-bound leukocytes into the tumour nests jointly restoring the antitumorigenic immunity[238]. Although there are currently no TNC inhibitors approved in the clinical setting, the highly restricted TNC expression in cancer can be used for effective drug delivery, as recently reviewed[239].

## 1.5 Project aims and summary

As outlined throughout this introduction, cancer cells employ diverse mechanisms to escape immune surveillance and sustain the tumour growth. One of these mechanisms was proposed to include the ability of cancer cells to produce ECM protein TNC that suppresses macrophage activation[228] and leads to an exclusion of lymphocytes[92], therefore enhancing the growth of primary tumours. Building on these results together with the phenotypical heterogeneity of macrophages in the TME (unpublished data, Midwood group), my initial aim was to further investigate mechanisms by which TNC drives the macrophage diversity. However, due to the early discovery of prevalent eosinophil population in two independent mouse models of breast cancer, and the concurrent recognition of a) the eosinophil plasticity in healthy and diseased tissues[125] and b) eosinophils as important players in response to ICB in breast cancer[184], the role of eosinophils in the tumour microenvironment became a central topic of this thesis.

Eosinophils were linked to anti-tumorigenic properties in metastatic breast cancer and primary colorectal cancer models[166,167,171], intriguingly, neither eosinophilia nor depletion of eosinophils had an effect on tumour growth in murine models of breast cancer[184,240]. This led to a hypothesis that the breast TME might be capable of exploiting the eosinophil heterogeneity to avoid their inherent cytotoxicity.

Based on this, the aims of this project were three-fold:

1. Characterise the phenotypic and functional heterogeneity of eosinophils in the breast tumour microenvironment.
2. Elucidate mechanisms that could reactivate eosinophils toward a more cytotoxic state.
3. Understand the impact of TNC-modulated macrophages on eosinophil behaviour.

Therefore, Chapter 3 focuses on characterisation of eosinophil phenotypical plasticity by utilising a complex spectral flow cytometry staining panel and unbiased dimensionality

reduction analysis, aiming to recognise markers that define tumour-associated eosinophil subsets. This initial analysis revealed 2 novel subsets of eosinophils that were well-conserved across different breast cancer models and associated with disease progression. Differences between these subsets were further functionally validated ex vivo to ensure of their biological relevance.

Chapter 4 follows up on these findings and adds to the eosinophil characterisation by bulk RNA sequencing of the 2 tumour-associated eosinophil subsets defined in Chapter 3. These results revealed a potential exhaustion phenotype of eosinophils associated with later stages of TME development and led to experiments that aimed to reactivate eosinophils to a more cytotoxic state ex vivo and in vivo. Additionally, as described in section 1.2.2, ICB treatment is increasingly used for the treatment of hard-to-treat metastatic but also early-stage TNBC patients, with eosinophils being a good prognostic marker of treatment response[184]. Therefore, baseline eosinophil density was analysed in primary and recurrent breast cancer patients with the aim of providing a preliminary dataset that could uncover eosinophil infiltration of specific breast cancer subtypes for future treatment stratification.

Finally, Chapter 5 aims to characterise the TNC-macrophage interaction in relation to eosinophil biology through characterising both macrophages and eosinophils on temporal, spatial, and functional levels. These results provide novel insights into eosinophil development and dynamics under the influence of the breast TME.

## Chapter 2 | Materials and Methods

## 2.1 Mice

FVB wild-type mice were bred in-house, except for anti-Siglec-F depletion and anti-IFN treatment experiments, on these occasions FVB/N mice were ordered from Charles River. Balb/cAnNCrl (Balbc) and C57BL/6J (Bl6) mice were purchased from Charles River for all experiments; all animals did not undergo any experimental procedures for at least 7 days post arrival. All mice were housed under pathogen-free conditions in individually ventilated cages. A maximum of 7 mice were maintained per cage, and the mice had access to water and food ad libitum. In all experiments with primary tumours, female mice were orthotopically grafted at 8–13 weeks of age. In experiments involving pulmonary metastasis, female mice aged 7–8 weeks were intravenously grafted. Schedule 1 method of exposure to increasing $CO_2$ concentration was applied at the final time point in all animal experiments. All mouse experiments were performed in accordance with the UK Home Office guidelines under project license PP3609558.

## 2.2 Cancer cell lines

The NT193 murine breast cancer cell line, derived from a spontaneous MMTV-NeuNT primary tumour with control (shCTL/TNC+/NT193) and conditional knockdown of tenascin-C (shTNC/TNC-)[231], was provided by Dr. Gertraud Orend. The 4T1 cell line used for the generation of primary mammary tumours was obtained from the ATCC. E0771, E0771-mCherry$^{+}$hCD2 and 4T1-Cherry$^{+}$GFP$^{+}$ cell lines with mCherry labelling tool[233,241] stably transfected with sLP-Cherry and human CD2 receptor or GFP were a gift from Dr. Ilaria Malanchi.

NT193 cells were cultured in Dulbecco's Modified Eagle Medium (DMEM) (cat. 10566016, Gibco) supplemented with 10% fetal bovine serum (FBS) (cat. 10500064, Gibco), 1% Penicillin-Streptomycin (P/S) (cat. 15140122, ThermoFisher), and 10$\mu g/ml$ puromycin (cat. A1113803, Gibco). The 4T1- and E0771-derived cell lines were cultured in DMEM (cat.

41965039, Gibco) supplemented with 10% FBS and 1% P/S. All cells were maintained at 37°C with 5% $CO_2$ in a humidified atmosphere.

The NT193 cell line was passaged once a week at full confluence. Briefly, the cells were washed once with PBS, incubated for 5 minutes or until detached with 0.25% Trypsin-ethylenediaminetetraacetic acid (EDTA) (cat. 25200072, Gibco) at 37°C with 5% $CO_2$ in a humidified atmosphere, trypsin was quenched with the NT193 cell culture media, cells were harvested and spun down for 5 minutes at 1500rpm at room temperature, supernatant was discarded and cells were split at 1:15 ratio into a new T-175 cell culture flask (cat. 83.3912.002, Sarstedt) with fresh NT193 culture media. The media was changed after 3 days and on the day of splitting. 4T1 cell line was split every 2-3 days when reaching 70% confluence; cells were washed once with PBS, incubated for 3 minutes with 0.25% Trypsin-EDTA at room temperature, trypsin was quenched with 4T1 cell culture media, cells were harvested and spun down for 5 minutes at 1500rpm at room temperature, supernatant was discarded and cells were split at 1:10 ratio into a new T-75 cell culture flask (cat. 83.3911.002, Sarstedt) with fresh 4T1 culture media. The E0771 cell line grows in suspension and was split every 2-3 days; cells were harvested by resuspension in cell culture media, spun down for 5 minutes at 1500rpm at room temperature, supernatant was discarded, and cells were split at 1:10 ratio into a new T-75 cell culture flask (cat. 83.3911.002, Sarstedt) with fresh E0771 culture media.

All cell lines were tested for mycoplasma with MycoAlert® Mycoplasma Detection Kit (cat. LT07-318, Lonza) according to the manufacturer's instructions. TNC expression of the NT193 cell line was assessed by the quantitative PCR method as described in section 2.16.

## 2.3 Tumour models

The NT193 cell line was used for orthotopic engraftment at full confluence, 4T1- and E0771-derived cell lines were used at 70-80% confluence for both orthotopic and intravenous grafting.

The NT193 and 4T1 cell lines were harvested with 0.25% Trypsin-EDTA, washed 3 times with PBS (cat. 10010023, Gibco) and resuspended at the desired concentration in PBS. E0771 cells were harvested by ice-cold PBS, washed 3 times and resuspended in PBS. Prior to the orthotopic injection, mice were anaesthetised with isoflurane (IsoFlo, Zoetis) and the 4$^{th}$ right mammary fat pad area was shaved and sterilised with betadine (cat. 3030440, Vidine antiseptic solution 10% w/w). Tumour-bearing mice were housed on alpha-dry bedding to avoid irritation of the skin during tumour development and tumour growth was monitored every 2-3 days, starting 4 days after the tumour injection until the final time point or up to reaching the humane endpoint (12mm in any dimension). Tumour volume was calculated by the formula $V$ = ($length$ × $width$ × width)/2. Treatment-naïve mice with spontaneously regressing tumour volume were excluded from analysis.

To study primary tumour development, NT193 (5 000 000 cells), 4T1 WT (50 000 cells), and E0771 WT (100 000 cells) cell lines were orthotopically grafted with Micro-Fine+ 29G needles (cat. 324892, BD) in 100μl of Phosphate Buffered Saline (PBS) (ThermoFisher, 10010023) into the 4th right mammary fat pad of FVB, Balb/c and C57/Bl6 female mice, respectively. For induction of lung metastases, 4T1 mCherry-GFP (1000 000 cells) and E0771 mCherry-hCD2 (1000 000 cells) were intravenously grafted with Micro-Fine+ 29G needles through the tail vein into 6-7 weeks old Balb/c and C57/Bl6 mice, respectively.

For induction of lung metastasis, 4T1 and E0771 wild-type or mCherry labelled cells were grafted at a final concentration 1x10$^7$ cells/ml in 100μl of PBS, filtered through a 70μm cell strainer (cat. CLS352350, Corning) and administered intravenously within 30 minutes after the last filtration. Mice were monitored for loss of weight and a decrease in BCS (body condition score) every 2 days. Intravenous injections were performed by Albertino Bonifacio and Karolina Kaczkowska.

## 2.4 Administration of cell labelling agents and treatments

For experiments in Chapter 3 that utilised SUrface SEnsing of Translation (SUnSET) method[242] to assess translational activity in vivo, 100μl of 10mg/ml of puromycin (Gibco, A1113803) was administered intravenously through the tail vein 30 minutes prior to tumour harvest. The puromycin dose and incubation period were picked based on previous protocols using O-propargyl-puromycin in vivo[243]. All puromycin injections were done by Daniel Andrews. For experiments in Chapter 3, 5-ethynyl-2'-deoxyuridine (EdU) (cat. A10044, ThermoFisher) was reconstituted in PBS to a concentration of 5mg/ml and 1mg per mouse was administered intravenously 24 hours prior to harvest by Albertino Bonifacio and Karolina Kaczkowska.

For all experiments involving treatments, mice were divided into groups based on their weight, age, and tumour size at the start of the treatment. For the eosinophil depletion, anti-Siglec-F antibody (cat. MAB17061-500, R&D systems) and IgG2a isotype control (cat. BE0089, BioXCell) were reconstituted in PBS, and 20μg per mouse was intraperitoneally injected using BD Micro Fine Plus 0.5ml U100 30G 8mm syringes (cat. 324893, BD) every 3 days, starting on the day of orthotopic engraftment. For the anti-PD-L1 treatment, Ultra-LEAF Purified anti-mouse CD274 (cat. 124339, BioLegend) or Ultra-LEAF Purified Rat IgG2b antibodies (cat. 400672, BioLegend) were administered by intraperitoneal injection at a final dose of 10mg/kg, starting on day 7. For anti-IFN treatment, combination of Ultra-LEAF Purified anti-mouse IFNAR-1 (cat. 400198, BioLegend) and Ultra-LEA Purified anti-mouse IFN-γ (cat. 505848, BioLegend) or a control Ultra-LEA Purified Mouse IgG1, Isotype antibody (cat. 400198, BioLegend) was administered by intraperitoneal injection in the following order: day prior to orthotopic injection, 1.5mg of anti-IFNAR-1 antibody was used, on the day of orthotopic engraftment 250μg of anti-IFNγ was administered, from day 2 post-engraftment onwards, every 3 days a combination of 300μg of anti-IFNAR1 and 250μg of anti-IFNγ was administered to block IFNγ and IFNβ signalling. For the macrophage depletion experiments in NT193

tumours, PBS or clodronate liposomes (Liposoma) were administered at $10\mu l/g$ of mice by intravenous injection on day 1 and day 8 post-engraftment by Dr. Andrew MacLean and Karolina Kaczkowska.

## 2.5 Tissue processing

At experimental timepoint or when tumours reached 12mm in any calliper measurement, mice were culled using the Schedule 1 method, and tumours were collected into ice-cold PBS. Tumours and mammary fat pads were manually minced using scissors, resuspended in tumour digestion media (Roswell Park Memorial Institute 1640 medium (RPMI), 10% FBS, 500μg/ml Liberase TM (cat. 5401127001, Roche), 100μg/ml DNAse I (cat. 11284932001, Sigma)) and digested for 30 minutes at 37°C under gentle agitation. Following enzymatic digestion, tumour suspensions were kept at 4°C at all times, mechanically passed through $70\mu m$ cell strainers (cat. 83.3945.070, Starstedt) and washed once with FACS buffer (PBS with 5% FBS and $10\mu g/ml$ DNAse I) to obtain a single cell suspension. In case of apparent cell clumps, tumours were refiltered through $70\mu m$ cell strainers.

Lungs were minced by the gentleMACS OctoDissociator machine in GentleMACS C Tubes (cat. 130-093-237, Miltenyi) in digestion media containing PBS with 0.1% collagenase I (cat. LS004196, Worthington Biochemical) and 0.1% collagenase III (cat. LS004182, Worthington Biochemical). Cell suspensions were digested for 30 minutes at 37°C under gentle agitation prior to further processing with the gentleMACS OctoDissociator. Afterwards, cells were spun for 10 minutes at 300xg, washed with FACS buffer, passed through $70\mu m$ cell strainers to obtain a single cell suspension, treated with ACK buffer (cat. A1049201, Gibco) for 1 minute at room temperature, and red blood cell lysis was stopped by 10ml of PBS.

For confirmation of eosinophil depletion, 25μl of blood was taken by tail vein puncture using Jaytec Glass™ Micro-Haematocrit Tubes (cat. 12306297, FisherScientific) and resuspended

in 25μl of 0.5 M EDTA (cat. 15575020, ThermoFisher) straight after blood collection. For experiments comparing matched tumour and blood samples in Chapter 3, approximately 300$\mu l$ of blood per mouse was collected by cardiac puncture into an EDTA-coated tube (cat. 367527, BD). All samples were treated with 5ml of ACK buffer for 10 minutes at room temperature, and lysis was stopped by adding 10ml ice-cold PBS.

Bone marrow used for flow cytometry analysis was collected by flushing the femur bones with 5ml of cRPMI by using a 23G needle (cat. AN2325R1, Terumo). All cell suspensions were spun down at 1500 rpm for 5 minutes, resuspended in FACS buffer and kept at 4°C for flow cytometry staining.

## 2.6 Flow cytometry staining and sorting

All samples stained for flow cytometry analysis were plated into V-shaped 96-well plates at a maximum 2x$10^6$ cells per well for tissue samples, a minimum of 50 000 cells per well was plated for eosinophil developmental assays and IFN stimulations, and approximately 15 000 cells per condition was used in assays with FACS-sorted eosinophils that underwent development ex vivo. All cells were incubated with TruStain FcX (cat. 101319, ThermoFisher) in 100μl of FACS buffer at a 1:200 dilution for 15 minutes. Blocked samples were stained with LIVE/DEAD Fixable Blue, Near-IR or Yellow Dead Cell Stain Kits (cat. L23105, L34975, L34959, ThermoFisher) in 50μl at a 1:200 dilution in PBS for 30 minutes. For surface staining, cells were incubated with 50μl of primary antibodies described in Table 2.1 in FACS buffer for 30 minutes. Lung samples and samples in Chapter 4 were kept unfixed to preserve better mCherry staining of the niche, all other samples were incubated with Fixation buffer (cat. 420801, BioLegend) for 15 minutes, washed and resuspended in FACS buffer. For intracellular staining, samples were further incubated in 1X BD Cytofix/cytoperm (cat. 51-2090KZ, BD Biosciences) for 1 hour, washed once in 1X BD Perm/Wash 10x (cat. 51-2091KZ, BD Biosciences) and incubated with intracellular antibodies described in Table 2.2 diluted in 1X

Perm/Wash for 30 minutes, washed once in 1X Perm/Wash and resuspended in FACS buffer. All incubations were done at 4°C, and cells were spun at 1600rpm for 2 minutes. All data were acquired by LSRFortessa X-20 (BD Biosciences) or Aurora (Cytek) spectral flow cytometer using DIVA or SpectroFlo software, respectively. Flowcytometry data was analysed with FlowJo v10.9.0 and OMIQ (Dotmatics).

In experiments studying cell proliferation by EdU incorporation, cells were first stained for surface antigens as described above and afterwards EdU was detected with Click-iT™ EdU Alexa Fluor™ 647 Flow Cytometry Assay Kit (cat. C10424, ThermoFisher) following the manufacturer's instructions.

For fluorescence-activated cell sorting (FACS) experiments, single cell suspensions after digest were enriched with mouse anti-CD11b (cat. 130-126-725, Miltenyi), mouse anti-Siglec-F (cat. 130-118-513, Miltenyi), or mouse anti-CD45 (cat. 130-110-618, Miltenyi) magnetic micro-beads using MS columns (cat. 130-042-201, Miltenyi) in combination with OctoMACS™ Separator (Miltenyi) following manufacturer's instructions. Enriched cells were further stained with LIVE/DEAD Fixable Blue Dead Cell Stain Kit with surface receptors as described above, and resuspended in PBS, 2 mM EDTA, and 0.5% FBS before sorting with a 100μm nozzle size on Aria III. All sorting experiments were done with the help of Jonathan Webber.

The sorting strategy used for isolation of myeloid populations infiltrating 4T1 tumours is explained in Chapter 3, section 3.2.2. The sorting strategy used for isolation of Ly6C+ and Ly6C- tumour-associated eosinophils used for cytotoxic assays, imaging, and stimulations in Chapters 3 and 4, is described in Figure 2.1. The sorting strategy used for isolation of bone marrow-derived eosinophils on day 18 of cell culture, described below in section 2.7, is shown in Figure 2.2. The sorting strategy used for isolation of tumour-associated Ly6C+ and Ly6C- eosinophils, joint with tumour-associated macrophages that were all directly sorted into RLT

buffer and used for bulk RNA-sequencing is shown in Figure 2.3; this analysis is associated with the bulk RNA-sequencing data in Chapter 4 (eosinophils) and Chapter 5 (macrophages).

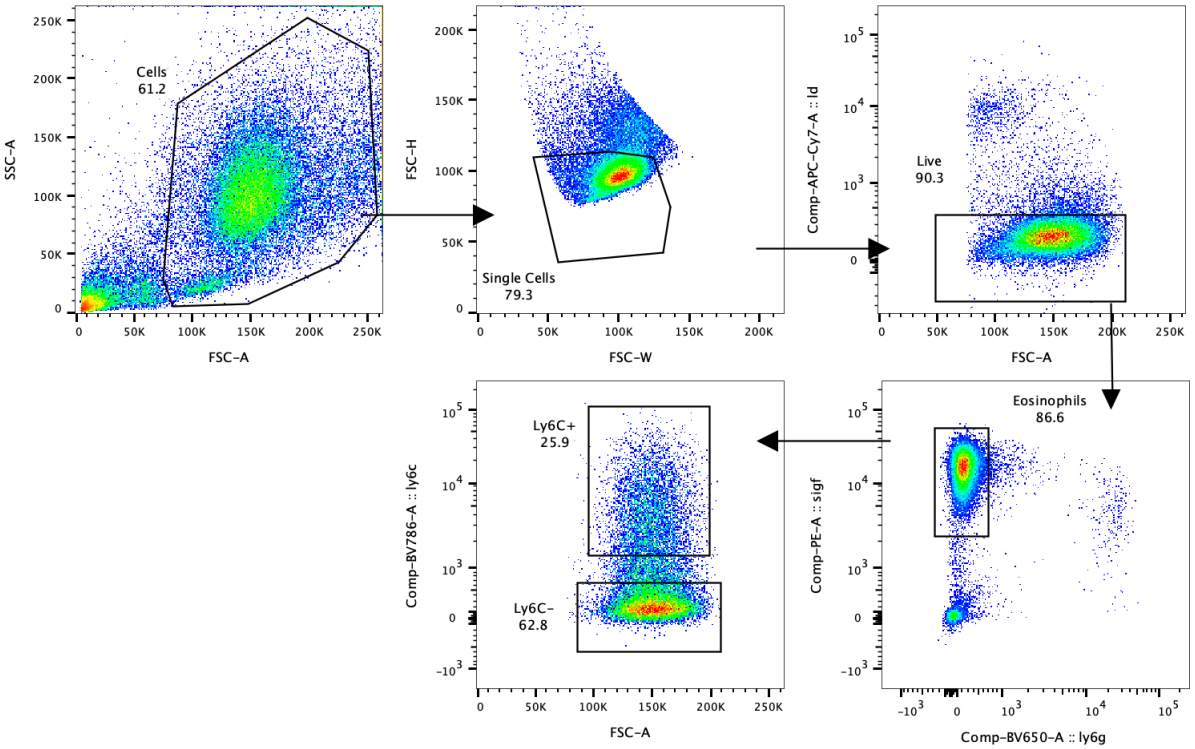


**Figure 2.1. FACS sorting of tumour-associated eosinophils.** Whole tumour lysates were enriched by mouse anti-Siglec-F magnetic micro-beads using MS columns in combination with OctoMACS™ Separator following manufacturer's instructions, as described above. Afterwards, cells were stained with Live/dead cell stain kit and surface receptors, to enable getting of single cell, alive, Siglec-F+ cells. Eosinophils were further distinguished based on their expression of Ly6C.

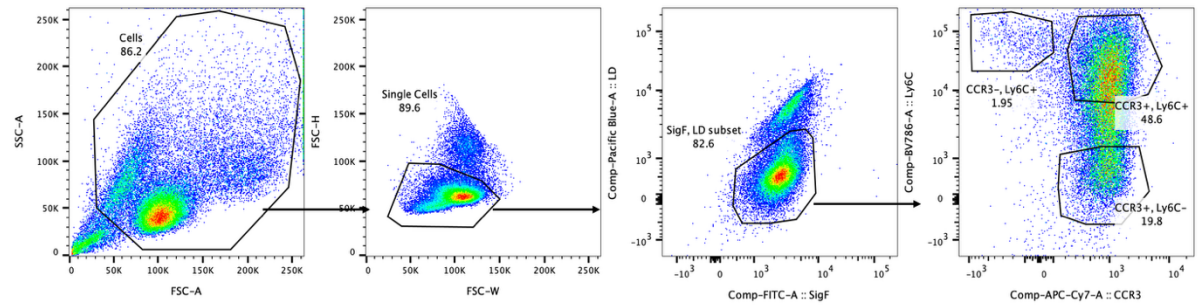


**Figure 2.2. FACS sorting of bone marrow-derived eosinophils.** Bone marrow-derived eosinophils were collected on day 18, cells were stained with Live/dead cell stain kit and surface receptors, to enable getting of single cell, alive, Siglec-F+ cells. Eosinophils were further distinguished based on their expression of Ly6C and CCR3.

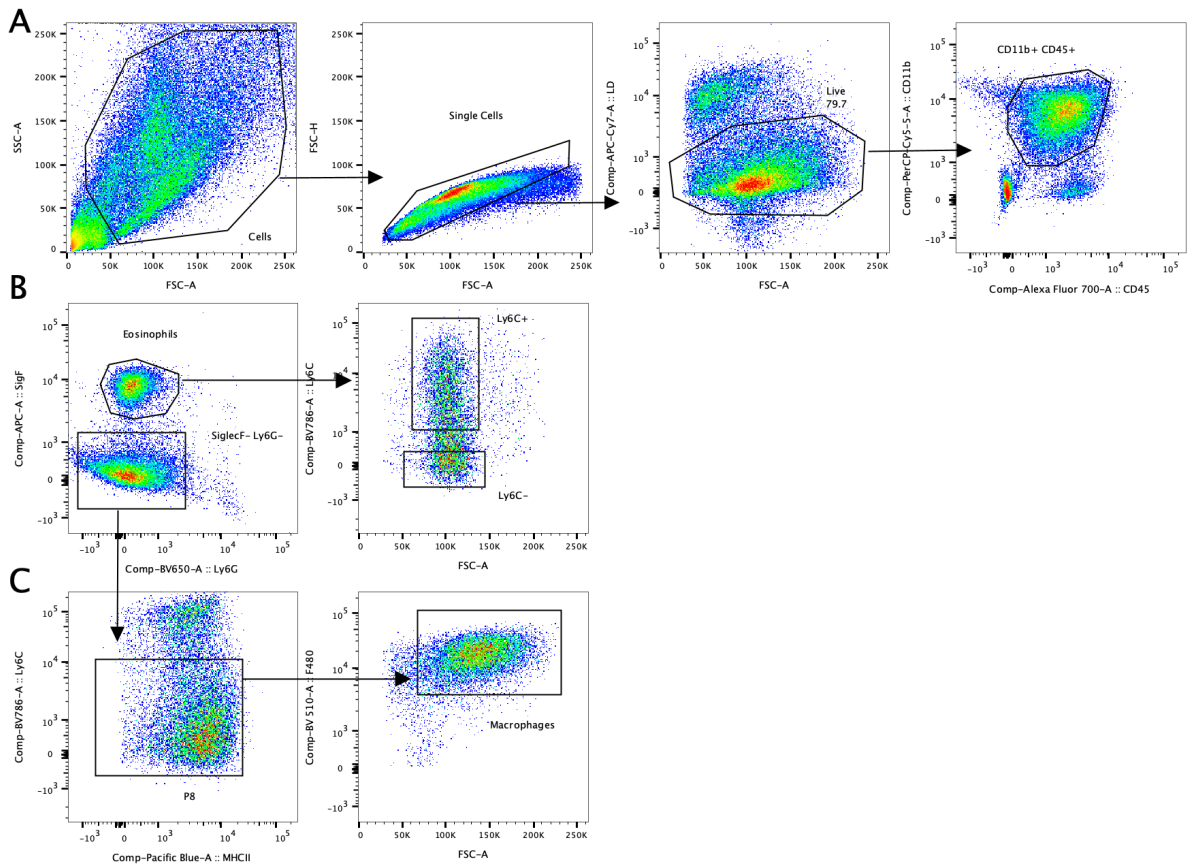


**Figure 2.3. FACS sorting of tumour-associated eosinophils and macrophages for bulk RNA-sequencing. (A)** Whole tumour lysates were enriched by mouse anti-CD11b magnetic micro-beads using MS columns in combination with OctoMACS™ Separator following manufacturer's instructions, as described above. Afterwards, cells were stained with Live/dead cell stain kit and surface receptors, to enable getting of single cell, alive, CD45+, CD11b+ cells. **(B)** Eosinophils were gated based on their Siglec-F surface expression and further split into Ly6C+ and Ly6C- population. **(C)** Siglec-F-, Ly6G- population of cells that excluded granulocytes, was further gated for Ly6C- cells to exclude monocytes. Afterwards, a population of F4/80+ cells was isolated as macrophages.

## 2.7 Cell culture

The immortalised Hoxb8 macrophage cell line was a gift from Prof. Irina Udalova. Hoxb8 cells contain a Hoxb8-ER construct (estrogen-binding domain fused to homeobox B8) that inhibits myeloid differentiation and keeps cells in their progenitor state in the presence of estrogen[244]. Hoxb8 progenitors were cultured in suspension below $1x10^6$ cells/ml confluence in RPMI (cat. R8758-1L, Sigma) supplemented with 10% FBS, 1% P/S, 30μM beta-Mercaptoethanol (cat. 31350010, ThermoFisher), 10μM estradiol (cat. E2758, Sigma) and 10mg/ml murine GM-CSF (cat. AF-315-03-50UG, Peprotech). Confluence was assessed every 2 days; cells were stained by resuspension in trypan blue (cat. T8154-100ML, Sigma) at a 1:1 ratio (cell suspension to trypan blue), applied onto EVE Cell Counting C-Slide (cat. NE-EVS-50, EVE)

and analysed by automatic cell counter Countess 3 (Thermofisher). Cells were split 1:10 when they reached confluence 1x$10^6$ cells/ml into a new flask; briefly cell suspension was spun for 5 minutes at 1500rpm at room temperature, supernatant was discarded, cells were resuspended in Hoxb8 cell culture media and split into a fresh T-75 flask. For utilization of SUnSET assay in vitro, Hoxb8 progenitors were cultured in presence of estrogen at all times, 2x$10^6$ cells in 2ml were plated into a 6-well plate (cat. 353046, Falcon), pre-stimulated with 10$\mu$g/ml of cycloheximide (cat. 239763-M, Sigma) to block protein translation or equal volume of DMSO for 15 minutes and afterwards incubated with 10$\mu$g/ml puromycin for 15 minutes. Afterwards, cells were washed twice with PBS before proceeding with flow cytometry staining. All incubation steps were performed at 37°C with 5% $CO_2$ in a humidified atmosphere.

For bone-marrow derived cultures, femur and tibia of 8-14 weeks old mice were flushed with RPMI (cat. 11875093, ThermoFisher) using a 23G needle (cat. AN2325R1, Terumo), spun at 500xg for 5 minutes, treated with ACK buffer for 2 minutes at room temperature and washed with 5ml of RPMI before filtering through a 70$\mu m$ cell strainer.

To culture bone marrow-derived macrophages (BMDMs), bone marrow cell suspension prepared above was cultured on non-tissue culture treated plates (cat. CLS431301, Corning) in RPMI supplemented with 10% FBS, 1% P/S, 1% sodium pyruvate (cat. 11360070, Gibco), 10% 4-(2-hydroxyethyl)-1-piperazineethanesulfonic acid (HEPES) (1 M) (cat. 15630080, Gibco) and 50ng/ml macrophage colony-stimulating factor (cat. 300-25, Peprotech) for 7 days, and one third of fresh media was added on day 5 of culture. For tenascin-C stimulations with FBG domain (purification performed by Linda Mies), BMDMs were harvested by resuspension with ice-cold PBS on day 5, 1x$10^6$ cells were plated into 6-well plates (cat. 353 046, Falcon), rested for 1 day, washed with PBS and stimulated with 1$\mu$M FBG domain of tenascin-C or 1$\mu$M FBG domain incubated at 90°C for 15 minutes (heat-denatured) in RPMI supplemented with

0.5% FBS, 1% P/S (starvation media) for 24 hours. Afterwards, conditioned media was collected, spun at 1000xg for 10 minutes and used for migration assays.

To obtain eosinophils from primary murine bone marrow cells, cells were cultured as previously described[245]. Freshly isolated bone marrow cells were cultured in RPMI 1640 supplemented with 20% FBS, 25 mM HEPES, 1% P/S, 2 mM glutamine (cat. 25030-024, Gibco), 1x NEAA (cat. 11140-035, Gibco), and 1 mM sodium pyruvate (cat. 11360070, Gibco) (eosinophil media) for 4 days supplemented with 100 ng/ml mSCF (cat. 250-03, PeproTech) and 100 ng/ml mFLT3-Ligand (cat. 250-31L, PeproTech), and 10ng/ml IL-5 (cat. 215-15, PeproTech) from day 4 onwards. Half of the media was replaced every 2 days; during all media replacements, eosinophils were spun at 300xg for 7 minutes. On days 4 and 8, cells were plated into a new flask to minimise the culture of adherent cells. Cell culture was kept at $1x10^6$ cells/ml confluence; cell density was assessed every 2 days by resuspension of cells in trypan blue (cat. T8154-100ML, Sigma) at a 1:1 ratio (cell suspension to trypan blue), applied into EVE Cell Counting C-Slide (cat. NE-EVS-50, EVE) and analysed by automatic cell counter Countess 3 (Thermofisher). In experiments with bone marrow-derived eosinophils, both Bl6 male and female mice were used. Culture of eosinophils from FVB mice resulted in comparable eosinophil populations when assessed by Ly6C and CCR3 expression, analysed by flow cytometry, however, much lower yields were gained compared to Bl6 mice, as previously reported[246], and therefore FVB mice were not used for further experiments.

In experiments studying chronic eosinophil stimulations in Chapter 4, $1x10^5$ eosinophils were harvested on day 10 and cultured for 4 days in 96-well flat-bottom plates (cat. 353072, Falcon) in eosinophil media supplemented with IL-5 and cultured with 10ng/ml of IFN-γ (cat. 575304, BioLegend), IL-4 (cat. 214-14, PeproTech), IL-13 (cat. 210-13, PeproTech) or IL-33 (cat. 210-33, PeproTech) with half of the media topped up on day 12. For acute 24-hour stimulations, $1x10^5$ eosinophils were plated and incubated with 10ng/ml IFNγ or IFN-β (cat. 581304, BioLegend) as described above.

## 2.8 mCherry in vitro labelling

Labelling efficiency of sLP-mCherry transfected cells was tested in vitro as previously described[241], by both a) conditioned media labelling and b) direct co-culture with 4T1 mCherry-GFP cells. Briefly, 4T1 mCherry-GFP cells were cultured to 80% confluency and incubated with fresh 4T1 media for 2 days. Media was afterwards collected, spun down at 800xg for 15 minutes and the supernatant was further used for experiments with mCherry conditioned media. Labelling efficacy of mCherry conditioned media was tested with HEK293 cells. HEK293 cell line was maintained in DMEM (cat. D6429, Sigma) supplemented with 10% FBS and 1% P/S at 80% confluency and cultured with the conditioned media for 2 days to allow the mCherry penetration of cells. In parallel with the conditioned media labelling assay, mCherry labelling was also examined in direct co-culture experiments; 4T1 mCherry-GFP cells were cultured with HEK293 cell line at a 2:1 ratio at $1x10^6$ cells/ml density for 2 days in a 6-well plate (cat. 353 046, Falcon). Afterwards, both 1) HEK293 cells cultured with conditioned media and b) HEK293 cells cultured with 4T1 mCherry-GFP cells were harvested by incubation with 0.25% Trypsin-EDTA for 3 minutes at 37°C with 5% $CO_2$, washed with PBS and stained with LIVE/DEAD Fixable Blue or Near-IR Dead Cell Stain Kits (cat. L23105, L34975, ThermoFisher) at 1:200 dilution in PBS for 30 minutes. All samples were acquired on the Aurora (Cytek) spectral flow cytometer without any fixation, and all live cells were analysed for mCherry and GFP expression. For unmixing purposes, 4T1 WT and HEK293 cells without mCherry were used as negative controls to extract the intrinsic autofluorescence of both cell lines.

## 2.9 Cytotoxic assay

For eosinophil cytotoxic assays with unstimulated tumour sorted Ly6C+ and Ly6C- eosinophils (Figure 2.1), eosinophils were mixed with NT193 tumour cells at a 1:1 ratio and cultured in 96-well flat-bottom plates for 3 days. For eosinophil cytotoxic assays with unstimulated bone marrow-derived eosinophils, sorted CCR3+ Ly6C+ and CCR3+ Ly6C- eosinophils (Figure 2.2)

were mixed with E0771 tumour cells at a 1:1 ratio and cultured in 96-well flat-bottom plates for 1 day. Because the yields of sorted eosinophils differed between individual mice and individual experiments, the absolute cell numbers were always different, however, the absolute cell density would never be below 20 000 cells or exceed 200 000 cells in total, in any of the assays.

In assays using tumour-associated eosinophils stimulated with cytokines, sorted Ly6C+ and Ly6C- cells (Figure 2.1) were spun down in 96-well V-shaped plate for 2 minutes at 1600rpm, resuspended in eosinophil media supplemented with 10ng/ml of IL-5, or with IL-5 supplemented with IFNγ (10ng/ml) (cat. 575304, BioLegend) and IFNβ (10ng/ml) (cat. 581304, BioLegend) and incubated in 96-well flat-bottom plates for 24 hours at 37°C with 5% $CO_2$ in humidified atmosphere. Cells were afterwards collected, washed once in a 96-well V-shaped plate with PBS, and cultured at a 1:1 ratio with NT193 tumour cells in a 96-well flat-bottom plate for 3 days. In assays using bone marrow-derived eosinophils stimulated with cytokines, sorted CCR3+ Ly6C+ and CCR3+ Ly6C- cells (Figure 2.2) were spun down in 96-well V-shaped plate for 2 minutes at 1600rpm, resuspended in eosinophil media supplemented with 10ng/ml of IL-5, or with IL-5 supplemented with a) IFNγ (10ng/ml) (cat. 575304, BioLegend) or b) IFNβ (10ng/ml) (cat. 581304, BioLegend) and incubated in 96-well flat-bottom plates for 24 hours at 37°C with 5% $CO_2$ in humidified atmosphere. Cells were afterwards collected, washed once in a 96-well V-shaped plate with PBS, and cultured at a 1:1 ratio in a 96-well flat-bottom plate with E0771 tumour cells for 24 hours.

All cytotoxic assays were stopped by the collection of cells into a separate 96-well V-shaped plate. Afterwards, the 96-well flat-bottom plate with attached ancer cells would be washed once with PBS, incubated with 0.25% Trypsin-EDTA for 2 minutes at 37°C with 5% $CO_2$ in a humidified atmosphere, and the trypsin was quenched with complete DMEM (DMEM + 10%FBS). During all washing steps, supernatants were collected and merged with the cells

collected in the first step into the 96-well V-shaped plate. Cells were spun down in the 96-well V-shaped plate for 2 minutes at 1600rpm, blocked with 1:200 Fc-block, and stained with Live/dead cell stain kit together with surface receptor Siglec-F, as described in section 2.6. Stained cells were washed once with 1X Annexin-V binding buffer (cat. 422201, BioLegend), and stained with Annexin-V (cat. 640920, BioLegend) reconstituted in 1X Annexin-V binding buffer at a 1:60 dilution for 15 minutes at room temperature in the dark. Afterwards, cells were washed once more, resuspended in 1X Annexin-V binding buffer and acquired without fixation. SiglecF- cells were considered as tumour cells and were further analysed for Annexin-V and Live/dead staining, with double positive cells labelled as apoptotic.

## 2.10 Transwell migration assay

For eosinophil migration assays, bone marrow-derived eosinophils were harvested at day 14, washed with PBS and resuspended at 250 000 cells/100$\mu$l in starvation media (RPMI supplemented with 0.5% FBS, 1% P/S). Migration assay was set-up in 24-well plate (cat. 353 047, Falcon) with 5$\mu$m pore-size tissue culture inserts (cat. 83.3932.500, Sarstedt), 100$\mu$l of eosinophils were gently applied to the top chamber above the 600$\mu$l conditioned media in the bottom chamber for 3 hours at 37°C. Conditioned media was prepared as described in section 2.6, with BMDMs stimulation by active or heat-denatured FBG domain. After 3 hours the tissue culture insert with the cells remaining in the top chamber was discarded and the cells that migrated to the bottom chamber of the migration assay were analysed by either Incucyte S3 Live-Cell Analysis System automatic density measurement or resuspended in 1:1 ratio with trypan blue (cat. T8154-100ML, Sigma), applied into EVE Cell Counting C-Slide (cat. NE-EVS-50, EVE), and analysed by automatic cell counter Countess 3 (Thermofisher).

## 2.11 Adhesion assay

For eosinophil adhesion assays, 96-well plate (cat. 353 072, Falcon) was coated with 100$\mu$l/well of full length TNC (1$\mu$M; purification done by Linda Mies), FBG domain (10$\mu$M;

purification done by Linda Mies), or MAPTrix TNC peptide (10μM; cat. 168312K-2.5MG, Merck) diluted in 0.01% PBS-Tween (cat. P1379, Sigma) at 4°C overnight. Afterwards, the supernatant was aspirated to discard the peptides, wells were washed 3 times with 1x PBS, blocked with 200μl/well 1% BSA (cat. A7906-100g, Sigma) in PBS for 3 hours at 37°C, and washed 3 times with 1x PBS. Bone marrow-derived eosinophils grown in suspension were collected on day 14, washed in 1x PBS, resuspended to a concentration of 100 000 cells/100μl in 1x HBSS (cat. 14065-056, Gibco) and 50μl of cell suspension was applied to the prepared plate for 2 hours at 37°C. Non-adherent cells were removed by gently tapping the plate upside-down, wells were carefully washed with 200μl of 1xPBS and spun for 5 minutes at 40xg upside-down. Afterwards, cell density was estimated by Incucyte SX5 (Sartorius) by Anja Schwenzer or Leia Worthington.

## 2.12 Immunofluorescent imaging

Harvested murine tumours were fixed in PFA-based fixative Antigenfix (cat. P0014, DiaPath) for 12-24 hours at 4°C. Tumours were afterwards washed twice with PBS for 1 hour at 4°C and dehydrated in 30% sucrose (cat. S9378-5KG, Sigma) for 24-48 hours. Following dehydration, tumours were embedded in Tissue-Tek® OCT compound (cat. 16-004004, Tissue-Tek) and snap frozen using methanol with dry ice. OCT blocks were sectioned using Leica CM3050 S Cryostat, sections of 5-10$\mu$m were mounted on positively charged VWR SuperFrost Plus, Adhesion Slides (cat. 631-0108, Avantor) and stored at -80°C. For immunofluorescent staining, sections were incubated for 5 minutes at room temperature, rehydrated with PBS for 5 minutes, washed 3 times with PBS for 5 minutes to remove OCT and incubated with PBS with 2% FBS, 0.1% Triton X-100 (cat. X100, Sigma), 5% donkey serum (cat. D9663, Sigma) (blocking solution) and 1:200 dilution of TruStain FcX for 4 hours in a humid chamber at room temperature. Blocked samples were incubated with primary antibodies as described in table 2.3 diluted in blocking solution over night at 4°C. Primary antibodies were washed 3 times for 5 minutes with blocking buffer and incubated with

secondary antibodies diluted in blocking solution at room temperature for 4 hours in humid chamber, sections were covered by parafilm (cat. HS234526B, Merck) to avoid drying of the tissue. After the final staining, sections were washed 3 times for 5 minutes with PBS. In experiments with nuclear staining, sections were stained with 1 $\mu$g/mL DAPI (cat. D3571, ThermoFisher) for 15 minutes at room temperature and washed 3 times with PBS for 15 minutes. Samples were mounted using FluorSave reagent (cat. 345789, Millipore) and imaged on ZEISS Axioscan 7 slide scanner unless stated otherwise. All images were analysed using QuPath v0.5.0.

## 2.13 DAB chromogenic staining

Tumour sections from breast cancer patients were received from Oxford Centre for Histopathology Research (REC reference 23/A034) and Breast Cancer Now Tissue Bank (REC Reference 23/EE/0229). All formalin-fixed paraffin-embedded sections were of 5$\mu$m thickness and mounted on positively charged microscopy slides (cat. 631-0108, VWR). Prior to staining, sections were deparaffinized by immersion in xylene (cat. 247642, Sigma) for 10 minutes and a decreasing gradient of absolute ethanol (cat. 32221, Sigma) (95%, 70%, and 50%). Following deparaffinization, slides were washed with deionised water, rehydrated in 1x Tris Buffer Saline (TBS) (cat. sc-24951, Santa Cruz) with 0.05% Tween20 (cat. P2287, Sigma) and permeabilised for intracellular staining by incubation in 1x TBS with 0.3% Triton X100 (cat. X100RS, Sigma) for 15 minutes. Antigen retrieval steps were optimised for eosinophil peroxidase staining as described in Chapter 4. The final protocol used for immunohistochemistry staining of breast cancer samples is described below.

First, citrate antigen retrieval solution pH 6 (cat. S169984-2, Agilent Technologies) was brought to 80°C in a NxGen Decloaking Chamber (pressure chamber) and slides were immersed in the solution for a total of 20 minutes while the pressure chamber reached and maintained 110°C for 5 minutes. Slides were then removed from the pressure chamber, left to adjust to

room temperature in citrate buffer and washed once with 1x TBS. Endogenous horseradish peroxidases and alkaline phosphatases were blocked by incubation with 3% peroxide (cat. 216763, Sigma) for 15 minutes. Samples were washed with 1x TBS and blocked in 1x TBS supplemented with 5% bovine serum albumin (cat. A9418, Sigma), and 5% horse serum (cat. H0146, Sigma) (blocking buffer) for 1 hour in a humid chamber. Sections were further blocked with the avidin/biotin blocking kit (cat. SP-2001, Vector Laboratories) following the manufacturer's instructions. Primary antibody staining was done in blocking buffer with a 1:1000 dilution of mouse anti-EPX antibody (MM25-82.2.1, provided by Dr. Elizabeth Jacobsen) overnight at 4°C in a humid chamber. Sections were washed 3 times with 1x TBS and samples were incubated with biotinylated Horse Anti-Mouse IgG Antibody (cat. BA-2000-1.5, Vector Laboratories) at a 1:500 dilution in blocking buffer for 1 hour. Afterwards, samples were washed 3 times in 1x TBS and processed with VECTASTAIN® ABC-HRP Kit, Peroxidase ABC complex (cat. PK-4000, Vector) following the manufacturer's protocol and washed 3 times with 1x TBS, prior to incubation with DAB substrate kit (cat. SK-4100, Vector Laboratories) for a maximum of 20 minutes. For contrast staining, samples were stained with freshly filtered Mayer's Haematoxylin (cat. MHS1, Sigma) and washed for a minimum of 3 times in deionised water to remove any excess Haematoxylin stain. Slides were dehydrated using an increasing gradient of ethanol once (50%, 70%, 95%) and xylene buffer twice for 10 minutes.

Slides were mounted using Sakura Tissue-Tek Glas Automated Glass Coverslipper and imaged on ZEISS Axioscan 7 slide scanner. In Chapter 4, for optimisation of EPX and MBP, sections were imaged using a Zeiss LSM 880 confocal microscope. All washing steps were done for 5 minutes at room temperature unless stated otherwise.

## 2.14 Cytospin imaging

For Cytospin imaging, up to 100 000 cells in 100$\mu$l were cytospun with Shandon Cytospin 3 Cytocentrifuge at 300xg for 3 minutes, with Scientific CytoSep Filter Papers for Shandon Cytospin Centrifuges (cat. 22-045-305, ThermoFisher) onto a positively charged slide (cat. 631-0108, VWR). Exact numbers varied across the experiments and were limited by the number of sorted cells. The absolute number of cells cytospun would never be lower than 20 000 cells or exceed 100 000 cells, and the absolute volume would always be 100 $\mu$l, despite the different cell densities.

Slides were left to air dry for 15 minutes, fixed with ice-cold Fixation buffer for 15 minutes, washed and left to air dry overnight. Haematoxylin and eosin staining was performed by the Histopathology facility using an autostainer Sakura TissueTek DRS. Briefly, slides were fixed in methanol (cat. 322415, Sigma) for 5 seconds, air dried, stained with Harris Hameatoxylin (cat. 3801560E, Leica) for 11 minutes, washed, incubated with acid alcohol (0.1% hydrochloric acid (cat. 10763124, FisherScientific), 70% absolute ethanol in distilled water) for 40 seconds to remove excess Haematoxylin, washed, and incubated with ammoniated water (0.3% ammonia solution (cat. 87766.290, VWR) in tap water) to enhance contrast staining. Slides were then washed in tap water and stained in eosin (cat. RBC-0100.00A, CellPath) for 2.5 minutes, prior to 3 washes with tap water and dehydration in 100% ethanol (3 times, 1 minute) and xylene (2 times, 1 minute). Dehydrated slides were cover-slipped using an automatic Sakura Tissue-Tek Glas Automated Glass Coverslipper and imaged on ZEISS Axioscan 7 slide scanner.

## 2.15 Antibodies

**Table 2.1Flow cytometry surface antibodies**

| Fluorochrome | Marker | Clone | Manufacturer | Cat. No. | Dilution (1:x) |
|---|---|---|---|---|---|
| BUV395 | CX3CR1 | ZM-50 | BD Biosciences | 567821 | 100 |
| APC-Cy7 | CCR3 | J073E5 | BioLegend | 144528 | 100 |
| BUV737 | CCR5 | C34-3448 | BD Biosciences | 749670 | 100 |
| PerCP-Cy5.5 | CD11b | M1/70 | BioLegend | 101227 | 200 |
| AF594 | CD11c | N418 | BioLegend | 117346 | 200 |
| BV605 | CD206 | C068C2 | BioLegend | 141721 | 200 |
| BV421 | CD3 | 17A2 | BioLegend | 100227 | 200 |
| BUV805 | CD44 | IM7 | BD Biosciences | 741921 | 200 |
| AF700 | CD45 | 30-F11 | BioLegend | 103127 | 200 |
| APC | CD64 | X54-5/7 | BioLegend | 139305 | 200 |
| PE-Cy7 | CD64 | X54-5/7 | BioLegend | 139313 | 200 |
| FITC | CD69 | H1.2F3 | BioLegend | 104505 | 200 |
| PE | CD86 | A17199A | BioLegend | 159203 | 200 |
| FITC | CXCR2 | SA044G4 | BioLegend | 149309 | 200 |
| Pacific blue | F4/80 | BM8 | BioLegend | 123124 | 100 |
| PE-Cy5 | hCD2 | RPA-2.10 | ThermoFisher | 15-0029-42 | 200 |
| BUV563 | IL33r (ST2) | U29-93 | BD Biosciences | 749324 | 100 |
| PE-Cy7 | IL33r (ST2) | DIH4 | BioLegend | 146609 | 200 |
| PE-Cy7 | IL5Ra | DIH37 | BioLegend | 153407 | 100 |
| APC | Ly6C | HK1.4 | BioLegend | 128015 | 200 |
| BV785 | Ly6C | HK1.4 | BioLegend | 128041 | 200 |
| BV650 | Ly6G | 1A8 | BioLegend | 127641 | 200 |
| FITC | MHC-I (H-2Kd/H-2Dd) | 34-1-2S | BioLegend | 114706 | 200 |
| BV510 | MHC-II (I-A/I-E) | M5/114.15.2 | BioLegend | 107635 | 200 |
| APC | MHC-II (I-A/I-E) | M5/114.15.2 | BioLegend | 107613 | 200 |
| PE-Fire640 | PD-L1 | B7-H1 | BioLegend | 124345 | 200 |
| PE | Siglec-F | E50-2440 | BD Biosciences | 562068 | 200 |
| FITC | Siglec-F | S17007L | BioLegend | 155503 | 200 |
| PE-Dazzle 594 | Siglec-F | S17007L | BioLegend | 155529 | 200 |
| APC | Siglec-F | S17007L | BioLegend | 155508 | 200 |
| Blue | Live/dead fixable dye | | ThermoFisher | L23105 | 400 |
| Yellow | Live/dead fixable dye | | ThermoFisher | L34967 | 400 |
| Near IR | Live/dead fixable dye | | ThermoFisher | L34975 | 400 |

**Table 2.2 Flow cytometry intracellular antibodies**

| Fluorochrome | Marker | Clone | Manufacturer | Cat. No. | Dilution (1:x) |
|---|---|---|---|---|---|
| AF488 | anti-Puromycin | 2A4 | BioLegend | 381505 | 200 |
| AF647 | EdU Click-iT | | ThermoFisher | C10419 | 50 |

**Table 2.3 Immunofluorescent staining antibodies**

| Type | Fluorochrome | Marker | Host | Reactivity | Clone | Manufacturer | Cat. No. | Dilution (1:x) |
|---|---|---|---|---|---|---|---|---|
| Primary | unconjugated | TNC | Rat IgG1 | Mouse/ Human | MTn-12 | Invtirogen | MA1-26778 | 150 |
| Primary | AF647 | CD68 | Rat IgG2a | Mouse | FA-11 | BioLegend | 137003 | 100 |
| Primary | PE | Siglec-F | Rat IgG2a | Mouse | E50-2440 | BD Biosciences | 562068 | 100 |
| Primary | AF647 | CD31 | Rat IgG2a | Mouse | MEC13.3 | BioLegend | 102515 | 400 |
| Primary | BV421 | Ly6C | Rat IgG2c | Mouse | HK1.4 | BioLegend | 128031 | 50 |
| Primary | unconjugated | Major Basic Protein (MBP) | Mouse IgG1 | Human | BMK-13 | Bio-Rad | MCA5751 | 50 |
| Primary | unconjugated | Eosinophil peroxidase (EPX) | Rabbit | Human | Polyclonal | Abcam | ab238506 | 100 |
| Secondary | FITC (AF488) | anti-Rat IgG (H+L) | Donkey | Rat | Polyclonal | BioLegend | A-21208 | 400 |
| Secondary | AF647 | anti-Mouse IgG | Goat | Mouse | Polyclonal | Invitrogen | A-21235 | 400 |
| Secondary | AF647 | anti-Rabbit IgG | Goat | Rabbit | Polyclonal | Invitrogen | A-21244 | 400 |
| Primary | AF647 | Isotype Ctrl | Rat IgG2a | | RTK2758 | BioLegend | 400526 | 400 |
| Primary | PE | Isotype Ctrl | Rat IgG2a | | RTK2758 | BioLegend | 400507 | 100 |
| Primary | BV421 | Isotype Ctrl | Rat IgG2c | | RTK4174 | BioLegend | 400725 | 50 |

## 2.16 qPCR

Eosinophils, macrophages, monocytes and neutrophils were FACS sorted as described in section 2.6, using the gating strategy described in Chapter 3, section 3.2.2. Sorted cells were collected directly into RNeasy lysis buffer (RLT) (cat. 79216, Qiagen), frozen on dry ice and stored at -80 °C. The NT193 cells were collected during cell passaging as described in section 2.2, washed once with PBS, $1x10^6$ cells of shCTL or shTNC phenotype were lysed in 350μl of RLT buffer by resuspension, frozen on dry ice and stored at -80 °C. RNA was isolated from RLT lysates with RNeasy Micro kit (cat. 74004, Qiagen) following Qiagen protocol. RNA was then reverse transcribed using High-Capacity RNA-to-cDNA Kit (cat. 4387-406, ThermoFisher) following the manufacturer's protocol to generate complementary DNA (cDNA). The resulting cDNA was diluted 1:5 in nuclease-free water (New England BioLabs, cat. no. B1500S) and used for real-time quantitative PCR (RT-qPCR) with TaqMan Fast Advanced Master Mix (ThermoFisher, cat. no. 4444557) and individual probes. Gene expression was measured using TaqMan probes for tenascin-c (cat. 4331182, assay ID: Mm00495662_m1, ThermoFisher), eosinophil peroxidase (cat. 4331182, assay ID:

Mm00514768_m1, ThermoFisher), GAPDH (cat. 4331182, assay ID: Mm99999915_g1, ThermoFisher), or Hprt (cat. 4331182, assay ID: Mm00446968_m1, ThermoFisher). qPCR reactions were run on a ViiA 7 Real-Time PCR System (ThermoFisher) and analysed using Design&Analysis 2 software (Applied Biosystems). Relative expression was calculated as a percentage of the housekeeping gene, as indicated, using the comparative Ct method: $2^{(Ct_{(reference)} - Ct_{(target)}} * 100$.

## 2.17 bulk RNA sequencing

Eosinophils (20 000 cells per condition – Ly6C+ and Ly6C-) and macrophages (200 000 cells) were FACS sorted from NT193 tumours as described above and collected into RLT (cat. 79216, Qiagen) with 1% β-mercaptoethanol (cat. M6250, Sigma). Samples were snap frozen on dry ice and RNA extraction, library preparation, sequencing, quality control and read processing were performed by Azenta Life Sciences using an ultra-low input RNA-seq workflow for eosinophils and a standard bulk RNA-seq pipeline for macrophages. Sequencing was conducted on the Illumina (2×150 bp, ~20 million paired-end reads per sample). Reads were trimmed with *Trimmomatic* (v0.36) and quality-checked with FastQC. Alignment to the Mus musculus reference genome (GRCm38, available on ENSEMBL) was performed using *STAR aligner* (v2.5.2b). Gene-level read counts were generated with *featureCounts* (Subread v1.5.2) using exon-overlapping, uniquely mapped reads.

All subsequent analyses were conducted in R version 4.4.0 within RStudio. Gene expression analysis was performed on raw counts. Lowly expressed genes were filtered out by removing genes with a total count of ≤400 across all samples. Ensembl gene identifiers were mapped to mouse gene symbols using the *org.Mm.eg.db* package (v3.19.1) via the *AnnotationDbi* package (v1.66.0). Genes lacking annotations were excluded. Differential gene expression analysis was performed using *DESeq2* (v1.44.0), with tumour identity included as a covariate to account for paired samples, with the primary comparison being between Ly6C+ and Ly6C- eosinophils. Log2 fold changes and Benjamini–Hochberg adjusted p-values (padj) were calculated using the Wald test. Genes with padj < 0.05 were considered significantly differentially expressed.

Variance-stabilising transformation (VST) was applied to the DESeq2 object for dimensionality reduction and visualisation. Principal component analysis (PCA) was performed using *plotPCA* from DESeq2 and visualised with *ggplot2* (v3.5.2). Volcano plots were generated with the *EnhancedVolcano* package (v1.22.0). For visualisation, the top 20 differentially expressed genes (DEGs) were selected based on descending padj values. Transformed expression values were z-score scaled across genes, and heatmaps were plotted using *pheatmap* (v1.0.13). Fold changes were also calculated per tumour to compare Ly6C+ versus Ly6C- eosinophils within individual tumours. Gene set enrichment analysis (GSEA) was conducted using the *clusterProfiler* package (v4.12.6). Genes were ranked by $\log_2$ fold change and mapped to Entrez IDs. The *gseGO* function was used to identify enriched Gene Ontology (GO) terms across biological process, molecular function, and cellular component categories altogether, with significance defined as padj < 0.05. For selected GO terms of interest, core enrichment genes were extracted and annotated. Heatmaps of these gene sets were generated using z-score-scaled expression values. The *ggVennDiagram* package (v1.5.2) was used to visualise overlaps in core enrichment genes across functionally related GO terms identified by GSEA.

In Chapter 5, publicly available gene expression data[232] (GSE184299) were obtained from the Gene Expression Omnibus (GEO) using the *GEOquery* package (v2.70.0). Expression data were derived from the Affymetrix Mouse430A_2 array platform and annotated using Ensembl gene symbols via the *biomaRt* package (v2.60.1). Probe-level data were mapped to gene symbols, and probes without gene annotations were removed. Differential gene expression analysis was performed using the *limma* package (v3.60.6), and heatmaps were generated with *pheatmap* to visualise z-score transformed expression profiles.

## 2.18 Data analysis

Unless otherwise specified, statistical analysis was performed using GraphPad Prism v10.5. One-way or two-way ANOVA using Holm-Šídák correction, or unpaired Student's t-test were applied as indicated in figure legends. Statistical significance was set at p-value < 0.05.

# Chapter 3 | Exploring eosinophil heterogeneity in the breast tumour microenvironment

## 3.1 Introduction

Over the past decade, single cell RNA sequencing (scRNA-seq) has helped reveal the transcriptional heterogeneity of myeloid cells in the breast tumour microenvironment (TME)[247,248]. However, validating these findings on the protein level presents a significant challenge, as protein expression often does not correspond to the transcriptomic data[249,250]. Building on analysis of a scRNA-seq data set that identified 5 distinct subsets of tumour-associated macrophages previously generated in the Midwood lab (unpublished data), we hypothesised that the TME keeps one subset of macrophages in a non-differentiated, translationally rich state, which helps the tumour to avoid immune recognition. Therefore, this chapter first introduces the SUnSET assay[242] used for validating these results by assessing the translational activity of cells in an in vitro and in vivo setting. However, technical aspects of these experiments led us to discover that a) eosinophils non-specifically bind antibodies used for intracellular staining and b) eosinophils represent a prevalent myeloid population in some murine models of breast cancer.

This chapter therefore further focuses on the role of eosinophils in the breast TME and explores their phenotypical and functional heterogeneity. Eosinophils, granulocytes mostly studied in the context of allergy and parasite infections, recently emerged as important players in a favourable response to immune checkpoint blockade in both breast cancer patients and mouse models of the disease[184]. However, their role across different cancer types and treatment-naïve murine tumours is less clear. While depletion of eosinophils in models of colon cancer or lung metastasis correlates with enhanced tumour growth and spread[102,166], depletion of eosinophils in orthotopic or subcutaneous models such as breast or melanoma had no effect on tumour growth[184,188,199]. Additionally, induction of eosinophilia in murine models of breast cancer did not affect tumour size[240], in contrast to tumour-burden reduction in both colon cancer and lung metastases[102,167]. How breast tumours escape eosinophil-mediated cytotoxicity remains unclear.

Three orthotopic murine models of breast cancer were used to explore eosinophil phenotype by spectral flow cytometry. This analysis revealed a) that eosinophils can represent up to 30% of all CD45+ immune cells in the NT193 model and b) the presence of 2 distinct eosinophil subsets, clearly distinguished by Ly6C expression. While up to 90% of eosinophils expressed Ly6C glycoprotein at early stages of tumour development, at the final time point of tumour growth, eosinophils downregulated Ly6C in all studied models. Furthermore, in NT193 tumours, an increased proportion of Ly6C+ eosinophils correlated with lower tumour volumes. Additionally, the Ly6C+ subset of eosinophils was more cytotoxic than the Ly6C- subset ex vivo. Lastly, depletion of eosinophils throughout the entire NT193 tumour development enhances tumour growth. Together, these data indicate that the breast TME is capable of altering eosinophil phenotype in a way that compromises their cytotoxic abilities late during tumour development.

Ly6C expression was also investigated as a marker of eosinophil development. To achieve this, I cultured bone marrow-derived eosinophils in vitro and observed a novel pathway of how eosinophils naturally progress through different stages defined by Ly6C and CCR3 expression, pointing to Ly6C as a potentially important developmental marker of eosinophils, beyond its well-established expression by monocytes.

Collectively, these data provide new evidence that eosinophils are a highly plastic population of granulocytes that are shaped into a less active state by the progressing breast TME and this functional change is associated with downregulation of Ly6C.

## 3.2 Results

### 3.2.1 Optimisation of the SUnSET assay to study translational differences of myeloid cells

Our first aim was to study the role of tumour-associated macrophages by using the NT193 murine model of breast cancer, as previously described[228]. Briefly, the NT193 cancer cell line was derived from spontaneous MMTV-NeuNT mammary tumours that developed in FVB/N female mice genetically engineered to express a constitutively active form of the Erbb2 oncogene (NeuNT) under the control of the mouse mammary tumour virus (MMTV) promoter, leading to cancer growth that represents a model of human HER2-positive breast cancer. NT193 cancer cells were orthotopically grafted into the mammary fat pad of FVB mice, myeloid cells (CD45+, CD11b+, CD3-) infiltrating NT193 tumours were isolated by fluorescence-activated cell sorting method (FACS), and analysed by scRNA-seq. Previous analysis of this dataset revealed 5 phenotypically different subsets of macrophages, a cluster of dendritic cells and a cluster of myeloid-derived suppressor cells (data generated and analysed by A. Gammage, Figure 3.1A-C). Building on this work, I aimed to validate a macrophage cluster 1 (Mac1), proposed to be enriched in ribosomal gene expression (Figure 3.1B) and serving as a root cluster for other macrophage subsets based on the pseudo-time analysis (Figure 3.1C).

To validate the increased levels of ribosomal gene expression on a protein level, we hypothesised that the Mac1 cluster has a higher level of transcriptional activity represented by increased protein synthesis. For quantification of protein synthesis of the Mac1 subset at a single cell level, we chose to use the surface sensing of translation (SUnSET) assay[242]. This assay uses puromycin, an aminoacyl t-RNA analogue, that is incorporated into the C-terminus of nascent proteins and can be detected by intracellular antibody-based fluorescent staining (Figure 3.1D). To validate the specificity of the SUnSET assay, the immortalised Hoxb8 macrophage progenitor cell line was used as previously described[244]. Hoxb8 cells were pulsed with puromycin in the presence or absence of pre-treatment with translation inhibitor cycloheximide (CHX), and compared to cells cultured without either CHX or puromycin (Figure

3.1E). As expected, flow cytometry analysis of intracellular puromycin staining of cells pulsed with puromycin in the absence of the translation inhibitor CHX had the highest fluorescence intensity of puromycin staining. Pre-treatment of Hoxb8 cells with the translation inhibitor CHX prior to puromycin pulsing showed reduced puromycin staining compared to cells not treated with CHX. Finally, cells that were not treated with either puromycin or CHX but were stained with the anti-puromycin antibody presented with background puromycin staining, lower than both puromycin-pulsed and CHX-pre-treated puromycin-pulsed cells (Figure 3.1F). These results suggested that a) CHX effectively blocked translation prior to the puromycin pulse and b) that puromycin labelling specifically detected puromycin-labelled proteins with a minimal background staining in translationally inhibited or puromycin-free cells.

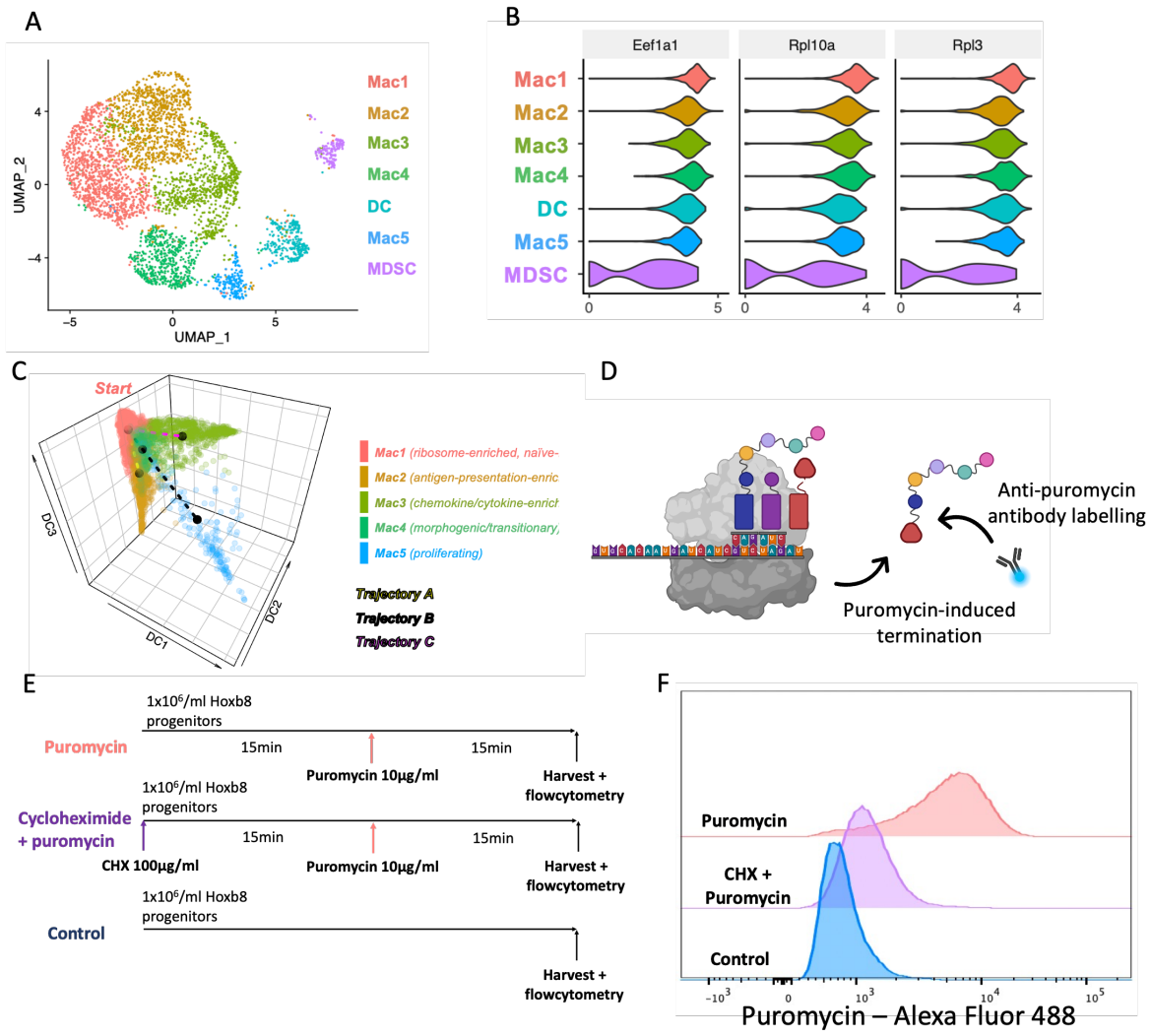


**Figure 3.1. Optimising the SUnSET assay to assess the translational rate of cells in vitro. (A-C)** The NT193 cancer cell line was orthotopically grafted into the 4th mammary fat pad of FVB female mice, tumours were harvested on day 18 and myeloid cells (CD11b+ CD3-) were isolated by fluorescence-

activated cell sorting and underwent single cell RNA sequencing (scRNA-seq). All single cell sequencing data and analysis were generated and performed by A. Gammage. **(A)** Uniform Manifold Approximation and Projection (UMAP) visualisation of tumour-associated myeloid clusters analysed by scRNA-seq. Macrophages (Mac1-Mac5), dendritic cells (DC), and myeloid-derived suppressor cells (MDSC). **(B)** Violin plots visualising z-scored expression of the top 3 macrophage cluster 1 (Mac1) discriminating markers. **(C)** Diffusion map analysis visualising macrophage pseudotemporal macrophage ordering using the first 3 diffusion map components (DC1-DC3). **(D)** Schematic of the surface sensing of translation (SUnSET) experimental approach detecting translation activity of cells through puromycin incorporation into nascent proteins and antibody detection. Puromycin (P) is an aminoacyl t-RNA analogue that is incorporated into the C-terminus of nascent proteins, terminates the translation and leads to the release of truncated protein labelled with puromycin. Puromycin-labelled proteins can be detected by intracellular antibody-based fluorescent staining and analysed by flow cytometry. **(E)** Overview of the experimental set-up designed to test the specificity of puromycin activity and detection. Hoxb8 cells were plated at $1x10^6$/ml cell density and were a) pulsed with puromycin for 15 minutes, b) pre-treated with translation inhibitor cycloheximide (CHX) for 15 minutes and then pulsed with puromycin for 15 minutes, or c) left untreated for 30 minutes. All conditions were then analysed by intracellular anti-puromycin flow cytometry staining. **(F)** Flow cytometry histogram plot of puromycin staining fluorescent intensity detected in puromycin pulsed cells (orange), cells pretreated with CHX and afterwards pulsed with puromycin (pink), or puromycin untreated cells (blue). Flow cytometry staining of CHX pre-treated cells is representative of one experiment. Flow cytometry staining of puromycin-pulsed and puromycin-free cells is representative of 3 independent experiments.

Following these results, the suitability of the SUnSET assay for quantification of translational activity in vivo was tested in tumour-bearing mice. The NT193 cell line was orthotopically grafted in FVB mice, mice were pulsed with puromycin by tail vein injection and puromycin incorporation into nascent proteins of tumour-infiltrating lymphocytes (TILs) was analysed by flow cytometry using staining described in Appendix Table 3.1 (Figure 3.2.A). Because CHX is highly toxic, it was not used in vivo as a negative control in this set of experiments. Instead, tumours of mice that were not injected with puromycin were used as a negative control (puromycin-free), and were stained exactly as tumours from puromycin-injected mice, including the intracellular staining with the anti-puromycin antibody.

All viable TILs (CD45+) were subsampled (Figure 3.2.B) and analysed by a non-linear dimension reduction method, t-Distributed Stochastic Neighbour Embedding (t-SNE), optimised for large cytometry datasets (opt-SNE)[251]. The puromycin staining was excluded from the parameter selection used for the opt-SNE analysis to avoid any clustering bias towards cells with increased protein synthesis and allowed pooling of puromycin-free and puromycin-pulsed mice. Using the CD45+ compartment pooled from puromycin-free and puromycin-pulsed mice for the opt-SNE analysis revealed distinct subsets of TILs (Figure

3.2C). Heatmap analysis of puromycin staining showed diverse levels of puromycin incorporation into nascent proteins across CD45+ cells in puromycin-treated mice (Figure 3.2.D). As expected, intracellular puromycin staining of the CD45+ compartment of mice not treated with puromycin did not detect any puromycin in most of the immune cells. However, a distinct subset of TILs in the puromycin-free mice was labelled with the anti-puromycin antibody (Figure 3.2.E). Furthermore, this cluster of cells differed from other TILs by high surface expression of myeloid marker CD11b (Figure 3.2F). These results suggested that while the SUnSET assay detects puromycin incorporation into proteins in cell culture with high accuracy, detecting puromycin in vivo is less specific and might be prone to non-specifically labelling myeloid cells, as even cells without the puromycin pulse were actively being labelled by the anti-puromycin antibody.

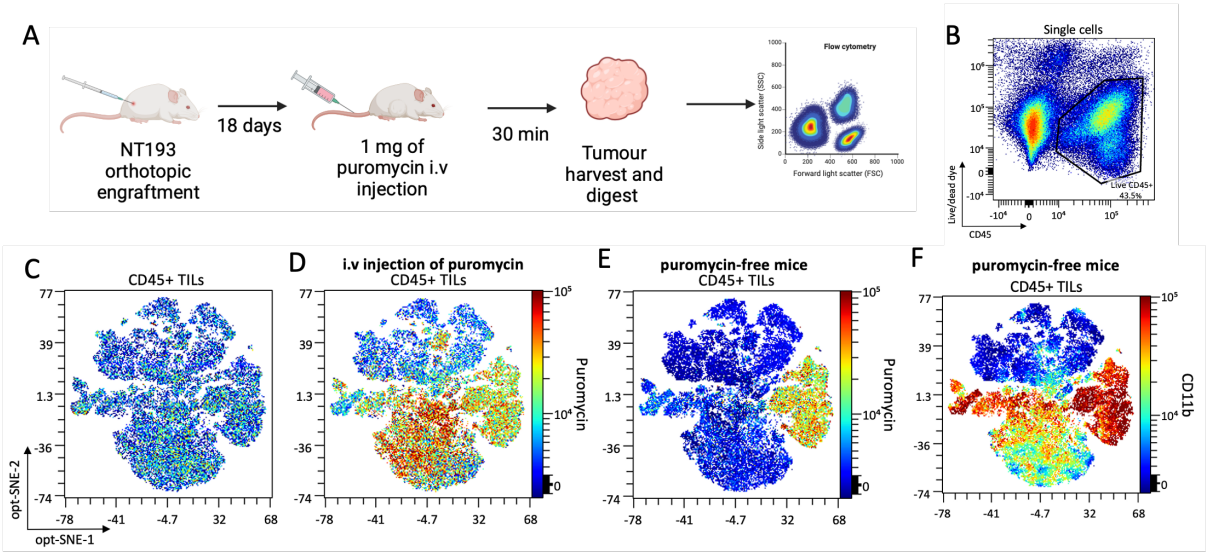


**Figure 3.2. Optimising the SUnSET assay to assess the translational rate of cells in vivo. (A)** Overview of the experimental set-up. The NT193 cancer cell line was grafted into the 4$^{th}$ mammary fat pad of FVB female mice, on day 18, tumour-bearing mice were pulsed with puromycin or left untreated (puromycin-free), and puromycin incorporation into nascent proteins was assessed by intracellular flow cytometry staining. **(B)** Representative flow cytometry plot for the gating of tumour-infiltrating lymphocytes (TILs). **(C-F)** opt-SNE analysis of TILs pooled from puromycin pulsed (*n* = 4) and puromycin-free mice (*n* = 8). opt-SNE analysis was informed by the set of myeloid markers described in Appendix Table 3.1, puromycin staining was excluded from parameter selection to avoid clustering bias towards cells with higher protein synthesis and to allow pooling of puromycin-pulsed and puromycin-free mice. Opt-SNE analysis was performed using OMIQ software. **(C)** Density plot showing cell distribution using opt-SNE components 1 and 2. **(D)** Heatmap analysis of the opt-SNE map showing different intensities of puromycin staining of TILs in mice pulsed with puromycin. **(E)** Heatmap analysis of the opt-SNE map showing different intensities of puromycin staining of TILs in puromycin-free mice. **(F)** Heatmap analysis of the opt-SNE map showing different intensities of CD11b staining of TILs in puromycin-free mice. Data are representative of 2 independent experiments.

Physical properties of puromycin+ cells were further compared to all puromycin- myeloid cells, revealing the increased granularity by side scatter area (SSC-A) of the puromycin+ population (Figure 3.3.A and B). Tumour infiltrating lymphocytes were therefore stained with Siglec-F, a canonical eosinophil marker, to investigate if puromycin+ cells could be a population of eosinophils, granulocytes known to be expressing CD11b and F4/80. Siglec-F staining co-stained puromycin+ cells and clearly separated them from the puromycin- population (Figure 3.3.C). These results led to the conclusion that eosinophils might be an overlooked myeloid population in the NT193 model.

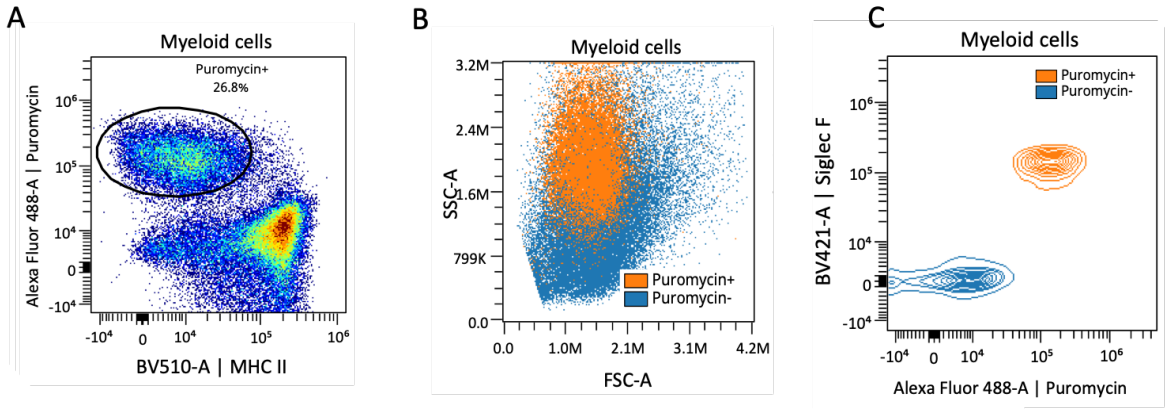


**Figure 3.3. Identification of eosinophils in NT193 tumours.** FVB female mice were grafted into the 4th mammary fat pad with the NT193 cancer cell line, and tumours were analysed on day 18 post-engraftment (n = 6). **(A)** Flow cytometry gating strategy for identification of puromycin+ myeloid cells. **(B)** Density plot with overlay of puromycin+ (orange) and puromycin- (blue) myeloid cells comparing their physical granularity (SSC-A) and size (FSC-A). **(C)** Contour plot overlay of puromycin+ (orange) and puromycin- (blue) myeloid population showing distinct expression of Siglec-F, analysed by flow cytometry. Data are representative of 2 independent experiments.

### 3.2.2 Eosinophil validation in murine models of breast cancer

Following the unexpected finding of such a high eosinophil infiltration in the NT193 tumours grafted in FVB mice, eosinophil (CD45+, CD11b+, Siglec-F+, Ly6G-) infiltration was further investigated in two other well-studied syngeneic murine models of breast cancer – the 4T1 cancer cell line derived from the Balb/c mouse background and the E0771 cancer cell line derived from the C57/Bl6 background mouse. Both of these orthotopic models representing triple-negative breast cancer were selected based on their previous extensive usage in the literature[252,253]. Eosinophils represented on average 30% of all TILs (CD45+) in the NT193 tumours, 10% in the 4T1 tumours grafted in Balb/c mice, and up to 2% in the E0771 tumours grafted in C57/Bl6 mice (Figure 3.4 A). Because wild-type 4T1 tumours were previously

reported to bear only up to 1% of eosinophils relative to all TILs[189], their cellular identity was further confirmed by morphology, gene expression and a combination of surface proteins expression.

Eosinophils (CD11b+, Siglec-F+), monocytes (CD11b+, Siglec-F-, Ly6G-, Ly6C+), macrophages (CD11b+, Siglec-F-, Ly6G-, Ly6C-low), and neutrophils (CD11b+, Siglec-F-, Ly6G+, Ly6C-int) were isolated from 4T1 tumours by fluorescence-activated cell sorting method (FACS sorting) (Figure 3.4.B). Haemoxylin and Eosin (H&E) staining using Cytospin prepared sorted samples confirmed the well-established eosinophil morphology, ring-shaped nucleus and bright eosin staining[104], exclusively in the eosinophil population (Figure 3.4.C). H&E staining also showed the typical bi-lobular nucleus of neutrophils and separated both granulocytic populations from monocytes and macrophages. As expected, the real-time qPCR (RT-qPCR) analysis of these sorted populations confirmed higher expression of eosinophil peroxidase (EPX) in the Siglec-F+ eosinophils compared to the other sorted myeloid populations (Figure 3.4.D).

Surface levels of Siglec-F, IL5Ra and CCR3 were compared among the myeloid populations to understand if the relatively high eosinophil infiltration is a result of a false positive identification. Siglec-F is a receptor expressed on eosinophils[104], alveolar and peritoneal macrophages[254] and a small subset of long-lived Siglec-F+ neutrophils in the TME[255]. Interleukin 5 receptor (IL5Ra) is an eosinophil marker that is essential for eosinophil expansion, however, it is not restricted to the eosinophil lineage and can also be found on B cells[256]. CCR3 is a receptor that binds eotaxins (CCL11, CCL24, and CCL26) and is expressed on eosinophils, however, it can also be present on Th2 lymphocytes, mast cells and basophils[113,257,258]. In agreement with the H&E staining and qPCR analysis, the eosinophil population has a unique phenotype presenting with statistically significant increased expression of Siglec-F and IL5Ra compared to all myeloid subsets, and CCR3 expression significantly higher than neutrophils and macrophages (Figure 3.4. E). While monocytes

presented with higher expression of CCR3, the absence of Siglec-F and IL5Ra expression clearly distinguished them from eosinophils. Expression of Siglec-F, IL5Ra, and CCR3 was then compared on the myeloid populations infiltrating the NT193 tumours. While Siglec-F and CCR3 receptors were significantly upregulated on eosinophils compared to neutrophils, macrophages, and monocytes, surface expression of IL5Ra was equal among all myeloid populations in the NT193 model (Figure 3.4F).

These data indicate that a) the population of Siglec-F+ eosinophils I observed is not a false positive result, and b) that eosinophils are an easy to miss population of TILs that might be more prevalent in murine models of breast cancer than previously thought.

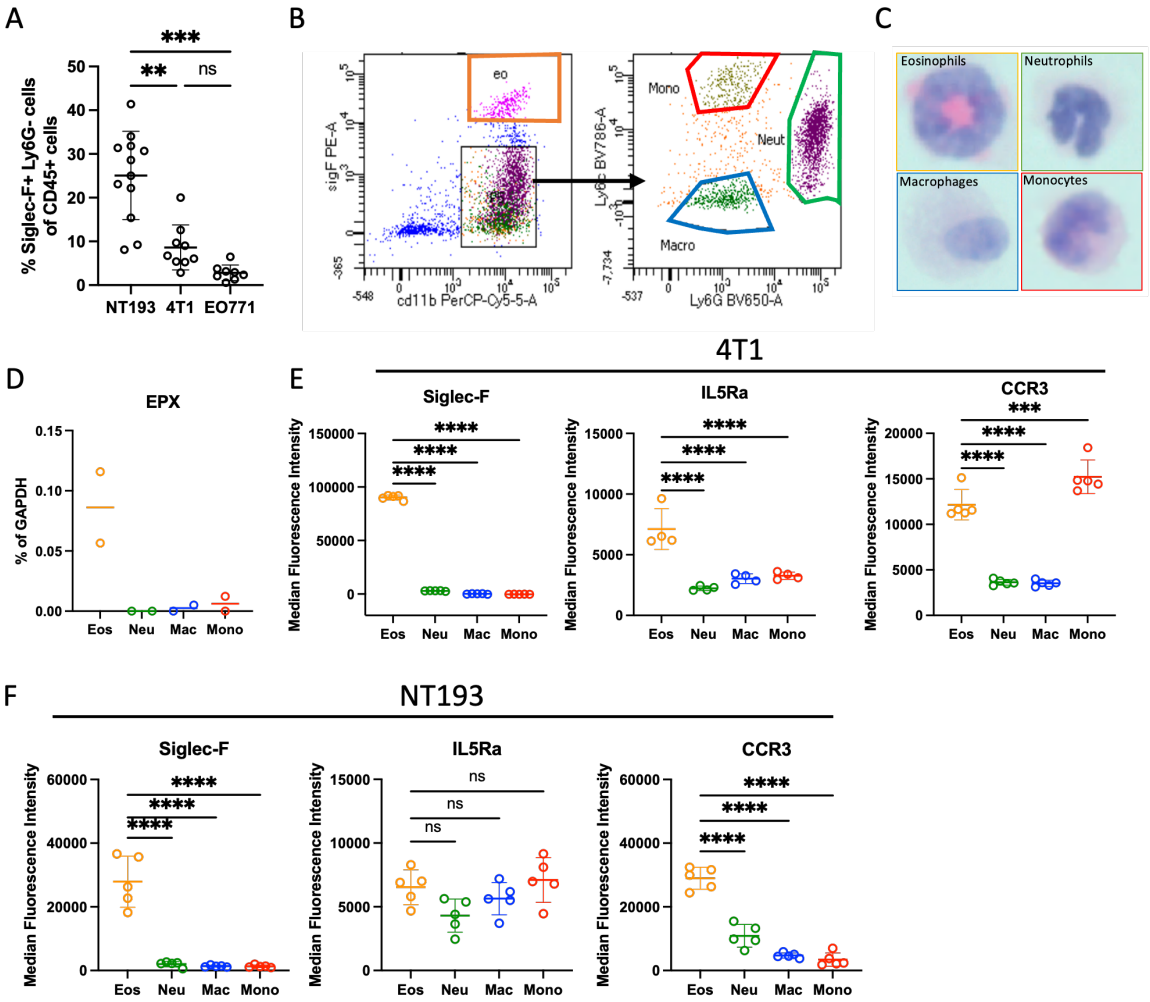


**Figure 3.4. Validation of eosinophil infiltration in murine breast cancer models and confirmation of their distinct phenotype from other myeloid cell types. (A)** Infiltration of eosinophils at the final time point in NT193 (*n*=12) (day18), 4T1 (*n*=9) (day 17-20), and E0771 (*n*=8) (day18-22) orthotopic mammary tumours engrafted into the 4th mammary fat pad of FVB, Balb/c, and C57/BL6 females,

respectively. **(B)** Sorting strategy applied to isolate macrophages (CD45+, CD11b+, Siglec-F-, Ly6C-, Ly6G-), monocytes (CD45+, CD11b+, Siglec-F-, Ly6C+, Ly6G-), neutrophils (CD45+, CD11b+, Siglec-F-, Ly6C$^{int}$, Ly6G+) and eosinophils (CD45+, CD11b+, Siglec-F+) from 4 pooled 4T1 tumours on day 14. **(C)** Haematoxylin and eosin staining of sorted myeloid populations after Cytospin preparation. Cells are representative of 1x10$^5$ cytospun cells. **(D)** RT-qPCR analysis of EPX from the sorted myeloid populations. Data represent 2 technical repeats of 4 pooled mice for each myeloid population. **(E)** Comparison of median fluorescent intensities (MFIs) of well-established eosinophil markers on the myeloid population described above. MFIs presented are analysed from each of the four 4T1 tumours before pooling. **(F)** Comparison of MFIs of well-established eosinophil markers on the myeloid population infiltrating NT193 tumours on day 18 (*n*=5). Data show individual values and mean ± SD and were analysed by two-way ANOVA using Holm-Šídák's multiple comparisons test for comparison of two or more groups. Statistical significance is displayed on figures as follows: *p < 0.05, **p < 0.01, ***p<0.001, ****p<0.0001. No statistical analysis was performed on the RT-qPCR data as the data represent only 2 technical repeats from 4 pooled tumours.

### 3.2.3 Phenotypical and functional heterogeneity of eosinophils in the NT193 model

Eosinophils are bone marrow-derived granulocytes, mostly studied in the context of lung and colon tissue biology, where they are most abundant. They were thought to be terminally differentiated and fully mature once they emerge from bone marrow[104], however, recent data show that they are a plastic cell type and are adapting to their local tissue niche on both gene and protein expression levels[125]. Eosinophils are known to play a role in the healthy mammary gland where they promote the development of the ductal tree[131], and their role in breast cancer is being increasingly studied[135,184]. Despite this, how and if eosinophils adapt to their niche in the mammary fat pad and the breast TME during cancer progression is not known.

To understand eosinophil heterogeneity, the NT193 model was used for explorative analysis due to the naturally higher levels of tumour-infiltrating eosinophils (Figure 3.4A). A multiparameter spectral flow cytometry approach assessing the surface expression of myeloid markers was used to avoid issues with sequencing of eosinophils that contain a low amount of mRNA and high levels of RNases and were previously missed in the single cell sequencing of myeloid cells infiltrating NT193 tumours (Figure 3.1A). It is important to notice that these experiments were performed before the publication of the stress-free protocol optimised for single cell sequencing of murine eosinophils[126].

NT193 tumours were harvested on day 18 post-engraftment and the population of eosinophils (CD45+, CD11b+, F4/80+, Siglec-F+, Ly6G-) pooled from 6 tumours was pre-gated for

subsequent analysis (Figure 3.5A). Eosinophils were further analysed by opt-SNE analysis informed by a set of lineage markers of myeloid populations (Siglec-F, CD11b, F4/80, Ly6G, Ly6C), eosinophil chemokine/alarmin receptors (CCR3, IL33r, CCR5), maturation and activation markers (IL5Ra, CD11c) and antigen-presenting marker (MHC-II), detailed in Appendix Table 3.2. opt-SNE visualisation suggested the presence of 2 eosinophil populations (Figure 3.5B). Individual myeloid markers were then overlaid on the opt-SNE map and heatmaps were individually scaled to demonstrate the different levels of myeloid receptor expression (Figure 3.5C). The canonical eosinophil markers – Siglec-F, F4/80, and CD11b were ubiquitously expressed on all eosinophils, together with the CD11c receptor, previously linked to eosinophil activation[259]. While CCR5 and IL33r were almost non-detectable, heatmap analysis of IL5Ra, CCR3 and MHC-II revealed overlapping patterns of expression. Most notably, Ly6C expression has split the eosinophil population into 2 subsets, suggesting the existence of Ly6C+ and Ly6C- eosinophil populations (Figure 3.5C).

Eosinophil expression of Ly6C was further investigated by density plots to better understand the separation between Ly6C+ and Ly6C- eosinophils. Additionally, the Ly6C phenotype of tumour-associated eosinophils (TAE) was compared between tumours harvested on day 7 (early tumours) and day 18 (late tumours). Ly6C+ eosinophils represented over 95% of all TAE in the early NT193 tumours, however, only 60% in the late tumours in which a clear separation between Ly6C+ and Ly6C- subsets was observed (Figure 3.5D). This drop in prevalence of Ly6C+ eosinophils in late tumours was statistically significant (Figure 3.5E).

To explore if the Ly6C downregulation is a conserved mechanism of eosinophils adapting to the progressing TME, Ly6C expression in early and late E0771 and 4T1 orthotopic tumours was assessed. Similarly to the NT193 tumour model, more than 90% of TAE in the early E0771 tumours were Ly6C+, and the Ly6C+ TAE population decreased to 70% in late TME (Figure 3.5F). While Ly6C+ eosinophils followed the same trend in 4T1 tumours, their baseline level of Ly6C expression in early tumours was only around 50% (Figure 3.5E). This led to a

hypothesis that Ly6C downregulation is a TME-regulated mechanism that might have wider implications on eosinophil functionality.

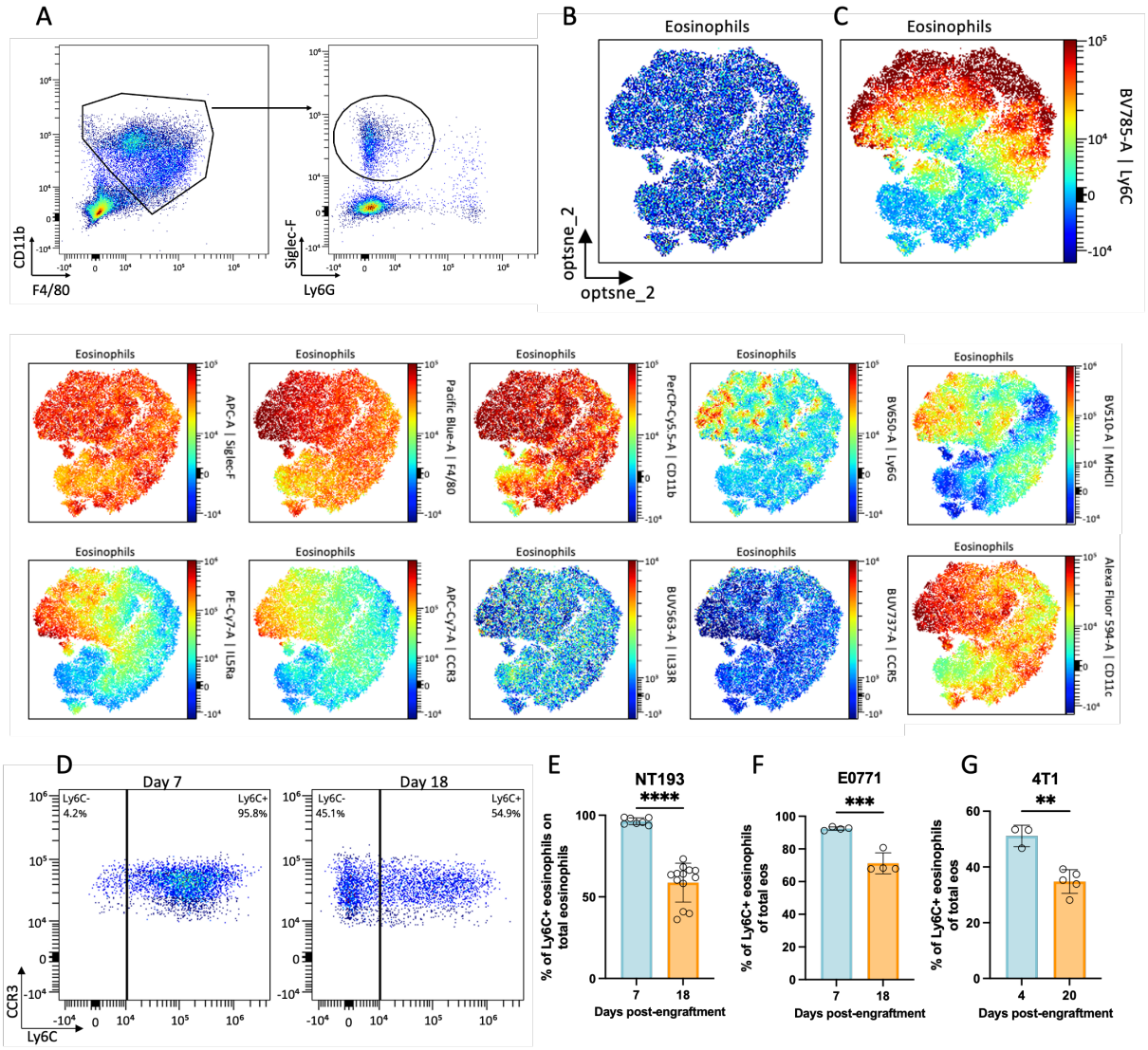


**Figure 3.5. Exploring heterogeneity of tumour-infiltrating eosinophils by spectral flow cytometry.** **(A)** Gating strategy used to identify myeloid cells (Live, CD45+, CD11b+, F4/80+) and follow-up gating for eosinophils (Live, CD45+, CD11b+, F4/80+, Siglec-F+, Ly6G-) in NT193 tumours. **(B)** opt-SNE high-dimensional analysis of eosinophils concatenated from 6 NT193 tumours on day 18 performed using OMIQ software. opt-SNE analysis was informed by the expression of 11 myeloid markers detailed in Appendix Table 3.2 and data were acquired using Cytek Aurora. **(C)** Heatmap analysis overlayed on opt-SNE density plots, each coloured-continuous plot represents expression of 1 myeloid marker, each marker is scaled individually, as shown on the adjacent scale bars. **(D)** Flow cytometry analysis of NT193 infiltrating eosinophils, identifying Ly6C+ and Ly6C- population on days 7 and 18 of tumour development. Data are representative of 6 tumours per condition. **(E-G)** Proportion of Ly6C+ eosinophils to total eosinophils in NT193 ($n_{day7}$=7, $n_{day18}$=13), E0771 ($n_{day7}$ = 4, $n_{day18\text{-}22}$ = 4) and 4T1 tumours ($n_{day4}$ = 3, $n_{day20}$=5) on day 7 and day 18-20. NT193 data are representative of 3 independent experiments, E0771 data are representative of 2 independent experiments, 4T1 experiment performed once on indicated time points and repeated with harvest days 7 and 14. Data show individual values and mean ± SD and were analysed by an unpaired Student's t-test. Statistical significance is displayed on figures as follows: *p < 0.05, **p < 0.01, ***p<0.001, ****p<0.0001.

To understand if and how tumour-infiltrating eosinophils play a role in the TME development, the relationship between total eosinophil infiltration and tumour weight on day 18 post-engraftment was analysed by simple linear regression and a correlation with a squared correlation coefficient ($R^2$) of 0.013 was observed (Figure 3.6A), showing no linear relationship between these two variables. However, the simple linear regression analysis of the proportion of Ly6C+ eosinophils and tumour weight showed a statistically significant negative correlation (Figure 3.6B). These results suggested that while the total level of eosinophils is not indicative of tumour weight on day 18, the proportion of Ly6C+ eosinophils negatively correlates with tumour weight, pointing to a potential anti-tumorigenic effect of this population.

To investigate anti-tumorigenic properties of Ly6C+ and Ly6C- eosinophils, these populations were FACS sorted from NT193 tumours on day 18 and characterised by the following analyses. Firstly, H&E staining of both populations revealed similar morphology of the nucleus (Figure 3.6C). However, the maximum optical density of eosin was significantly increased in Ly6C+ eosinophils (Figure 3.6D) compared to equal levels of haematoxylin staining in both populations (Figure 3.6E). Eosin stains the cytoplasm of cells by non-specifically binding to all proteins. Due to the high granule content of basic peroxidases, eosinophils are typically stained with eosin more than other cell types. This staining is, however, diminished in degranulating eosinophils with lower granule content[260]. Therefore, the increased eosin staining in the Ly6C+ but not the Ly6C- population of eosinophils suggested an increased granularity and cytotoxic potential. The granularity difference between the two eosinophil subsets was further investigated by comparing side-scatter (SSC) flow cytometry measurements. Ly6C+ eosinophils had increased SSC compared to their Ly6C- counterparts matched within the same tumour (Figure 3.6F). Furthermore, Ly6C+ eosinophils had also increased expression of CD63 degranulation marker (Figure 3.6G), but their levels of CD11b integrin were not significantly changed compared to Ly6C- eosinophils (Figure 3.6H). These data indicated that Ly6C+ eosinophils could present a more active degranulating population with enhanced cytotoxic properties.

Cytotoxic abilities of the sorted eosinophils were further tested in direct co-cultures with NT193 cells and a combination of apoptotic annexin-V and fixable live/dead staining was used to evaluate cell death of the NT193 cells. Co-culture of NT193 cells with Ly6C+ eosinophils resulted in 12% of annexin-V+ apoptotic NT193 cells, which was a slight but statistically significant increase compared to 7% of apoptotic cells detected in co-culture with Ly6C- eosinophils (Figure 3.6I).

Together, this indicates that Ly6C+ eosinophils compared to Ly6C- eosinophils represent a more granular eosinophil population with better cytotoxic abilities, and that under the influence of the breast TME, eosinophils may differentiate into a Ly6C- state that is less cytotoxic. If this transition is specific to the primary breast TME was further investigated.

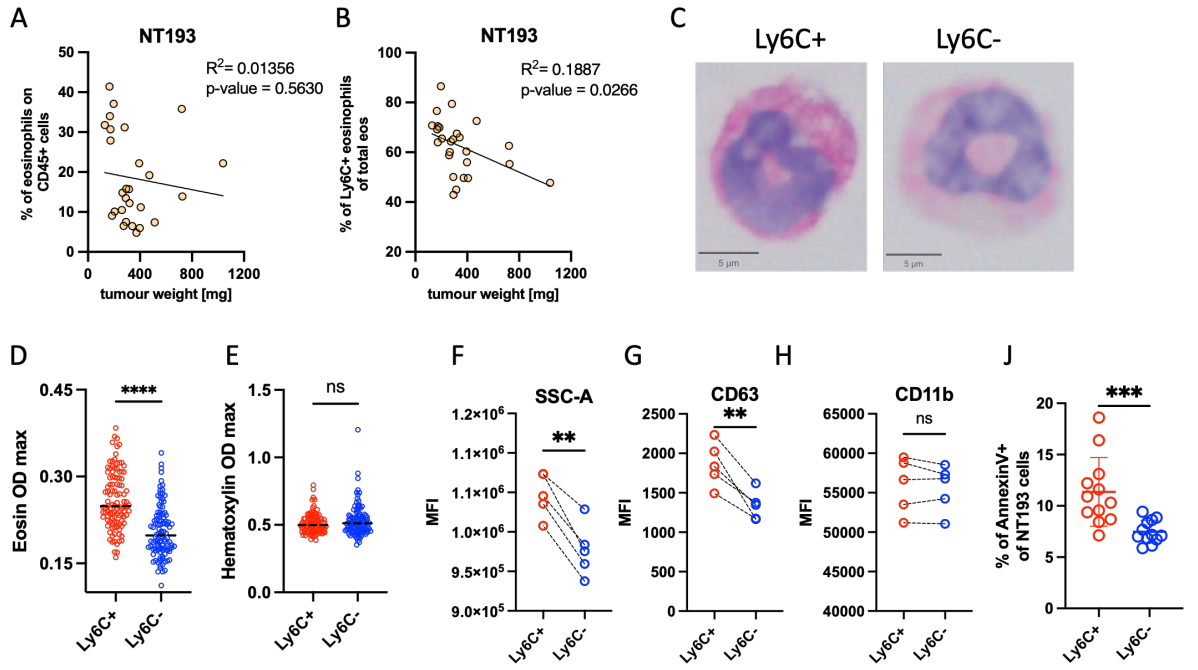


**Figure 3.6. Ly6C+ eosinophils represent a more granular phenotype with better cytotoxic properties. (A and B)** Correlation between NT193 tumour weight on day 18 and relative proportion of total eosinophils of CD45+ cells **(A)** and relative proportion of Ly6C+ eosinophils to total eosinophils **(B)**. Data are pooled from 4 independent experiments and show individual values of 27 tumours harvested on day 18. Simple linear regression was performed in GraphPad Prism; the reported $R^2$ corresponds to the Pearson correlation. **(C)** Haematoxylin and eosin (H&E) staining of cytospun Ly6C+ and Ly6C- eosinophils sorted from tumour harvested on day 18. **(D-E)** Analysis of the eosin **(D)** and haematoxylin **(E)** intensity of the H&E stained Ly6C+ eosinophils (n = 106) and Ly6C- (n = 108). Haematoxylin and eosin vector stains were automatically deconvoluted by QuPath, before extracting the maximal optical density measurements of individual cells. Data are representative of 2 experiments, in each experiment Ly6C+ or Ly6C- eosinophils were pooled from 3 NT193 tumours after sorting. **(F-H)**

Flow cytometry analysis of tumour-associated eosinophils. Comparison of side scatter **(F)**, CD63 expression **(G)**, and CD11b expression **(H)** between Ly6C+ and Ly6C- eosinophils on day 18 of NT193 tumour growth (n = 5). **(I)** NT193 tumour cells were co-cultured with sorted Ly6C+ or Ly6C- sorted tumour-associated eosinophils used as individual biological replicates (n=12), stained by Annexin-V and analysed by flow cytometry. Comparison of proportion of Annexin-V+ NT193 cells to all NT193 cells after direct co-culture with Ly6C+ and Ly6C- eosinophils. Annexin-V staining data are representative of 3 pooled experiments; mice were harvested between days 12-18. All data are representative of at least 2 biological experiments and show individual values and mean or mean ± SD and were analysed by unpaired Student's t-test. Statistical significance is displayed on figures as follows: *p < 0.05, **p < 0.01, ***p<0.001, ****p<0.0001.

### 3.2.4 Studying eosinophil heterogeneity in the lung metastatic niche

To investigate the effect of the metastatic environment on the balance between proportions of Ly6C+ and Ly6C- eosinophils, a murine model of breast cancer-derived lung metastasis was selected. Eosinophils represent 3% of the CD45+ immune cell population in healthy murine lungs[127], which allows comparison with metastasis-associated eosinophils during disease progression. Additionally, eosinophils are known to have an anti-tumorigenic role in breast cancer lung metastasis formation[167] and adapt their phenotype in metastatic lungs[166]. Therefore, the E0771 and 4T1-mCherry GFP breast cancer cell lines with high metastatic potential were injected into the circulation through the tail vein to induce pulmonary metastases and the eosinophil phenotype from diseased animals was compared with that in healthy mice.

Flow cytometry analysis revealed that Ly6C+ eosinophils represented 80% of all eosinophils in the healthy lungs of C57/Bl6 mice, and these levels were decreased by 20% in mice bearing E0771 metastases (Figure 3.7A). Ly6C+ eosinophils accounted for 40% of all eosinophils in the lungs of healthy Balb/c mice and their proportion decreased by 20% in Balb/c mice bearing 4T1 metastases (Figure 3.7B). To understand whether a decrease in the proportion of Ly6C+ eosinophils is associated with disease severity, similarly to higher proportions of Ly6C+ eosinophils associated with lower NT193 tumour weight (Figure 3.6B), the proportion of Ly6C+ eosinophils was correlated with proportions of 4T1 cancer cells and analysed by simple linear regression. The proportion of the 4T1 cancer cells to all acquired cells was used as an indicator of disease severity and the 4T1 cancer cells were identified based on their expression of both

mCherry and GFP. The higher proportions of Ly6C+ eosinophils of total eosinophils negatively correlated with increased proportions of 4T1 cancer cells (GFP+ mCherry+) as a proportion of total cells (Figure 3.7C).

To investigate if Ly6C- eosinophils are more prevalent specifically in the metastatic niche compared to the unaffected distant lung, a mCherry niche labelling model was used as previously described[233]. Briefly, by using cancer cells expressing a lipid-permeable mCherry vector that is actively secreted and permeabilizes neighbouring cells, up to 5 layers of neighbouring cells can be detected and distinguished from distant lung post-harvest by flow cytometry[233] (Figure 3.7D). The labelling efficiency of the 4T1 cells was first assessed in vitro, HEK293 fibroblasts were used as a receiving “neighbouring” cell line to repeat the same conditions as recommended[241]. mCherry and GFP expression were first confirmed in the 4T1 mCherry-GFP cell line by flow cytometry (Figure 3.7E). Afterwards, HEK293 cells in direct co-culture with 4T1 mCherry-GFP or cultured with conditioned media derived from this cell line were compared to wild-type non-labelled HEK293s. This analysis confirmed that 4T1 mCherry-GFP cells do label HEK293 cells in direct co-culture, as 2 populations were observed, 1) the original 4T1 cells expressing both mCherry and GFP and 2) GFP negative HEK293 cells with an increased level of mCherry (Figure 3.7E). While a small increase in mCherry positivity was observed in the culture of HEK293 cells with conditioned media compared to wild-type HEK293s, this was lower than in direct co-culture.

Labelling efficiency was further investigated in vivo by harvesting lungs 7 days post tail vein engraftment of 4T1 mCherry-GFP cells and staining with the panel detailed in Appendix Table 3.3. As expected, 3 populations of viable cells were observed when analysing mCherry GFP signal in lungs; 1) mCherry+ GFP+ cancer cells, 2) mCherry+ GFP- niche cells, and 3) mCherry- GFP- cells of distant lung (Figure 3.7F). Following this analysis, all CD45+ immune cells were analysed and a clear eosinophil population (CD45+, CD11b+, Siglec-F+, CD64-) was identified. Afterwards, mCherry presence specifically in the eosinophil population was

compared between mice with 4T1 WT and 4T1 mCherry-GFP metastases (Figure 3.7G). These results did not reveal any clear mCherry+ eosinophil population present in the niche. An identical analysis was performed on alveolar macrophages, a cell type reported to be abundant in metastatic TME[261]. Up to 70% of alveolar macrophages (CD45+, Siglec-F+, CD11b+, CD64+) were labelled by mCherry in mice grafted with 4T1 mCherry-GFP cells compared to 4T1 WT cells (Figure 3.7 H).

The absence of eosinophils in the mCherry+ metastatic niche is in contradiction with the reports showing that eosinophils were located in lung metastatic lesions when investigated by histopathology[166]. However, the absence of labelling of eosinophils by the mCherry vector could be explained by the study showing that not all cells might receive the lipid-permeable mCherry vector with the same efficiency[241]. These results suggest that while the mCherry labelling model is a powerful tool for exploring the metastatic niche, eosinophils were not detected in the metastatic niche based on the labelling by the mCherry lipid vector. Additional in vitro experiments of eosinophils cultured with the mCherry-conditioned media would be necessary to understand why eosinophils were not labelled with mCherry in metastatic lungs.

Overall, these data suggest that reduction of Ly6C+ eosinophil proportions as a response to cancer progression is a conserved mechanism in primary and lung metastatic models of breast cancer. Furthermore, higher proportions of Ly6C+ eosinophils might be indicative of better prognosis in both the NT193 primary tumour model and the 4T1 metastatic lung model. However, I was not able to identify eosinophil infiltration in the metastatic niche and more experiments would be needed to investigate if eosinophils locate outside of the metastatic niche or are labelled by the mCherry vector to a lesser extent.

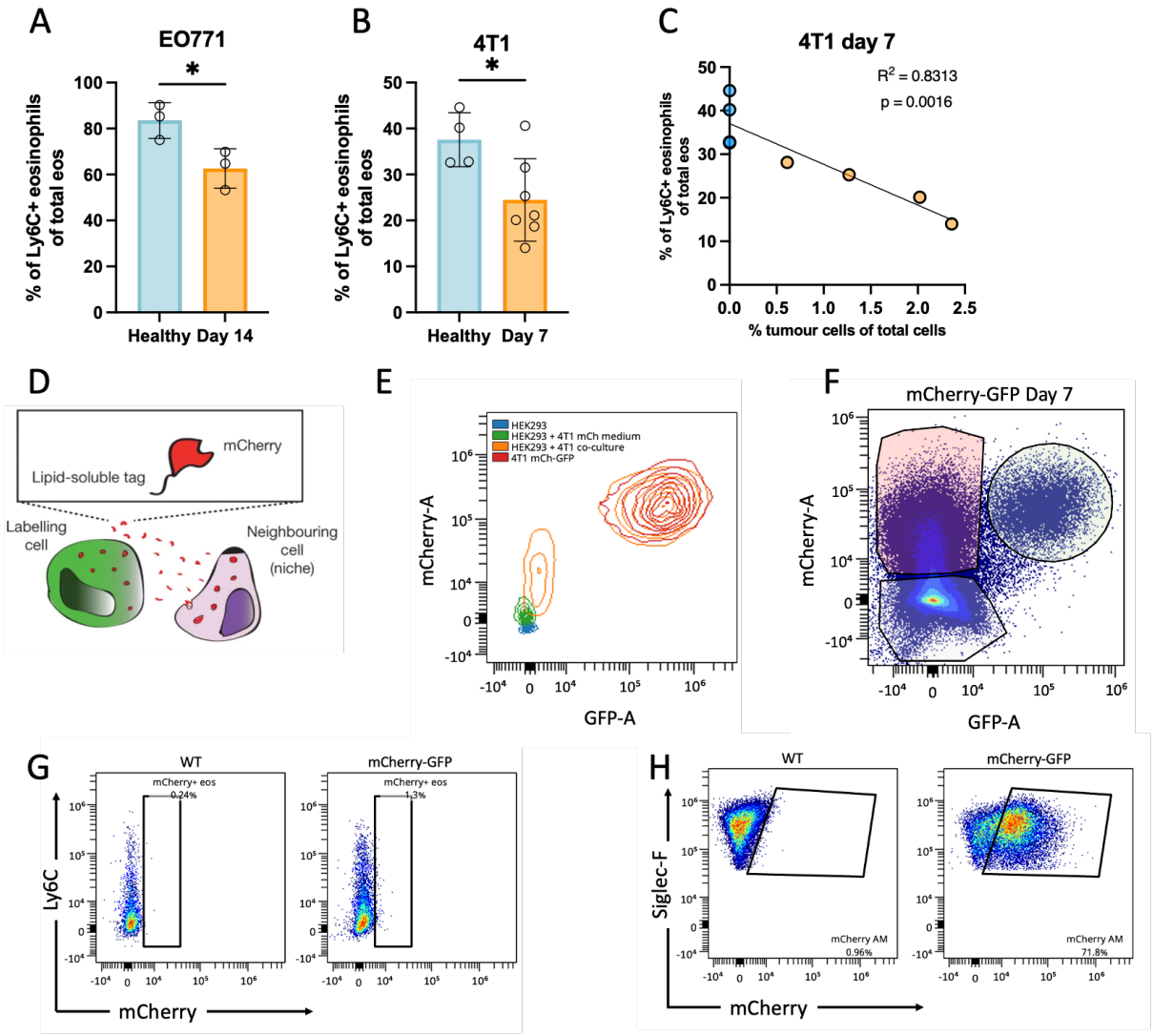


**Figure 3.7. Investigating the kinetics of Ly6C+ and Ly6C- eosinophils in the 4T1 and E0771 breast cancer lung metastases models. (A and B)** Bl6 and Balb/c female mice were injected with E0771 (1000 000 cells) and 4T1 mCherry-GFP cells (1 500 000 cells), respectively. Metastatic lungs were harvested on day 14 and day 7 as indicated on the plots, analysed by spectral flow cytometry and the proportion of Ly6C+ eosinophils to all eosinophils was compared between diseased and healthy animals of the same strain. ($n_{Bl6}$=3, $n_{day14}$=3), ($n_{Balb/c}$=4, $n_{day7}$=7). **(C)** Correlation between tumour cells (mCherry+ GFP+) of 4T1 lung metastasis (orange, $n_{day7}$=4), healthy lungs (blue, $n_{Balb/c}$=3), and percentage of Ly6C+ eosinophils. Data are representative of one experiment. **(D)** Schematics of the mCherry labelling system adapted from (Ombrato et al., 2019). mCherry is linked to lipid-soluble vector (sLP-mCherry) that is being secreted from the 4T1 mCherry-GFP cells and is capable of permeabilising neighbouring cells in vitro and labelling tumour niche in vivo. **(E)** Flow cytometry analysis of mCherry and GFP signal in HEK293 cells 1) cultured in conditioned media derived from 4T1 mCherry-GFP cells (green), 2) in direct co-culture with 4T1 mCherry-GFP (orange) or 3) on their own (blue) compared with 4) 4T1 mCherry-GFP (red) cell line by flow cytometry. Data are representative of one repeat, and two replicates per condition. **(F-H)** 4T1 mCherry-GFP cancer cells were intravenously engrafted into Balb/c female mice and lungs were harvested and analysed by flow cytometry 7 days after ($n_{day7}$=7). **(F)** Flow cytometry analysis of sLP-mCherry and GFP signal in 4T1 metastatic lungs distinguished tumour niche (red) from tumour cells (green) and distal lung (grey). **(G-H)** Uptake of sLP-mCherry by eosinophils (Siglec-F+, CD11b+, CD64-) **(G)** and alveolar macrophages (Siglec-F+, CD11b+, CD64+) **(H)** in comparison with mice bearing metastasis of 4T1 wild-type cell line. Alveolar macrophages were identified as a myeloid population expressing both Siglec-F and CD64, eosinophils were gated as myeloid cells with expression of Siglec-F but absence of CD64 expression. Data show individual values and mean ± SD and were analysed by an unpaired Student's t-test. Statistical significance is displayed on figures as follows: *p < 0.05.

### 3.2.5 Ly6C+ eosinophils transition into Ly6C- state

Next, the relationship between Ly6C+ and Ly6C- eosinophil subsets was investigated. Eosinophils are a bone marrow-derived population of granulocytes, originating from *Gata1+* progenitors that give rise to erythroid cells, megakaryocytes, basophils, mast cells and eosinophils[98]. Eosinophils undergo 4 stages of maturation in the bone marrow, each stage associated with increasing expression of CCR3, the receptor essential for binding eotaxins. Afterwards, mature CCR3+ eosinophils migrate through circulation to distant tissues based on the local eotaxin gradient and internalise CCR3 after entering the tissue as a response to eotaxin exposure[262,263], recently demonstrated in a model of skin cancer[264]. To better understand the dynamics of the 2 eosinophil subsets in NT193 tumours, Ly6C and CCR3 expression of eosinophils was investigated in the mammary fat pad of healthy mice, and bone marrow, blood, and tumours on day 7 and day 18 of NT193 tumour-bearing mice. Because Ly6C is not a marker commonly associated with eosinophils, eosinophils were compared to monocytes ($Ly6C^{high}$, Ly6G-, Siglec-F- population), neutrophils ($Ly6C^{int}$, Ly6G+, Siglec-F-) and all immune cells (CD45+ lymphocytes) to understand the Ly6C expression differences in broader context of tissue biology (Figure 3.8A), with gating strategies used to identify these individual populations, described in Figure S1.

Mammary fat pad (MFP) was analysed to investigate the Ly6C expression on tissue resident eosinophils, which represent a minor resident population[38]. As expected, tissue resident eosinophils in MFPs of healthy FVB female mice express low levels of CCR3 compared to eosinophils in bone marrow or blood. Even though MFP resident eosinophils express less Ly6C than monocytes or neutrophils, the contour plot indicates that the majority of this population is Ly6C+ compared to the rest of the lymphocytes (Figure 3.8A). Eosinophils were further analysed from the bone marrow of mice bearing tumours for 18 days; all bone marrow eosinophils had a baseline level of Ly6C expression comparable to neutrophils, and previously described populations of immature (CCR3-) and mature (CCR3+) eosinophils were

observed[98,266] (Figure 3.8A). Subsequently, mature CCR3+ eosinophils emerging from the bone marrow were identified in blood, where all eosinophils expressed ubiquitous levels of Ly6C, above some of the lymphocytes (CD45+) but below monocytes or neutrophils and remained CCR3+ (Figure 3.8A). To this point, these data suggest that eosinophils are predominantly Ly6C+ in the mammary fat pad, bone marrow and blood of healthy and tumour-bearing animals.

Therefore, Ly6C and CCR3 expression was investigated on eosinophils infiltrating NT193 tumours on day 7 and day 18. In agreement with eosinophils internalising CCR3 as a response to migrating towards inflamed tissue[262,263], surface expression of CCR3 on TAE was reduced on both day 7 and day 18 post-engraftment compared to the blood and bone marrow of matched animals. As described above in section 3.2.3 (Figure 3.5E), eosinophils are predominantly Ly6C+ in early tumours, however, they downregulate Ly6C expression and up to 50% of eosinophils become Ly6C- by day 18 post-engraftment in tumours (Figure 3.8A). Additionally, eosinophil prevalence as a proportion of all immune cells (CD45+) or all acquired single cells was compared in MFP, bone marrow, blood and tumours. Eosinophils represented a minor immune and resident population in MFP, bone marrow or blood and were accumulating in tumours over time, with the highest levels of eosinophils identified in tumours on day 18 (Figure 3.8 B and C). These data pointed to the possibility of Ly6C+ eosinophils infiltrating tumours early on day 7 and then transitioning into the Ly6C- state.

To understand whether the Ly6C+ population of eosinophils detected in tumours on day 7 represents the circulating population present in the vasculature at the time of harvest, co-localisation of eosinophils (Siglec-F) and vasculature (CD31) was compared between day 7 and day 18 by confocal imaging (Figure 3.8D). While some Siglec-F+ cells directly co-localised with the CD31 staining, most of the tumour-infiltrating Ly6C+ eosinophils identified on day 7 and day 18 were located outside of the vasculature.

Overall, because a) eosinophil ontogeny occurs in the bone marrow, b) eosinophils express high levels of Ly6C in blood of tumour bearing mice and in tumours at early stages, c) eosinophils accumulate in tumours over time, and d) both Ly6C+ and Ly6C- eosinophils are residing in the tissue outside of the vasculature, these data suggest that Ly6C+ eosinophils might be transitioning into Ly6C- state after entering tumours.

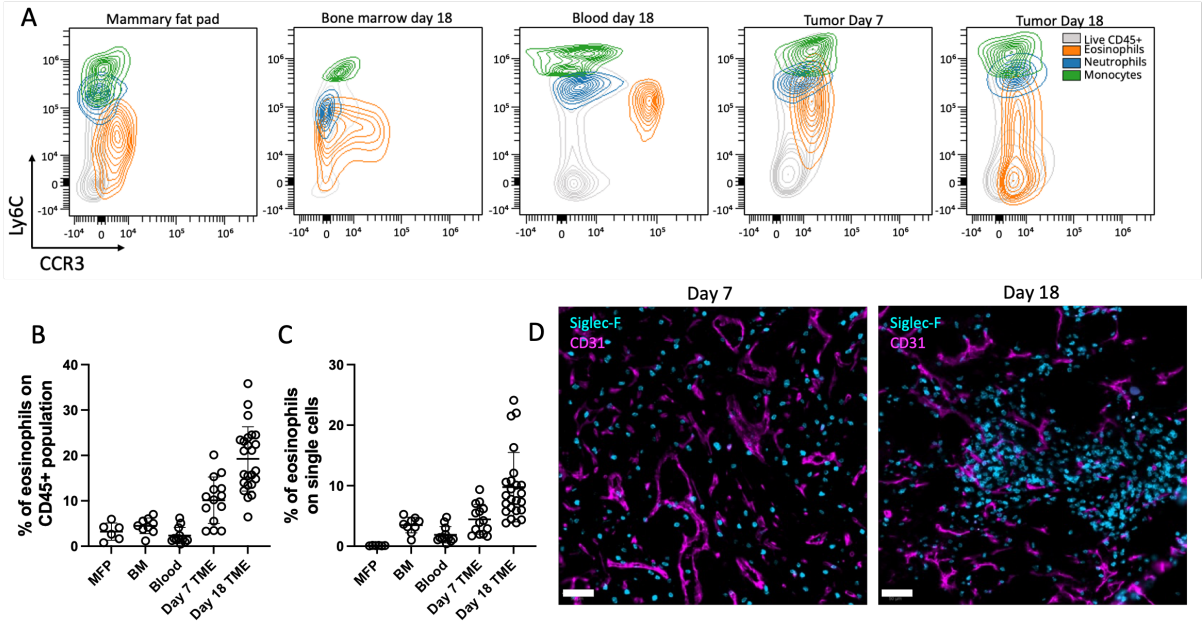


**Figure 3.8. Ly6C+ eosinophils transition into the Ly6C- state after entering NT193 tumours. (A)** Flow cytometry analysis comparing Ly6C and CCR3 expression between eosinophils (CD11b+, SiglecF+, Ly6G-), neutrophils (CD11b+, SiglecF-, Ly6G+), monocytes (CD11b+, Siglec-F-, Ly6G-, MHC-II$^{low}$, Ly6C+) and all immune cells (CD45+) in healthy mammary fat pads (MFP), bone marrow (BM) and blood of FVB mice orthotopically engrafted with NT193 cancer cell line, and early (day7 TME) and late NT193 tumours (day18 TME). **(B and C)** Quantification of total eosinophil population as a proportion of immune cells (CD45+) **(B)** or all acquired single cells **(C)**. (A-C, $n_{MFP}$ = 6, $n_{BM}$=9, $n_{blood}$ = 12, $n_{day7TME}$ = 14, $n_{day18TME}$ = 24). Data are representative of at least 2 experiments for blood (harvested between day 14 to day 18), and at least 3 experiments for tumour-associated eosinophils infiltrating NT193 tumours on day 7 or day 18. **(D)** Immunofluorescent staining of Siglec-F+ eosinophils (cyan) and CD31+ vasculature (magenta) of NT193 tumours on the indicated days. Scale bar = 50 µm. Data are representative of two experiments, and represent analysis of 4 individual tumours on day 7 and day 18, a full section was acquired by Axio Slide scanner.

To further understand the potential of Ly6C+ eosinophils to give rise to the Ly6C- population, NT193 tumour infiltrating eosinophils were isolated on day 7, kept in culture with interleukin-5 (IL-5), and the expression of Ly6C and CCR3 was analysed 1-, 2-, 4-, and 8-days post-isolation (Figure 3.9A). IL-5 is a cytokine essential for eosinophil survival and expansion[267]. Therefore, IL-5 was used in all ex vivo cultures to keep eosinophils viable and capable of

differentiation. As described above, eosinophils freshly isolated from early tumours internalised CCR3 and over 90% of them expressed the Ly6C receptor as measured by flow cytometry. However, after only 1 day in culture with IL-5, 80% of these eosinophils re-expressed CCR3 on the surface, and 4 days after isolation from tumours, over 95% of eosinophils were CCR3+ (Figure 3.9B). More importantly, Ly6C+ viable eosinophils spontaneously differentiated into the Ly6C- population and this transition represented a 20% decrease of the Ly6C+ population on day 4 and almost 30% on day 8 post-isolation (Figure 3.9C). To prove that in culture with IL-5, only Ly6C+ eosinophils have the potential to differentiate into the Ly6C- population and this transition does not happen both ways, both Ly6C+ and Ly6C- populations were FACS sorted from late NT193 tumours and kept in culture for a maximum of 4 days (Figure 3.9D). Within 2 days post-sorting, 40% of Ly6C+ eosinophils differentiated to the Ly6C- population, however, Ly6C- eosinophils remained in the Ly6C- state throughout the whole ex vivo culture experiment.

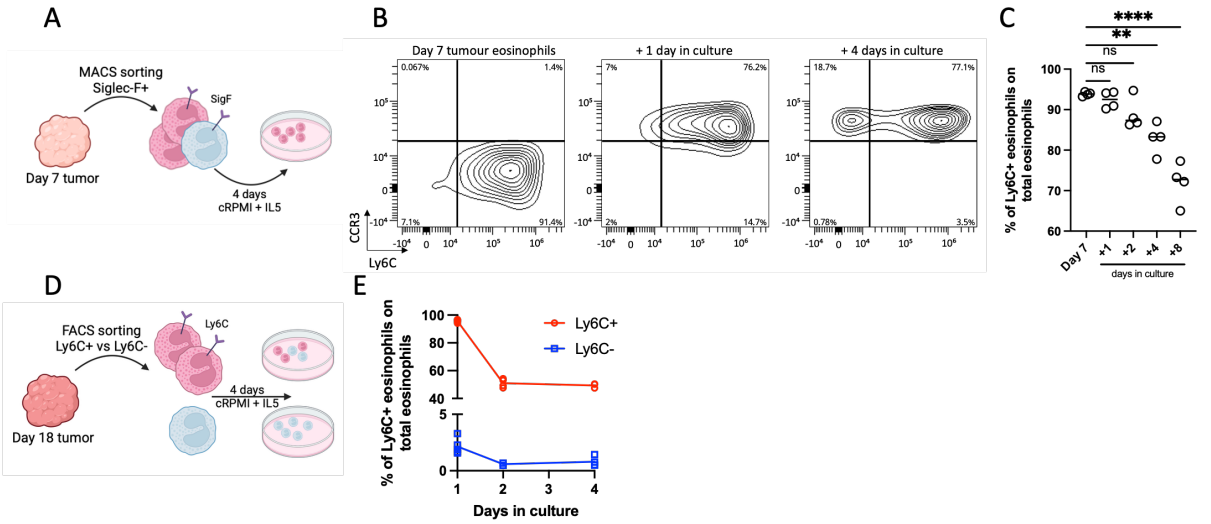


**Figure 3.9. Ex vivo culture of Ly6C+ and Ly6C- eosinophils. (A)** Overview of the experimental plan, NT193 tumours were harvested on day 7, digested and magnetic cell separation (MACS) was used to enrich Siglec-F+ cells. Siglec-F+ cells were afterwards cultured up to 8 days with IL-5 and analysed by flow cytometry on days 1, 2, 4 and 8 of culture. **(B)** Contour plots showing eosinophil (Siglec-F+, Ly6G-) expression of Ly6C and CCR3 after MACS enrichment on the day of harvest and on day 1 and day 4 of ex vivo culture, as indicated on the plots. **(C)** Relative proportion of Ly6C+ eosinophils gated on all eosinophils (n = 4). **(D)** Overview of the experimental plan, NT193 tumours were harvested on day 18, digested and FACS sorted for Siglec-F+ Ly6C+ and Ly6C- eosinophils. Both populations were afterwards cultured up to 4 days with IL-5 and analysed by flow cytometry on days 1, 2, and 4 of culture. **(E)** Relative proportion of Ly6C+ eosinophils gated on all eosinophils sorted as Ly6C+ or Ly6C-. (n = 3). Data are representative of two independent experiments, show individual values and median and were analysed by 2-way ANOVA. Statistical significance is displayed on figures as follows: *p < 0.05, **p < 0.01, ***p<0.001, ****p<0.0001.

These results made me hypothesise that the loss of Ly6C is not only a consequence of the TME deactivation, but possibly a mechanism by which eosinophils undergo a terminal differentiation after entering a tissue that is capable of providing them with an IL-5-rich condition.

### 3.2.6 Role of Ly6C glycoprotein in eosinophil development

Knowing that Ly6C expression on eosinophils is associated with enhanced cytotoxic activity and possibly a differentiation status in the TME of primary and metastatic breast cancer, I further wanted to investigate if Ly6C expression defines eosinophil subsets maturing in a controlled ex vivo setting. Eosinophils can be derived from bone marrow progenitors with a well-established protocol[245]. Briefly, following isolation of bone marrow from C57/Bl6 mice, progenitor cells are expanded for 4 days in the presence of murine stem cell factor (mSCF) and FMS-related tyrosine kinase 3 ligand (Fltl3) and afterwards eosinophil differentiation is driven by IL-5 for at least 10 days (Figure 3.10A). Following this protocol, Siglec-F expression was investigated every 2 days and over 95% of viable cells were Siglec-F+ after exposure to IL-5 for 10 days (Figure 3.10B).

Surface expression of Ly6C and CCR3 was analysed by flow cytometry every 2 days from day 8 onwards of ex vivo culture. Day 8 was selected as the first day to assess the surface expression of Ly6C and CCR3 on eosinophils, as they represented at least 10% of all viable cells at this time point. This analysis revealed that while eosinophils are defined by homogenous expression of Siglec-F (Figure 3.10C), the population of eosinophils is heterogeneous and actively transitioning through different Ly6C and CCR3 defined states. Eosinophils on day 8 were all CCR3-, however, split into 2 subsets based on their Ly6C positivity – CCR3- Ly6C- and CCR3- Ly6C+. On day 10, the appearance of a Ly6C+ CCR3+ population was observed and the time course analysis revealed that between day 12 and day 14, this subset became the most abundant. Afterwards, from day 14 onwards, the CCR3+

Ly6C- eosinophil population was increasingly more prevalent. While the original protocol suggests culturing eosinophils only up to day 14, continuous culture for 4 extra days showed that all eosinophils became CCR3+, and were divided into CCR3+ Ly6C+ and CCR3+ Ly6C- populations (Figure 3.10D and E).

To better understand the continuity of bone marrow-derived eosinophil development, the CCR3- Ly6C+, CCR3+ Ly6C+, and CCR3+ Ly6C- populations were FACS sorted and cultured in the presence of IL-5. After 2 days in the presence of IL-5, over 95% of the CCR3- Ly6C+ eosinophil population transitioned to the CCR3+ Ly6C+ state (Figures 3.10F and G). Furthermore, the population of CCR3+ Ly6C+ eosinophils was gradually transitioning to the CCR3+ Ly6C- state over 10 days, with over 60% of the parental CCR3+ Ly6C+ eosinophils fully transitioned on day 10 (Figure 3.10G). In contrast to the populations of CCR3- Ly6C+ and CCR3+ Ly6C+ eosinophils, the sorted population of CCR3+ Ly6C- eosinophils remained unchanged over the whole 10 days of IL-5 culture (Figure 3.10G).

These results were used to propose a model in which eosinophils in ex vivo culture undergo 3 steps of maturation: 1) from CCR3- Ly6C- population to CCR3- Ly6C+, 2) from CCR3- Ly6C+ to CCR3+ Ly6C+, and 3) downregulation of Ly6C by the CCR3+ Ly6C+ population, resulting in CCR3+ Ly6C- eosinophils subset (Figure 3.10H). To further confirm that all eosinophils eventually lose their Ly6C expression and remain in the terminally differentiated CCR3+ Ly6C- state, eosinophil differentiation was continued until day 30, double the time previously reported by others[245]. As expected, all CCR3+ Ly6C+ eosinophils gradually lost the expression of Ly6C (Figure 3.10I). Supportive of the fact that the CCR3+ Ly6C- population might represent the terminal stage of eosinophil development was the decreasing viability from day 27 onwards (Figure 3.10J).

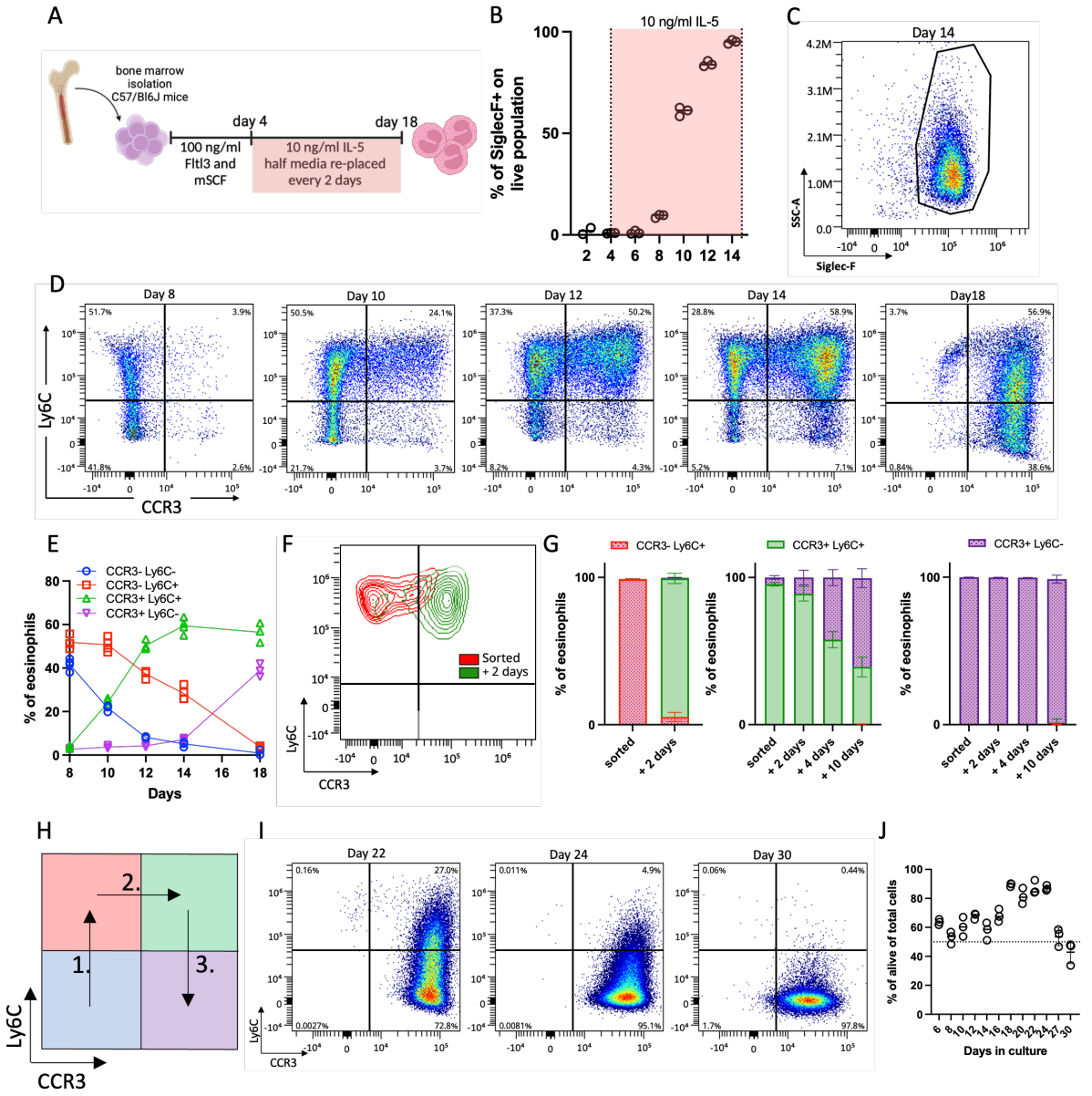


**Figure 3.10. Role of Ly6C and CCR3 expression in eosinophil development in vitro. (A)** Overview of the bone marrow-derived eosinophil culture from C57/Bl6 mice. Bone marrow cells were first cultured with Fltl3 and mSCF for 4 days and then differentiated into eosinophils with IL-5 until day 18. **(B)** Relative proportion of eosinophils (Siglec-F+) in cell culture analysed by flow cytometry on the indicated days. Data are representative of 2 independent experiments (n = 3). **(C)** Representative density plot showing the gating strategy used to identify eosinophils based on Siglec-F expression. **(D)** Representative flow cytometry plots showing different expressions of Ly6C and CCR3 receptors on a population of Siglec-F+ eosinophils on the indicated days. **(E)** Time course analysis of the proportion of the Ly6C- CCR3-, Ly6C+ CCR3-, Ly6C+ CCR3+, and Ly6C- CCR3+ eosinophils analysed by flow cytometry every 2 days from day 8 onwards. **(F)** Flow cytometry contour plot showing Ly6C and CCR3 expression of sorted Ly6C+ CCR3- cells on day of sorting (red) and after 2 days in culture with IL-5 (green), **(G)** with quantification of Ly6C+ CCR3- and Ly6C+ CCR3+ populations on day 0 and day 2 of culture; and quantification of CCR3+ Ly6C+ and CCR3+ Ly6C- (purple) eosinophils on day 0, day 2, day 4 and day 10 post sorting of CCR3+ Ly6C+ and CCR3+ Ly6C- as indicated. Data are representative of two independent experiments (n = 3). **(H)** Schematic overview of the proposed eosinophil differentiation model ex vivo, defined by Ly6C and CCR3 expression. **(I)** Representative flow cytometry plots showing different expressions of Ly6C and CCR3 receptors on a population of Siglec-F+ eosinophils on the indicated days. **(J)** Viability of eosinophils throughout the ex vivo differentiation experiment (n=3). Data are representative of 2 independent experiments and show individual values + median.

### 3.2.7 Investigating anti-tumorigenic properties of bone marrow-derived eosinophils

Following the results pointing at eosinophil heterogeneity when differentiated ex vivo, I hypothesised that CCR3+ eosinophil subsets could be representative of the tumour-infiltrating eosinophil population. The CCR3+ population of the bone marrow-derived eosinophils was selected as it is a fully mature population that would be the most representative of the mature tissue resident eosinophils that internalised the CCR3 receptor upon the tumour infiltration. To investigate the cytotoxic potential of these 2 subsets, CCR3+ Ly6C+ (Ly6C+) and CCR3+ Ly6C- (Ly6C-) eosinophils were differentiated from the bone marrow for 18 days, FACS sorted, characterised by H&E staining and used in a direct co-culture with E0771 mCherry-hCD2 cancer cell line of Bl6 background (Figure 3.11A).

Firstly, eosinophil subsets present in bone marrow-derived eosinophil culture were characterised by histopathology and flow cytometry. Both, Ly6C+ and Ly6C- sorted eosinophils had similar nuclear morphology, however, Ly6C+ eosinophils were more granular and had a higher intensity of eosin stain (Figure 3.11B). Eosinophil maturity, granularity and activation of the three eosinophil subsets on day 18 were investigated by flow cytometry. While CCR3+ Ly6C- eosinophils presented with the highest expression of Siglec-F (Figure 3.11C), suggesting their terminal differentiation and maturity, CCR3+ Ly6C+ eosinophils were the most granular of the 3 studied populations (Figure 3.11D) and expressed higher levels of degranulation marker CD63 than CCR3+ Ly6C- eosinophils (Figure 3.11E). CCR3- Ly6C+ eosinophils were not used for the cell killing assays because based on the studied markers, they represented a more immature population that would not be representative of the tumour-associated eosinophils.

To optimise the cell killing assays, E0771 cells were first co-cultured with unsorted eosinophil population at following eosinophil to E0771 ratios – 0:1, 1:1, 5:1. Annexin-V flow cytometry read-out has clearly separated Annexin-V+ apoptotic E0771 cells stained by fixable live/dead dye in all conditions (Figure 3.11F), and eosinophils induced apoptosis at both 1:1 and 5:1

ratios compared to E0771 cells cultured without eosinophils (Figure 3.11G). The lower ratio of 1:1 was used with sorted eosinophils to enable more biological and technical repeats with sorted cells. The fold change difference of apoptotic dead E0771 cells analysed in Ly6C+ co-cultures was approximately 3-fold higher than from co-cultures with Ly6C- eosinophils (Figure 3.11H). These results suggested that Ly6C+ and Ly6C- eosinophils are a good substitute for studying cytotoxic properties of Ly6C-related phenotype outside of tumours.

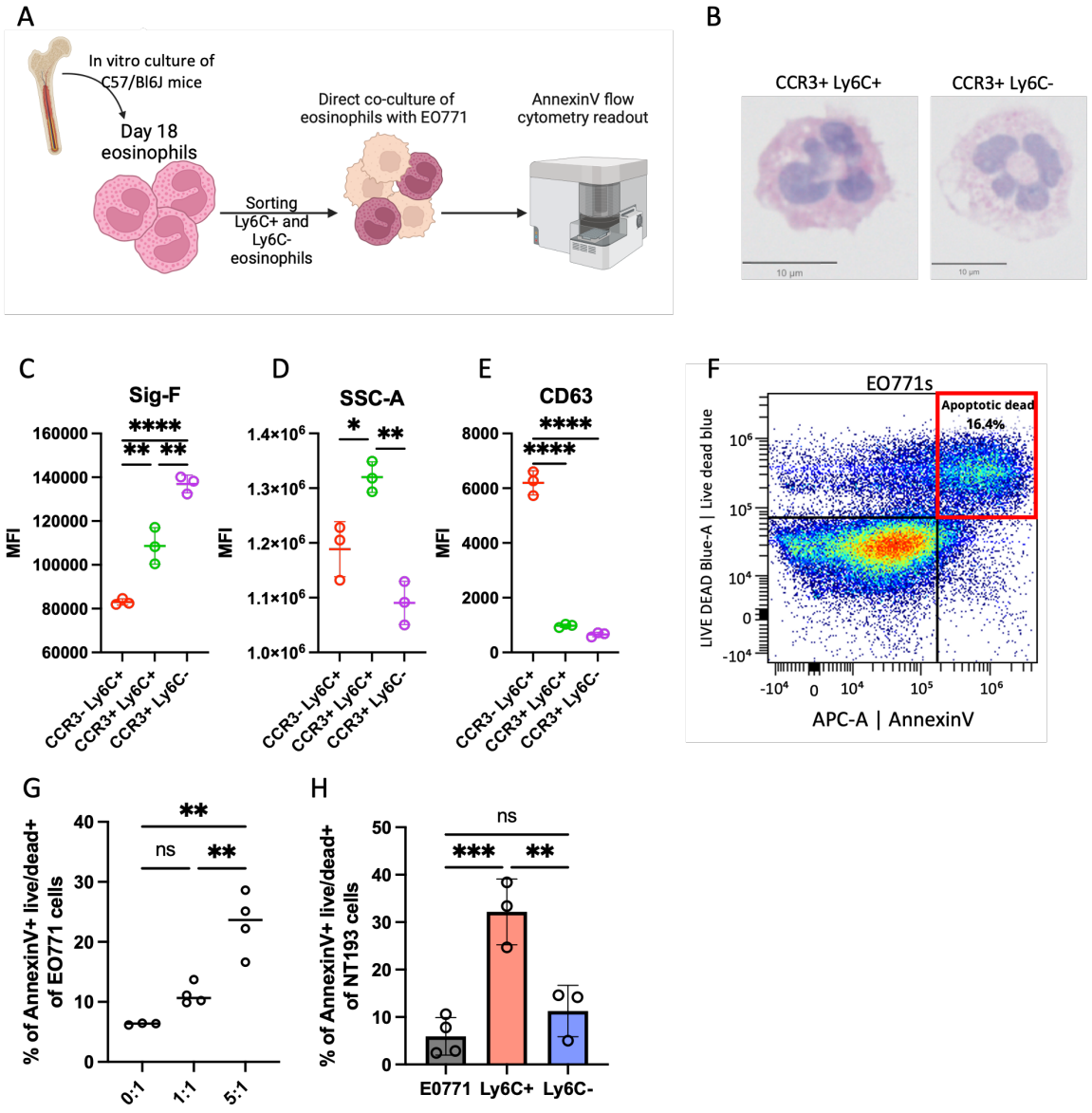


**Figure 3.11. Direct co-culture of eosinophils with the E0771 tumour cell line results in increased apoptosis of cancer cells. (A)** Overview of the experimental approach. Bone marrow-derived eosinophils from C57/Bl6 mice were cultured for 18 days and FACS sorted into CCR3+ Ly6C+ and CCR3+ and Ly6C- populations that were directly co-cultured with E0771 cancer cells for 24 hours and analysed by Annexin-V and fixable live/dead staining. **(B)** Haematoxylin and eosin (H&E) staining of cytospun Ly6C+ and Ly6C- eosinophils sorted on day 18. The image is representative of $10x10^5$ cells cytospun for each subset. **(C-E)** Flow cytometry analysis of ex vivo cultured eosinophils on day 18. Comparison of Siglec-F expression **(C)**, side-scatter intensity **(D)**, and CD63 expression **(E)** between

Ly6C+ and Ly6C- eosinophils on day 18 of cell culture (n = 3). **(F)** Representative flow cytometry plot showing Annexin-V and fixable live/dead staining that distinguishes the apoptotic E0771 cancer cell population. **(G)** Optimisation of cell killing assay with unsorted eosinophils on day 14 of in vitro culture (n = 4). Different ratios of eosinophils to E0771 cells were tested and the relative proportion of annexin-V+ Live/dead stained E0771 population was quantified. **(H)** Proportion of E0771 apoptotic cells after 24 hours of co-culture with no eosinophils or FACS-sorted Ly6C+ or Ly6C- BM-derived eosinophils. Data are representative of 2 independent experiments. E0771 n=4, Ly6C+ n=3, Ly6C- n=3. Data show individual values + median and were analysed by 2-way ANOVA for comparison of 2 and more groups. Data show individual values + median and were analysed by Student's t-test. Statistical significance is displayed on figures as follows: *p < 0.05, **p < 0.01, ***p<0.001, ****p<0.0001.

### 3.2.8 Eosinophil depletion in the NT193 model enhances tumour growth

Given the evidence that Ly6C+ eosinophils are present in NT193 tumours from day 7 onwards, are more cytotoxic than Ly6C- eosinophils, and represent 60% of total TAE on day 18, their function was further investigated in vivo. FVB mice were grafted with the NT193 cell line and eosinophils were depleted by anti-Siglec-F antibody on the day of engraftment. Afterwards, anti-Siglec-F treatment or IgG2a isotype control was administered 3 times per week to maintain eosinophil reduction. Eosinophil depletion was confirmed in blood on day 0, 7 and at the final harvest on day 14 in both blood and tumours by flow cytometry (Figure 3.12A). To confirm depletion of eosinophils in blood, expression of CCR3 was used instead of Siglec-F, to avoid potential internalisation of Siglec-F in response to the treatment (Figure 3.12B). Eosinophil levels were significantly reduced on day 7 and day 14 in mice treated with anti-Siglec-F (Figures 3.12C and D). Because eosinophils internalise the CCR3 receptor in the TME, the combination of CCR3 and low expression of MHC-II was used when analysing the myeloid population (CD45+, CD11b+, F4/80+) (Figure 3.12E). Eosinophils were significantly reduced in the TME of the anti-Siglec-F- compared to isotype- treated mice (Figure 3.12F) and eosinophil depletion resulted in increased tumour weight on day 14 (Figure 3.12G) and enhanced tumour growth (Figure 3.12H).

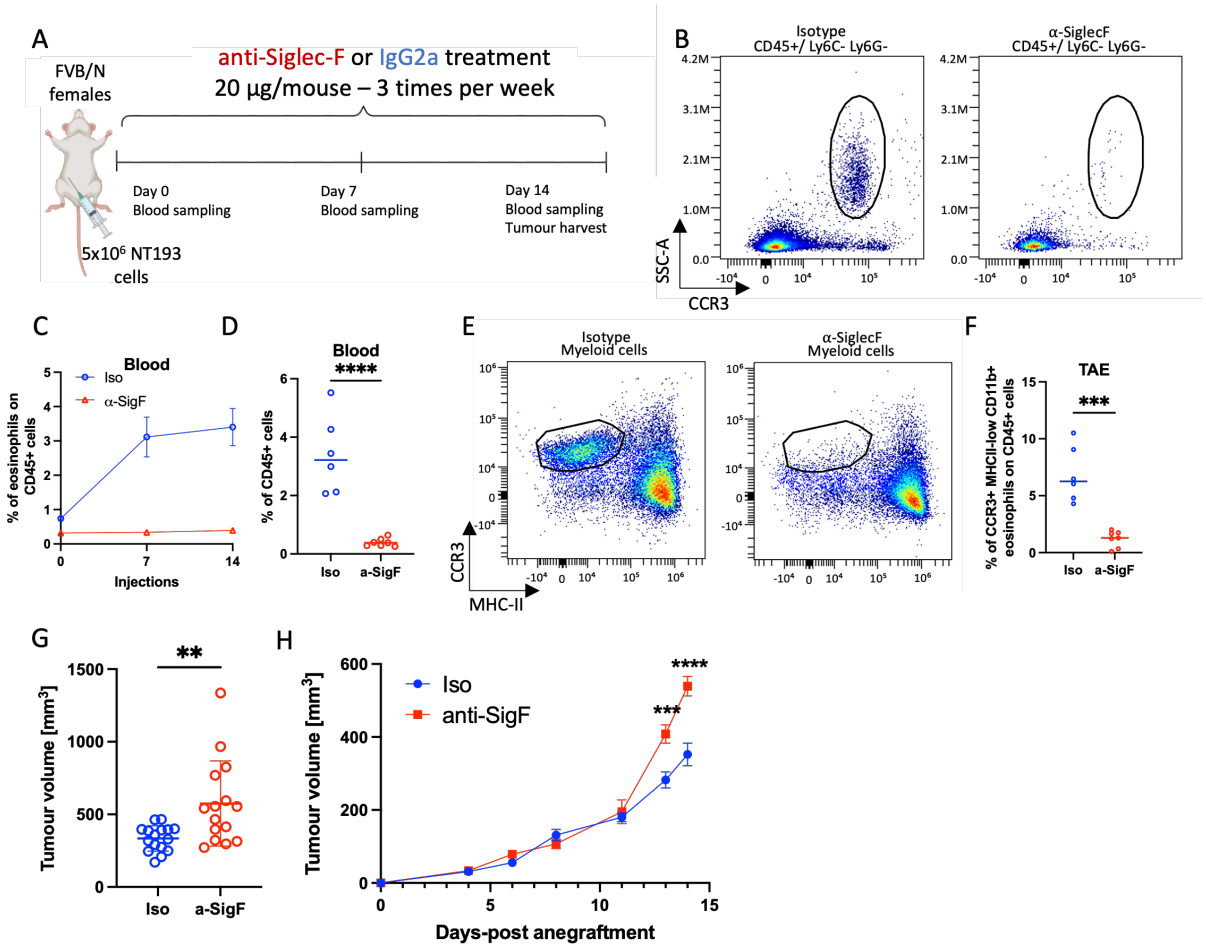


**Figure 3.12. Depletion of eosinophils in NT193 tumours does not alter tumour growth. (A)** Overview of experimental plan. FVB mice bearing orthotopic NT193 tumours were treated with anti-Siglec-F or IgG2a (n = 6) antibodies 3 times a week and eosinophil depletion was confirmed throughout the experiment by blood sampling and at the final time point in tumours. **(B)** Representative flow cytometry plot comparing eosinophil gating in the blood of anti-Siglec-F and IgG2a (Isotype) treated mice. **(C)** Quantification of relative eosinophil proportions in the blood of eosinophil-depleted (a-SigF, n=7) and control (Iso, n=6) animals on the indicated days. **(D)** Quantification of relative eosinophil proportions in the blood of a-SigF and Iso animals on day 14. **(E)** Representative flow cytometry plot comparing eosinophil gating in tumours. Alternative markers such as CCR3 and low levels of MHC-II were used to identify eosinophils independently of Siglec-F expression. **(F)** Quantification of relative eosinophil (CD11b+, CCR3+, MHC-II-low) proportions in tumours of Iso (n=6) and a-SigF (n=7) mice on day 14. **(G)** Tumour volumes of Iso (n=16) and a-SigF (n=15) mice on day 14. Data are pooled from 3 independent experiments. **(H)** Tumour growth curves of Iso and a-SigF mice, data represent mean + SEM. Data are representative of 3 experiments, show individual values + median unless otherwise stated, and were analysed by Student's t-test. Statistical significance is displayed on figures as follows: *p < 0.05, **p < 0.01, ***p<0.001, ****p<0.0001.

## 3.3 Technical discussion

The initial aim of this chapter was to study the translational activity of tumour-associated macrophages in NT193 tumours. To do this, we chose to first optimise the SUnSET assay[242] based on puromycin incorporation into nascent proteins. This method has several advantages compared to other methods used for studying translational activity, 1) puromycin is a non-radioactive labelled substrate with an equivalent incorporation rate to radioactively labelled amino acids, 2) it provides easily accessible flow cytometry read-outs, and 3) is an affordable alternative to *O*-propargyl-puromycin (OP-Puro), an analogue of puromycin detectable by Click-chemistry that can be used for both fluorescent labelling and purification of nascent proteins[243]. Because of the similarities with the OP-Puro, the low toxicity and the initial in vitro tests showing the high specificity of the intracellular staining by anti-puromycin antibody (Figure 3.1F), I used the SUnSET assay to study protein synthesis in NT193 tumours.

These experiments, however, detected a subset of tumour-infiltrating lymphocytes (TILs) specifically labelled by anti-puromycin antibody in mice that were not injected with puromycin (Figure 3.2). At first, the non-specific binding of anti-puromycin antibody led us to speculate whether these cells might be an artefact caused by the presence of puromycin used in the media during the culture of NT193 cells. However, the puromycin staining of myeloid cells was still present even after withdrawing puromycin from the NT193 culture prior to engraftment (Figure 3.13). Therefore, a more detailed characterisation of this cell cluster led to the identification of a previously missed eosinophil population. Technical challenges of studying this cell type and explanations for non-specific antibody staining are discussed below.

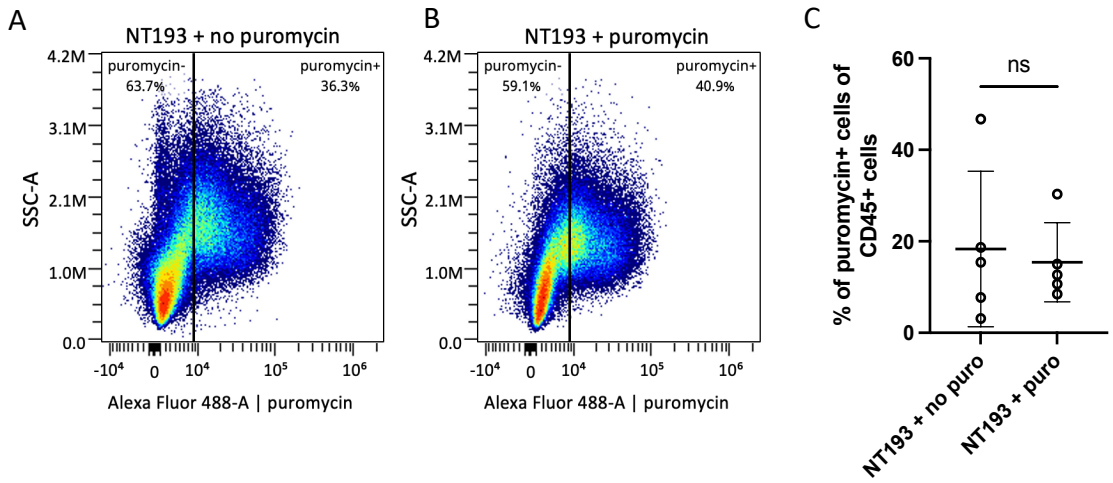


**Figure 3.13. Withdrawal of puromycin from NT193 tumour cells in culture does not alter puromycin staining of tumour-associated myeloid cells.** NT193 cancer cells were cultured in the presence of puromycin as previously reported[228], or puromycin was withdrawn from the culture immediately after the cells were thawed. Afterwards, $5x10^6$ NT193 cells cultured in the presence or absence of puromycin were grafted into the 4th mammary fat pad of FVB/N female mice, tumours were monitored, harvested on day 18 and processed for intracellular puromycin staining. **(A, B)** Representative flow cytometry plot of intracellular puromycin staining of tumour-associated myeloid cells in tumours generated with NT193 cancer cells cultured in the absence (NT193 + no puromycin, n = 5) or presence (NT193 + puromycin, n = 5) of puromycin. **(C)** Quantification of the relative proportion of puromycin+ cells of CD45+ immune cells in NT193 + no puromycin and NT193+ puromycin generated tumours. Data are representative of one experiment. Data show individual values + mean with SD and were analysed by Student's t-test. Statistical significance is displayed on figures as follows: *p < 0.05, **p < 0.01, ***p<0.001, ****p<0.0001.

### 3.3.1 Technical challenges of studying eosinophils

Eosinophils are a population of granulocytes that are often missed or overlooked in many tissues, tumour microenvironment included, due to technical caveats as previously summarized[268]. The first encountered challenge of working with eosinophils in this chapter is the non-specific staining with intracellular antibodies. Even though not mentioned in the results, I observed that eosinophils are non-specifically stained even with 5-ethynyl 2´-deoxyuridine (EdU) click-chemistry staining based on the biorthogonal azide-alkyne reaction (Figure 3.14). Both of these staining methods, antibody or click chemistry-based, require permeabilisation of the cytoplasmic membrane, which is likely to result in permeabilisation of the membrane of eosinophilic granules. Eosinophils carry cationic protein-rich granules that maintain an acidic pH of around 5.1[269], enabling the canonical staining with negatively charged eosin dye. It is possible that the pH is altering the affinity of antibodies which afterwards non-

specifically label the granules. This, however, does not explain the high background of click-chemistry-based staining.

It was previously shown that heparin reduced the background of intracellular antibody staining in mass cytometry experiments, due to the reduction of negatively charged metal-based interactions[270]. The charge-based interactions might also be present in flow cytometry staining, as a group of Alexa Fluor (AF) fluorochromes is known to be negatively charged. The negative charge of AF-conjugated antibodies might be enhancing their affinity towards the acidic granules. All intracellular staining performed in this chapter was done with either AF488 or AF647 which might have affected the click chemistry reaction.

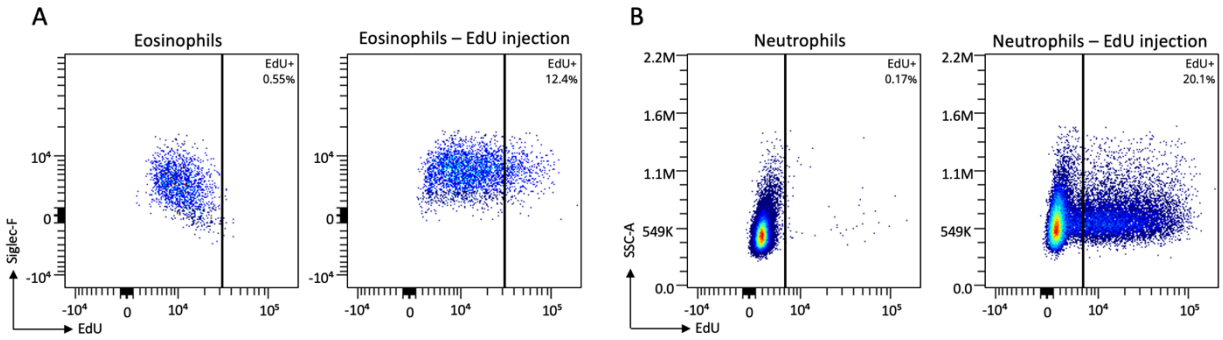


**Figure 3.14. Non-specific staining of eosinophils by EdU click-reaction kit.** FVB mice bearing NT193 tumours were intravenously injected with 1mg of EdU to understand eosinophil proliferation in bone marrow and tumours. Healthy mice not injected with EdU were used as controls to determine EdU background staining. **(A)** Representative flow cytometry plot comparing EdU signal in eosinophils of healthy mice (n =3) and EdU pulsed mice (n =3) in eosinophils and **(B)** neutrophils in the bone marrow. Data are representative of one experiment.

Another caveat of studying eosinophils is their low amount of mRNA and high levels of RNases stored in the granules, making it difficult to capture their transcriptomic signature. This explains why eosinophils were absent from the scRNA-seq dataset of CD11b+ myeloid cells previously generated in the Midwood lab. Furthermore, eosinophils are not present in any of the current datasets looking at myeloid cells in orthotopic breast tumours[271] and are absent even in murine tissues where their presence is well established, such as lungs[272]. It is important to notice that new protocols are being developed to obtain high-quality RNA that allows sequencing of eosinophils at single cell level[126].

As eosinophils express low levels of Ly6G receptor, a well-established neutrophil marker, and neutrophils express low levels of Siglec-F, the main eosinophil marker, I wanted to confirm that these two populations are distinct. In this chapter, I used real-time qPCR to compare levels of eosinophil peroxidase on the transcriptional level (Figure 3.4D). Because neutrophils are of low abundance in NT193 tumours at late stages of tumour growth, I used the 4T1 model for sorting of myeloid populations to obtain enough cells of both, eosinophil and neutrophil populations, needed for RNA processing. Because analysis of granulocytes is affected by the low RNA levels and transcriptional activity, I optimised the qPCR protocol in the following way, 1) all myeloid populations were sorted directly into RNA lysis buffer (RLT) to minimise loss of cells after sorting, 2) RLT was enriched with 1% beta-mercaptoethanol to denature RNases, 3) RNA was isolated with RNeasy Micro Kit suitable for isolating small amounts of RNA, and 4) carrier RNA was added to the samples before isolation to improve RNA recovery. In further sorting experiments, MACS enrichment steps were used to reduce sorting time and avoid pooling of tumours.

MACS enrichment steps were also utilised to enrich eosinophils through Siglec-F magnetic beads prior to sorting tumour-associated eosinophils used in cell killing assays. As previously reported, eosinophils are prone to degranulation as a response to physical stress[126], therefore, the FACS sorting strategy was adjusted to obtain viable eosinophils with minimal impact on their functionality. First, I used the 100 μm nozzle for FACS sorting, the largest available at our facility, with a low sheath pressure to reduce microfluidic pressure. Second, eosinophils were collected into complete RPMI media containing IL-5 to increase their long-term viability. Third, all isolated eosinophils were spun down at a lower g-force for longer times to prevent any additional cell damage and degranulation. While all of these steps allowed us to sort highly viable eosinophils capable of cell killing, I noticed that the overall cell killing capability is higher in eosinophils sorted from cell culture when compared to TAE. It is possible that the tumour digestion causes additional stress that stuns eosinophils' cytotoxicity. Because reducing the

time of digestion would result in much lower cellular yield, cell killing assays were prolonged to 3 days, to allow eosinophils to recover from the tissue processing.

### 3.3.2 Utilisation of the mCherry niche-labelling model for eosinophil labelling

Eosinophils were previously associated with anti-tumorigenic properties in the context of breast cancer lung metastasis in murine models[166,167]. To fully explore how the metastatic niche affects eosinophil phenotype, the mCherry niche labelling strategy was used (Figure 3.7)[233,241]. Even though eosinophils were previously reported to be present in the metastatic lesions by histopathology techniques[166,167], I was not able to detect eosinophils by flow cytometry in the mCherry niche. In contrast, there was a clear population of alveolar macrophages used as a positive control. As mentioned in the original protocol[241], not all cell types are equally efficient in receiving the lipid-soluble mCherry (sLP-mCherry) vector. It is therefore possible that eosinophils are not an efficient recipient cell type. Alternatively, if the sLP-mCherry vector permeabilizes eosinophils and reaches the eosinophil granules, mCherry fluorescent intensity is likely to decrease[273].

Additionally, it was recently shown that macrophages are labelled by mCherry protein expressed by cancer cells even in the absence of the lipid-soluble linker attached to the mCherry protein. These results suggest that more technical controls are necessary to understand the extent of mCherry uptake by phagocytic cells[30]. In this chapter, CD64+ macrophages were the most abundant population identified in the metastatic niche. However, non-myeloid lymphocytes labelled by mCherry also presented with an expression of phagocytic receptor CD64. It is unclear if this signal was a result of CD64 surface expression or an artefact of cellular interactions in situ. There is therefore a possibility that the mCherry niche labelling might be enhanced by mCherry+ macrophage fragments attached to neighbouring cells, as the effect of macrophage fragmentation was already observed and described in other tissues[45]. More technical controls and imaging techniques would be

necessary to understand the extent of potential macrophage fragmentation artefacts in these experiments.

### 3.3.3 Limitations of eosinophil depletion through antibody targeted treatment

To understand how eosinophils contribute to pro- or anti-tumorigenic properties of the NT193 TME, tumour growth of eosinophil-depleted mice was compared to the control isotype-treated group (Figure 3.12). A treatment strategy using an anti-Siglec-F antibody used for selective depletion of eosinophils in FVB mice with spontaneous tumours[184] was adopted. As previously reported, the treatment with the anti-Siglec-F antibody might lead to internalisation of Siglec-F receptors, and incomplete depletion of eosinophils and subsequent false-positive reporting of absence of Siglec-F+ cells[274]. Therefore, alternative gating strategies were used to identify eosinophils without the potential bias of staining for Siglec-F (Figures 3.12B and E). CCR3 expression, high granularity and low levels of MHC-II expression were used to analyse blood and tumours, with a clear eosinophil population identified in control mice but not the mice treated with anti-Siglec-F antibody. Additionally, eosinophil-deficient mouse models were considered[275]. However, all of the currently available strains are on C57/Bl6 or Balb/c background and back-crossing these strains with FVB mice would be necessary for at least 10 generations. This was not possible in the time available within this project.

## 3.4 Biological discussion

Eosinophils (Siglec-F+, F4/80+ myeloid population) represented up to 30% of all tumour-infiltrating lymphocytes (TILs) in NT193 orthotopic mammary tumours grafted in FVB mice (Figure 3.4A). This population was previously unrecognised in the NT193 model and all F4/80+ cells were attributed to macrophages when analysed by immunofluorescent staining[92,228,238]. This issue is not restricted to the NT193 model, with F4/80 being commonly used as a sole marker of macrophages for imaging[276,277] or MACS isolations of macrophages[278]. Therefore, the usage of additional markers to define macrophages should be considered when using the NT193 or other murine breast cancer models in the future. How eosinophil presence might influence the previously described macrophage findings in the NT193 tumour model is further studied in Chapter 5.

Because eosinophils are otherwise reported to be a rare type of TILs, mouse models overexpressing IL-5[125,170] or intraperitoneal injections of IL-5[240] are being used in order to induce eosinophil infiltration and enable their further study. However, the NT193 model has a naturally high level of eosinophils and thus represents a great tool for studying eosinophils in wild-type animals without affecting other parts of immune responses through unphysiological levels of IL-5. Whether the NT193 tumours possess higher levels of IL-5 compared to the 4T1 or E0771 tumours was not investigated; however, IL-5 levels could be assessed by Enzyme-Linked Immunosorbent Assay (ELISA) of tumour supernatants in future experiments.

Following the surprising finding of eosinophil infiltration in NT193 tumours, eosinophil presence was investigated in 2 other well-established murine breast cancer models – E0771 and 4T1 on C57/Bl6 and Balb/c background, respectively. As expected, eosinophils represent up to 3% of all TILs in E0771 tumours 18-22 days post engraftment (Figure 3.4A)[199]. These findings also fit well with the C57/Bl6 mouse model known to be skewed towards stronger Th1 immune responses[85]. However, eosinophils represented around 10% of all TILs in 4T1

tumours (Figure 3.4A). While this is not matched with the published data reporting eosinophils below 1% of all TILs[189], similar levels were previously reported in a publicly available thesis[240]. Because of these discrepancies with the literature and neutrophils are known to express Siglec-F, eosinophil cell identity was confirmed in 4T1 tumours by comparison of eosinophil peroxidase expression to mRNA levels, surface expression of canonical eosinophil markers and morphology of other myeloid cell types to confirm their cell identity (Figure 3.4). These data collectively prove that eosinophils are an overlooked population in certain orthotopically engrafted mammary tumours.

### 3.4.1 Selection of Ly6C marker to define eosinophil subpopulations

Despite known eosinophil infiltration in breast tumours, there is currently no available dataset describing their phenotypical adaptation on transcriptomic or translational levels in this disease. Ly6C glycoprotein, commonly used as a marker of monocytes or short-lived CD4+ T cells, has clearly defined 2 populations of eosinophils in NT193 tumours, using spectral flow cytometry (Figure 3.5C and D). Ly6C receptor, encoded by *Ly6c1* and *Ly6c2* genes, is a member of the lymphocyte antigen-6 family (Ly6) of GPI-anchored proteins, with currently no known human ortholog[279]. The functional role of Ly6C on cell types defined by its expression is currently unknown, even though Ly6C expression was suggested to be regulated by type I and II interferons and IL-27 on CD4 and CD8 T-cells[280]. Eosinophil plasticity was recently investigated in the context of colorectal cancer, and two eosinophil subsets matched in murine and human scRNA-seq analysis were described, both differing from control eosinophils by their response to interferon gamma (IFNγ)[170]. However, in that study, eosinophils were analysed by scRNA-seq without pre-sorting for Siglec-F+ cells as part of all CD45+ cells. Further transcriptomic analysis of this data set revealed that even though *Ccr3* expression was recognised to be upregulated in the cluster that was assigned eosinophil identity, *Siglecf* or *Adgre1* (F4/80) gene transcripts were not detectable. Therefore, *Ly6c1* and *Ly6c2* gene expression was not further investigated in this dataset.

Ly6C surface expression, or *Ly6c1* and *Ly6c2* gene expression can be observed in publicly available datasets focusing on eosinophil biology, however, it was previously not used as a cluster-defining marker. *Ly6c2* is in the top 100 markers for immature and progenitor eosinophils present in the bone marrow and blood of IL5-Tg mice[125]. In a recent study, eosinophilopoiesis occurring in murine bone marrow was described to consist of 4 maturation stages. Ly6C protein is one of the 6 most overexpressed surface receptors during stage II and III of eosinophilopoiesis, and is detected among the top gene markers for stage III maturation[98]. Furthermore, in a systematic review analysing publicly available bulk RNAseq data of tissue-resident eosinophils from bone marrow, lung, and gastrointestinal tract together with bone marrow-derived cultured eosinophils, the *Ly6C2* gene is detected as differentially expressed in each comparison performed, with the highest expression recorded in cultured and tissue-resident bone marrow eosinophils[281]. Overall, Ly6C expression on both mRNA and protein levels in eosinophils is well documented and under homeostatic conditions seems to be regulated during eosinophil differentiation.

While other eosinophil markers important for eosinophil survival and migration, such as CCR3 or IL-5Ra, were investigated by flow cytometry (Figure 3.5C), the levels of their expression were not usable for distinguishing different eosinophil subsets. Therefore, this work further focused on understanding the regulation and functional differences between Ly6C+ and Ly6C- eosinophils in the TME.

### 3.4.2 Ly6C is an important marker for eosinophil maturity/differentiation

Ly6C+ eosinophils represent 95% of all eosinophils at an early time point of tumour development and this subset was reduced to around 50-70% 18 days post-engraftment in both NT193 and E0771 tumours (Figure 3.5 E and F). As discussed above, Ly6C was previously linked with eosinophil differentiation. Therefore, I hypothesised that the Ly6C- population appearing at later stages of tumour development is derived from Ly6C+ eosinophils infiltrating

the tumours early on. In favour of this hypothesis, eosinophils in the bone marrow and blood of the corresponding mice on day 18 of tumour development were exclusively Ly6C+. As the half-life of eosinophils in circulation can be as short as 3 hours[282] and all circulating eosinophils were found to be Ly6C+, it is unlikely that Ly6C- eosinophils are infiltrating tumours straight from circulation on day 18 of tumour growth. Furthermore, even though there is a minor tissue-resident population of eosinophils in mammary fat pads expressing relatively high levels of Ly6C compared to other lymphocytes (Figure 3.8A), eosinophils are not known to be proliferating out of bone marrow and therefore resident eosinophils are a minor contribution to the eosinophilic population observed during tumour progression. Additionally, the isolation of Ly6C+ tumour-infiltrating eosinophils and their culture under homeostatic IL-5-rich conditions led to the downregulation of Ly6C (Figure 3.9). It is important to notice that IL-5 shares a common β-chain receptor with GM-CSF and IL-3[283] and therefore IL-5 might not be an exclusive factor supporting this transition in tissue.

Tracking the development of eosinophils derived from bone marrow progenitors has revealed that Ly6C is not only an important differentiation marker in TME but that in combination with the CCR3 receptor distinguishes 4 different stages of eosinophilopoiesis ex vivo (Figure 3.10). These results are of particular importance as the well-established protocol for bone marrow-derived eosinophil culture leading to these results was used to draw conclusions based on a number of assays such as 1) response of eosinophils to cytokines analysed by bulk RNA sequencing[125], 2) studying effect of gene knockouts on eosinophil development[284], and 3) tracking eosinophil migration post in vivo transfer[285] – all using Siglec-F+ cells as a homogenous population on day 14 of culture. However, Siglec-F+ cells on day 14 consist of four eosinophil subsets, differing by their granularity and presumably with different migration abilities based on the diverse expression of the CCR3 eotaxin receptor. Altogether, this is likely to impact the results of these assays in an unpredictable manner, and further characterisation of these clusters and their responses to cytokine stimulation is described in more detail in Chapter 4.

Finally, data in this chapter suggest that the lungs of mice bearing breast cancer metastasis induced by E0771 and 4T1 also present with reduced levels of Ly6C+ eosinophils, with preliminary data linking this phenotype to more advanced disease. However, analysis of the bulk RNAseq dataset of eosinophils isolated from healthy and PyMT metastatic lungs of C57/Bl6 wild-type mice did not confirm differential expression of *Ly6c1* or *Ly6c2* between these 2 conditions[166]. Therefore, a thorough analysis with more biological replicates in each of these tumour models inducing lung metastasis would be needed to understand the adaptation of eosinophils to the metastatic TME.

### 3.4.3 Loss of cytotoxic properties in Ly6C- eosinophils

Eosinophil infiltration did not correlate with tumour sizes in the NT193 model (Figure 3.6A), however, higher infiltration of Ly6C+ eosinophils is linked with smaller tumour weights (Figure 3.6B). Ly6C+ eosinophils sorted from late tumours were also more granular and cytotoxic in direct co-cultures with the NT193 cancer cell line (Figure 3.6 C-J). However, lower granularity and cytotoxicity of Ly6C-eosinophils might not be directly indicative of the eosinophil role in tumour progression in all cases. The TME of subcutaneous MC38 colon cancer also shapes eosinophils into a less degranulated phenotype, when compared with circulating eosinophils from the same C57/Bl6 mice[102], but in this model, depletion of eosinophils resulted in greater tumour sizes. Therefore, decreased granularity might also be interpreted as capturing eosinophils that had already degranulated in the TME and contributed to the anti-tumorigenic response. It would be interesting to know the Ly6C status of eosinophils in the MC38 tumours and whether they are also transitioning into the Ly6C- state or maintain the proposed active Ly6C+ phenotype during the whole study.

Supporting the hypothesis of tumour-infiltrating eosinophils being directly cytotoxic in our in vivo model is also the fact that systemic depletion of eosinophils in FVB mice bearing NT193

tumours resulted in increased tumour weight (Figure 3.12G, H). As mentioned before, eosinophil depletion was not previously not observed to alter the tumour growth in other murine models of primary breast cancer[184,188,199]. It is possible that this is due to the lower eosinophil prevalence in the orthotopic 4T1 and E0771 models or the spontaneous KEP model; however depletion of highly prevalent eosinophil population in NT193 tumours pointed to eosinophil cytotoxicity. In the experiment with the NT193 model, eosinophils were depleted on the day of the tumour engraftment, therefore, tumours developed in the absence of all eosinophils, predominantly Ly6C+ cytotoxic eosinophils representing up to 95% of all eosinophils until day 7. It is therefore possible that TME actively shapes eosinophils into a less active Ly6C- state and evades the eosinophil cytotoxicity even in eosinophil-rich tumours. However, testing of eosinophil depletion treatment during late stages of development was not possible as tumours were reaching the humane endpoint on day 18 when Ly6C- eosinophils were becoming more prevalent.

In agreement with the ex vivo cell killing assays from the NT193 tumours, Ly6C+ bone marrow-derived eosinophils of C57/Bl6 mice were more granular and cytotoxic than the Ly6C- eosinophils (Figure 3.11). While this experiment does not recapitulate the complexity of the TME-shaped eosinophils, it provides evidence that in a controlled environment, Ly6C- eosinophils derived from the Ly6C+ subset are losing their cytotoxic properties. These data collectively suggest that breast TME actively shapes eosinophils into a less active state incapable of cell killing and that Ly6C might be one of the markers indicating the functional change of these eosinophil subsets. To further investigate how breast TME shapes eosinophils on a functional level, a comparison of the cytotoxicity of circulating to the tumour-infiltrating eosinophils would be necessary. However, such an experiment was not performed as eosinophils represent a minor population in the blood of all tested models using wild-type mice.

To more comprehensively compare these 2 newly described subsets with eosinophil phenotypes reported in the literature, a detailed characterisation of Ly6C+ and Ly6C- eosinophils was performed and is described in Chapter 4.

## 3.5 Appendix

**Appendix Table 3.1 Flow cytometry panel used for the SUnSET in vivo experiments**

| Fluorochrome | Marker | Clone | Manufacturer | Cat. No. | Dilution (1:x) |
|---|---|---|---|---|---|
| Blue | Live/dead fixable dye | | ThermoFisher | L23105 | 400 |
| Pacific blue | F4/80 | BM8 | BioLegend | 123124 | 100 |
| BV510 | MHC-II | M5/114.15.2 | BioLegend | 107635 | 200 |
| BV605 | CD206 | C068C2 | BioLegend | 141721 | 200 |
| BV650 | CD86 | GL-1 | BioLegend | 105035 | 200 |
| BV785 | Ly6C | HK1.4 | BioLegend | 128041 | 200 |
| PerCP-Cy5.5 | CD11b | M1/70 | BioLegend | 101227 | 200 |
| AF488 | Puromycin | 12D10 | Sigma-Aldrich | MABE-343 | 200 |
| PE | CD11c | N418 | BioLegend | 117307 | 200 |
| PE-Dazzle 594 | CD4 | GK1.5 | BioLegend | 100455 | 200 |
| APC | MHC-I | 34-1-2S | BioLegend | 114713 | 200 |
| AF700 | CD45 | 30-F11 | BioLegend | 103127 | 200 |

**Appendix Table 3.2 Flow cytometry panel used for eosinophil opt-SNE analysis**

| Fluorochrome | Marker | Clone | Manufacturer | Cat. No. | Dilution (1:x) |
|---|---|---|---|---|---|
| BUV395 | CX3CR1 | ZM-50 | BD Biosciences | 567821 | 100 |
| Blue | Live/dead fixable dye | | ThermoFisher | L23105 | 400 |
| BUV563 | IL33r (ST2) | U29-93 | BD Biosciences | 749324 | 100 |
| BUV737 | CCR5 | C34-3448 | BD Biosciences | 749670 | 100 |
| BUV805 | CD44 | IM7 | BD Biosciences | 741921 | 200 |
| Pacific blue | F4/80 | BM8 | BioLegend | 123124 | 100 |
| BV510 | MHC-II | M5/114.15.2 | BioLegend | 107635 | 200 |
| BV605 | CD206 | C068C2 | BioLegend | 141721 | 200 |
| BV650 | Ly6G | 1A8 | BioLegend | 127641 | 200 |
| BV785 | Ly6C | HK1.4 | BioLegend | 128041 | 200 |
| FITC | CXCR2 | SA044G4 | BioLegend | 149309 | 200 |
| PerCP-Cy5.5 | CD11b | M1/70 | BioLegend | 101227 | 200 |
| PE | CD86 | A17199A | BioLegend | 159203 | 200 |
| AF594 | CD11c | N418 | BioLegend | 117346 | 200 |
| PE-Cy7 | IL5Ra | DIH37 | BioLegend | 153407 | 100 |
| APC | Siglec-F | S17007L | BioLegend | 155508 | 200 |
| AF700 | CD45 | 30-F11 | BioLegend | 103127 | 200 |
| APC-Cy7 | CCR3 | J073E5 | BioLegend | 144528 | 100 |

**Appendix Table 3.3 Flow cytometry panel used for mCherry-niche labelling experiments in vivo**

| Fluorochrome | Marker | Clone | Manufacturer | Cat. No. | Dilution (1:x) |
|---|---|---|---|---|---|
| Blue | Live/dead fixable dye | | ThermoFisher | L23105 | 400 |
| BUV563 | IL33r (ST2) | U29-93 | BD Biosciences | 749324 | 100 |
| BUV737 | CCR5 | C34-3448 | BD Biosciences | 749670 | 100 |
| BUV805 | CD44 | IM7 | BD Biosciences | 741921 | 200 |
| Pacific blue | F4/80 | BM8 | BioLegend | 123124 | 100 |
| BV510 | MHC-II | M5/114.15.2 | BioLegend | 107635 | 200 |
| BV605 | CD206 | C068C2 | BioLegend | 141721 | 200 |
| BV650 | Ly6G | 1A8 | BioLegend | 127641 | 200 |
| BV785 | Ly6C | HK1.4 | BioLegend | 128041 | 200 |
| GFP | tumour | | | | |
| PerCP-Cy5.5 | CD11b | M1/70 | BioLegend | 101227 | 200 |
| PE | Siglec-F | E50-2440 | BD Biosciences | 552126 | 200 |
| mCherry | tumour/niche | | | | |
| PE-Cy7 | CD64 | X54-5/7.1 | BioLegend | 139313 | 200 |
| AF700 | CD45 | 30-F11 | BioLegend | 103127 | 200 |
| APC-Cy7 | CCR3 | J073E5 | BioLegend | 144528 | 100 |

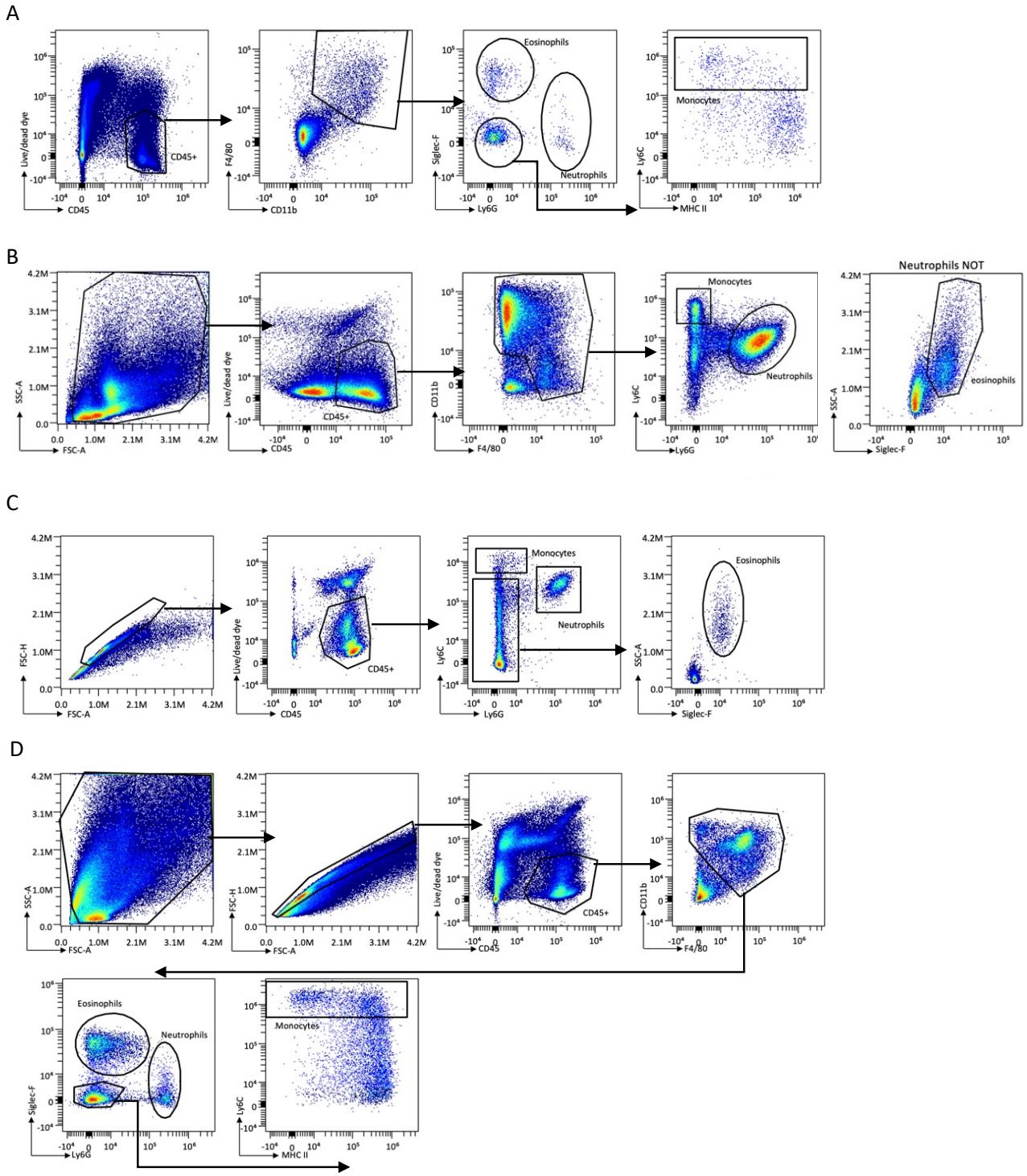


**Figure S1. Gating strategies used to analyse flow cytometry data.** Myeloid populations in following tissues were analysed **(A)** mammary fat pad, **(B)** bone marrow, **(C)** blood, **(D)** tumours on both day 7 and day 18.

## Chapter 4 | Eosinophil cytotoxicity is regulated by interferons

## 4.1 Introduction

The spectral flow cytometry analysis of tumour-associated eosinophils in Chapter 3 revealed two subsets of eosinophils distinguished by the expression of the Ly6C glycoprotein. Ly6C+ eosinophils infiltrated tumours early during tumour development and presented with a more cytotoxic phenotype, while Ly6C- eosinophils differentiated from the Ly6C+ subset in the progressing tumour microenvironment (TME) and lost their anti-tumorigenic properties. It is currently known that 1) eosinophils are highly plastic cells adapting their phenotype to the local tissue niche[125], and 2) direct eosinophil cytotoxicity towards cancer cells can be enhanced by various stimuli, such as IFNγ[171]. How different eosinophil subsets respond to the progressing TME milieu and how these interactions shape eosinophil cytotoxicity remains unclear. The first part of this chapter is therefore focused on gaining a deeper understanding of differences between Ly6C+ and Ly6C- eosinophils and identifying potential drivers of the enhanced eosinophil cytotoxicity in the Ly6C+ subset.

To this end, both Ly6C+ and Ly6C- eosinophils were analysed by bulk RNA-sequencing and analysis of the transcriptomic dataset revealed responsiveness to interferons (IFNs) among the most upregulated pathways in Ly6C+ eosinophils. Following these results, the next part of this chapter focuses on validating these findings. A series of experiments utilising ex vivo IFN stimulation of tumour-associated and bone marrow (BM)-derived eosinophils 1) confirmed the enhanced responsiveness of Ly6C+ eosinophils to interferons, 2) characterised the broader effects of IFNs on both subsets of eosinophils and 3) suggested that IFN stimulation enhances cytotoxic activity of Ly6C- tumour-associated eosinophils and both Ly6C+ and Ly6C- BM-derived eosinophils. Therefore, I next sought to examine how and if IFNs regulate the dynamics and phenotype of these two eosinophil states in vivo.

Because immune checkpoint blockade (ICB) treatment is known to induce IFN-rich TME during a successful response phase[286], eosinophils play an important role in response to ICB[184], and Ly6C+ eosinophils are responsive to IFNs, this raises multiple questions: a) does eosinophil cytotoxicity depend on IFNs in vivo, b) does the absence or abundance of IFNs

shift proportions of Ly6C+ eosinophils and c) how does successful ICB response affect eosinophil phenotype? To answer some of these questions, the second part of this chapter is aimed at regulating levels of IFNs in TME by using the NT193 murine model of breast cancer. First, IFNs were neutralised (anti-IFN) during the whole NT193 tumour growth and the effect on eosinophils was examined by flow cytometry and ex vivo cytotoxic assays, which suggested reduced cytotoxic abilities of eosinophils in the anti-IFN treated mice. Afterwards, the tumour-associated eosinophil phenotype was characterised after successful ICB treatment. Although the ratio of Ly6C+ eosinophils did not change, Ly6C+ eosinophils presented with an increased degranulation and activation marker phenotype.

Lastly, the relevance of these eosinophil findings for human diseases was examined. Despite the evidence that an eosinophil gene signature correlates with improved overall survival in breast cancer patients[135,160], a study using histological detection of eosinophils in tumour microarrays (TMAs) of 576 treatment naïve patients reported low eosinophil infiltration[162]. Understanding this discrepancy is particularly important, as eosinophils play a role in maintaining ICB[184,199] and radiotherapy[189] treatment response in human and murine studies. To understand if TMA-based studies might be underestimating eosinophil presence, full tumour sections of a small group of 48 breast cancer patients were analysed with anti-eosinophil peroxidase immunohistochemistry staining. This analysis revealed that TNBC patients with local recurrence had a higher density of eosinophils compared to the primary tumours, with the eosinophil accumulation occurring at the periphery of the tumours, partially explaining why eosinophils can be easily missed in other studies analysing TMAs.

In summary, this chapter provides a more comprehensive understanding of the Ly6C+ and Ly6C- eosinophil subset differences, reveals a specific interferon signalling in Ly6C+ eosinophils and points to the potential of activating eosinophil cytotoxicity during ICB treatment. Additionally, the data in this chapter provide new evidence of eosinophil infiltration in locally recurrent TNBC patients.

## 4.2 Results

### 4.2.1 Bulk RNA sequencing of tumour-associated eosinophils reveals an IFN-responsive signature in the Ly6C+ subset

The first aim of this chapter was to complement the phenotypic and functional characterisation of tumour-associated eosinophils (TAE) described in Chapter 3 by exploring the transcriptional differences between Ly6C+ and Ly6C- subsets of eosinophils. Therefore, both subsets of TAE (CD11b+, Siglec-F+, Ly6G-) were FACS sorted from NT193 tumours on day 18 post-engraftment and examined by an ultra-low input RNA sequencing (bulk RNA-seq) method, suitable for capturing mRNA signatures of a small number of cells with low yield of mRNA (Figure 4.1A and B). Principal component analysis of the bulk RNA-seq results revealed a clear separation between Ly6C+ and Ly6C- eosinophils (Figure 4.1C). Furthermore, differential gene expression analysis (DESeq2) of these two eosinophil subsets identified 112 differently expressed genes (DEGs) (logFC > 1, p-value < 0.05). Of these DEGs, 37 were downregulated and 75 were upregulated in Ly6C+ eosinophils compared to the Ly6C- subset (Figure 4.1D, Appendix Table 4.1). Notably, the *Ly6c2* gene was among the most significantly upregulated genes in Ly6C+ eosinophils, validating the increased expression of Ly6C observed by flow cytometry (Figure 4.1D).

Even though both eosinophil subsets were FACS sorted as CD11b+, Siglec-F+, Ly6G- ensuring of the high purity of eosinophils, potential contamination on the transcriptional level by other cell types was investigated by comparing normalised gene counts of a manually curated gene panel focused on different cell identities (Appendix Table 4.2). As expected, genes associated with eosinophils (*Siglecf*, *Ccr3*, *Adgre1* (F4/80), *Itgam* (CD11b)) were all highly expressed across all eosinophil samples (Figure 4.2E). In comparison, genes commonly associated with macrophages (*Cd68*, *Mrc1*, *Cd86*), monocytes (*Cx3cr1*, *Ccr2*), dendritic cells (*Flt3*, *Siglech*), neutrophils (*Cd177, S100a8, S100a9*), lymphocytes (*Cd3e, Cd79a*), and stromal cells (*Pdgfra*, *Pdgfrb*, *Pecam1*) were detected at low levels (Figure 4.2E). Although there is a moderate expression of *Cd68* and *Mrc1* markers, the strong expression of

*Siglecf* and *Ccr3*, and the absence of the macrophage/monocyte lineage marker *Cx3cr1* confirms the high purity of the sorted eosinophil population.

Interestingly, *Il5ra*, the receptor of IL5, which is essential for eosinophil survival[287] and a common marker for identifying eosinophils in transcriptomic datasets[125], was present at lower levels compared to *Siglecf,* based on normalised counts. However, further analysis confirmed its expression above 2000 normalised counts, a level well above typical low-expression thresholds used in RNA-seq analyses and indicative of a robustly expressed gene. Additionally, genes encoding eosinophil granule proteins were excluded from this analysis as their mRNA expression is known to be uncoupled from the protein levels[98,125], as later discussed in section 4.3.2.

Overall, these results confirmed eosinophil identity of all sequenced samples at the transcriptomic level, validated the high Ly6C expression observed by flow cytometry in the Ly6C+ eosinophil subset, and pointed to robust transcriptional differences between Ly6C+ and Ly6C- eosinophils.

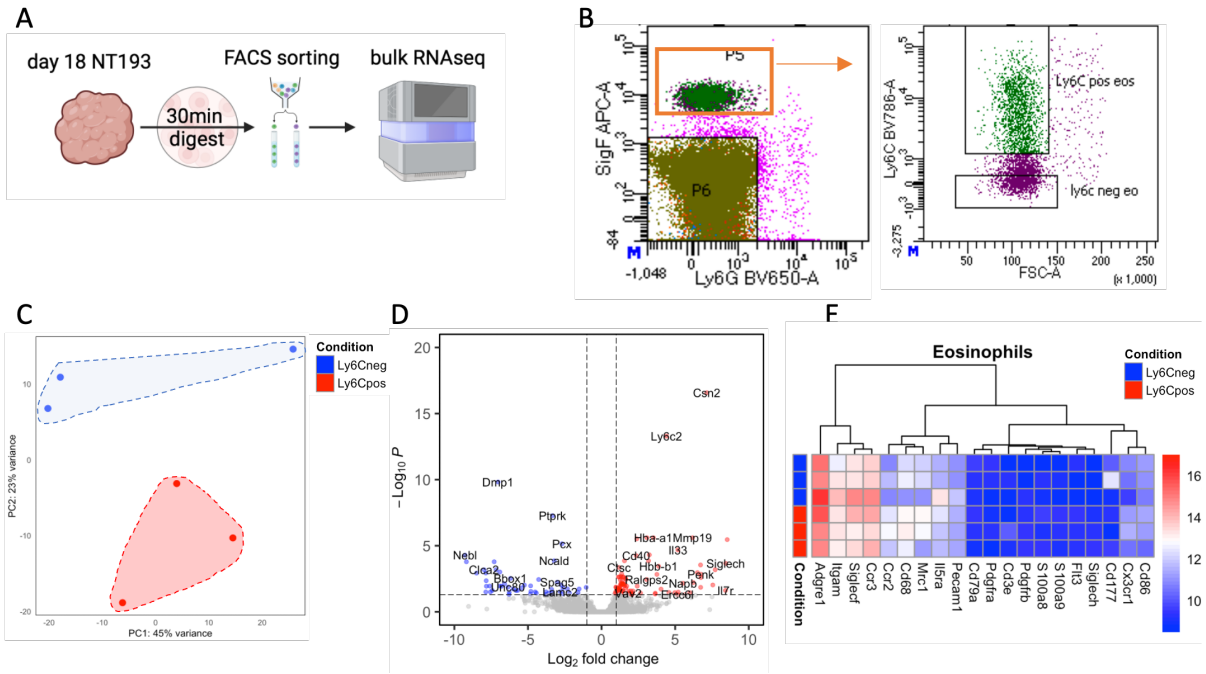


**Figure 4.1. bulk RNA sequencing analysis of NT193 tumour-associated Ly6C+ and Ly6C- eosinophils. (A)** Overview of the experimental set-up. The NT193 cancer cell line was grafted into the 4th mammary fat pad of FVB female mice; on day 18, tumours (n = 3) were harvested, and Siglec-F+

CD11b+ eosinophils were sorted based on their expression of Ly6C receptor. Ly6C+ and Ly6C- sorted eosinophils were then processed and analysed by bulk RNA sequencing. **(B)** Representative image of the gating strategy applied to sort Ly6C+ and Ly6C- eosinophils. **(C)** Visualisation of principal components (PC) 1 and 2 of PCA analysis performed on all sequenced samples after DESeq2 normalisation. Each point represents an individual sample, colour-coded by experimental condition as indicated - Ly6C+ (red) and Ly6C- (blue). **(D)** Volcano plot of differentially expressed genes between Ly6C+ and Ly6C- eosinophils. Each point represents a gene; all genes are plotted by fold change ($\log_2$) against statistical significance ($-\log_{10}$ adjusted p-value). Significantly upregulated genes in Ly6C+ eosinophils are marked in red, significantly downregulated genes are marked in blue. **(E)** Heatmap of normalised gene expression in both eosinophil subsets. Rows represent individual samples and columns represent genes. Expression levels are colour-coded according to a custom palette.

To understand the gene expression differences in a broader functional context, the bulk RNA-seq dataset was further analysed by gene set enrichment analysis (GSEA) using the gene ontology (GO) resource. GSEA analysis identified "*response to type II interferon (IFNγ)*" and "*response to interferon-beta (IFNβ)*" as the two most significantly upregulated pathways in Ly6C+ eosinophils compared to the Ly6C- subset (Figure 4.2A, Appendix Tables 4.3 and 4.4). Furthermore, this analysis has also identified pathways related to cytotoxicity, such as "*killing of cells of another organism*" and "*disruption of cells in another organism*" among the most overrepresented pathways in Ly6C+ eosinophils (Appendix Table 4.5). This is in line with the increased cytotoxic properties of Ly6C+ eosinophils characterised in Chapter 3 (Figure 3.6J).

Genes driving these pathway annotations were further investigated to understand the potential overlaps of these gene signatures. For this purpose, DEGs recognised in the three most up- and down-regulated pathways in Ly6C+ eosinophils were extracted (Figure S3), and the number of shared genes was assessed. The comparison revealed that genes associated with the response to IFNγ, IFNβ and cytotoxic pathways ("*killing of cells of another organism*" and "*disruption of cell in another organism*") were mostly distinct, with only 3 genes (*Gbp2, Gbp2b, Gbp3*) being shared between all of these gene sets (Figure 4.2B). In contrast, genes involved in mesonephric epithelium, ureteric bud, and renal tubule development, overrepresented in Ly6C- eosinophils, showed substantial overlap (Figure 4.2C, Appendix Tables 4.6,4.7), with an absolute match observed between gene sets of "*mesonephric epithelium development*" and "*ureteric bud development*" pathways (Appendix Table 4.7). Because pathways related to the tubule development consisted of a low number of genes and were not directly related to

the TME eosinophil biology, the further analysis focused on the IFN-related pathways and their potential relevance to eosinophil cytotoxicity of the Ly6C+ phenotype.

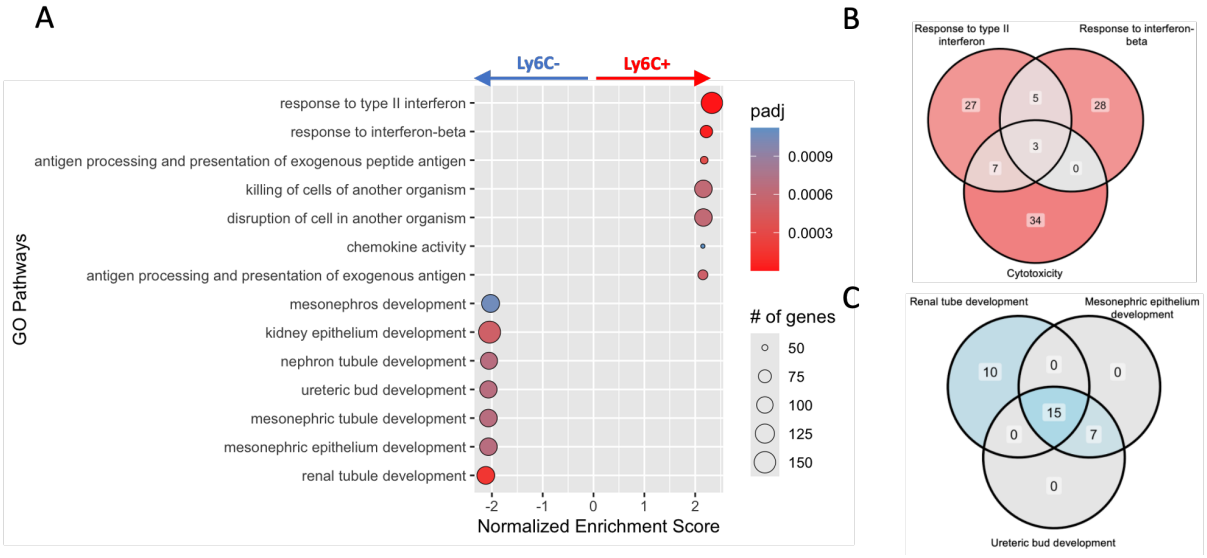


**Figure 4.2. Gene set enrichment analysis based on the GO resource. The** NT193 cancer cell line was grafted into the 4th mammary fat pad of FVB female mice on day 18, tumours (n=3) were harvested, and Siglec-F+ CD11b+ eosinophils were sorted based on their Ly6C surface expression. Ly6C+ and Ly6C- sorted eosinophils were then processed and analysed by bulk RNA sequencing. **(A)** Gene Set Enrichment Analysis (GSEA) using Gene Ontology (GO) database was performed using ranked gene expression data. Genes were ranked by differential expression and converted to Entrez IDs before enrichment testing across all GO categories (Biological process, Molecular function, and Cellular component). Enriched pathways were identified based on normalised enrichment scores (NES) and adjusted p-values (adjusted p-value < 0.05). The dot plot displays the top significantly enriched GO terms for upregulated (NES>0) and downregulated (NES<0) gene sets in Ly6C+ eosinophils, dot size represents the number of genes in each pathway and dot colour intensity indicates statistical significance (adjusted p-value). **(B and C)** Venn diagrams comparing gene overlaps of the three most upregulated **(B)** and downregulated **(C)** pathways in Ly6C+ eosinophils.

### 4.2.2 Validation of bulk RNA sequencing data

Following the DEG and GO-based GSEA analyses, I aimed to validate the identified key transcriptomic changes at the protein level. To do this, I first compared an expression of two receptors that were present in both the transcriptomic dataset and the flow cytometry panel detailed in Table 3.2.

*Il1rl1* gene, which encodes the IL-33 receptor (IL33r), was identified to be overexpressed in Ly6C- eosinophils based on normalised counts (p-value = 0.08) (Figure 4.3A). Therefore, IL-33r expression was analysed on NT193 infiltrating eosinophils by flow cytometry. First, Ly6C+ and Ly6C- eosinophils were identified as described in Chapter 3, section 3.2.3. Il33r+

eosinophils were gated based on Fluorescence minus one (FMO) control, and the proportion of Ly6C- IL33r+ eosinophils to the parental Ly6C- population was compared with the proportion of Ly6C+ IL33r- eosinophils to the parental Ly6C+ population (Figure 4.3B). In line with the transcriptomic data, Ly6C- IL33r+ population was significantly more prevalent compared to the Ly6C+ IL33r+ subset.

In contrast, to validate a receptor overexpressed on Ly6C+ eosinophils, major histocompatibility complex class II (MHC II) was selected as it was present in both bulk RNA-seq data and flow cytometry analysis. *H2-Aa* and *H2-Eb1*, which encode the MHC II, were both overexpressed in Ly6C+ eosinophils, with *H2-Aa* overexpression being statistically significant (Figures 4.3D and E). Consistent with these findings, flow cytometry analysis of MHC-II+ eosinophil subsets identified based on FMO controls (Figure 4.3F) showed a higher prevalence of Ly6C+ MHC-II+ eosinophils compared to the Ly6C- MHC-II+ subset, both gated on their respective parental populations (Figure 4.3G). These data collectively suggest that the transcriptional differences are reflected on a protein level to a certain extent, beyond the Ly6C overexpression used for FACS sorting.

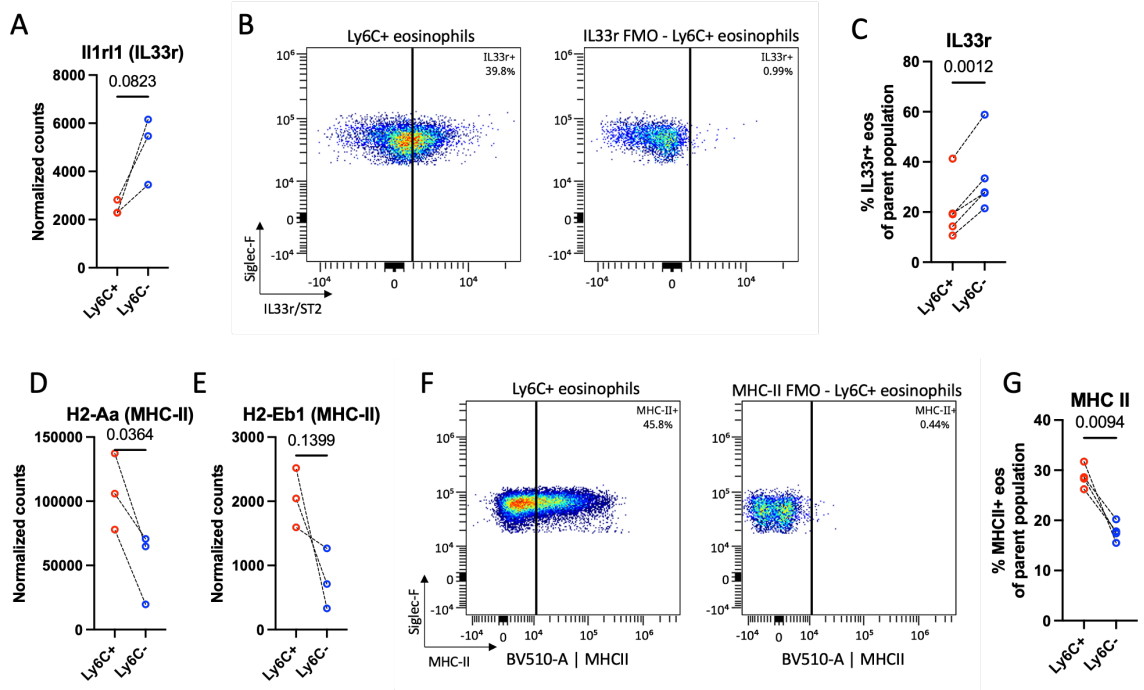


**Figure 4.3. Validation of bulk RNA sequencing data on the protein level.** The NT193 cancer cell line was grafted into the 4th mammary fat pad of FVB female mice, on day 18, tumours were harvested

and Siglec-F+ CD11b+ eosinophils were sorted based on their Ly6C surface expression. Ly6C+ and Ly6C- sorted eosinophils were then processed and analysed by bulk RNA sequencing (n = 3) or flow cytometry (n = 5). **(A)** Normalised counts for *Il1rl1* (IL-33 receptor) extracted from bulk RNA-seq dataset of Ly6C+ and Ly6C- eosinophils. **(B)** Representative gating strategy for identifying IL33r+ eosinophils by flow cytometry based on IL-33R fluorescence minus one (FMO) staining. **(C)** Comparison of the prevalence of IL33r+ Ly6C+ and IL33r+ Ly6C- eosinophils identified by flow cytometry. **(D and E)** Normalised counts for *H2-Aa* **(D)** and *H2-Eb1* **(E),** both encoding MHC-II, extracted from bulk RNA-seq data of Ly6C+ and Ly6C- eosinophils. **(F)** Representative gating strategy for identifying MHC-II+ eosinophils by flow cytometry using MHC-II FMO staining. **(G)** Comparison of the prevalence of MHC-II+ Ly6C+ and MHC-II+ Ly6C- eosinophils identified by flow cytometry. Separate NT193 tumours were used for flow cytometry validation (n = 5); flow cytometry data are representative of 3 independent experiments. Data show individual values and were analysed by a two-tailed paired Student's t-test.

To further validate the upregulation of interferon (IFN) signalling pathways in Ly6C+ eosinophils, both Ly6C+ and Ly6C- eosinophils were FACS-sorted from NT193 tumours on day 18 post-engraftment, stimulated ex vivo with IFNγ or IFNβ in the presence of IL-5, and compared to control tumour eosinophils cultured in the presence of IL-5 exclusively (Figure 4.4A). Because the expression of PD-L1 receptor is known to be regulated by IFNs through the JAK-STAT signalling pathway[288], PD-L1 was selected as a main marker of IFN responsiveness in this assay. Following stimulation with IFNγ or IFNβ, Ly6C+ eosinophils showed a significantly greater fold increase of PD-L1 expression compared to the Ly6C- eosinophils (Figure 4.4 B and C). MFI of IFNγ receptor (IFNGR2) and receptor for IFNβ (IFNAR1) were assessed by flow cytometry, however, low MFI signal for both was detected at baseline (Figure S4A), indicating their potential internalisation.

These data are in line with the observed increased responsiveness of Ly6C+ eosinophils to IFNs and further validate the transcriptomic dataset on a protein level. Therefore, the downstream analyses in this chapter focus on understanding the broader effects of IFN stimulation of both subsets and investigating the potential link to increased cytotoxic properties of Ly6C+ eosinophils.

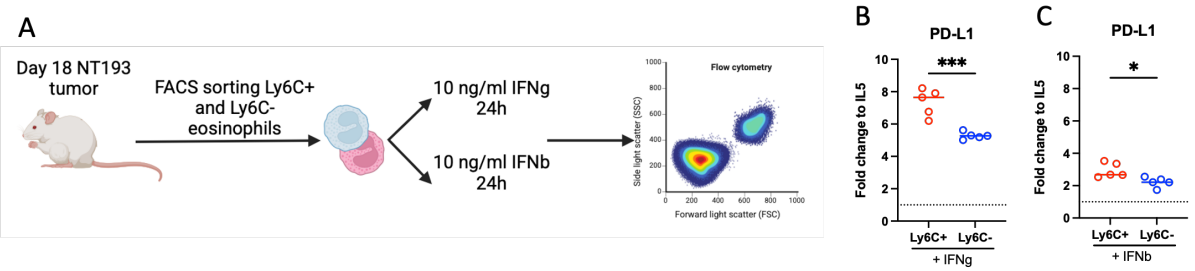


**Figure 4.4. Measuring response of Ly6C+ and Ly6C- eosinophils by PD-L1 expression. (A)** Overview of the experimental plan. FVB mice were orthotopically grafted with the NT193 cell line, tumours (n =5) were harvested on day 18 post-engraftment and Ly6C+ and Ly6C- eosinophils were isolated by FACS sorting. Both subsets of eosinophils were afterwards incubated with IFNγ or IFNβ in the presence of IL-5, or cultured in the absence of IFNs in the presence of only IL-5. All treatment groups were analysed with flow cytometry. **(B, C)** Fold change difference of PD-L1 expression of Ly6C+ and Ly6C- eosinophils treated with IFNγ **(B)** or IFNβ **(C)** to matched Ly6C+ and Ly6C- eosinophils cultured in the absence of IFNs (IL-5 controls). Data show individual values and mean ± SD and were analysed by two-tailed unpaired Student's t-test. Statistical significance is displayed on figures as follows: *p < 0.05, **p < 0.01, ***p<0.001, ****p<0.0001. Data are representative of 2 independent experiments.

### 4.2.3 IFN stimulation of eosinophils ex vivo leads to re-expression of Ly6C and degranulation

To investigate the effects of IFNs on eosinophil activation, Ly6C+ and Ly6C- eosinophils infiltrating NT193 tumours were FACS-sorted, and IL-5 cultured eosinophils were left untreated or treated with IFNγ or IFNβ, as described in section 4.2.2 (Figure 4.4A). Cells were analysed by flow cytometry (Figure 4.4A) using a panel of markers previously associated with eosinophil activation, maturity and IFN signalling.

Briefly, granularity (SSC-A) was assessed as a proxy for degranulation, with reduced granularity interpreted as a result of active degranulation in the presence of IFNs and therefore suggesting increased cytotoxicity. CD63, also known as LAMP-3 is a transmembrane protein involved in vesicular transport. Detection of CD63 by surface staining indicates release of granules with membrane-bound CD63 and, therefore, was included as a second marker of eosinophil degranulation[289]. Siglec-F was included as a marker of maturity[98,102]; however, as Siglec-F is also an apoptotic marker, it is possible that stimulation by IFNs might also lead to its internalisation. Lastly, CCR3, Ly6C, MHC-I, MHC-II, and PD-L1 were used as indirect markers of IFN responsiveness; CCR3 was previously shown to be internalised following IFN signalling[290]. In contrast, Ly6C is known to be upregulated upon IFNγ stimulation on certain

cell types, such as T-cells[15] and MHC-I, MHC-II and PD-L1 are also known to be induced by IFN signalling[288,291,292].

Stimulation of FACS-sorted eosinophils with either IFNγ or IFNβ reduced the viability of both eosinophil subsets to a similar extent (Figure 4.5A), indicating an IFN sensitivity of TAE ex vivo. Viable eosinophils were further analysed and a significant decrease in granularity of Ly6C+ eosinophils was observed following IFNγ but not IFNβ exposure (Figure 4.5B). In contrast to this, IFNs did not affect the granularity of Ly6C- eosinophils (Figure 4.5B). These results suggested potential degranulation of Ly6C+ eosinophils upon IFNγ stimulation, therefore, levels of CD63 were further investigated.

Ly6C+ and Ly6C- eosinophils stimulated with either IFNγ or IFNβ presented with a reduced median fluorescence intensity of CD63 compared to control IL-5 treated eosinophils (Figure 4.5C). The combination of a) lower granularity suggesting degranulation caused by IFNγ and b) the diminished presence of CD63 on the surface, suggests a potential decoupling of the surface CD63 presence and release of the granules in this context. It is also possible that IFNγ causes cytolytic degranulation. However, these eosinophils would not be viable and, therefore, would be mostly excluded from this analysis. Additionally, the Siglec-F signal was reduced in both subsets following IFNγ but not IFNβ stimulation (Figure 4.5D). Whether this reflects internalisation or a downregulation would have to be further investigated by qPCR to understand the relevance of this change. Internalisation of receptors could also be investigated by intracellular flow cytometry staining, however, this experiment was not performed due to the non-specific intracellular staining problems discussed in section 3.3.1.

In agreement with the literature, CCR3 was downregulated in both eosinophil subsets following IFNγ and IFNβ stimulation (Figure 4.5E). Furthermore, Ly6C expression was upregulated in response to both IFNs, with the overexpression being more dominant after IFNβ stimulation (Figure 4.5F). Finally, as discussed previously, interferons are potent

inducers of MHC-I, MHC-II and PD-L1 expression. As expected, all three of these receptors were significantly upregulated following both IFNγ and IFNβ stimulation (Figure 4.5G-I).

As mentioned above, IFN stimulation led Ly6C- eosinophils towards re-expression of the Ly6C glycoprotein (Figure 4.5F). Therefore, differences in Ly6C expression between these two subsets were further investigated to understand if IFNs have the potential to reverse the Ly6C- eosinophils back to a more "Ly6C+ –like" state.

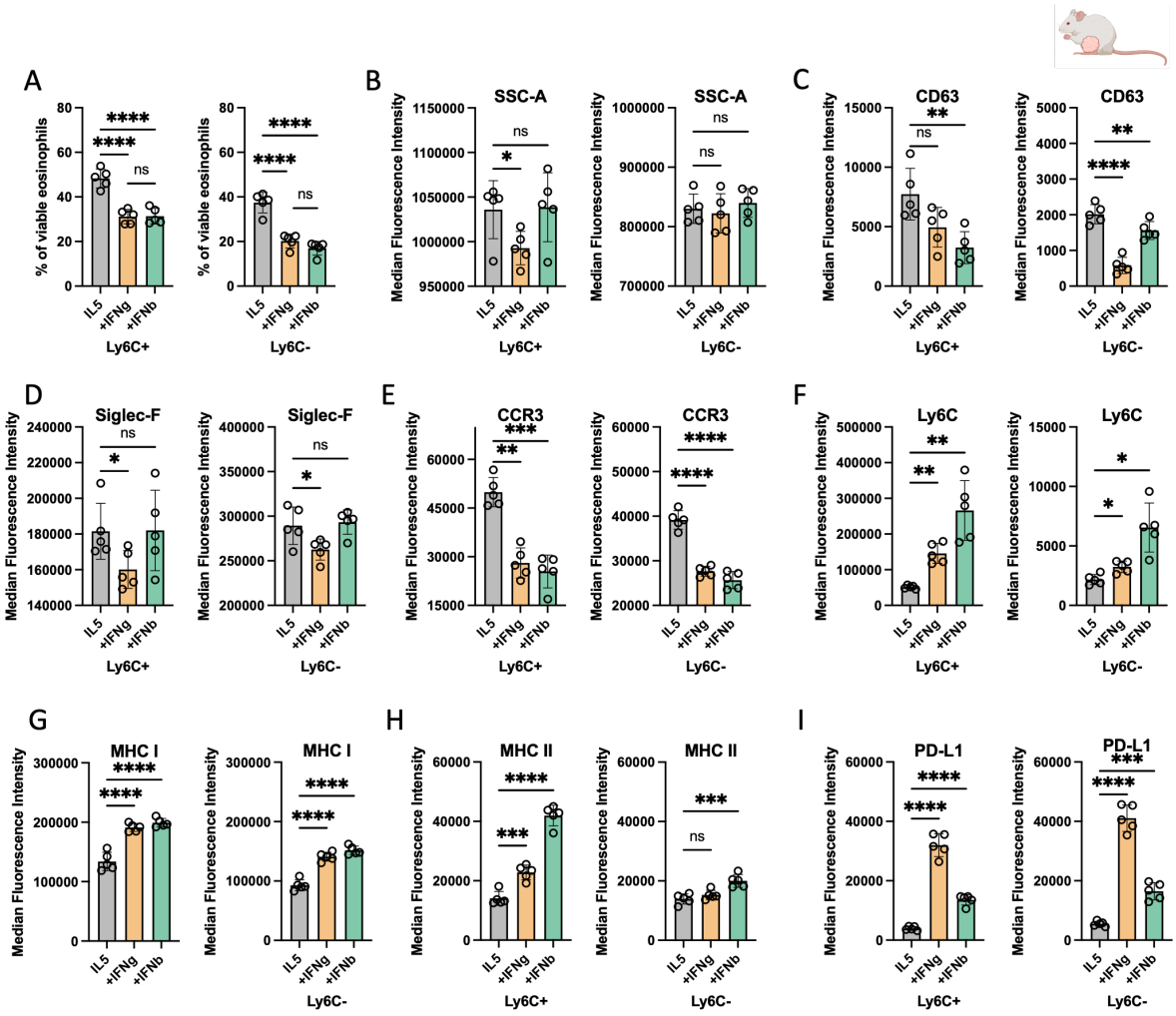


**Figure 4.5. Effect of IFN stimulation on Ly6C+ and Ly6C- tumour-associated eosinophils ex vivo.** FVB mice were orthotopically grafted with the NT193 cell line, tumours (n =5) were harvested on day 18 post-engraftment and Ly6C+ and Ly6C- eosinophils were isolated by FACS sorting. Both subsets of eosinophils were afterwards incubated with IFNγ or IFNβ in the presence of IL-5, or cultured in the absence of IFNs in the presence of only IL-5. All treatment groups were analysed with flow cytometry. **(A-F)** Comparison of Ly6C+ and Ly6C- eosinophils after incubation with IL-5 (grey), IL-5+ IFNγ (+IFNγ, yellow), and IL-5 + IFNβ (+IFNβ, green), as indicated. **(A)** Proportion of viable eosinophils to total cell population. **(B)** Median side-scatter values of viable eosinophils. Median fluorescence intensity of **(C)** CD63, **(D)** Siglec-F, **(E)** CCR3, **(F)** Ly6C, **(G)** MHC-I, **(H)** MHC-II, and **(I)** PD-L1 on viable eosinophils. Data show individual values and mean ± SD and were analysed by one-way ANOVA test using Holm-Šídák correction for comparison of IFN treatments to IL-5 control group, or two-way ANOVA using Holm-

Šídák correction for comparison of viability between all groups. Statistical significance is displayed on figures as follows: *p < 0.05, **p < 0.01, ***p<0.001, ****p<0.0001. Data are representative of 2 independent experiments.

To understand the extent of Ly6C overexpression upon the IFN stimulation of both Ly6C+ and Ly6C- eosinophils, both subsets were FACS sorted from NT193 tumours on day 18 and Ly6C surface distribution was analysed by comparing density plots of a) Ly6C+ eosinophils cultured in presence of IL-5, and with addition of IFNγ or IFNβ (Figure 4.6A), and b) Ly6C- eosinophils cultured in presence of IL-5, and with addition of IFNγ or IFNβ (Figure 4.6B).

This analysis revealed that following the stimulation with either of the IFNs, a subpopulation of the Ly6C- eosinophils re-expressed Ly6C receptor to levels comparable with native Ly6C+ eosinophils (Figure 4.6B). Whether these eosinophils with newly re-expressed Ly6C receptor (Ly6C+$^{new}$) were phenotypically different from cells that remained Ly6C- was unclear. Therefore, Ly6C- and Ly6C+$^{new}$ eosinophils were gated as two separate populations (Figure 4.6B). Afterwards, granularity, CD63, and MHC-II surface expression were compared between these two newly gated subsets, as these markers were previously shown to be upregulated in the native Ly6C+ eosinophils compared to Ly6C- TAE (Figure 3.6F&G, Figure 4.3G). However, this analysis showed that following the IFN stimulation with either of the IFNs, the Ly6C+$^{new}$ subset of eosinophils did not differ from Ly6C- eosinophils in terms of granularity (Figure 4.6C), CD63 (Figure 4.6D), or MHC-II expression (Figure 4.6E).

In summary, while IFNs impact eosinophil viability and induce phenotypic changes related to activation, based on the selected markers, the re-expression of Ly6C on its own does not directly lead to recapitulation of the Ly6C+ phenotype. Further experiments are needed with sorted tumour-associated eosinophils, focused on the potential effect of IFN stimulation on cytotoxic properties.

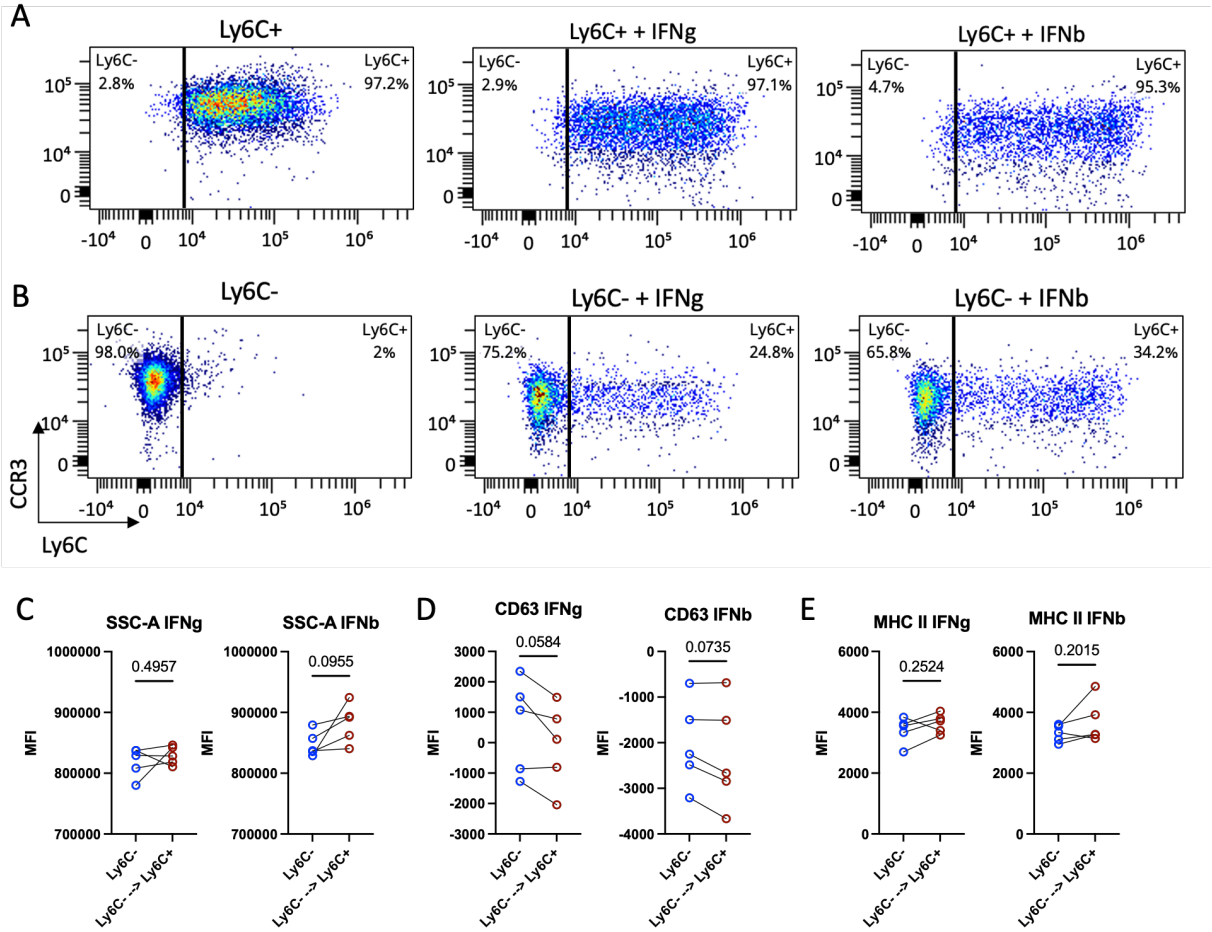


**Figure 4.6. Re-expression of Ly6C after IFN stimulation does not translate into a native Ly6C+ phenotype.** FVB mice were orthotopically grafted with the NT193 cell line, tumours (n =5) were harvested on day 18 post-engraftment and Ly6C+ and Ly6C- eosinophils were isolated by FACS sorting. Both subsets of eosinophils were afterwards incubated with IFNγ or IFNβ in the presence of IL-5, or cultured in the absence of IFNs in the presence of IL-5 only for comparison. All treatment groups were analysed by flow cytometry. **(A, B)** Representative density plots showing Ly6C expression of sorted **(A)** Ly6C+ eosinophils and **(B)** Ly6C- eosinophils under the three culture conditions. **(C-E)** Comparison of Ly6C- eosinophils that remained Ly6C- after stimulation with IFNs and Ly6C- eosinophils that re-expressed Ly6C receptor after IFN stimulation (Ly6C+$^{new}$ labelled as Ly6C- --> Ly6C+). Comparison of **(C)** granularity (SSC-A), and expression of **(D)** CD63, and **(E)** MHC-II between Ly6C- and Ly6C+$^{new}$ subsets after stimulation with IFNγ or IFNβ as indicated. Data show individual values, are representative of 2 independent experiments, and were analysed by a two-tailed paired Student's t-test; statistical significance is displayed above the figures.

### 4.2.4 Bone marrow-derived eosinophils as a model to study IFN responses

In Chapter 3, I have established a model of bone marrow (BM)-derived eosinophils that resemble the Ly6C+ and Ly6C- tumour-associated eosinophils in terms of increased granularity, CD63 expression and cytotoxicity of the Ly6C+ CCR3+ BM-derived eosinophil subset. Following the transcriptomic and proteomic signatures pointing to the higher IFN responsiveness of Ly6C+ eosinophils infiltrating NT193 tumours, my next aim was to understand if BM-derived eosinophils are capable of recapitulating this phenotype. Therefore,

BM progenitors were cultured in the presence of Ftl3 and mSCF for 4 days and then further cultured in the presence of IL-5 to allow their maturation until day 18. Afterwards, CCR3+ Ly6C+ and CCR3+ Ly6C- BM-derived eosinophils were FACS sorted and stimulated with a) IFNγ and IL-5, b) IFNβ and IL-5, or c) cultured in the presence of IL-5 alone, and analysed by flow cytometry (Figure 4.7A). Identically to section 4.2.2, expression of PD-L1 was used as a measurement of response to IFNs. This analysis confirmed that following the stimulation with either of the IFNs (Figure 4.7B, C), CCR3+ Ly6C+ eosinophils upregulate expression of PD-L1 to a greater extent than CCR3+ Ly6C- eosinophils, when compared to eosinophils cultured with IL-5 alone.

The overall fold change difference of PD-L1 expression in bone marrow-derived eosinophils stimulated with either of the IFNs is visibly higher (up to 100-fold with Ly6C+ eosinophils stimulated with IFNγ), compared to the FACS-sorted TAE (Figure 4.4). This is due to the very low baseline MFI signal for PD-L1 expression of the naïve bone marrow eosinophils, compared to the TAE eosinophils sorted from the immunosuppressed TME that present with higher baseline PD-L1 expression and therefore the fold change difference to IFNγ and IFNβ stimulated eosinophils was lower. Furthermore, expression of IFNGR2 on CCR3+ Ly6C+ and CCR3+ Ly6C- eosinophils was compared by flow cytometry (Figure S4B). Although CCR3+ Ly6C- presented with slightly increased IFNGR2 MFI, the overall MFI levels were comparable with the FMO controls. Similarly to the TAE eosinophils (Figure S4A), this could be a result of internalisation of the IFNGR2 upon engagement. Expression of IFNAR1 was not assessed, however, it could be interesting to investigate in the future.

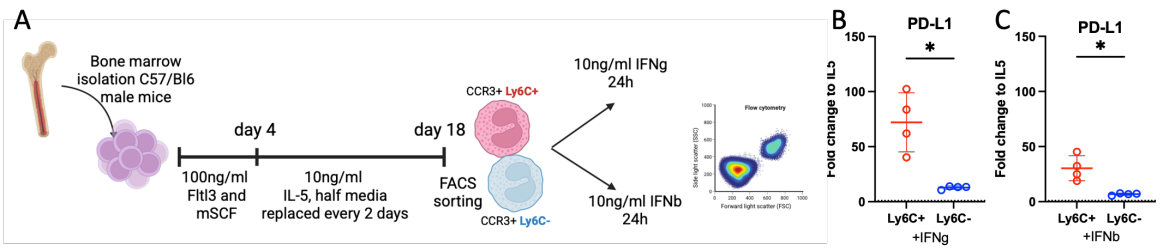


**Figure 4.7. Measuring response of Ly6C+ and Ly6C- BM-derived eosinophils by PD-L1 expression. (A)** Schematic of experiment, bone marrow cells of C57/Bl6 male mice (n = 4) were first cultured with Fltl3 and mSCF for 4 days, then differentiated into eosinophils with IL-5 until day 18 and CCR3+ Ly6C+ and CCR3+ Ly6C- eosinophils were FACS sorted. Both subsets of eosinophils were

afterwards incubated with IFNγ or IFNβ in the presence of IL-5, or cultured in the absence of IFNs in the presence of only IL-5. All treatment groups were analysed by flow cytometry. **(B, C)** Fold change difference of PD-L1 expression of Ly6C+ and Ly6C- eosinophils treated with IFNγ **(B)** or IFNβ **(C)** to matched Ly6C+ and Ly6C- eosinophils cultured in the absence of IFNs (IL-5 controls). Data show individual values and mean ± SD and were analysed by two-tailed unpaired Student's t-test. Statistical significance is displayed on figures as follows: *p < 0.05, **p < 0.01, ***p<0.001, ****p<0.0001. Data are representative of 2 independent experiments.

To further understand if IFNs cause similar phenotypical changes on BM-derived eosinophils, viability, granularity, CD63, Siglec-F, CCR3, MHC-I, MHC-II, and PD-L1 expression were compared by flow cytometry following the IFN stimulation. As expected, both IFNγ and IFNβ reduced the eosinophil viability by approximately 10% (Figure 4.8A). The viability of Ly6C+ eosinophils was lower compared to the Ly6C- subset cultured with IL-5; this was observed in 3 independent experiments and is in contrast with the viability of Ly6C+ and Ly6C- eosinophils sorted from tumours (Figure 4.5A). It is unclear why Ly6C+ eosinophils were less viable; one explanation could be that they carry more granular content and therefore are more prone to degranulation during the FACS sorting.

Stimulation of CCR3+ Ly6C+ eosinophils with IFNγ led to reduced granularity, while no difference was observed with IFNβ, or upon stimulation of Ly6C- eosinophils with either of the IFNs (Figure 4.8B). Furthermore, as previously observed with sorted TAEs, lower granularity was not matched to an increase in surface CD63. Both CCR3+ Ly6C+ and CCR3+ Ly6C- eosinophils presented with lower CD63, Siglec-F, and CCR3 expression after stimulation with either IFNγ or IFNβ (Figure 4.8C-E). In contrast, MHC-I, MHC-II and PD-L1 were all overexpressed on both Ly6C+ and Ly6C- subsets following either IFNγ or IFNβ stimulation (Figure 4.8F-H).

To understand if BM-derived eosinophils also re-express Ly6C receptor as a response to IFN stimulation, Ly6C distribution was compared on a) CCR3+ Ly6C+ eosinophils cultured in the presence of IL-5, and with addition of IFNγ or IFNβ (Figure 4.8I), and b) CCR3+ Ly6C- eosinophils cultured in the presence of IL-5, and with addition of IFNγ or IFNβ (Figure 4.8J).

This analysis led to the conclusion that while CCR3+ Ly6C- eosinophils do re-express Ly6C receptor following the IFN stimulation, this is to a lesser extent compared to Ly6C- IFN stimulated tumour-associated eosinophils (Figure 4.6B).

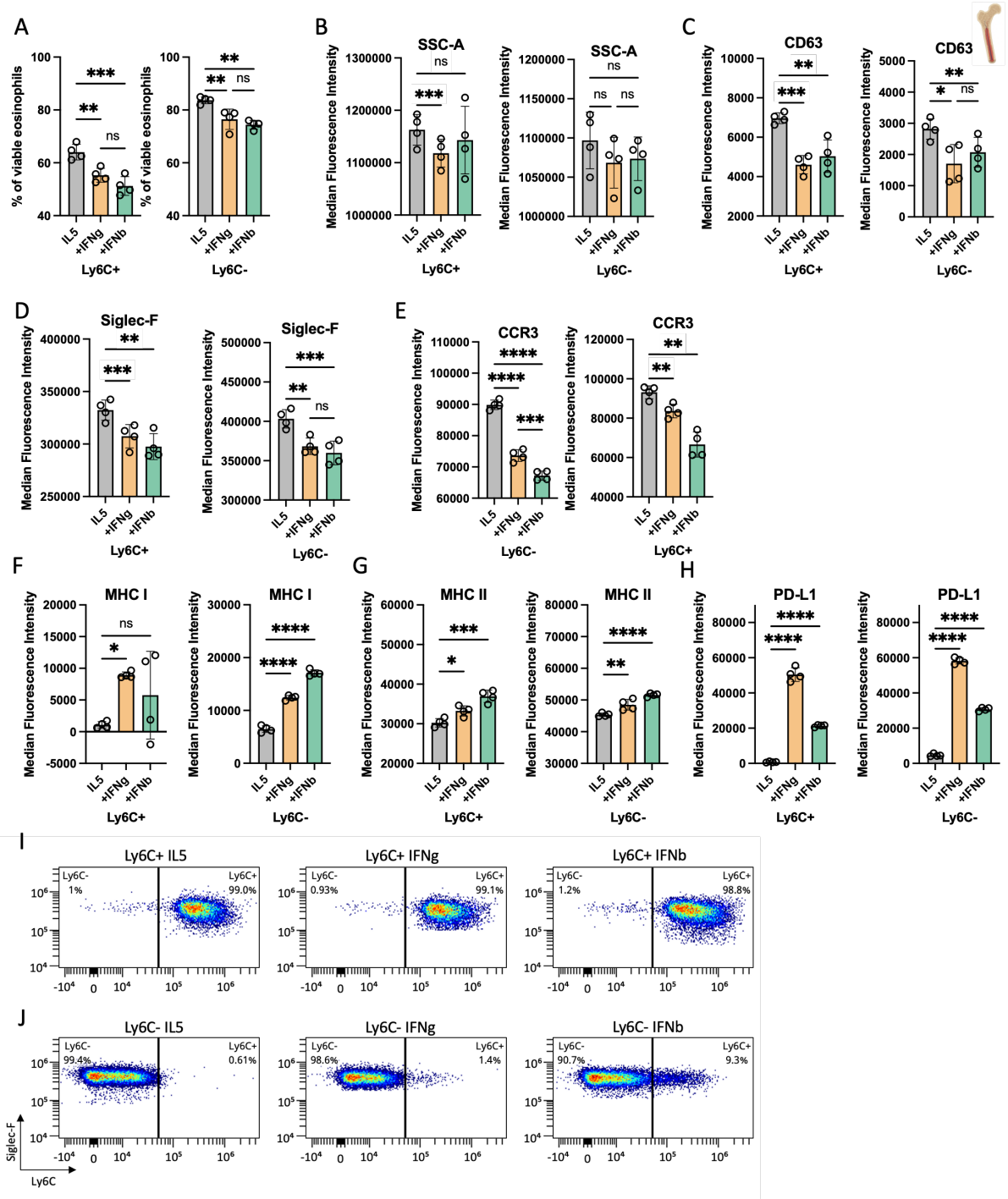


**Figure 4.8. Effect of IFN stimulation on Ly6C+ and Ly6C- bone marrow-derived eosinophils ex vivo.** Bone marrow cells of C57/Bl6 male mice (n = 4) were first cultured with Fltl3 and mSCF for 4 days, then differentiated into eosinophils with IL-5 until day 18 and CCR3+ Ly6C+ and CCR3+ Ly6C- eosinophils were FACS sorted. Both subsets of eosinophils were afterwards incubated with IFNγ or IFNβ in the presence of IL-5, or cultured in the absence of IFNs in the presence of only IL-5. All treatment groups were analysed with flow cytometry. **(A-E)** Comparison of Ly6C+ and Ly6C- eosinophils after incubation with IL-5 (gray), IL-5+ IFNγ (+IFNγ, yellow), and IL-5 + IFNβ (+IFNβ, green), as indicated.

**(A)** Proportion of viable eosinophils to total cell population. **(B)** Median side-scatter values of viable eosinophils. Median fluorescence intensity of **(C)** CD63, **(D)** Siglec-F, **(E)** CCR3, **(F)** MHC-I, **(G)** MHC-II, and **(H)** PD-L1 on viable eosinophils. **(I, J)** Representative density plots showing Ly6C expression of sorted **(I)** Ly6C+ eosinophils and **(J)** Ly6C- eosinophils under the three culture conditions, as indicated. Data show individual values and mean ± SD and were analysed by one-way ANOVA test using Holm-Šídák correction for comparison of IFN treatments to the IL-5 control group. Statistical significance is displayed on figures as follows: *p < 0.05, **p < 0.01, ***p<0.001, ****p<0.0001. Data are representative of at least 2 independent experiments.

These data collectively prove that both Ly6C+ and Ly6C- subsets of eosinophils isolated from NT193 tumours or bone marrow culture respond to IFNγ and IFNβ ex vivo. In both of these models, Ly6C+ eosinophils are more responsive to IFNs, and present with a more degranulated phenotype following the IFNγ stimulation. IFNγ stimulation of peritoneal eosinophils was previously associated with enhanced cytotoxic properties towards cancer cells[171]. Therefore, my next aim was to test whether IFNγ and/or IFNβ stimulation helps improve cytotoxicity of tumour-associated or BM-derived eosinophils in direct co-culture with cancer cell lines.

### 4.2.5 IFN stimulation enhanced eosinophil cytotoxicity

To test the effect of IFN stimulation on eosinophil cytotoxicity, Ly6C+ and Ly6C- eosinophils were sorted from NT193 tumours, cultured in the presence of IL-5 and with the addition of IFNγ and IFNβ or in the absence of IFNs, used in direct co-culture with the NT193 cell line and apoptosis of NT193 cells was assessed by Annexin-V staining (Figure 4.9A). The NT193 cell line was used because it is of the same genetic background as tumour-associated eosinophils. While IFN stimulation did not increase cytotoxicity of Ly6C+ eosinophils compared to IL-5-treated control (Figure 4.9B), Ly6C- eosinophils treated with IFNs were more cytotoxic compared to Ly6C- eosinophils cultured in the presence of IL-5 alone (Figure 4.9C).

To test the effect of IFN stimulation on eosinophil cytotoxicity of bone marrow-derived eosinophils, CCR3+ Ly6C+ and CCR3+ Ly6C- eosinophils were sorted on day 18 of bone marrow culture, cultured with IL-5 in the presence of a) IFNγ, b) IFNβ, or C) absence of both IFNs, and afterwards used in a direct co-culture assay with the E0771 cell line, and apoptosis of E0771 cells was assessed by Annexin-V staining (Figure 4.9D). The E0771 cell line was

used because it is of the same genetic background as bone marrow-derived eosinophils. To control for the baseline apoptosis rate of this cell line, E0771 cells were stained with Annexin-V in the absence of any eosinophils or IFNs in the culture. As expected, unstimulated CCR3+ Ly6C+ eosinophils were cytotoxic against the E0771 cell line, but no significant increase of apoptosis of cancer cells was detected when co-cultured with CCR3+ Ly6C- eosinophils. Furthermore, cytotoxicity of the CCR3+ Ly6C- eosinophils stimulated with either IFNγ or IFNβ was restored to a level matching the unstimulated CCR3+ Ly6C+ eosinophils. Cytotoxicity of CCR3+ Ly6C+ eosinophils was significantly increased when stimulated with both IFNγ and IFNβ compared to unstimulated eosinophils, however, this effect was more pronounced with IFNβ stimulated eosinophils (Figures 4.9 E and F).

In summary, in line with the published literature, IFNγ enhanced the anti-tumorigenic activity of eosinophils ex vivo. Moreover, these results provide evidence that IFNβ may be a more potent activator of eosinophil cytotoxicity than IFNγ, which was previously not investigated. Even though this effect was not as potent when using eosinophils isolated from NT193 tumours. Possible explanations for this difference are discussed in section 4.4.1. Briefly, eosinophils sorted from tumours were responsive to IFNs on a phenotypical level, however, their viability was significantly lower compared to BM-derived eosinophils and this has likely impacted their cytotoxic properties. Therefore, the impact of altered IFN signalling on tumour-associated eosinophils was investigated in vivo using different treatment regimens.

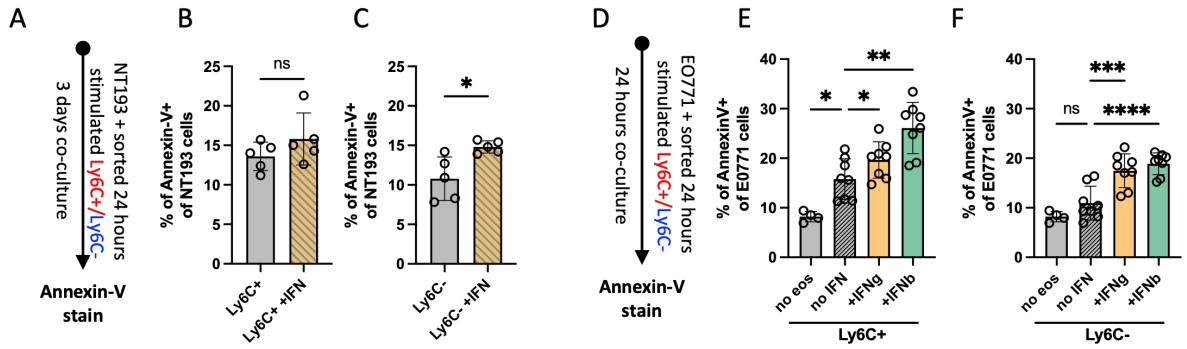


**Figure 4.9. IFN stimulation of eosinophils ex vivo results in increased cell killing properties of Ly6C- eosinophils. (A)** Schematics of the experimental approach. Tumour-associated Ly6C+ and Ly6C- eosinophils sorted from NT193 tumours (n = 5) 18 days post-engraftment were cultured in the

presence of IL5 with IFNγ and IFNβ (+IFN) or only IL5 and afterwards used in direct co-culture with the NT193 cell line for 3 days. NT193 cells were stained with Annexin-V and analysed by flow cytometry to detect apoptosis. **(B, C)** Comparison of apoptotic Annexin-V+ NT193 cells after co-culture with control or IFN treated Ly6C+ eosinophils **(B)** and Ly6C- eosinophils **(C)**. Data show individual values and mean ± SD and were analysed by two-tailed unpaired Student's t-test. **(D)** Schematics of the experimental approach. Bone marrow-derived eosinophils (n = 8) were in culture for 18 days prior to FACS sorting of CCR3+ Ly6C+ and CCR3+ Ly6C- eosinophils. Both subsets were afterwards cultured in the presence of IL-5 (no IFN), or IL-5 supplemented with IFNγ or IFNβ for 24 hours, and afterwards used in direct co-culture with the E0771 cell line for 1 day. E0771 cells were stained by Annexin-V and analysed by flow cytometry to detect apoptosis. **(E, F)** Comparison of apoptotic Annexin-V+ E0771 cells cultured without eosinophils, Ly6C+ eosinophils **(E)**, or Ly6C- eosinophils **(F)** stimulated with no IFN, IFNγ (+IFNg), or IFNβ (+IFNb). Data show individual values and mean ± SD and were analysed by one-way ANOVA test using Holm-Šídák correction for comparison of IFN treatments to the IL-5 control group. Data of tumour-associated eosinophils are representative of one experiment; data of bone marrow-derived eosinophils are pooled from 2 independent experiments. Statistical significance is displayed on figures as follows: *p < 0.05, **p < 0.01, ***p<0.001, ****p<0.0001.

### 4.2.6 Blocking of IFN during tumour development leads to reduced eosinophil cytotoxic activity ex vivo

To understand if the Ly6C expression or cytotoxicity of eosinophils depends on the presence of IFNγ or IFNβ in the tumour microenvironment, NT193 tumours were treated with a combination of anti-IFNγ and anti-IFNAR1 antibodies to block IFNγ and IFNβ signalling, or with an equal amount of isotype control (Figure 4.10A). As previously reported[293,294], blocking IFN signalling resulted in increased tumour weight on day 12 post-engraftment (Figure 4.10B). These results were expected as IFNs are essential for initiating and sustaining anti-tumour immunity by promoting antigen presentation and innate immune activation. However, the absence of IFN signalling did not result in differences in proportions of Ly6C+ eosinophils (Figure 4.10C).

To further investigate if blocking of IFNs had a phenotypical impact on eosinophils, a set of markers known to be regulated by IFNγ or IFNβ was assessed by flow cytometry and Ly6C+ and Ly6C- eosinophils were compared between isotype and anti-IFN treated tumours. In anti-IFN treated tumours, MHC-I, MHC-II and PD-L1 expression was downregulated (Figure 4.10D-F), suggesting a successful blocking of the IFN signalling. Next, the effect of the IFN depletion on eosinophil degranulation was assessed by comparing granularity and CD63 expression. While no differences in granularity were observed during the first experiment (Figure 4.10G), during the second experimental repeat, eosinophils presented with a more

granular phenotype in IFN-blocked tumours (Figure 4.10H). Two experimental repeats are shown only for parameters that differed between the two experiments (Figures 4.10 G and H). At the same time, no differences were observed in the expression of CD63 in either of these experiments (Figure 4.10I).

Lastly, the effect on Siglec-F, CCR3 and Ly6C expression was examined, as data in sections 4.2.3 and 4.2.4 suggest that the presence of IFNs causes downregulation of Siglec-F and CCR3 and upregulation of Ly6C. However, the absence of IFN signalling did not affect the expression of these receptors on either of the eosinophil subsets (Figure 4.10 J-L). Interestingly, I have noticed that in the anti-IFN treated tumours, Ly6C- eosinophils strongly overexpress the CD45 receptor compared to Ly6C- eosinophils from control tumours (Figure 4.10M). CD45 is a protein tyrosine phosphatase receptor present on all leukocytes, with known inhibitory function of interferon-induced JAK-STAT signalling in mast cells[295]. Therefore, this raises a question of the role of CD45 in eosinophil interferon regulation.

Because the blocking of IFN signalling through antibody depletion and receptor blocking broadly affects all cells present in the TME and system response, the enhanced tumour growth could not be directly linked with altered eosinophil phenotype. To partially address this limitation, Ly6C+ and Ly6C- eosinophils were FACS sorted from the control isotype-treated and anti-IFN blocked tumours and their cytotoxic properties were assessed ex vivo after a direct co-culture with NT193 cells by Annexin-V staining (Figure 4.10N). Ly6C+ eosinophils sorted from isotype-treated tumours were significantly more cytotoxic compared to Ly6C+ eosinophils isolated from anti-IFN-treated tumours, or Ly6C- eosinophils isolated from both control and anti-IFN treated tumours (Figure 4.10 O).

In summary, these results suggested that while depletion of IFNγ or IFNβ signalling does not affect the transition of Ly6C+ eosinophils to the Ly6C- state, the absence of IFNs in the TME might lead to less degranulation and a reduction of their cytotoxic potential ex vivo. Therefore,

how eosinophils change their phenotype in IFN-rich TME upon response to ICB was further investigated.

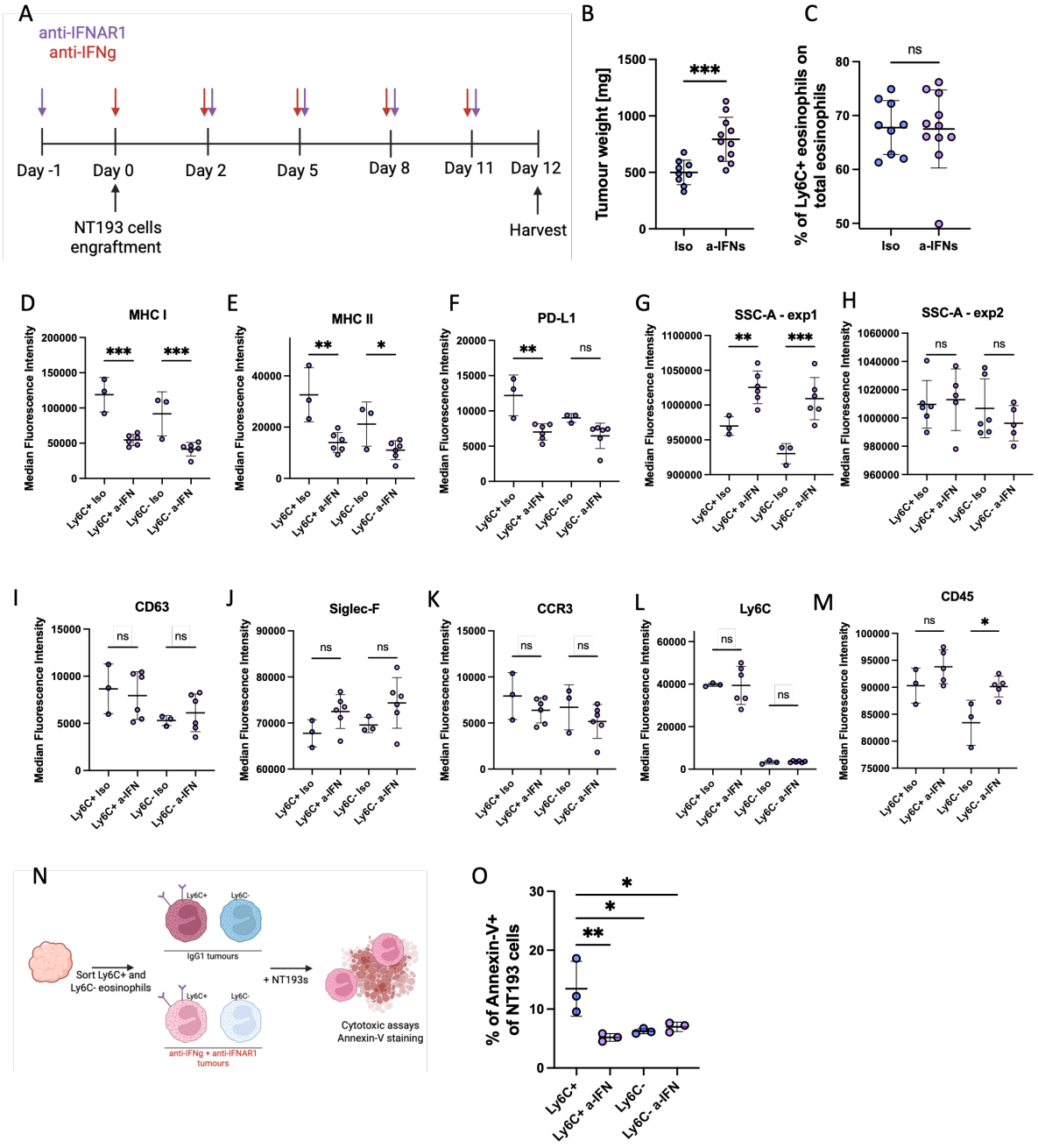


**Figure 4.10. In vivo blocking of IFNs leads to reduced cell activation of eosinophils. (A)** FVB mice were orthotopically grafted with the NT193 cell line into the 4th mammary fat pad and treated every 3 days with anti-IFNAR1 and anti-IFNγ antibodies (anti-IFNs) or isotype control (Iso), until reaching the humane end-point on day 12. **(B, C)** Tumour weight **(B)** and proportion of Ly6C+ eosinophils of total eosinophil population **(C)** of mice treated with isotype control (n = 9) and anti-IFNs (n = 11). Data are pooled from 2 independent experiments and show individual values and mean ± SD. Data were analysed by a two-tailed unpaired Student's t-test. **(D-M)** Comparison of MHC-I **(D)**, MHC-II **(E)**, and PD-L1 **(F)** expression, granularity in two independent experiments **(G, H)**, CD63 **(I)**, Siglec-F **(J)**, CCR3 **(K)**, Ly6C **(L)**, and CD45 **(M)** expression on Ly6C+ and Ly6C- eosinophils treated with isotype control (Iso, $n_{exp1}$ = 3, $n_{exp2}$ = 6) or anti-IFNs (a-IFNs, $n_{exp1}$ = 6, $n_{exp2}$ = 5). Data are representative of 2 independent experiments, except for granularity, for which both experimental repeats are shown. Measurements shown only in one experimental repeat are representative of both experiments. Data

show individual values and mean ± SD and were analysed by one-way ANOVA test using Holm-Šídák correction for comparison of anti-IFN treatments to the Isotype control group. **(N)** Schematics of the experimental approach. Ly6C+ and Ly6C- tumour-associated eosinophils were FACS sorted on day 12 from Isotype treated (n = 3) or anti-IFN (n = 3) treated mice, used in direct co-culture with NT193 cells for 3 days and NT193 cells were stained with Annexin-V to determine levels of apoptosis. **(O)** Comparison of Annexin-V+ NT193 cells cultured with Ly6C+ or Ly6C- eosinophils from Isotype or anti-IFN (a-IFN) treated mice. Data show individual values and mean ± SD and were analysed by one-way ANOVA test using Holm-Šídák correction for comparison of Ly6C+ isotype treated eosinophils to other experimental conditions. Statistical significance is displayed on figures as follows: *p < 0.05, **p < 0.01, ***p<0.001, ****p<0.0001.

### 4.2.7 Anti-PD-L1 treatment of NT193 tumours leads Ly6C+ eosinophil to degranulation

Eosinophils play an important role in mediating the response to immune checkpoint blockade (ICB)[184,199]. I have therefore hypothesised that during a successful response to ICB, which is well-known to be associated with T-cell activation and an increase of IFN signature[184], eosinophils themselves present with a more activated phenotype. To investigate how eosinophils adapt to the ICB-responsive TME, and if this potentially IFN-rich TME leads to increased eosinophil activation, NT193 tumour-bearing mice with established tumours on day 7 were treated with anti-PD-L1 antibody and the phenotype of the tumour-associated eosinophils was investigated by flow cytometry.

ICB treatment successfully induced regression of NT193 tumours (Figure 4.11A) and reduced the tumour weight on day 18 post-engraftment (Figure 4.11B) compared to the control cohort. Response to the ICB was not associated with differences in the proportion of Ly6C+ tumour-infiltrating eosinophils (Figure 4.11C). To understand if anti-PD-L1 treatment induced “IFN-like” phenotype in eosinophils that would be similar to eosinophils stimulated with IFNs ex vivo, expression of MHC-I and MHC-II was compared between ICB and control mice. Indeed, both subsets of eosinophils that were present in the ICB-treated tumours overexpressed MHC-I and MHC-II, with Ly6C+ eosinophils showing a greater increase in the expression (Figures 4.11D and E). Additionally, expression of Siglec-F was significantly downregulated on Ly6C+ eosinophils during ICB response (Figure 4.11F). These results recapitulated the eosinophil phenotype observed with IFNγ and IFNβ stimulation ex vivo and therefore suggested an increased presence of IFNs in the ICB-treated tumours. However, a direct assessment of the IFN levels by enzyme-linked immunosorbent assay (ELISA) would be needed. These assays are currently being optimised, as discussed in section 4.3.3.

Afterwards, granularity and CD63 expression on eosinophils were compared between the control and ICB-treated tumours as markers of active degranulation. Granularity of both subsets was reduced following the ICB response (Figure 4.11G), however, only Ly6C+ eosinophils presented with increased surface CD63 (Figure 4.11H). These results point to the possibility that ICB drives Ly6C+ eosinophils towards a more actively degranulating phenotype. Therefore, eosinophils were FACS sorted from isotype and ICB-treated tumours and cultured with the NT193 cell line to assess their potential to induce apoptosis ex vivo. However, no differences in apoptosis of NT193 cells were detected when comparing Ly6C+ or Ly6C- eosinophils from ICB or Isotype-treated tumours (Figure 4.11I).

Overall, NT193 tumours are responsive to ICB, as previously reported[228], and Ly6C+ eosinophils in the responsive immunogenic TME present with a more actively degranulating phenotype, suggesting their increased cytotoxicity. However, to understand if the observed change of eosinophil phenotype during ICB response is caused directly by IFNs, this experiment would have to be complemented with data from mice simultaneously treated by ICB and anti-IFNs. This experiment was not conducted within the timeframe of this project.

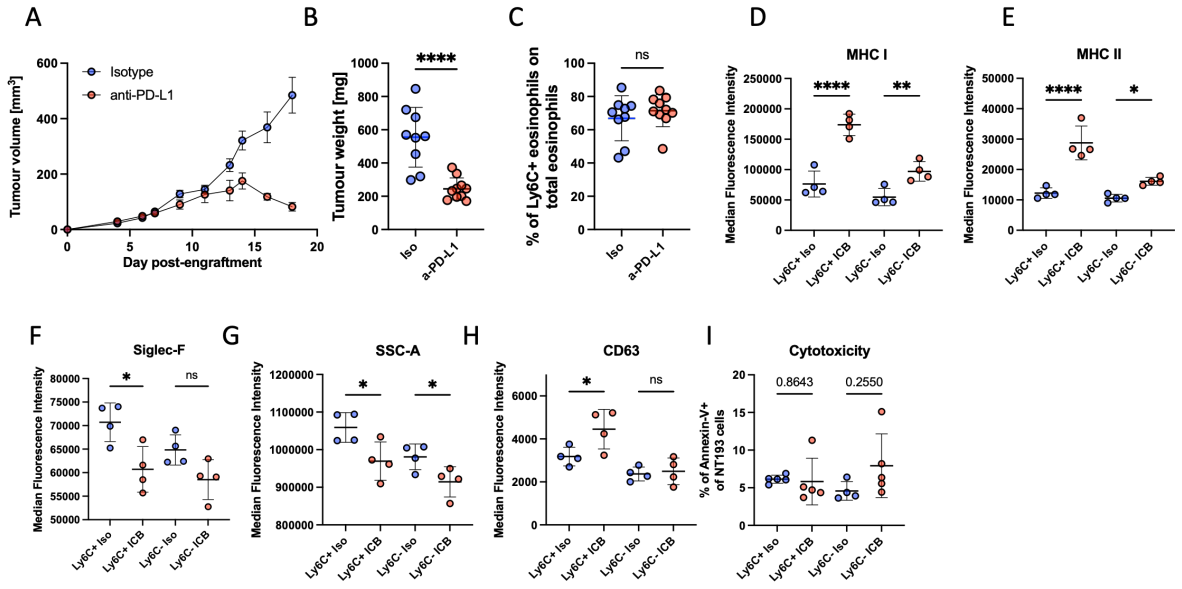


**Figure 4.11. anti-PD-L1 treatment results in tumour regression and a more degranulated eosinophil phenotype.** FVB mice were orthotopically grafted with the NT193 cell line into the 4th mammary fat pad and treated every 3 days with anti-PD-L1 or IgG2b isotype control antibodies up to day 18. **(A)** Tumour growth curve of mice treated with anti-PD-L1 (n = 6) or Isotype control (n = 5). Data show mean + SEM and are representative of 2 independent experiments. **(B, C)** Tumour weight **(B)** and proportion of Ly6C+ eosinophils of total eosinophil population **(C)** of mice treated with isotype (n = 9) or anti-PD-L1 (n = 10). Data are pooled from 2 independent experiments, show individual values and

mean ± SD, and were analysed by a two-tailed unpaired Student's t-test. **(D-G)** Comparison of MHC-I **(D)**, MHC-II **(E),** Siglec-F **(F)** expression, granularity (SSC-A) **(G)**, and CD63 expression **(H)** on Ly6C+ and Ly6C- eosinophils treated with isotype control (Iso, n = 4) or anti-PD-L1 (a-IFNs, n = 4). Data are representative of 2 independent experiments, show individual values and mean ± SD, and were analysed by one-way ANOVA test using Holm-Šídák correction for comparison of anti-PD-L1 treated eosinophils to the Isotype control group. CD63 expression was investigated in only one experimental repeat and a second experiment to confirm this result is planned. **(I)** Ly6C+ and Ly6C- tumour-associated eosinophils were FACS sorted on day 18 from isotype (n = 5) or anti-PD-L1 (n = 3) treated mice, used in direct co-culture with NT193 cells for 3 days and NT193 cells were stained with Annexin-V to determine levels of apoptosis. Data are representative of a single experiment, show individual values and mean ± SD, and were analysed by one-way ANOVA test using Holm-Šídák correction for comparison of anti-PD-L1 treated eosinophils to the Isotype control group. Statistical significance is displayed on figures as follows: *p < 0.05, **p < 0.01, ***p<0.001, ****p<0.0001, or above the figure.

### 4.2.8 Recurrent triple-negative breast cancer patients have higher levels of tumour-infiltrating eosinophils

Immunotherapy is a promising avenue for treating triple-negative breast cancer (TNBC), yet patient response remains variable[67,68]. Recent studies identified increased levels of eosinophils during responses to immune checkpoint blockade (ICB) in TNBC patients, with a lack of eosinophils diminishing the anti-tumorigenic effect of ICB in murine models[184]. How eosinophils infiltrate treatment-naïve breast tumours and whether a baseline increase of eosinophil infiltration could stratify patient responses to therapy is unknown. Current studies investigating eosinophil infiltration in primary breast cancer are mainly based on analysis of tumour microarrays (TMAs) and report an overall low density of eosinophils compared to many other tumour types[162]. Limitations of these approaches are discussed in section 4.3.5. Briefly, TMAs are a suitable tool for high-throughput screening and capturing inter-patient heterogeneity but due to the limited size of the cores, they are not suitable for studying the heterogeneity within individual tumours. Therefore, the final aim of this chapter was to analyse eosinophil infiltration in breast cancer patients using whole tumour sections.

To investigate if eosinophils are infiltrating primary breast tumours at a higher frequency than previously thought, full tumour sections were stained with anti-EPX antibody. The optimisation of anti-EPX antibody staining is discussed in section 4.3.5. The first analysed cohort consisted of 21 breast cancer patients received from the Oxford Biobank (REC reference 23/A034). These patients were evenly distributed among the 3 breast cancer subtypes, 6 HER2+, 7 ER+

and 8 TNBC patients (Figure 4.12A). Eosinophils were identified in all stained HER2+, ER+ and TNBC tumours at low density, except for 2 patients with increased eosinophil prevalence (Figure 4.12B). Overall, 18 patients were treatment-naïve with primary tumours, and 3 TNBC patients had locally recurrent disease, 2 of whom had the increased eosinophil infiltration. Eosinophils in these recurrent TNBC tumours were located at the tumour periphery, mostly in the tumour stroma (Figures 4.12C-E). However, no additional information in terms of previous radiotherapy or surgery could be assessed from the data acquired from the Oxford biobank. The accuracy of EPX staining was validated on colon samples (section 4.3.5, Figure 4.15), however, to confirm the accuracy of EPX staining in breast tumours, sequential tumour sections of both eosinophil-rich tumours were stained with isotype controls. This staining did not show any non-specific IHC staining in eosinophil-rich areas and therefore further validated the specificity of the anti-EPX staining in breast tissue (Figure 4.12.F).

Overall, anti-EPX IHC staining of a small cohort of 21 breast cancer patients identified TNBC patients with local recurrence as a potential group with higher infiltration of eosinophils. Recurrent and metastatic TNBC is a hard-to-treat disease, with these patients often being eligible for ICB therapy. Because increased eosinophil infiltration was linked to better responses to ICB, it would be interesting to know whether increased baseline presence of eosinophils could help with the stratification of TNBC patients prior to treatment.

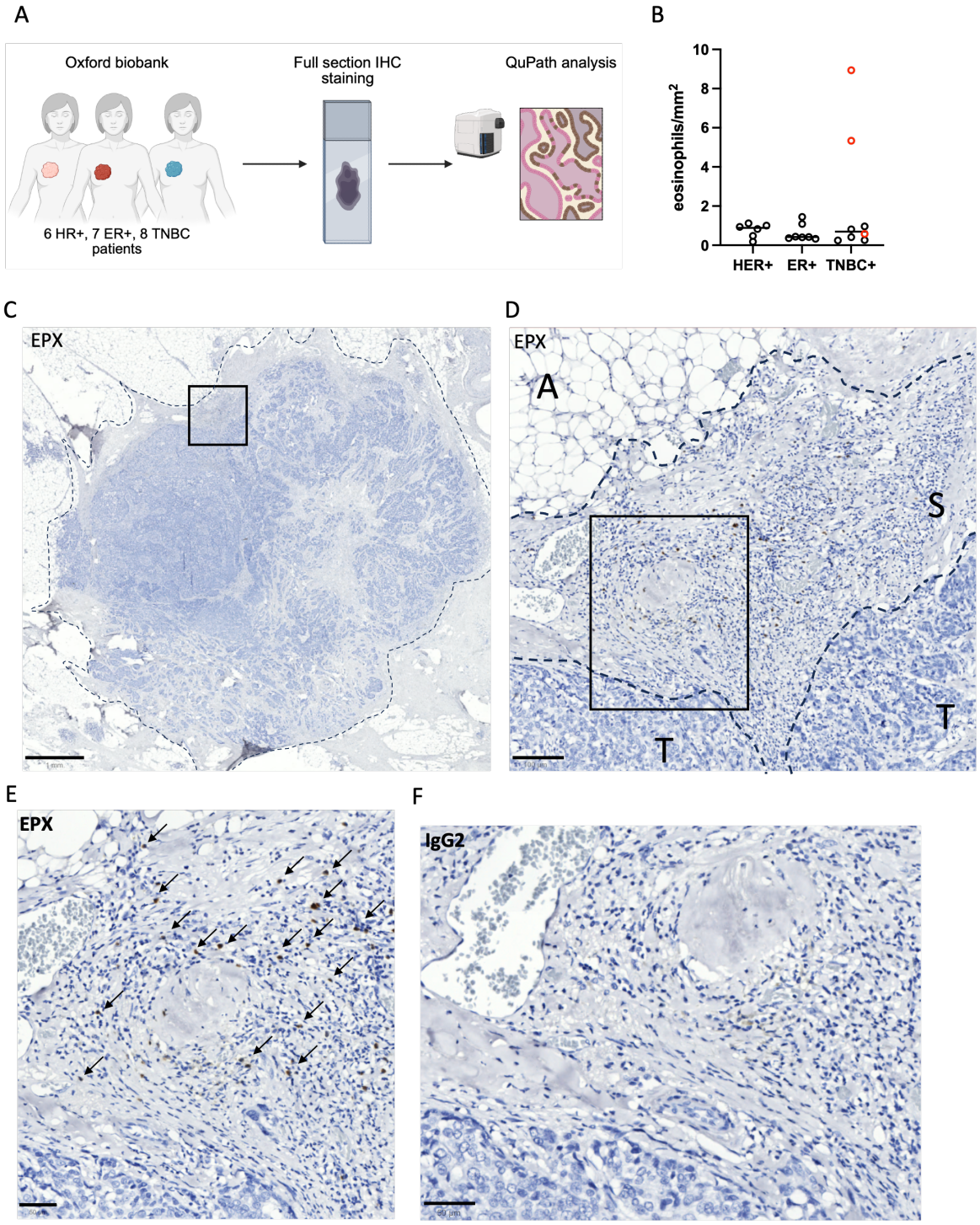


**Figure 4.12. Eosinophil infiltration in a cohort of breast cancer patients obtained from Oxford Biobank. (A)** Full sections obtained from 21 breast cancer patients with tumours at the primary site (6 HER2+, 7ER+, 8 triple negative (TNBC)) were stained by anti-EPX (eosinophil peroxidase) immunohistochemical staining (IHC) and analysed by QuPath. **(B)** Comparison of eosinophil densities. Locally recurrent TNBC patients are labelled in red. Each point represents an individual patient; breast cancer type is indicated. **(C)** Representative image of the anti-EPX IHC staining with contrast haematoxylin stain. Dashed lines represent tissue annotation. Cancerous tissue was annotated based on abnormal tissue structure and cell morphology, differing from the healthy breast tissue containing adipocytes. Annotations were consulted with a pathologist. Scale bar = 1mm. **(D)** Selected representative area of tumour periphery with eosinophil infiltration in tumour stroma (S) compared to no eosinophil detection in tumour nests (T) or healthy adjacent adipose tissue (A). Dashed lines represent

tissue annotation based on cell morphology; annotations were consulted with a pathologist. Scale bar = 100μm **(E-F)** Eosinophil detection by IHC staining with anti-EPX antibody (positive cells stained with DAB (brown)) **(E)** and serial section from the same patient stained with IgG2 isotype **(F)**. Scale bar = 50μm. Arrows indicated an EPX+ eosinophil

Following these preliminary results, a larger cohort obtained from Breast Cancer Now (REC reference 23/EE/0229) was stained with anti-EPX antibody, to test if locally recurrent TNBC patients have a higher likelihood of eosinophil infiltration. This cohort consisted of 5 HER2+, 5 ER+, and 5 TNBC patients with primary tumours and 13 TNBC patients with local recurrence, of whom 6 underwent radiotherapy and 7 were radiotherapy-naïve (Figure 4.13 A). Of these patients, two cases were excluded, one HER2+ tumour was excluded because there was no tumour tissue detected, and one recurrent TNBC tumour was removed because of a high background staining and therefore was not reliable for eosinophil detection. Analysis of the anti-EPX staining in this cohort of patients revealed that 4 out of 11 locally recurrent TNBC patients presented with eosinophil infiltration above 5 eosinophils/$mm^2$. In comparison, only one patient of either the TNBC or ER+ patient cohort with a primary tumour had eosinophil infiltration above the 5 eosinophils/$mm^2$ threshold (Figure 4.13B). Furthermore, analysis of recurrent TNBC patients obtained from Breast Cancer Now biobank allowed for comparison of patients previously treated with radiotherapy to radiotherapy-naïve, with the radiotherapy-naïve tumours presenting with a higher eosinophil count (Figure 4.13C).

Because of similar infiltration patterns, quality of tissue and IHC staining, patients from both Oxford Biobank and Breast Cancer Now cohorts were analysed together to empower the statistical analysis. This confirmed that locally recurrent TNBC patients had significantly elevated eosinophil infiltration compared to TNBC patients with primary tumours, ER+ and HER2+ breast cancer patients (Figure 4.13D).

In summary, analysis of samples obtained from two independent breast cancer biobanks suggested that TNBC patients with local recurrence might present with increased eosinophil

infiltration. To confirm these results and their potential relevance for breast cancer patients, a larger cohort of patients with more detailed clinical information would be needed.

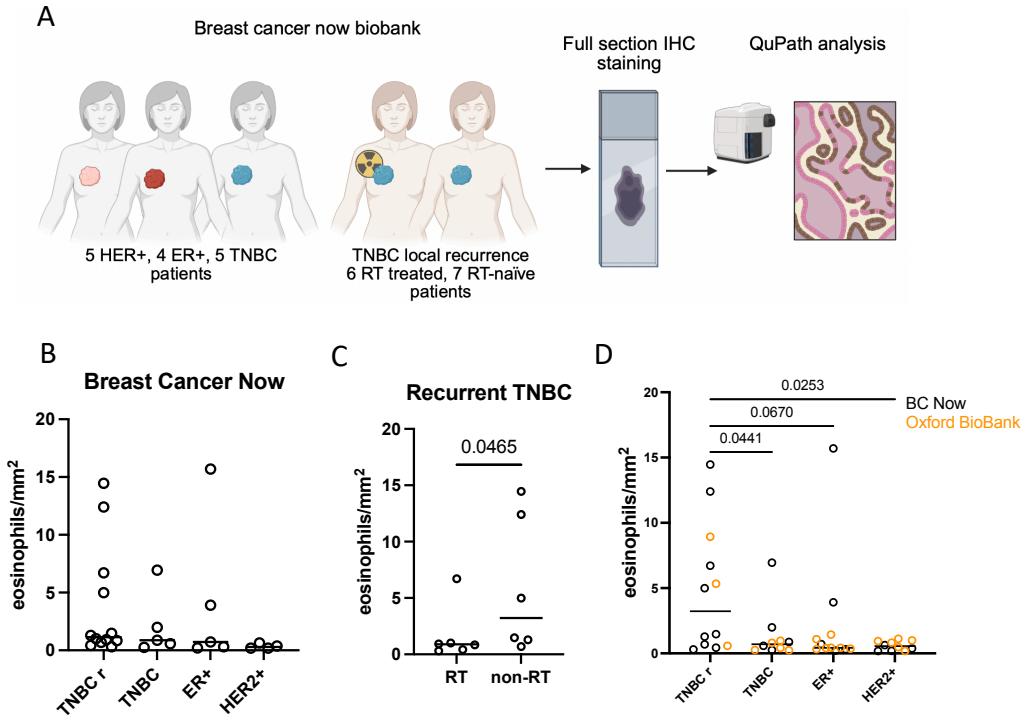


**Figure 4.13. Eosinophil infiltration is elevated in locally recurrent TNBC tumours. (A)** Full sections obtained from 27 breast cancer patients with tumours at the primary site (5 HER2+, 4ER+, 5 triple negative (TNBC), 13 locally recurrent TNBC – 7 treated with radiotherapy (RT), 6 RT-naïve) were stained by anti-EPX (eosinophil peroxidase) immunohistochemical staining (IHC) and analysed by QuPath. **(B)** Comparison of eosinophil densities. **(C)** Comparison of eosinophil densities of locally recurrent TNBC patients previously treated with RT compared to RT-naïve patients. All samples were obtained from Breast Cancer Now biobank. **(D)** Comparison of eosinophil densities merged from Oxford Biobank (orange) and Breast Cancer Now cohort (black).

## 4.3 Technical discussion

### 4.3.1 Technical challenges of eosinophil sequencing and their transcriptomic analysis

This chapter builds on the initial bulk RNA sequencing (bulk RNA-seq) analysis that revealed increased responsiveness of Ly6C+ tumour-associated eosinophils to interferons (IFN). However, studying the transcriptomic signature of eosinophils presents several challenges, such as the overall low yield of mRNA and high RNase activity, already discussed in section 3.3.1. While eosinophils were already successfully studied by single cell RNA-seq (scRNA-seq)[125,126], in this chapter bulk RNA-seq was prioritised over scRNA-seq for a number of reasons.

First, the two eosinophil subsets were clearly distinguished by Ly6C surface expression prior to sequencing. How this difference in surface expression would relate to mRNA levels of Ly6C was unclear. Therefore, the main concern was that while scRNA-seq is a powerful tool to explore eosinophil heterogeneity, it might not be sensitive enough to recognise different levels of *Ly6c1* or *Ly6c2* expression. In that case, this dataset would not be relatable to the already defined eosinophil subsets, impairing the downstream validation and analysis.

Second, bulk RNA-seq offers a greater sequencing depth per sample, enabling the detection of lowly expressed genes. This is especially important when sequencing eosinophils, due to their low mRNA levels. Therefore, using a bulk RNA-seq pipeline allowed for ultra-low input amplification and more robust sequencing results. As a result of this approach, genes encoding all essential eosinophil lineage markers, such as *Siglecf*, *Adgre1* (F4/80), and *Ccr3* were detected, suggesting a high eosinophil purity. Detection of these transcripts is not always possible in the publicly available scRNA-seq datasets focused on murine eosinophils[170].

Last, the current successful scRNA-seq protocol requires a minimum of 60 000 cells post-enrichment with anti-Siglec-F magnetic beads[126]. In this experiment, eosinophils were

enriched using CD45 magnetic beads as part of a shared sorting pipeline for tumour-associated macrophages sequenced in Chapter 5. This approach resulted in a lower yield of eosinophils, within a range of 10 000 – 50 000 cells due to the sorting time constraints. To minimise any further losses, eosinophils were sorted straight into RLT with β-mercaptoethanol. This would not be compatible with the scRNA-seq pipeline. However, it would be interesting to know if unbiased scRNA-seq would also reveal these two subsets of eosinophils and potentially help with elucidating the mechanism behind the transition of Ly6C+ to Ly6C- eosinophil subset through pseudo-time analysis. Furthermore, scRNA-seq could reveal an additional heterogeneity within the Ly6C+ and Ly6C- eosinophil subsets.

### 4.3.2 Validation of bulk RNA sequencing

To confirm the identity and purity of sorted Ly6C+ and Ly6C- eosinophils, the expression of canonical eosinophil lineage markers was compared to markers of other cell types. This analysis, described in section 4.2.1, showed an increased expression of eosinophil surface markers, however, consistently low expression of granule protein genes, including major basic protein (*Prg2*), eosinophil peroxidase (*Epx*), and eosinophil cationic protein 1 (*Ear1*), despite their well-known abundance at the protein level. This phenomenon is consistent with other published datasets and highlights the known discrepancy between the transcriptomic and proteomic profiles of eosinophils, likely due to post-transcriptional regulation and pre-packaged granules formed during eosinophil maturation in the bone marrow[98,125]. Low abundance of eosinophil cationic proteins on the gene level was also linked to eosinophil maturity[125], despite this, genes encoding granule proteins are part of the leukocyte signature matrix used by CIBERSORT to detect eosinophils[296]. Moreover, *Epx* was used as a part of 3 3-gene signature in a recent review comparing overall survival based on eosinophil presence[160]. Whether or not *Epx* or other eosinophil cationic proteins are reliable eosinophil markers when analysing transcriptomic datasets should be further considered.

Being aware of the discrepancies between mRNA and protein expression, the results of the bulk RNA-sequencing were validated through manually selected surface protein markers (Figure 4.3) or ex vivo stimulations (Figure 4.4), both analysed by flow cytometry. However, it would be interesting to see if an unbiased analysis of the proteome of the Ly6C+ and Ly6C- eosinophil subset by mass spectrometry would also validate some of the identified enriched gene sets. For example, Ly6C+ eosinophils were observed to be more granular through flow cytometry and H&E staining and upregulated pathways related to cell killing. Knowing if this difference translates into enrichment of eosinophil granule proteins could further complement the analysis.

### 4.3.3 Limitations of studying IFN effect on eosinophil cytotoxicity

Because of the increased IFN responsiveness of Ly6C+ eosinophils, I examined the effect of IFNγ and IFNβ stimulation on tumour-associated and bone marrow-derived eosinophils through a series of ex vivo experiments. The aims of these experiments were three-fold: 1) validate IFN responsiveness based on PD-L1 expression, 2) characterise the effect on a broader set of surface markers and granularity, and 3) study the effect of IFN stimulation on eosinophil cytotoxic potential. However, in all ex vivo assays, stimulation with both types of interferons resulted in decreased viability (Figures 4.5A, 4.8A). While this does not affect flow cytometry analysis of receptor expression of live cells in the first two aims, the decreased viability might be affecting the physical properties, such as granularity, of early apoptotic but still viable eosinophils (Figures 4.5B and 4.8B) and their cytotoxic properties.

Considering that following the IFN stimulation the viability of Ly6C+ and Ly6C- tumour-associated eosinophils was reduced 1.5-fold and 2-fold, respectively, and the rate of NT193 cell line apoptosis was unchanged or slightly increased after co-culture with the stimulated eosinophils, this points to a possibility that the remaining eosinophils at lower density were significantly more cytotoxic. While a similar trend of reduced viability was observed on the

bone marrow-derived eosinophil population, the impact on eosinophil viability was less pronounced, which enabled more direct comparison of the cytotoxic effects.

It is important to notice that IFNs were found to be directly cytotoxic towards cancer cell lines in some studies[297,298], but not in others[171]. To prevent direct IFN interference with the cytotoxic assays, stimulated eosinophils were washed prior to co-culture with cancer cell lines, however, it is possible that traces of IFNs could still be present in the culture. No data exploring the direct cytotoxic effect of IFNs on NT193 or E0771 cell lines were found in the literature. Therefore, further experiments testing the cytotoxicity of different IFN concentrations on cancer cell lines might help with understanding the extent of this issue with the NT193 and E0771 cell lines used in this chapter.

Additionally, due to limited eosinophil yield from tumours, direct comparisons between IFNγ and IFNβ stimulation in tumour-associated eosinophils could not be tested independently. Instead, both Ly6C+ and Ly6C- eosinophils were stimulated with a 1:1 mixture of IFNγ and IFNβ at a total concentration of 20ng/ml. However, this might have further affected the eosinophil viability as bone marrow-derived eosinophils were stimulated with a lower concentration of IFNs separately (10ng/ml).

Overall, the viability of sorted tumour-associated eosinophils is lower compared to sorted bone-marrow-derived eosinophils, even prior to IFN stimulation (Figures 4.5A, 4.8A). This is likely due to the enzymatic and mechanical digestion of tumours, necessary to isolate eosinophils from a single cell suspension. This partially explains why tumour-associated eosinophils appeared less cytotoxic than bone marrow-derived eosinophils in assays used in section 4.2.5. Because these technical limitations cannot be overcome, bone marrow-derived eosinophils represent a better model to study the effects of eosinophil cytotoxicity ex vivo.

### 4.3.4 Limitations of studying IFN blocking in an in vivo setting

To complement the ex vivo finding of IFNs enhancing eosinophil cytotoxicity and possibly Ly6C expression, I sought to examine the effect of IFNs on eosinophil phenotype in vivo. To do this, two antibody-based methods were used to alter eosinophil phenotype infiltrating NT193 tumours: 1) neutralisation of IFNγ and simultaneous blocking of IFNAR1 (anti-IFN), and 2) immune checkpoint blockade treatment with anti-PD-L1 antibody known to result in endogenous IFNs expression[299]. Both anti-IFN and anti-PD-L1 treatment regimens affected eosinophil phenotype in terms of MHC-I, MHC-II, PD-L1 expression, or granularity (Figures 4.10 and 4.11). However, while neutralisation of IFNs clearly links this altered phenotype to the absence of IFN signalling in the TME, it is less clear how anti-PD-L1 treatment altered IFNγ and IFNβ levels. Therefore, I have tried to quantify IFN levels in tumour lysates by ELISA. However, both IFNs were below the detection threshold. This is likely due to the short half-life of interferons and their degradation during the 30 minutes enzymatic digestion at 37°C. To optimise the IFN detection, tumour lysates will be taken after the mechanical mincing of tumours before the enzymatic digestion, to decrease the IFN degradation. In immediate terms, for validation of successful IFN depletion or induction, a decrease or increase in MHC-I and MHC-II expression was used, respectively.

While both anti-IFN and anti-PD-L1 treatments showed that a proportion of Ly6C+ eosinophils is not regulated by IFNs, the main limitation is that these treatments do not target eosinophils specifically but remodel the whole TME. IFNs have a major effect on the overall immunogenicity of the TME, with a well-established role in regulating antigen presentation[300], activation of the myeloid compartment[301], and having a direct cytotoxic effect against cancer cells[302]. Therefore, changes in the tumour growth are not directly linkable to the altered eosinophil phenotype. To isolate the specific contribution of IFN signalling in eosinophils on the TME and tumour growth, we would need to generate a mouse model with conditional IFNGR2 or IFNAR1 knockout under *Epx* promoter, to specifically deplete IFNγ or IFNβ

signalling in eosinophils. This approach was considered, however, all currently available eosinophil mouse models are on the C57/Bl6 background, and therefore, any generated model would have to be backcrossed for at least 10 generations to the FVB background. This was not feasible within the timeline of this project.

Lastly, to evaluate functional consequences of altered eosinophil phenotypes related to anti-IFN and anti-PD-L1 treatments in NT193 tumours, I used ex vivo cytotoxicity assays. As discussed above in section 4.3.3, these assays present multiple technical challenges, especially when conducted with tumour-sorted eosinophils. One additional limitation is the sorting of potentially activated granulocytes that have already degranulated in the tissue and therefore might not have the cytotoxic potential ex vivo. It is difficult to estimate what could be the extent of this limitation; however, it would explain why the difference between Ly6C+ and Ly6C- eosinophil cytotoxicity is smaller when sorting tumour-associated eosinophils compared to BM-derived eosinophils, or eosinophils from ICB IFN-rich TME compared to eosinophils from isotype-treated mice. To avoid using the ex vivo apoptotic assay, an alternative assay detecting cell death in situ could be used. For example, co-staining of frozen sections with anti-Siglec-F antibody and terminal deoxynucleotidyl transferase dUTP Nick End Labelling (TUNEL) kit or antibodies against cleaved caspase-3 to detect late and early apoptosis could reveal increased cell death in close proximity to eosinophils, suggesting their increased cytotoxicity.

### 4.3.5 Optimisation of eosinophil staining in human tissue

Eosinophils are vastly understudied in human disease, mostly because of their absence in scRNA-seq datasets and also the low abundance of their signature in bulk RNA transcriptomic studies[268]. Therefore, eosinophil infiltration in breast tumours was recently assessed by immunohistochemistry staining of 576 TMAs, with this analysis pointing to an overall low infiltration in breast tumours[162]. However, TMAs represent only a limited area of the tumour (1-

2 $mm^2$), are often taken from the tumour core and therefore do not capture the intra-tumoral heterogeneity. For this reason, we aimed to investigate eosinophil infiltration in full sections obtained from 42 breast cancer patients.

Because the well-established Giemsa staining method used for the detection of eosinophils based on their protein-rich granules might be impacted by eosinophil degranulation in the tissue, I first needed to optimise a robust staining method that would be highly specific. All optimisation steps were performed on a healthy colon with steady levels of eosinophils. First, I tried immunofluorescent (IF) staining with an antibody against major basic protein (MBP) and eosinophil peroxidase (EPX), previously reported to be a useful marker for eosinophils in the colon[120,125] (Figure S5). However, in my hands, this staining was not specific for eosinophils and a fluorescent signal was detected even on isotype-stained controls (Figure S5). This is likely caused by a) incomplete antigen processing that did not reveal the eosinophilic granule epitopes or b) the presence of highly autofluorescent macrophages reported in colon samples[303].

To address these issues, different antigen processing methods combined with immunohistochemistry (IHC) staining were optimised. First, IHC EPX staining of samples retrieved with heat-induced antigen retrieval using a citrate solution (pH = 6) was compared to samples treated with Tris (pH = 9) or samples that did not undergo any antigen retrieval (Figure 4.14).

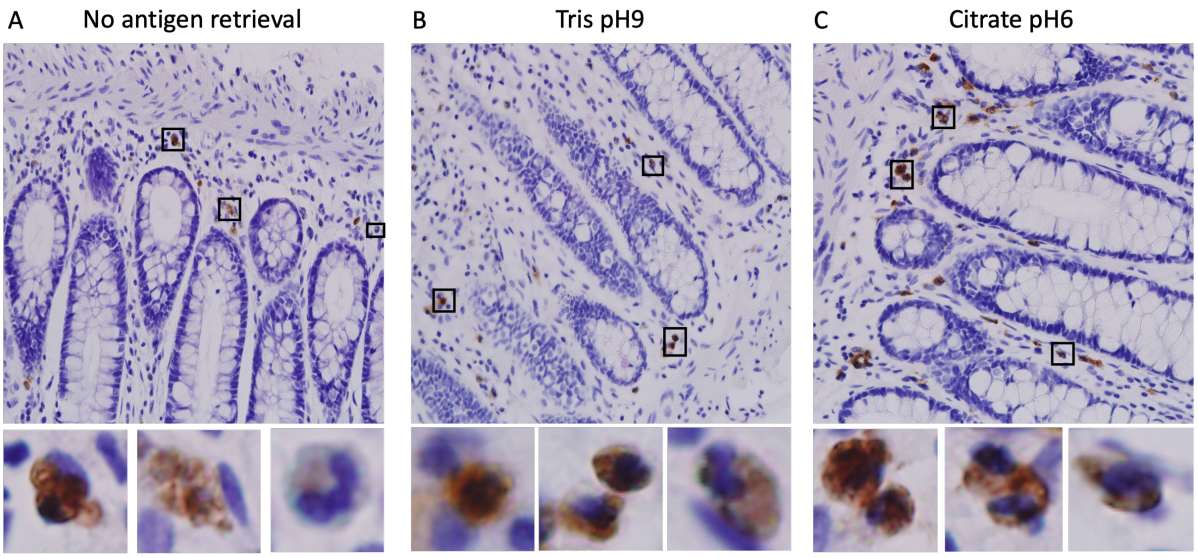


**Figure 4.14 Optimisation of antigen retrieval for EPX immunohistochemistry chromogenic staining.** Healthy human colon slides underwent **(A)** no antigen retrieval, or heat-induced antigen retrieval with **(B)** Tris pH9, or **(C)** citrate pH6. Afterwards, slides were stained with the immunohistological protocol for anti-EPX staining and imaged on Zeiss Axio Scan7.

Based on these results, citrate solution was selected for further assays due to the higher signal-to-noise ratio of eosinophils and more specific detection of eosinophils. Isotype staining with IgG2 antibody further validated the high specificity of the anti-EPX staining in the healthy colon samples (Figure 4.15).

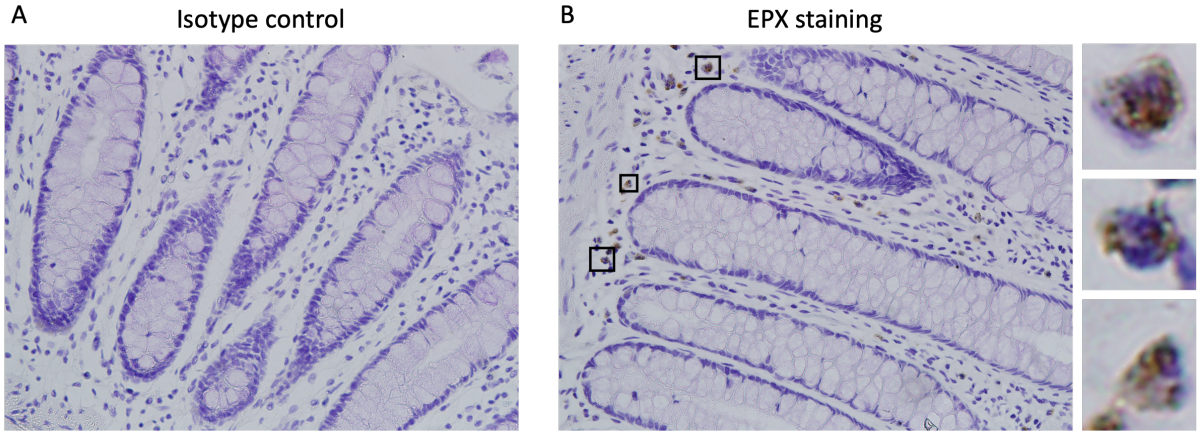


**Figure 4.15 Validation of EPX staining specificity on human colon samples.** Healthy human colon slides underwent heat-induced antigen retrieval with citrate pH6. Afterwards, slides were stained with the immunohistological protocol for **(A)** IgG2a and **(B)** anti-EPX staining and imaged on Leica microscope.

While IHC detection of eosinophils with anti-EPX staining was optimised and validated, this method also presents technical limitations. First, for amplification of signal, secondary

antibody with horse radish peroxidase (HRP) was used, as HRP enables strong signal amplification by catalysing a colourimetric reaction of chromogenic substrate DAB in the presence of hydrogen peroxide. However, this reaction can be catalysed by a number of peroxidases including cell-endogenous ones. Even though all samples were pretreated with hydrogen peroxide prior to staining to quench their activity, some cells retained their intrinsic peroxidase activity and were recognised even in isotype-treated sections (Figure 4.16A).

As this staining was non-specific for the EPX antigen, these areas were manually curated to remove these cells. Furthermore, all cells annotated as positive based on a DAB threshold set up in QuPath software were manually curated to exclude any tissue artefacts (Figure 4.16B). Additionally, tissue sections that were of poor quality, likely destroyed by treatment, were also excluded from further analysis (Figure 4.16C, D).

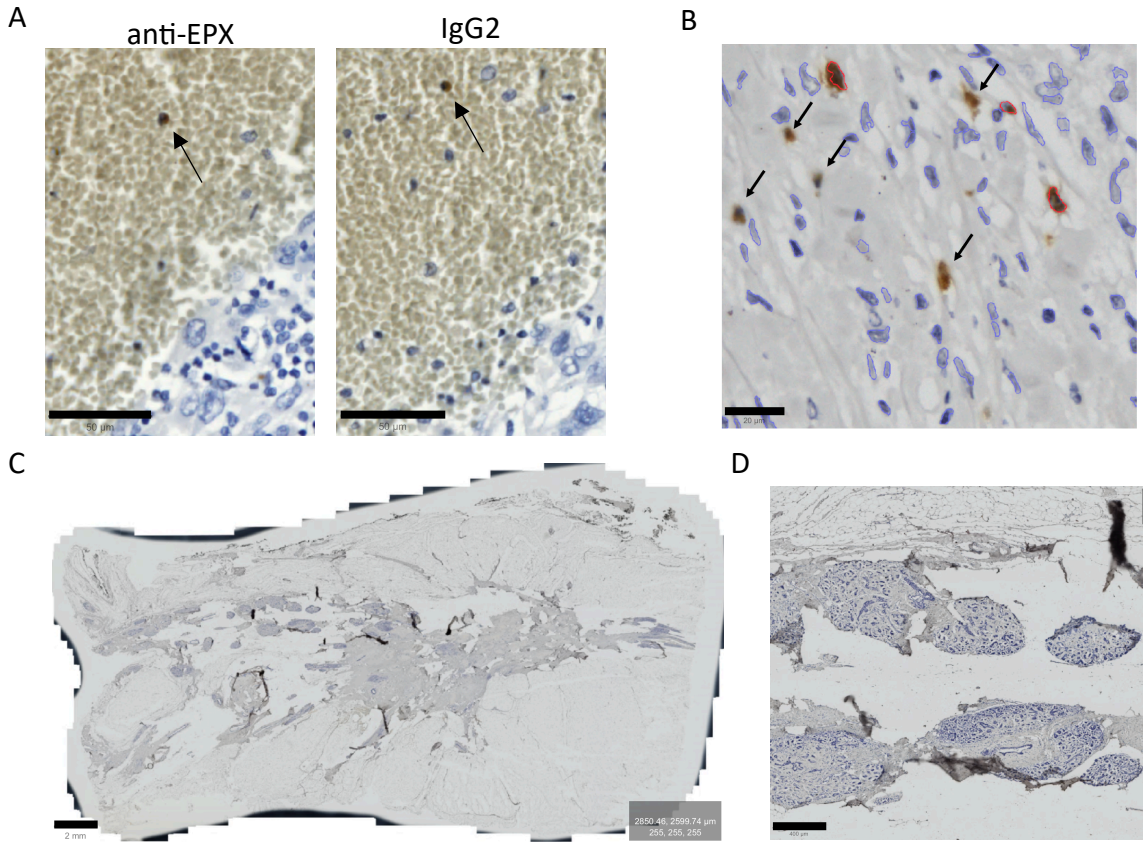


**Figure 4.16. Limitations of the immune histochemistry anti-EPX staining.** Full sections obtained from breast cancer patients were stained with anti-EPX or control IgG2 immunohistochemistry staining

and analysed by QuPath **(A)** Comparison of anti-EPX and control IgG2 staining on 2 serial sections from the identical donor. Arrow points at the cell type identified in both staining conditions. Scale bar = 50 µm**. (B)** QuPath cell annotation of the anti-EPX IHC stained section (negative cells – blue, positive cells – red, arrow pointing at non-nucleated DAB-positive staining). Scale bar = 20 µm. **(C-D)** Representative image of a tissue not analysable with QuPath cell annotations. **(C)** Scale bar = 2mm. **(D)** Scale bar = 400 µm.

Overall, the IHC anti-EPX presented a robust method to reliably detect eosinophils with high accuracy. However, macrophage and mast cell markers could be tested to exclude the possibility that the DAB staining is a result of endogenous peroxidases. Additionally, these sections could be further stained by a Giemsa staining that could confirm eosinophil identity independently of antigen staining.

## 4.4 Biological discussion

### 4.4.1 How do IFNs enhance eosinophil cytotoxicity?

Eosinophils, bone marrow-derived granulocytes, dynamically adapt their phenotype to their local niche. A growing body of literature describes their functional heterogeneity across different organs and disease states, including cancer[94,159]. Tumour-associated eosinophils were recently found to be responsive to IFNγ in murine models of colorectal cancer (CRC)[170]. Furthermore, IFNγ stimulation of splenic eosinophils ex vivo resulted in increased apoptosis of CRC cell lines[171]. Additionally, only 90-minute incubation of active eosinophils with IFNγ led to their degranulation ex vivo[125], pointing to the strong effect of IFNs on eosinophil biology. In this chapter, Ly6C+ eosinophils represent a more cytotoxic eosinophil subset with increased responsiveness to IFNγ and IFNβ. This led to the hypothesis that their IFN responsiveness potentiates the increased cytotoxicity of the Ly6C+ subset, likely through direct degranulation.

Indeed, ex vivo, BM-derived Ly6C+ eosinophils had enhanced cytotoxic properties following IFN stimulation. However, IFN stimulation also led to increased cytotoxicity of Ly6C- BM-derived and tumour-associated eosinophils (TAE), even though they were less responsive to IFNs (Figure 4.9). These data are in line with the previously described enhanced cytotoxicity upon IFNγ stimulation[171], but also suggest that Ly6C- eosinophils are capable of increasing their cytotoxicity in the ex vivo setting with unlimited access to IFNs. It is possible that Ly6C- eosinophils present with a less responsive IFN phenotype not due to their differentiation or exhaustion state, but simply due to the inaccessibility of IFNs in their local niche. As the Ly6C+ eosinophils transition to the Ly6C- state during the exponential tumour growth phase, it may be that the more established pro-tumorigenic TME has lower levels of type I cytokines and this further impacts the immune suppression of the newly transitioned Ly6C- eosinophils. This points at the complexity of the spatial and temporal eosinophil regulation in vivo.

To test whether Ly6C+ or Ly6C- eosinophils have different co-localisation patterns with IFNs in murine models of breast cancer, I have attempted to optimise an immunofluorescent staining with Ly6C and Siglec-F that would help to spatially distinguish these 2 subsets. For this experiment, early tumours containing eosinophils predominantly of Ly6C+ phenotype were picked as a positive control. However, due to the high expression of Ly6C by monocytes, this staining is technically challenging, and only very few eosinophils were specifically stained with the Ly6C antibody at the exposure time that distinguishes them from monocytes (Figure 4.17).

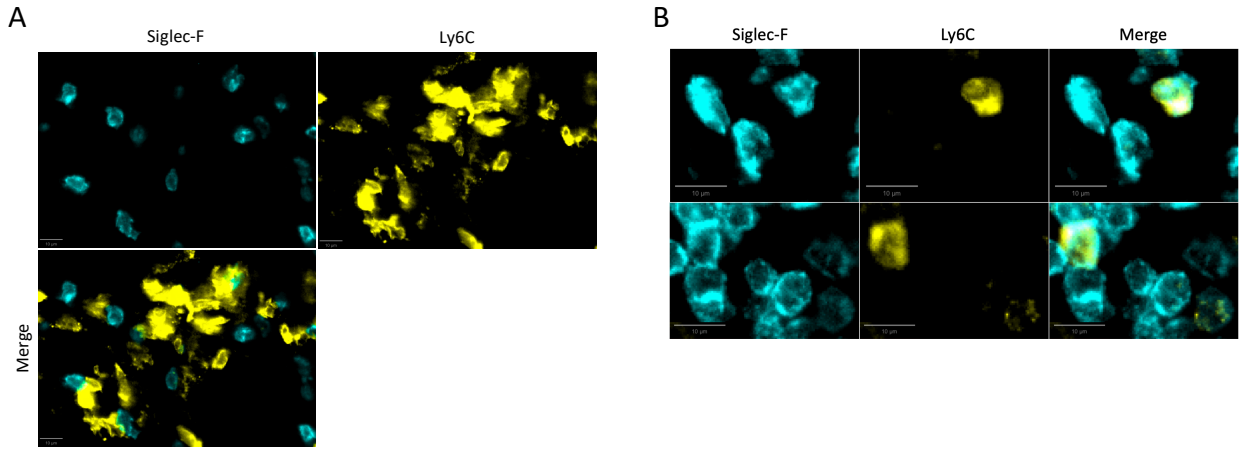


**Figure 4.17. Immuno-fluorescent staining of NT193 tumours with Siglec-F and Ly6C antibodies.** Tumours harvested at day 7 were fixed with PFA-based fixative, dehydrated in sucrose and frozen in OCT, prior to cryosectioning and staining with immunofluorescent antibodies. Day 7 tumours were imaged with **(A)** longer exposure times to capture lower intensity of Ly6C staining on eosinophils and **(B)** shorter exposure times capturing only eosinophils with the highest Ly6C expression. Scale = 10um.

Ex vivo, IFNγ stimulation but not IFNβ stimulation, led to decreased granularity of Ly6C+ eosinophils (Figures 4.5 and 4.8). This suggests that Ly6C+ eosinophils are actively degranulating upon IFNγ signalling. However, it is important to notice that this change in granularity was not associated with increased expression of CD63, a common marker of piecemeal degranulation[289]. Together with the fact that IFN stimulation decreases eosinophil viability, the decreased granularity in the absence of surface expression of CD63 might be caused by cytolytic degranulation that results in cell death due to cell wall rupture. Results of these assays are therefore inconclusive and to prove the active degranulation of Ly6C+ eosinophils ex vivo upon IFNγ signalling, additional ELISA assays detecting eosinophil

peroxidase or major basic protein in the supernatant of IFN-stimulated eosinophils would be needed.

In one of the experimental repeats, blocking of IFNγ and IFNβ signalling in vivo led to a significant increase in granularity of both Ly6C+ and Ly6C- TAE with no differences in CD63 expression, suggesting a blocked eosinophil degranulation. In contrast, treatment of NT193 tumours with anti-PD-L1 ICB therapy, commonly associated with IFN-rich TME, led to a significant decrease in granularity of both TAE subsets and overexpression of CD63 only by the Ly6C+ eosinophil subset. This suggests an activation and more pronounced degranulating phenotype of Ly6C+ eosinophils during ICB response. Therefore, these experiments collectively point to the importance of interferons regulating eosinophil degranulation and also present a potentially new mechanism by which eosinophils might contribute to treatment response during ICB treatment[184].

It is also important to comment on the fact that while stimulation with either of the IFNs enhanced the eosinophil cytotoxicity ex vivo, IFNβ stimulation did not affect the eosinophil granularity. This suggests that IFNβ signalling activated different pathways leading to the anti-tumorigenic effect. As discussed in the introduction section 1.3.4, overexpression of adhesion receptors CD11b, CD18, LFA-1, and ICAM-1 on bone marrow-derived eosinophils was previously linked to increased eosinophil-mediated cytotoxicity[177,181]. Moreover, IFNs can induce adhesion of leukocytes, such as monocytes[304]. Therefore, this raises a question of whether IFNs increased eosinophil cytotoxicity in the direct co-culture assays (Figure 4.9) through their enhanced attachment to the cancer cells. However, the flow cytometry analysis data obtained from the IFNγ and IFNβ stimulation of bone marrow-derived eosinophils suggest that Ly6C+ eosinophils downregulate CD11b receptor in response to both IFNs, and Ly6C- eosinophils downregulate CD11b only in response to IFNγ (Figure S6); therefore, suggesting a decrease in eosinophil adhesion upon IFN stimulation. These data are however limited, as

expression of the other adhesion surface proteins should be investigated in future experiments.

### 4.4.2 Do IFNs regulate eosinophils beyond degranulation?

Currently, most evidence describing eosinophil heterogeneity originates from studies on the gut and lungs, due to the increased eosinophil prevalence at mucosal sites[94]. Two populations of gut-resident eosinophils were observed at baseline level - active immunomodulatory (A-Eos) and basal (B-Eos) eosinophils involved in tissue remodelling. A-Eos express higher levels of PD-L1, are involved in immune regulation and were shown to have an important role in regulating a murine model of colitis[125]. Although ex vivo studies clearly point to different eosinophil regulation by Th1 (IFNγ – inflammatory phenotype similar to eosinophils present in colitis) and Th2 cytokines (IL-4, IL-33 – regulation of T cell differentiation and leukocyte cell-cell adhesion phenotype similar to eosinophils in asthma)[125,179,180], in vivo, A-Eos are jointly regulated by both IL-33 and IFNγ. IL-33 is essential for A-Eos development and IFNγ increases their immunoregulatory properties[125]. Together, these findings highlight that eosinophil functional heterogeneity arises from the integration of both Th1- and Th2-derived signals, rather than being driven by a single cytokine pathway.

In line with the previously performed IFNγ stimulation of eosinophils[125,180], expression of immunomodulatory receptors, such as MHC-I, MHC-II and PD-L1 on eosinophils, was dependent on IFN signalling. Moreover, MHC-I and MHC-II expression was more affected on Ly6C+ eosinophils than Ly6C- eosinophils during ICB and anti-IFN treatment; even though this difference was not statistically significant, the data point at a clear trend with ICB-treated Ly6C+ eosinophils consistently upregulating MHC-I and MHC-II and anti-IFN treated Ly6C+ eosinophils downregulating expression of these receptors (Figure S7). These data however need further repeats to prove the biological relevance. Despite IFN-induced Ly6C expression ex vivo (Figure 4.6), blocking or enhancement of IFNs in vivo did not alter the ratio of

Ly6C+/Ly6C- subsets in the tumours or had a minor effect. To understand if a prolonged IFN signalling has the potential to impact eosinophil development in a controlled setting, BM-derived eosinophils were cultured with IFNγ for 4 days until day 14 and eosinophil distribution between the 4 eosinophil development stages described in Chapter 3 was investigated. However, only a minor statistically non-significant shift towards CCR3+ Ly6C- eosinophils was observed, with results likely to be impacted by the decreased viability (Figure 4.18). This shows that while IFNs are regulating eosinophil phenotype, they are not able to act as a single factor affecting their transition.

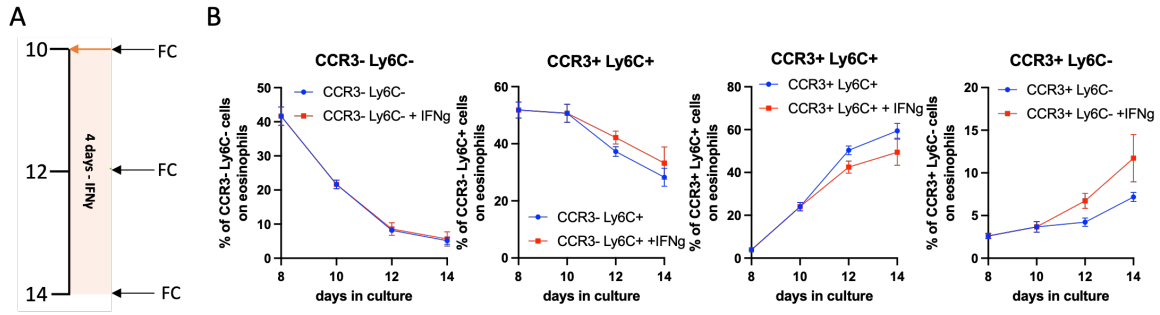


**Figure 4.18. IFNγ stimulation of BM-derived eosinophils. (A)** Overview of the experimental approach; bone marrow cells of C57/Bl6 male mice (n = 3) were first cultured with Fltl3 and mSCF for 4 days, then differentiated into eosinophils with IL-5 until day 14. Orange arrow indicates beginning of IFNγ treatment, black arrows indicate timepoints when eosinophils were investigated by flow cytometry. **(B)** Comparison of eosinophil development in the presence (red) or absence (blue) of IFNγ on the indicated days.

Following the reports of strong Th2 polarization of eosinophils by IL-4 and IL-33 and the importance of IL-33 for A-Eos development[125,179], I hypothesised that transition to the Ly6C- state could be impacted by Th2 cytokines. BM-derived eosinophils were incubated with IL-4, IL-13 or IL-33 from day 10 to day 14 and proportions of CCR3- Ly6C+, CCR3+ Ly6C+ and CCR3+ Ly6C- eosinophils were compared to IL-5 treated control. However, only minor effects were observed, suggesting IL-33 could be enhancing a shift towards the Ly6C- subset (Figure 4.19). This further shows that the transition to Ly6C- eosinophils is a complex process, beyond the classic Th1/Th2 polarisation of eosinophils.

To further test if Ly6C- transition is accommodated by a combination of cytokines, it would be important to first understand the differences in the cytokine milieu of day 7 and day 18 tumours. This could be tested for example with the Olink cytokine profiling platform, which can analyse up to 45 different targets from tumour lysates. A smaller LEGEND-plex pre-defined panel based on flowcytometry read-out could also be used as a more affordable approach, testing a combination of Th1 and Th2 cytokines.

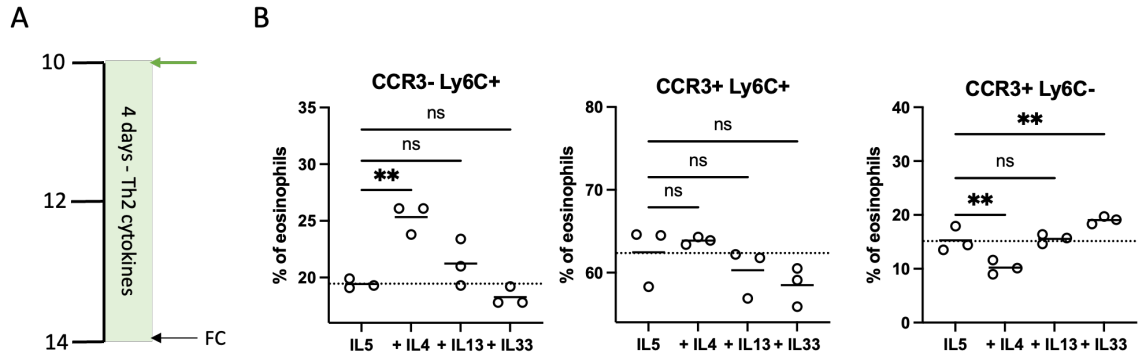


**Figure 4.19. Impact of Th2 cytokines on BM-derived eosinophil development. (A)** Overview of the experimental approach; bone marrow cells of C57/Bl6 male mice (n = 3) were first cultured with Fltl3 and mSCF for 4 days, then differentiated into eosinophils with IL-5 until day 14. The green arrow indicates the beginning of IL-4, IL-13, or IL-33 treatment, the black arrow indicates the time point when eosinophils were investigated by flow cytometry. **(B)** Comparison of eosinophil development in the presence of IL-5 compared to Th2 cytokines on day 14.

Lastly, eosinophils were previously shown to play an anti-tumorigenic role through activation of T cells in syngeneic models of CRC[102] or during ICB response in spontaneous models of breast cancer[184]. While this chapter is focused on studying direct eosinophil cytotoxicity, it would be important to understand if and how eosinophils contribute to T cell activation in these experiments, in light of their increased MHC-I, MHC-II and PD-L1 receptors in response to IFNs. This could be further explored through eosinophil depletion during anti-IFN or ICB treatment of NT193-bearing mice, and the prevalence of activated T cells would be compared to eosinophil-containing WT tumours.

The potential eosinophil-T cell crosstalk could also be studied in vitro, by comparing antigen-presenting abilities of Ly6C+ and Ly6C- bone marrow-derived eosinophils in combination with

OT-I or OT-II T cells, with both eosinophils and T cells being derived from the C57/Bl6 genetic background. It would be important to understand how pronounced the effect of eosinophil depletion on tumour growth during ICB treatment might be, as eosinophils are not the main antigen-presenting cell type in TME. Because eosinophil deletion during the combination of chemotherapy and anti-PD-1 treatment was observed to reduce T cell activation, it would be interesting if a similar effect would be observed in the NT193 model treated with the anti-PD-L1 antibody.

### 4.4.3 IFN stimulation leads to downregulation of Siglec-F expression

One of the most conserved IFN-dependent phenotypes in this chapter is the different regulation of the Siglec-F receptor. In both, BM-derived eosinophils and TAE ex vivo models, stimulation with either IFNγ or IFNβ led to Siglec-F downregulation. Additionally, ICB treatment, potentially associated with IFN-rich TME, led to Siglec-F downregulation (Figure 4.11). On the other hand, during the neutralisation of IFN signalling through IFNγ neutralisation and IFNAR1 blockade in vivo, eosinophils presented with a slight but statistically non-significant increase of Siglec-F (Figure 4.10). Altogether, the data in this chapter suggest that surface expression of Siglec-F is affected by IFNs.

Siglec-F is a sialic-acid binding receptor that upon interaction with its ligands induces eosinophil apoptosis[305]. Because of the Siglec-F ability to induce apoptosis upon antibody or ligand-mediated cross-linking, Siglec-F plays an important role in a negative feedback loop. SiglecF$^{-/-}$ mice partially lose the ability to induce eosinophil apoptosis through Siglec-F and therefore present with bone marrow, blood and lung eosinophilia during nasal OVA sensitisation[306]. Publicly available transcriptomic datasets comparing IL-5 and IFNγ stimulated eosinophils are inconsistent, peritoneal eosinophils isolated from IL5Tg mice significantly downregulated Siglec-F expression following IFNγ stimulation[180]; however, no differences in Siglec-F expression were observed after IFNγ stimulation of BM-derived eosinophils[125]. It

would therefore be interesting to know whether Siglec-F downregulation in IFN-stimulation assays presented in this chapter is caused by receptor internalisation or systemic gene downregulation. Either of these options could present a mechanism that protects eosinophils from excessive cell death upon IFNγ stimulation. This could explain how eosinophils survive in an IFN-rich TME environment during ICB response.

### 4.4.4 Could Ly6C- eosinophils be pro-tumorigenic?

Cytotoxic potential of Ly6C+ eosinophils and reactivation of Ly6C- eosinophils is the main focus of this chapter. Despite this, the possibility that Ly6C- eosinophils that are exclusively present during late stages of the TME development might have an important role beyond the suggested reduced cytotoxicity should not be omitted. Indeed, the GSEA-GO analysis in section 4.2.1 did not reveal any major pro-tumorigenic pathways associated with Ly6C- eosinophils, but broadly described gene sets associated with epithelial development, suggesting involvement of tissue remodelling pathways (Figure 4.2). To test if Ly6C- subset of eosinophils could be more skewed towards a pro-tumorigenic phenotype, the bulk RNA-seq dataset was revisited.

Additional GSEA analysis was performed with the KEGG database, which is more focused on signalling pathways[307]. This analysis revealed upregulation of Wnt signalling in Ly6C- eosinophils (Figure 4.20A). While abnormal Wnt signalling is a well-established driver of cancer proliferation and growth[308], its role in tumour-associated myeloid cells is less clear. Closer analysis of the gene transcripts associated with Wnt signalling in Ly6C- eosinophils revealed overexpression of three Wnt ligands associated with non-canonical Wnt signalling, *Wnt5b*, *Wnt7b*, and *Wnt11* (Figure 4.20B, Appendix Table 4.8). Of these, *Wnt11* was highly expressed, with an average of over 5500 normalised counts in Ly6C- eosinophils. Wnt11 is a secreted ligand that was previously associated with cell proliferation and migration[309], and was recently shown to mediate T-cell exclusion in murine models of liver metastasis[310]. Therefore,

it would be interesting to investigate if Ly6C- eosinophils are also capable of expressing Wnt11 protein and remodelling their local niche by secreting this pro-tumorigenic factor.

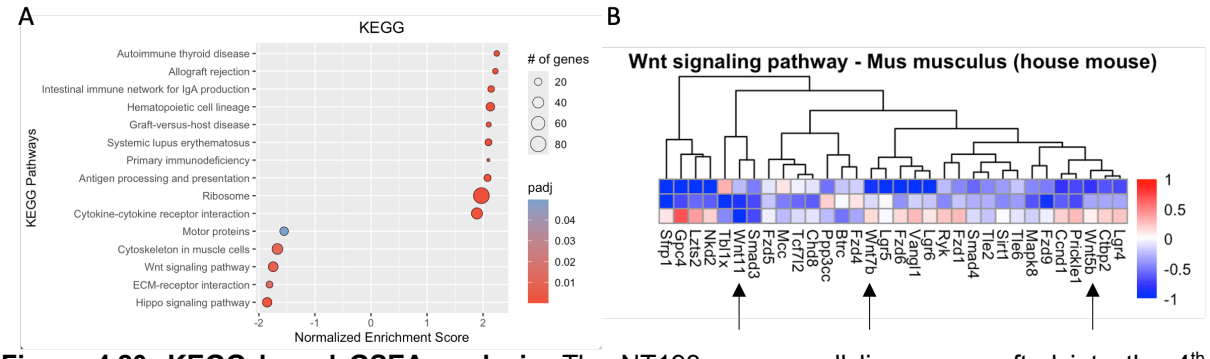


**Figure 4.20. KEGG based GSEA analysis.** The NT193 cancer cell line was grafted into the 4$^{th}$ mammary fat pad of FVB female mice; on day 18 tumours (n=3) were harvested and Siglec-F+ CD11b+ eosinophils were sorted based on their Ly6C surface expression. Ly6C+ and Ly6C- sorted eosinophils were then processed and analysed by bulk RNA sequencing and analysed by GSEA using the KEGG database. **(A)** Heat map of GSEA-KEGG recognised pathways. **(B)** Gene sets of the top 3 upregulated pathways in Ly6C- eosinophils were extracted and visualised by heatmaps. Heatmaps display fold change (FC) differences between Ly6C+ and Ly6C- eosinophils. Data were further normalised by z-scoring across all samples for visualisation. FC differences are colour-coded according to a custom palette; genes overexpressed in Ly6C+ eosinophils have FC > 0.

### 4.4.5 Can eosinophils help with TNBC patient stratification for ICB?

As previously discussed, eosinophils reside in mucosal tissues with higher frequency compared to non-mucosal organs; therefore, their infiltration in patients with lung or colorectal cancer is well documented[162]. Infiltration of eosinophils in melanoma or breast cancer is reported to be rare[162], with some studies suggesting a complete absence of eosinophils in invasive breast cancer[311]. Despite this, both human and murine studies suggests that an increase in eosinophil infiltration during ICB treatment is associated with better therapy response[184,189,199,312]. Furthermore, an increase in the eosinophilic gene signature at baseline in both breast cancer and melanoma patients predicted better overall survival[135,160]. Altogether, this strongly suggests that eosinophils are a good prognostic factor in breast cancer patients and are likely more than just bystanders. However, their presence is often missed in the analysis of TMAs, as discussed in section 4.3.5, and as shown later in Chapter 5, eosinophils can be excluded and reside at tumour periphery. Therefore, full tumour sections containing both tumour core and edge were stained with anti-EPX to evaluate eosinophil densities.

In line with the literature, eosinophils are indeed a rare infiltrating cell type in most breast tumours. However, the preliminary analysis in this chapter has revealed that TNBC patients with local recurrence are more likely to present with higher eosinophil levels. In contrast to previously reported data[162], these eosinophils were mostly residing in the stroma at the tumour periphery rather than tumour nests. The overall eosinophil infiltration, even in patients that were recognised as “eosinophil-rich”, is still relatively low compared to other cell types. Furthermore, eosinophils are not found to be evenly scattered across the tumours, they usually reside in distinct niches at the periphery and are present more closely together. Quantitative analysis of their infiltration patterns should be done to evaluate their spatial proximity to each other and the proximity to the tumour edge.

Because the increased tissue eosinophil levels were specifically observed in patients with local recurrence, this raises a question of whether eosinophils are infiltrating tumours of these patients due to a chronic wound response after radiotherapy. There are many vascular and fibrotic effects in radiotherapy-treated tissue. However, it may simply be that these are more aggressive tumours anyway. To test if this eosinophil infiltration is unique for TNBC patients, a) more TNBC patients with local recurrence would have to be analysed, and b) patients with local recurrence of other breast cancer subtypes should be compared.

Lastly, eosinophil upregulation during response to ICB is a good prognostic factor for both TNBC and melanoma patients[184,312]. TNBC is the most aggressive breast cancer subtype, which is hard to treat with standard chemotherapy and therefore these patients can greatly benefit from ICB. However, ICB works for some but not all patients. It would be interesting to know whether baseline increased eosinophil infiltration could help identify patients with higher chances of responding to ICB.

# 4.5 Appendix

## Appendix Table 4.1. List of DEGs between sorted tumour-associated Ly6C+ and Ly6C- eosinophils, organized by log2FoldChange

| Gene name | baseMean | log2FoldChange | pvalue | padj |
|---|---|---|---|---|
| Cd300e | 172.849026 | 8.525470146 | 2.54E-09 | 3.08E-06 |
| Siglech | 64.1476281 | 8.440396293 | 3.52E-07 | 0.0002019 |
| Il7r | 74.4980805 | 8.412987711 | 0.00018961 | 0.0241043 |
| Slc8a1 | 126.847065 | 7.70536741 | 1.44E-06 | 0.00062596 |
| Csn2 | 648.756766 | 7.141574797 | 2.00E-21 | 2.18E-17 |
| Htr7 | 78.5576898 | 6.740648532 | 8.16E-06 | 0.00246994 |
| Penk | 88.8794055 | 6.740356392 | 3.70E-06 | 0.00136928 |
| Zfp41 | 80.5535067 | 6.723329583 | 9.11E-05 | 0.01460865 |
| Sectm1b | 135.346161 | 6.716844447 | 4.90E-07 | 0.00026713 |
| Ifit1bl1 | 73.6960911 | 6.509376957 | 2.45E-06 | 0.00099041 |
| Zfp850 | 95.1917341 | 6.222089322 | 2.51E-05 | 0.00595504 |
| Mmp19 | 140.07228 | 6.180044153 | 1.08E-09 | 2.23E-06 |
| Napb | 72.9258738 | 5.525319743 | 2.83E-05 | 0.00655801 |
| Slc7a2 | 84.9403762 | 5.202836362 | 0.0002987 | 0.03354674 |
| Il33 | 308.570171 | 5.187998771 | 1.87E-08 | 1.85E-05 |
| Amigo3 | 77.6085079 | 4.975451914 | 0.00033394 | 0.03637901 |
| Fam185a | 97.1681254 | 4.574408754 | 0.00031433 | 0.0349418 |
| Ly6c2 | 3616.81403 | 4.413101765 | 8.88E-18 | 4.83E-14 |
| Mefv | 225.771489 | 4.03927638 | 0.00013801 | 0.01903151 |
| Hbb-b1 | 296.406773 | 3.8732438 | 6.22E-07 | 0.00032273 |
| Fbn1 | 120.178731 | 3.759708295 | 3.77E-06 | 0.00136928 |
| Enpp2 | 145.230759 | 3.647863633 | 0.00038911 | 0.04039894 |
| Ubd | 365.725584 | 3.64725926 | 0.00049464 | 0.04726827 |
| Hba-a1 | 1286.88922 | 3.523236369 | 1.43E-09 | 2.23E-06 |
| Cd209a | 1023.65759 | 3.246153438 | 4.89E-08 | 4.40E-05 |
| Chil3 | 863.5951 | 3.192853503 | 1.93E-07 | 0.0001239 |
| Ly6i | 635.989794 | 3.080235756 | 1.40E-09 | 2.23E-06 |
| Ralgps2 | 199.96867 | 3.060431488 | 1.23E-05 | 0.00343169 |
| Thbs2 | 329.07946 | 2.648925026 | 0.0003768 | 0.04024342 |
| Ccr7 | 218.01222 | 2.423291986 | 6.32E-05 | 0.01129017 |
| Ms4a4c | 1619.56189 | 2.39151335 | 2.20E-09 | 2.99E-06 |
| Cd40 | 718.206321 | 2.358288534 | 6.56E-08 | 5.10E-05 |
| Cd209e | 487.304071 | 2.139100892 | 0.0002207 | 0.02701453 |
| Jaml | 270.504156 | 2.114018471 | 0.0004039 | 0.04112228 |
| Tnip3 | 249.259886 | 2.007131342 | 0.00050663 | 0.04799355 |
| Tlr1 | 610.85433 | 1.987099515 | 0.0002144 | 0.02654185 |
| Scimp | 639.549502 | 1.87607717 | 0.0004733 | 0.04645165 |
| Ccl5 | 553.360198 | 1.851994355 | 0.00022877 | 0.02769158 |
| Vav2 | 315.802744 | 1.813169112 | 0.00036656 | 0.03953718 |
| Gm6377 | 762.67317 | 1.710664386 | 6.78E-05 | 0.01172449 |
| Serpina3f | 802.834953 | 1.660603638 | 1.33E-05 | 0.00353736 |
| Spon1 | 1140.03143 | 1.645058809 | 0.00010581 | 0.01623536 |
| Ms4a6c | 1778.51967 | 1.629130443 | 1.08E-05 | 0.00309038 |
| Clec4a1 | 1079.35656 | 1.591742 | 4.21E-05 | 0.00864891 |
| Ccr2 | 3300.5313 | 1.555835693 | 1.93E-07 | 0.0001239 |
| Ms4a6b | 1624.96394 | 1.54632207 | 5.95E-05 | 0.0109937 |
| Cd72 | 1613.15578 | 1.489569897 | 3.68E-05 | 0.00802098 |
| Ptpro | 831.438295 | 1.479586052 | 0.00024065 | 0.02849644 |
| Ciita | 1282.76884 | 1.478523145 | 7.22E-06 | 0.00236969 |
| Ms4a6d | 3456.16342 | 1.457722467 | 7.40E-06 | 0.00236969 |
| Il21r | 1009.87488 | 1.456505972 | 3.84E-05 | 0.00809487 |
| BC028528 | 753.001782 | 1.442298634 | 0.00018978 | 0.0241043 |
| Ms4a4a | 2724.76695 | 1.425959936 | 3.21E-05 | 0.00728626 |
| P2ry6 | 1349.30822 | 1.404840018 | 5.02E-05 | 0.00960222 |
| H2-DMb1 | 4834.48193 | 1.395225358 | 1.87E-05 | 0.00463393 |
| Ly6a | 5187.54316 | 1.389075156 | 3.86E-05 | 0.00809487 |
| Oas3 | 849.502844 | 1.377804432 | 0.00023261 | 0.02784714 |
| Otulinl | 2388.93678 | 1.363193686 | 3.64E-06 | 0.00136928 |
| Clec7a | 2753.74026 | 1.322279125 | 6.04E-06 | 0.00212243 |
| H2-DMb2 | 3983.11765 | 1.307651528 | 4.42E-05 | 0.00891661 |
| H2-Ab1 | 171122.571 | 1.305401041 | 3.67E-05 | 0.00802098 |
| Tifab | 1114.38566 | 1.276110749 | 0.00015721 | 0.0211437 |
| Clec4a3 | 3590.18595 | 1.273235924 | 1.59E-05 | 0.00412502 |
| Ctss | 32695.508 | 1.249361165 | 7.07E-05 | 0.0120319 |
| Cxcl16 | 5815.15768 | 1.244440438 | 0.00017541 | 0.0233033 |
| H2-Aa | 79763.8045 | 1.220719029 | 0.00012252 | 0.01779583 |
| Cd74 | 239070.713 | 1.202586527 | 0.0001145 | 0.01708763 |
| Plbd1 | 4939.99232 | 1.196631262 | 7.31E-06 | 0.00236969 |
| Ctsc | 23167.7158 | 1.189110242 | 9.53E-07 | 0.00047176 |
| Ms4a7 | 6318.82034 | 1.17868046 | 0.00019114 | 0.0241043 |
| Clec10a | 3169.0866 | 1.172196255 | 0.00046491 | 0.04604304 |
| Sdc3 | 5438.88309 | 1.147046056 | 7.75E-06 | 0.00241203 |
| Axl | 5708.69733 | 1.085086451 | 0.0001778 | 0.02333742 |
| Mgl2 | 3794.44015 | 1.083634245 | 0.00012062 | 0.01775697 |
| Ap2a2 | 2987.12531 | 1.023758419 | 0.00045653 | 0.04562764 |

| Gene name | baseMean | og2FoldChang | pvalue | padj |
|---|---|---|---|---|
| Actn4 | 12188.2235 | -1.0468341 | 0.00010078 | 0.01586498 |
| Car4 | 742.262267 | -1.5213007 | 0.00013551 | 0.01903151 |
| Ccn3 | 2230.16342 | -1.6027335 | 0.00032484 | 0.03574566 |
| Clca3a2 | 2344.5138 | -2.1777425 | 0.00038239 | 0.04039894 |
| Col11a1 | 1711.34365 | -2.3222828 | 0.00013681 | 0.01903151 |
| Kcnk5 | 356.501303 | -2.6270277 | 0.00010808 | 0.0163524 |
| Acox2 | 450.412035 | -2.6729279 | 0.00048439 | 0.04676001 |
| Pcx | 557.50816 | -2.6905065 | 5.89E-09 | 6.42E-06 |
| Large2 | 322.266997 | -2.741585 | 4.76E-05 | 0.00942952 |
| Lamc2 | 666.520182 | -2.8108215 | 0.00027993 | 0.03210098 |
| Spag5 | 175.327293 | -3.0076701 | 2.23E-05 | 0.00539918 |
| Ncald | 497.235131 | -3.2159613 | 1.74E-07 | 0.0001239 |
| Ptprk | 537.70497 | -3.3330241 | 1.50E-11 | 4.09E-08 |
| Syne3 | 94.1316727 | -3.3748594 | 0.00039235 | 0.04039894 |
| Myh14 | 453.294077 | -3.3943197 | 0.0001499 | 0.02041212 |
| Boc | 595.269265 | -3.5905873 | 0.00039309 | 0.04039894 |
| Pcdh18 | 243.115675 | -3.7684042 | 0.00028936 | 0.03283623 |
| Rem2 | 106.375991 | -3.7767965 | 0.00051537 | 0.04839998 |
| Dsc2 | 325.608456 | -4.2770188 | 1.33E-05 | 0.00353736 |
| Nat8f4 | 133.386463 | -4.8048254 | 0.00024484 | 0.02868033 |
| Ccser1 | 69.2829241 | -4.8189993 | 5.56E-05 | 0.01043403 |
| Cand2 | 97.5954164 | -4.8304637 | 0.00048503 | 0.04676001 |
| Hunk | 179.306934 | -5.2458291 | 4.96E-05 | 0.00960222 |
| Fzd9 | 82.4891333 | -5.4344183 | 0.00010194 | 0.01586498 |
| Osbpl10 | 81.2773891 | -6.0037766 | 0.00012976 | 0.01859966 |
| Bbox1 | 74.9099284 | -6.1838749 | 9.63E-06 | 0.00283516 |
| Unc80 | 75.851571 | -6.3546703 | 8.14E-05 | 0.01363895 |
| Adamts7 | 156.575708 | -6.9118379 | 2.20E-06 | 0.00092122 |
| Dmp1 | 646.83927 | -7.0324172 | 3.55E-14 | 1.29E-10 |
| Atp10b | 135.815546 | -7.1599502 | 1.43E-06 | 0.00062596 |
| Sh3tc2 | 155.510863 | -7.285191 | 2.56E-07 | 0.00015498 |
| Atp2c2 | 69.614551 | -7.423522 | 0.0001925 | 0.0241043 |
| Col25a1 | 68.09878 | -7.5964661 | 6.26E-05 | 0.01129017 |
| Al429214 | 67.4341591 | -7.8228074 | 6.77E-05 | 0.01172449 |
| Glt28d2 | 78.4912141 | -7.8358312 | 1.75E-05 | 0.00443468 |
| Clca2 | 64.69101 | -7.9831303 | 1.29E-06 | 0.00061062 |
| Nebl | 66.3839125 | -9.2740512 | 5.25E-08 | 4.40E-05 |

**Appendix Table 4.2. List of lineage markers used to validate eosinophil purity.**

| Gene name | Protein Name | Primary Cell Type(s) |
|---|---|---|
| **Adgre1** | F4/80 | Macrophages, eosinophils |
| **Itgam** | CD11b | Myeloid cells |
| **Siglecf** | Siglec-F | Eosinophils, alveolar macrophages |
| **Ccr3** | CCR3 | Eosinophils |
| **Il5ra** | IL-5Rα | Eosinophils |
| **Cx3cr1** | CX3CR1 | Monocytes, macrophages |
| **Cd86** | CD86 | Macrophages |
| **Cd68** | CD68 | Macrophages, monocytes |
| **Ccr2** | CCR2 | Inflammatory monocytes |
| **Mrc1** | CD206 | M2 macrophages, |
| **Flt3** | FLT3 | Dendritic progenitors |
| **Cd177** | CD177 | Neutrophils |
| **S100a8** | S100A8 | Neutrophils, monocytes |
| **S100a9** | S100A9 | Neutrophils, monocytes |
| **Siglech** | Siglec-H | Dendritic cells |
| **Cd3e** | CD3ε | T cells |
| **Cd79a** | CD79a | B cells |
| **Pdgfra** | PDGFRα | Fibroblasts |
| **Pdgfrb** | PDGFRβ | Pericytes, fibroblasts |
| **Pecam1** | CD31 | Endothelial cells |

**Appendix Table 4.3. List of genes associated with response to IFNγ in GSEA-GO analysis, organised by log2FoldChange**

| Gene | log2FoldChange | baseMean | pvalue | padj |
|---|---|---|---|---|
| Mefv | 4.03927638 | 225.771489 | 0.00013801 | 0.01903151 |
| Ubd | 3.64725926 | 365.725584 | 0.00049464 | 0.04726827 |
| Gbp5 | 2.483774211 | 149.556922 | 0.00077847 | 0.06145416 |
| Pparg | 2.107173847 | 212.842236 | 0.0058259 | 0.21465079 |
| Ccl17 | 2.067054206 | 127.805699 | 0.01182979 | 0.33267055 |
| Ccl22 | 1.988033143 | 167.556986 | 0.03750274 | 0.59817702 |
| Ccl5 | 1.851994355 | 553.360198 | 0.00022877 | 0.02769158 |
| Kynu | 1.76375872 | 71.374136 | 0.06529011 | 0.75804496 |
| H2-Eb1 | 1.59252504 | 1416.48128 | 0.00101138 | 0.07132814 |
| Ciita | 1.478523145 | 1282.76884 | 7.2167E-06 | 0.00236969 |
| Gbp4 | 1.424109928 | 925.632302 | 0.00275198 | 0.13698337 |
| Ccl24 | 1.396817973 | 1010.16846 | 0.00104987 | 0.07193267 |
| H2-Ab1 | 1.305401041 | 171122.571 | 3.6741E-05 | 0.00802098 |
| Rab7b | 1.268899395 | 709.317768 | 0.01375331 | 0.36428313 |
| Cxcl16 | 1.244440438 | 5815.15768 | 0.00017541 | 0.0233033 |
| H2-Aa | 1.220719029 | 79763.8045 | 0.00012252 | 0.01779583 |
| Rab12 | 1.210563777 | 149.972959 | 0.13950712 | 0.99077403 |
| Ifitm6 | 1.203802547 | 77.5360709 | 0.20465006 | 0.99985668 |
| Cd74 | 1.202586527 | 239070.713 | 0.0001145 | 0.01708763 |
| Tlr2 | 1.173589836 | 1260.34725 | 0.00085454 | 0.0655586 |
| Ccl12 | 1.1711968 | 2358.47965 | 0.00377211 | 0.1625519 |
| Irf8 | 1.108255786 | 2633.77586 | 0.0021572 | 0.11760805 |
| Gbp10 | 1.093402779 | 174.504425 | 0.17767503 | 0.99985668 |
| Dapk3 | 1.011748861 | 409.799229 | 0.15799483 | 0.99985668 |
| Ccl2 | 0.986277434 | 2369.71152 | 0.00689424 | 0.23885163 |
| Gbp2b | 0.90267656 | 2159.10415 | 0.00596118 | 0.21655081 |
| Ccl8 | 0.900387002 | 51924.0093 | 0.01829855 | 0.41428029 |
| Jak2 | 0.884804195 | 999.688722 | 0.06886941 | 0.7779074 |
| Gbp8 | 0.86604874 | 1221.9425 | 0.02314703 | 0.46439002 |
| Stxbp1 | 0.852668436 | 249.927728 | 0.12488059 | 0.96060871 |
| Ccl25 | 0.849442608 | 77.6713453 | 0.40201703 | 0.99985668 |
| Bst2 | 0.711384429 | 1212.77176 | 0.04815991 | 0.66580462 |
| Ccl7 | 0.706512907 | 6556.76433 | 0.03622809 | 0.58730481 |
| Gbp3 | 0.70299528 | 1749.16161 | 0.02814227 | 0.5091738 |
| Mrc1 | 0.674865634 | 4080.48215 | 0.01623991 | 0.39402583 |
| Rab11fip5 | 0.673163814 | 1033.25275 | 0.05267174 | 0.69197504 |
| Ifitm2 | 0.672885388 | 3793.22062 | 0.08313146 | 0.84010583 |
| Gbp2 | 0.645823097 | 5798.89894 | 0.04140989 | 0.63312138 |
| Vim | 0.64330812 | 4307.46949 | 0.02285475 | 0.46107349 |
| Arg1 | 0.592386497 | 1246.76106 | 0.17087361 | 0.99985668 |
| Irgm1 | 0.591370069 | 4573.36852 | 0.051672 | 0.68731961 |
| Ifitm3 | 0.582666701 | 7078.90745 | 0.13457233 | 0.98360438 |

**Appendix Table 4.4. List of genes associated with response to IFNβ in GSEA-GO analysis, organised by log2FoldChange**

| Gene | log2FoldChange | baseMean | pvalue | padj |
|---|---|---|---|---|
| Gm4841 | 3.108243655 | 80.7543329 | 0.03130333 | 0.53535086 |
| F830016B08Rik | 2.644866461 | 182.373676 | 0.03719653 | 0.59678785 |
| Gm5431 | 2.493496954 | 260.314267 | 0.02282118 | 0.46107349 |
| Ikbke | 1.46269251 | 344.269695 | 0.00943723 | 0.29168439 |
| Ifi213 | 1.388211012 | 65.383883 | 0.20277393 | 0.99985668 |
| Ifi211 | 1.294909202 | 70.658928 | 0.21746889 | 0.99985668 |
| Ifi202b | 1.269913474 | 713.01086 | 0.00377507 | 0.1625519 |
| Ifi208 | 1.203962065 | 140.75893 | 0.11311591 | 0.92652987 |
| Ifitm6 | 1.203802547 | 77.5360709 | 0.20465006 | 0.99985668 |
| Ifi203 | 1.12744975 | 474.049454 | 0.02695865 | 0.49538053 |
| Oas1g | 1.088811123 | 444.196152 | 0.03068733 | 0.52924818 |
| Iigp1 | 1.033634557 | 2960.44569 | 0.00188306 | 0.10629032 |
| Ifi204 | 1.011382586 | 524.396903 | 0.07878729 | 0.81977917 |
| Ifi214 | 0.924562839 | 174.449619 | 0.14840451 | 0.99985668 |
| Gbp2b | 0.90267656 | 2159.10415 | 0.00596118 | 0.21655081 |
| Ifit3 | 0.867352627 | 865.23926 | 0.0322774 | 0.54771025 |
| Ifi207 | 0.862441177 | 1197.21083 | 0.04317176 | 0.64196739 |
| Iigp1c | 0.751504741 | 350.031368 | 0.15791924 | 0.99985668 |
| Bst2 | 0.711384429 | 1212.77176 | 0.04815991 | 0.66580462 |
| Gbp3 | 0.70299528 | 1749.16161 | 0.02814227 | 0.5091738 |
| Ifi47 | 0.702141381 | 2487.46483 | 0.01733936 | 0.40276116 |
| Oas1a | 0.696609903 | 1731.14276 | 0.04531133 | 0.65200195 |
| Ifitm2 | 0.672885388 | 3793.22062 | 0.08313146 | 0.84010583 |
| Ifi209 | 0.660309843 | 1588.23437 | 0.02986161 | 0.52122408 |
| Gbp2 | 0.645823097 | 5798.89894 | 0.04140989 | 0.63312138 |
| Irgm1 | 0.591370069 | 4573.36852 | 0.051672 | 0.68731961 |
| Ifitm3 | 0.582666701 | 7078.90745 | 0.13457233 | 0.98360438 |
| Aim2 | 0.513639182 | 302.841009 | 0.39539959 | 0.99985668 |
| Tgtp2 | 0.479676626 | 2318.30234 | 0.22969331 | 0.99985668 |
| Sting1 | 0.403993686 | 2558.11618 | 0.17315203 | 0.99985668 |
| Oas1b | 0.380891374 | 67.2890065 | 0.6943274 | 0.99985668 |
| Stat1 | 0.380324741 | 10028.6809 | 0.21459492 | 0.99985668 |
| Irgm2 | 0.377100064 | 1480.83141 | 0.36647005 | 0.99985668 |
| Ifitm1 | 0.351306642 | 85.7287935 | 0.72136572 | 0.99985668 |
| Ifnar1 | 0.348268119 | 2247.14324 | 0.31821509 | 0.99985668 |
| Ifi205 | 0.345485501 | 86.6270277 | 0.69392069 | 0.99985668 |

**Appendix Table 4.5. List of genes associated with cell killing, in GSEA-GO analysis, organised by log2FoldChange**

| Gene | log2FoldChange | baseMean | pvalue | padj |
|---|---|---|---|---|
| Il7r | 8.412987711 | 74.4980805 | 0.00018961 | 0.0241043 |
| Gbp5 | 2.483774211 | 149.556922 | 0.00077847 | 0.06145416 |
| Ccl17 | 2.067054206 | 127.805699 | 0.01182979 | 0.33267055 |
| Ccl22 | 1.988033143 | 167.556986 | 0.03750274 | 0.59817702 |
| Klrb1b | 1.778418354 | 115.836117 | 0.03848417 | 0.60848557 |
| Rasgrp1 | 1.686371908 | 364.970327 | 0.00158534 | 0.09526435 |
| Cxcl9 | 1.585186303 | 820.112725 | 0.00366311 | 0.16193437 |
| Havcr2 | 1.493352627 | 559.826279 | 0.00265235 | 0.13377166 |
| Fcgr1 | 1.485810585 | 1339.691 | 0.00093989 | 0.06871943 |
| Il18 | 1.438604336 | 124.463293 | 0.08109796 | 0.83456246 |
| Cd1d1 | 1.370641186 | 334.336652 | 0.06179523 | 0.73734633 |
| Clec7a | 1.322279125 | 2753.74026 | 6.0396E-06 | 0.00212243 |
| Gzma | 1.299285124 | 82.096641 | 0.41476663 | 0.99985668 |
| Cxcl13 | 1.29040408 | 357.20353 | 0.02701083 | 0.49538053 |
| H2-Ea | 1.261792768 | 1569.96809 | 0.00062841 | 0.05657805 |
| Ccr5 | 1.256996771 | 966.077209 | 0.00066515 | 0.05796927 |
| Cx3cr1 | 1.194782934 | 1191.91993 | 0.00250005 | 0.1278662 |
| Ctsc | 1.189110242 | 23167.7158 | 9.5271E-07 | 0.00047176 |
| Fcgr4 | 1.149936182 | 496.697872 | 0.03249104 | 0.54933397 |
| Klrk1 | 1.048758865 | 641.312162 | 0.00968805 | 0.29563474 |
| Lyz2 | 0.998222186 | 112188.145 | 0.00076171 | 0.06145416 |
| Ccl2 | 0.986277434 | 2369.71152 | 0.00689424 | 0.23885163 |
| C3 | 0.973365829 | 6282.53237 | 0.00026821 | 0.03108388 |
| Cxcl12 | 0.95969922 | 393.360011 | 0.16497348 | 0.99985668 |
| Cxcl10 | 0.952386495 | 1349.32331 | 0.00350759 | 0.15843733 |
| Dnase1l3 | 0.951137563 | 878.672138 | 0.01366617 | 0.36400806 |
| Gbp2b | 0.90267656 | 2159.10415 | 0.00596118 | 0.21655081 |
| Ccl8 | 0.900387002 | 51924.0093 | 0.01829855 | 0.41428029 |
| Serpinb9 | 0.896299226 | 323.649341 | 0.08258459 | 0.83846833 |
| Ccl25 | 0.849442608 | 77.6713453 | 0.40201703 | 0.99985668 |
| Lamp1 | 0.796254155 | 17762.3728 | 0.0074877 | 0.24975921 |
| Hfe | 0.763949716 | 2156.17529 | 0.03252436 | 0.54933397 |
| Gbp3 | 0.70299528 | 1749.16161 | 0.02814227 | 0.5091738 |
| H2-T24 | 0.69477185 | 1557.68191 | 0.1067356 | 0.90213013 |
| Cadm1 | 0.685610149 | 620.723584 | 0.09419726 | 0.86551826 |
| Lyz1 | 0.675714447 | 1380.88803 | 0.05246475 | 0.69140796 |
| Ripk3 | 0.669143009 | 519.686829 | 0.16496743 | 0.99985668 |
| H2-M2 | 0.667980946 | 1544.44844 | 0.11351599 | 0.92910831 |
| Ap1g1 | 0.655596235 | 1428.30974 | 0.09758053 | 0.86992004 |
| Gbp2 | 0.645823097 | 5798.89894 | 0.04140989 | 0.63312138 |
| Cd2 | 0.640601311 | 192.344798 | 0.32346652 | 0.99985668 |
| Slamf6 | 0.622233391 | 351.406696 | 0.23466568 | 0.99985668 |
| Arg1 | 0.592386497 | 1246.76106 | 0.17087361 | 0.99985668 |
| Nkg7 | 0.580731461 | 383.928979 | 0.38983319 | 0.99985668 |

**Appendix Table 4.6. List of genes associated with renal tubule development, in GSEA-GO analysis, organised by log2FoldChange**

| Gene | log2FoldChange | baseMean | pvalue | padj |
|---|---|---|---|---|
| Sox8 | -4.508433936 | 88.5077489 | 0.0026042 | 0.13213711 |
| Hs3st3a1 | -2.941348513 | 92.5953789 | 0.05933548 | 0.72710991 |
| Prom1 | -2.636992282 | 90.8137025 | 0.06995664 | 0.78056154 |
| Prickle1 | -2.579346802 | 158.058326 | 0.01884585 | 0.422516 |
| Lgr5 | -2.550690786 | 62.4895704 | 0.278258 | 0.99985668 |
| Lgr4 | -2.26444038 | 82.5657682 | 0.10982115 | 0.91257939 |
| Pbx1 | -1.938234689 | 150.860269 | 0.0368381 | 0.59366011 |
| Npnt | -1.835665259 | 794.169346 | 0.02000064 | 0.43496774 |
| Hey1 | -1.460564231 | 176.896781 | 0.10128083 | 0.88480622 |
| Hs3st3b1 | -1.400327504 | 420.826929 | 0.02000307 | 0.43496774 |
| Dll1 | -1.348018861 | 147.995786 | 0.30508399 | 0.99985668 |
| Agt | -1.323329221 | 82.6989381 | 0.25265584 | 0.99985668 |
| Ttc8 | -1.243058326 | 99.9309426 | 0.24076045 | 0.99985668 |
| Sox9 | -1.240584237 | 453.371245 | 0.07545001 | 0.79943307 |
| Irx3 | -1.209349426 | 189.578478 | 0.18889192 | 0.99985668 |
| Lama5 | -1.072924141 | 301.602246 | 0.07541767 | 0.79943307 |
| Wnt7b | -1.057644488 | 270.321874 | 0.20201806 | 0.99985668 |
| Ptch1 | -1.037547201 | 72.3801187 | 0.39324475 | 0.99985668 |
| Aqp1 | -0.933136728 | 517.898864 | 0.18354289 | 0.99985668 |
| Lzts2 | -0.892156601 | 528.592936 | 0.16974661 | 0.99985668 |
| Col4a1 | -0.802229875 | 2431.39197 | 0.5601615 | 0.99985668 |
| Gata3 | -0.668266726 | 691.881704 | 0.29380709 | 0.99985668 |
| Irx2 | -0.656853979 | 179.181546 | 0.4542003 | 0.99985668 |
| Bcl2 | -0.644176758 | 317.396142 | 0.27843662 | 0.99985668 |
| Smad4 | -0.642316984 | 651.032017 | 0.12243342 | 0.95827724 |

**Appendix Table 4.7. List of genes associated with mesonephric epithelium and ureteric bud development, in GSEA-GO analysis, organised by log2FoldChange**

| Gene | log2FoldChange | baseMean | pvalue | padj |
|---|---|---|---|---|
| Sox8 | -4.508433936 | 88.5077489 | 0.0026042 | 0.13213711 |
| Hs3st3a1 | -2.941348513 | 92.5953789 | 0.05933548 | 0.72710991 |
| Fgfr2 | -2.65293425 | 178.32094 | 0.01476679 | 0.3746239 |
| Crlf1 | -2.57405094 | 140.984197 | 0.04448794 | 0.6470649 |
| Lgr4 | -2.26444038 | 82.5657682 | 0.10982115 | 0.91257939 |
| Pbx1 | -1.938234689 | 150.860269 | 0.0368381 | 0.59366011 |
| Npnt | -1.835665259 | 794.169346 | 0.02000064 | 0.43496774 |
| Sfrp1 | -1.71662669 | 503.388529 | 0.00824604 | 0.26499227 |
| Hey1 | -1.460564231 | 176.896781 | 0.10128083 | 0.88480622 |
| Hs3st3b1 | -1.400327504 | 420.826929 | 0.02000307 | 0.43496774 |
| Agt | -1.323329221 | 82.6989381 | 0.25265584 | 0.99985668 |
| Sox9 | -1.240584237 | 453.371245 | 0.07545001 | 0.79943307 |
| Bmp7 | -1.184529502 | 78.3163951 | 0.20393291 | 0.99985668 |
| Epcam | -1.125372469 | 5450.77236 | 0.04636487 | 0.65597257 |
| Smad3 | -1.110483769 | 1225.02538 | 0.00087693 | 0.06601565 |
| Lama5 | -1.072924141 | 301.602246 | 0.07541767 | 0.79943307 |
| Ptch1 | -1.037547201 | 72.3801187 | 0.39324475 | 0.99985668 |
| Lzts2 | -0.892156601 | 528.592936 | 0.16974661 | 0.99985668 |
| Gata3 | -0.668266726 | 691.881704 | 0.29380709 | 0.99985668 |
| Fgfr1 | -0.649688637 | 9446.91144 | 0.05129726 | 0.68484358 |
| Bcl2 | -0.644176758 | 317.396142 | 0.27843662 | 0.99985668 |
| Smad4 | -0.642316984 | 651.032017 | 0.12243342 | 0.95827724 |

## Appendix Table 4.8 List of genes associated with the top 3 KEGG pathways upregulated in Ly6C- eosinophils

| Gene | log2FoldChange | baseMean | pvalue | padj | Pathway |
|---|---|---|---|---|---|
| Lama3 | -9.03894771 | 133.7778 | 0.01833 | 0.41428 | ECM-receptor interaction |
| Dmp1 | -7.032417223 | 646.8393 | 3.55E-14 | 1.29E-10 | ECM-receptor interaction |
| Fzd9 | -5.434418256 | 82.48913 | 0.000102 | 0.015865 | Hippo signaling pathway; Wnt signaling pathway |
| Comp | -3.218679213 | 395.4339 | 0.002159 | 0.117608 | ECM-receptor interaction |
| Tle2 | -3.104290081 | 74.60271 | 0.001689 | 0.09794 | Wnt signaling pathway |
| Lamc2 | -2.810821463 | 666.5202 | 0.00028 | 0.032101 | ECM-receptor interaction |
| Col9a1 | -2.631932408 | 2840.689 | 0.035928 | 0.584184 | ECM-receptor interaction |
| Prickle1 | -2.579346802 | 158.0583 | 0.018846 | 0.422516 | Wnt signaling pathway |
| Lgr5 | -2.550690786 | 62.48957 | 0.278258 | 0.999857 | Wnt signaling pathway |
| Ajuba | -2.282776014 | 92.57062 | 0.10998 | 0.913206 | Hippo signaling pathway |
| Lgr4 | -2.26444038 | 82.56577 | 0.109821 | 0.912579 | Wnt signaling pathway |
| Col9a3 | -2.227180958 | 1216.964 | 0.002404 | 0.125157 | ECM-receptor interaction |
| Itgb4 | -2.125216965 | 604.4859 | 0.005847 | 0.214651 | ECM-receptor interaction |
| Pard3 | -2.018354093 | 118.6509 | 0.043858 | 0.64564 | Hippo signaling pathway |
| Itga3 | -1.997871503 | 315.1846 | 0.017006 | 0.400578 | ECM-receptor interaction |
| Wwc1 | -1.865931 | 139.1285 | 0.026462 | 0.49027 | Hippo signaling pathway |
| Npnt | -1.835665259 | 794.1693 | 0.020001 | 0.434968 | ECM-receptor interaction |
| Mcc | -1.806136105 | 94.19986 | 0.096541 | 0.869568 | Wnt signaling pathway |
| Mapk8 | -1.734356338 | 161.2407 | 0.014899 | 0.374624 | Wnt signaling pathway |
| Sfrp1 | -1.71662669 | 503.3885 | 0.008246 | 0.264992 | Wnt signaling pathway |
| Lamb2 | -1.689512225 | 409.164 | 0.013126 | 0.357524 | ECM-receptor interaction |
| Col9a2 | -1.610200155 | 560.4166 | 0.02909 | 0.514959 | ECM-receptor interaction |
| Nkd2 | -1.401003744 | 560.6063 | 0.047856 | 0.664864 | Hippo signaling pathway; Wnt signaling pathway |
| Hspg2 | -1.38988722 | 115.8029 | 0.252606 | 0.999857 | ECM-receptor interaction |
| Tgfb3 | -1.365357746 | 1605.253 | 0.011126 | 0.319461 | Hippo signaling pathway |
| Gpc4 | -1.287764236 | 413.2231 | 0.160714 | 0.999857 | Wnt signaling pathway |
| Tle6 | -1.246097359 | 104.0094 | 0.130292 | 0.975457 | Wnt signaling pathway |
| Bmp7 | -1.184529502 | 78.3164 | 0.203933 | 0.999857 | Hippo signaling pathway |
| Wnt5b | -1.157959383 | 203.3197 | 0.126428 | 0.967207 | Hippo signaling pathway; Wnt signaling pathway |
| Frmd6 | -1.150503678 | 320.9803 | 0.061962 | 0.737721 | Hippo signaling pathway |
| Smad3 | -1.110483769 | 1225.025 | 0.000877 | 0.066016 | Hippo signaling pathway; Wnt signaling pathway |
| Lgr6 | -1.110290503 | 324.3719 | 0.121476 | 0.958277 | Wnt signaling pathway |
| Fzd6 | -1.104655985 | 280.4937 | 0.134783 | 0.983604 | Hippo signaling pathway; Wnt signaling pathway |
| Lama5 | -1.072924141 | 301.6022 | 0.075418 | 0.799433 | ECM-receptor interaction |
| Wnt7b | -1.057644488 | 270.3219 | 0.202018 | 0.999857 | Hippo signaling pathway; Wnt signaling pathway |
| Cdh1 | -1.04233659 | 1895.562 | 0.057995 | 0.720478 | Hippo signaling pathway |
| Wnt11 | -1.024993363 | 5703.981 | 0.001112 | 0.074297 | Hippo signaling pathway; Wnt signaling pathway |
| Tgfb2 | -0.967009038 | 128.919 | 0.264977 | 0.999857 | Hippo signaling pathway |
| Vangl1 | -0.960771485 | 288.5269 | 0.263471 | 0.999857 | Wnt signaling pathway |
| Itga8 | -0.954685544 | 529.6165 | 0.100477 | 0.882025 | ECM-receptor interaction |
| Dag1 | -0.938890987 | 1902.35 | 0.01815 | 0.413542 | ECM-receptor interaction |
| Fzd5 | -0.916083652 | 84.16903 | 0.31542 | 0.999857 | Hippo signaling pathway; Wnt signaling pathway |
| Lzts2 | -0.892156601 | 528.5929 | 0.169747 | 0.999857 | Wnt signaling pathway |
| Col4a5 | -0.883696643 | 409.3655 | 0.171811 | 0.999857 | ECM-receptor interaction |
| Sdc1 | -0.880448761 | 513.8985 | 0.204906 | 0.999857 | ECM-receptor interaction |
| Fzd4 | -0.872328892 | 95.52638 | 0.343389 | 0.999857 | Hippo signaling pathway; Wnt signaling pathway |
| Patj | -0.858362846 | 339.9209 | 0.180022 | 0.999857 | Hippo signaling pathway |
| Col4a1 | -0.802229875 | 2431.392 | 0.560161 | 0.999857 | ECM-receptor interaction |
| Sirt1 | -0.773233092 | 308.8329 | 0.164692 | 0.999857 | Wnt signaling pathway |
| Tead2 | -0.768923577 | 130.9701 | 0.290352 | 0.999857 | Hippo signaling pathway |
| Tbl1x | -0.719593507 | 865.2986 | 0.154717 | 0.999857 | Wnt signaling pathway |
| Fzd1 | -0.678740736 | 105.0864 | 0.565871 | 0.999857 | Hippo signaling pathway; Wnt signaling pathway |
| Llgl2 | -0.653182661 | 288.6929 | 0.237365 | 0.999857 | Hippo signaling pathway |
| Ccnd1 | -0.645998772 | 1155.011 | 0.143216 | 0.999857 | Hippo signaling pathway; Wnt signaling pathway |
| Smad4 | -0.642316984 | 651.032 | 0.122433 | 0.958277 | Hippo signaling pathway; Wnt signaling pathway |
| Nf2 | -0.597380214 | 1247.983 | 0.073008 | 0.79229 | Hippo signaling pathway |
| Btrc | -0.586768758 | 479.0764 | 0.22108 | 0.999857 | Hippo signaling pathway; Wnt signaling pathway |
| Prkci | -0.563248602 | 659.4133 | 0.281221 | 0.999857 | Hippo signaling pathway |
| Ppp3cc | -0.557264892 | 313.9434 | 0.347531 | 0.999857 | Wnt signaling pathway |
| Bmpr1a | -0.553877855 | 165.7714 | 0.542511 | 0.999857 | Hippo signaling pathway |
| Pals1 | -0.546567208 | 434.9485 | 0.22393 | 0.999857 | Hippo signaling pathway |
| Chd8 | -0.543666558 | 655.0519 | 0.217903 | 0.999857 | Wnt signaling pathway |
| Llgl1 | -0.534519826 | 964.727 | 0.125179 | 0.96171 | Hippo signaling pathway |
| Tcf7l2 | -0.505424751 | 602.5596 | 0.250784 | 0.999857 | Hippo signaling pathway; Wnt signaling pathway |
| Ctbp2 | -0.496503599 | 623.2585 | 0.306992 | 0.999857 | Wnt signaling pathway |
| Ryk | -0.482345519 | 314.5314 | 0.420289 | 0.999857 | Wnt signaling pathway |

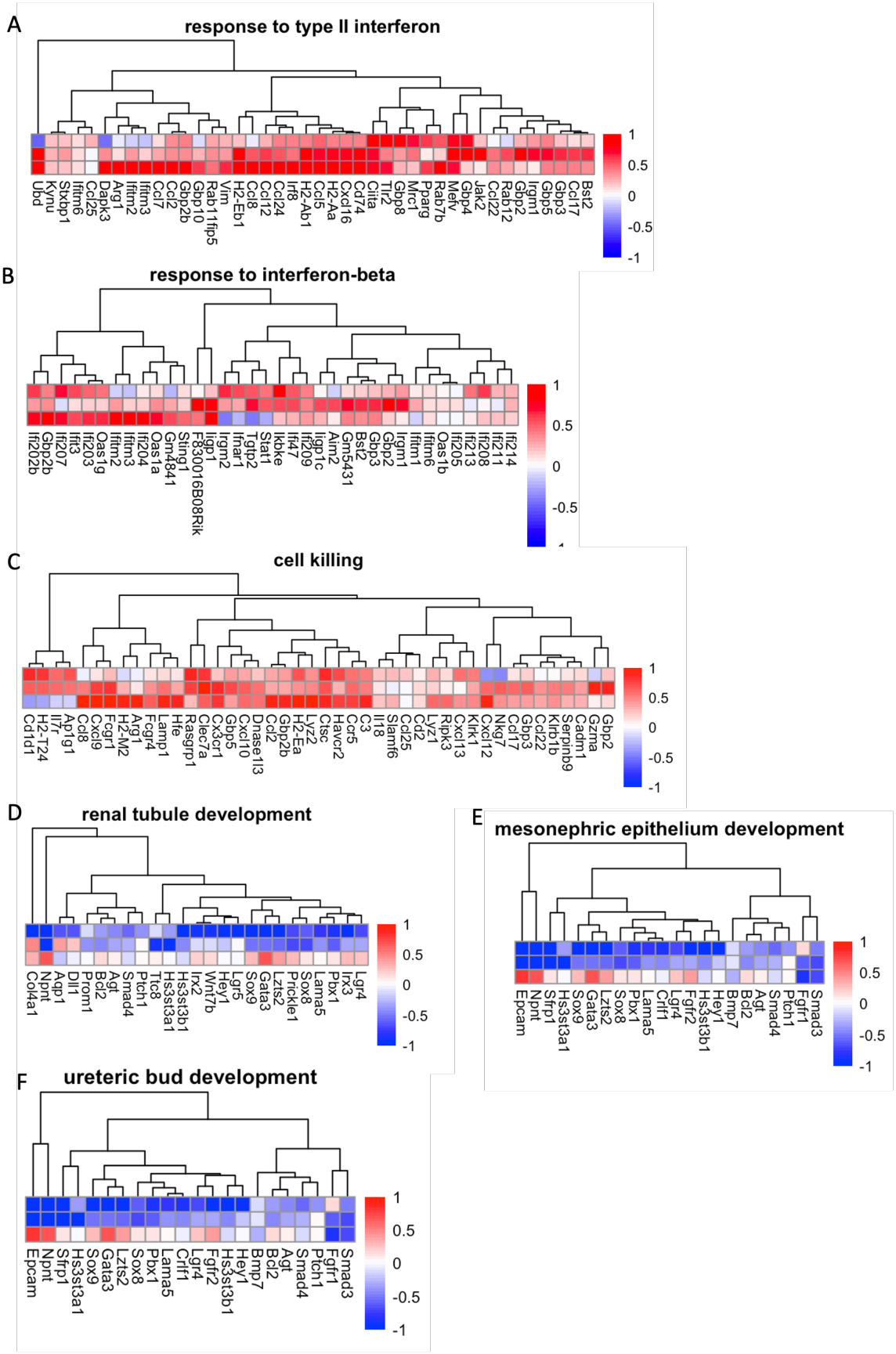


**Figure S3. Heatmaps of genes extracted from the GSEA-GO analysis. The** NT193 cancer cell line was grafted into the 4th mammary fat pad of FVB female mice, on day 18 tumours (n=3) were harvested and Siglec-F+ CD11b+ eosinophils were sorted based on their Ly6C surface expression. Ly6C+ and Ly6C- sorted eosinophils were then processed and analysed by bulk RNA sequencing and analysed by

GSEA-GO. Gene sets of top 3 up **(A-C)** and down **(D-F)** regulated pathways in Ly6C+ eosinophils were extracted and visualised by heatmaps. Heatmaps display fold change (FC) differences between Ly6C+ and Ly6C- eosinophils. Data were further normalised by z-scoring across all samples for visualisation. FC differences are colour-coded according to a custom palette; genes overexpressed in Ly6C+ eosinophils have FC > 0.

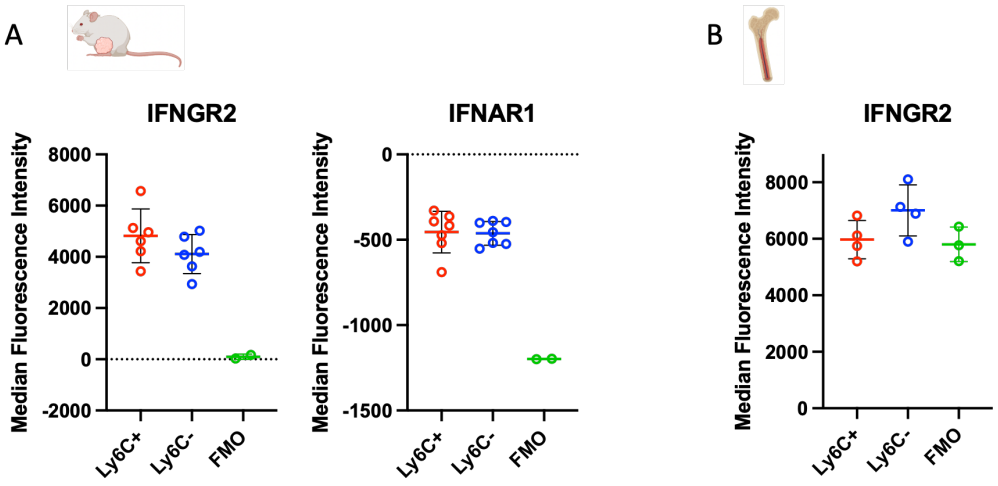


**Figure S4. Flow cytometry analysis of IFNGR2 and IFNAR1 on tumour-associated and bone marrow-derived eosinophils. (A)** The NT193 cancer cell line was grafted into the 4th mammary fat pad of FVB female mice, on day 18, tumours were analysed by flow cytometry and the median fluorescence intensity of IFNγ receptor 2 (IFNGR2) and IFN-alpha receptor 1 (IFNAR1) was compared between Ly6C+ eosinophils, Ly6C- eosinophils (n =6) and fluorescence minus one control on all eosinophils (n = 2). **(B)** Bone marrow cells of C57/Bl6 male mice (n = 4) were first cultured with Fltl3 and mSCF for 4 days, then differentiated into eosinophils with IL-5 until day 18 and and the median fluorescence intensity of IFNγ receptor 2 (IFNGR2) was compared between Ly6C+ eosinophils, Ly6C- eosinophils (n =4) and fluorescence minus one control on all eosinophils (n =3).

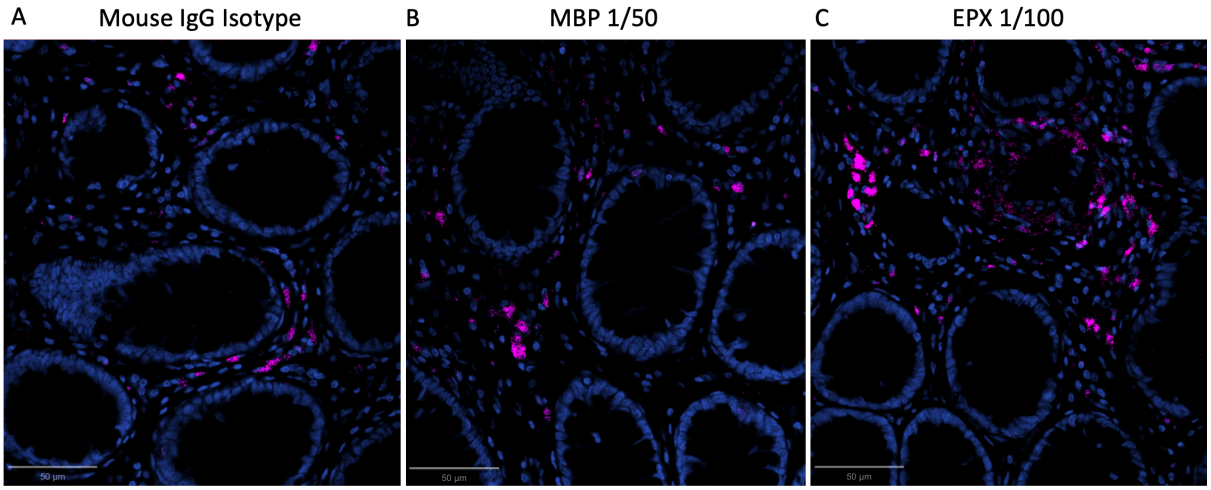


**Figure S5. Comparison of immunofluorescent staining with IgG isotype control and two eosinophil markers on healthy colon.** Healthy colon samples underwent heat-induced antigen retrieval with citrate and tris incubation and were stained with IgG isotype **(A)**, anti-major basic protein (MBP) **(B)**, and anti-eosinophil peroxidase (EPX) **(C)** antibodies and visualised with the confocal microscope Zeiss 880. Scale = 50μm.

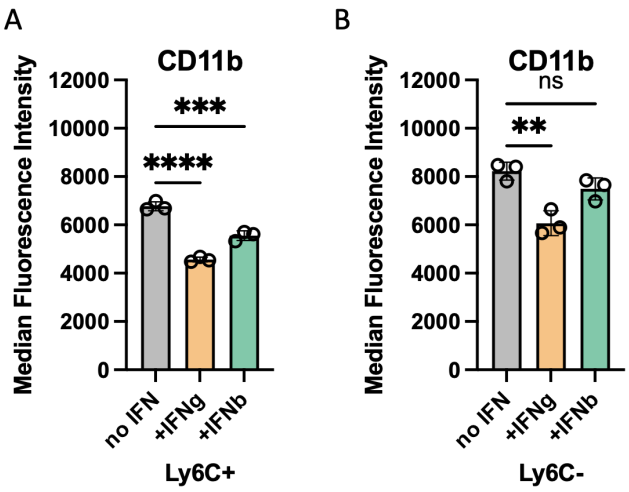


**Figure S6. Effect of IFN stimulation on CD11b expression of Ly6C+ and Ly6C- bone marrow-derived eosinophils ex vivo.** Bone marrow cells of C57/Bl6 male mice (n = 3) were first cultured with Fltl3 and mSCF for 4 days, then differentiated into eosinophils with IL-5 until day 18 and CCR3+ Ly6C+ and CCR3+ Ly6C- eosinophils were FACS sorted. Both subsets of eosinophils were afterwards incubated with IFNγ or IFNβ in the presence of IL-5, or cultured in the absence of IFNs in the presence of only IL-5. All treatment groups were analysed with flow cytometry. **(A, B)** Comparison of CD11b expression of Ly6C+ and Ly6C- eosinophils after incubation with IL-5 (gray), IL-5+ IFNγ (+IFNγ, yellow), and IL-5 + IFNβ (+IFNβ, green), as indicated. Data show mean + SEM and are representative of 2 independent experiments, and were analysed by a two-tailed paired Student's t-test. Statistical significance is displayed on figures as follows: **p < 0.01, ***p<0.001, ****p<0.0001.

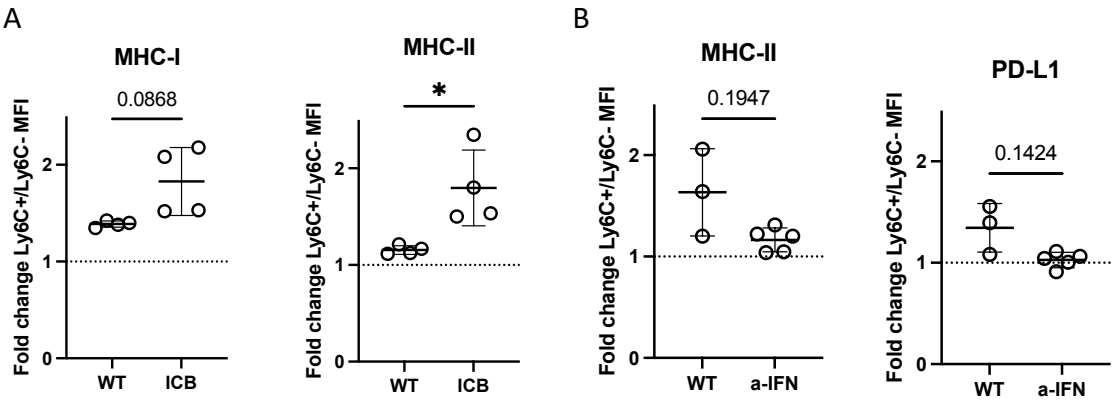


**Figure S7. MFI fold change differences of Ly6C+ to Ly6C- eosinophils in control and treated tumours. (A)** FVB mice were orthotopically grafted with the NT193 cell line into the 4th mammary fat pad and treated every 3 days with anti-PD-L1 or IgG2b isotype control antibodies up to day 18. Foldchange of MHC-I and MHC-II median fluorescence intensity on Ly6C+/Ly6C- eosinophils in WT (n = 4) and ICB (n = 4) treated tumours. **(B)** FVB mice were orthotopically grafted with the NT193 cell line into the 4th mammary fat pad and treated every 3 days with anti-IFNAR1 and anti-IFNγ antibodies (anti-IFNs) or isotype control (Iso), until reaching the humane end-point on day 12. Foldchange of MHC-II and PD-L1 median fluorescence intensity on Ly6C+/Ly6C- eosinophils in WT (n = 3) and a-IFN (n = 5) treated tumours. Data show mean + SEM and are representative of 1 experiment, and were analysed by two-tailed paired Student's t-test. Statistical significance is displayed on figures as follows: *p < 0.05, or p-value above the plot.

# Chapter 5 | Tenascin-C supports macrophage-eosinophil crosstalk

## 5.1 Introduction

Eosinophils represent a prevalent myeloid population in NT193 tumours, as described in Chapter 3. Intriguingly, the NT193 cancer cell line with genetically engineered low or high expression levels of extracellular matrix protein tenascin-C (TNC) was previously used to examine the effects of cancer-derived TNC on macrophage polarisation[228], metastatic blood vessel formation[231], and formation of a distinct tumour microenvironment (TME) resulting in a T-cell exclusion during breast cancer progression[92]. Therefore, this chapter uses the NT193 model with high (TNC+) and low (TNC-) levels of cancer-derived TNC to further understand eosinophil behaviour in the altered TME. The analysis of the myeloid compartment of TNC+ and TNC- tumours revealed that eosinophils are a major myeloid population exclusively in TNC+ tumours with wild-type levels of TNC. Moreover, comparison of early and late tumours revealed that while macrophages and eosinophils were excluded towards the tumour periphery in early tumours, eosinophils were more efficient in penetrating TNC+ tumours at the final time point. Although this phenotype was not associated with any differences in the tumour growth, the NT193 TNC-dependent model was used to explore why eosinophils infiltrated the TNC+ tumours at higher rates.

Following these initial findings and the fact that tumour-associated macrophages (TAMs) were previously proposed to be differentially polarised towards a more M2-like state in NT193 tumours with altered TNC[228], TAMs of both TNC+ and TNC- tumours were analysed by bulk RNAseq analysis. These results a) confirmed the altered phenotype of TAMs infiltrating these two distinct TMEs and b) revealed that TAMs infiltrating TNC+ tumours upregulated genes associated with granulocyte chemotaxis, including overexpression of *Ccl24*, eotaxin-2, a chemokine responsible for eosinophil migration[108]. Because TNC is a known activator of TLR4[234] and TNC stimulation of bone marrow-derived macrophages (BMDM) was previously linked to *Ccl24* expression[232], further analysis focused on understanding if and how TNC supports macrophage-eosinophil crosstalk in vitro and in vivo. To this end, I was able to

confirm that eosinophils and macrophages co-localised on TNC tracks and that in vitro stimulation of BMDMs with the tenascin-C domain binding TLR4 led to an increased eosinophil migration.

To investigate the potential macrophage-eosinophil cross-talk in vivo, TNC+ tumours were treated with clodronate liposomes, a treatment strategy used for the depletion of phagocytic cells and leading to a reduction of tumour growth. This treatment reduced TAM level by 33% one day after the last clodronate administration and caused eosinophil reduction in one experimental repeat. However, because of the systemic effect of clodronate liposome on the spleen and the incomplete macrophage depletion, these experiments were discontinued.

Overall, this chapter presents new findings on the TNC-dependent NT193 model, pointing to eosinophils as one of the major myeloid populations impacted by the knockdown of cancer-derived TNC. Furthermore, these results provide new insights into TNC macrophage activation, pointing to a possible mechanism by which TNC supports macrophage-eosinophil crosstalk in vitro and in vivo. Finally, while clodronate liposome treatment did not result in complete macrophage depletion, observations during these experiments raise a question of the potential systemic side effects of this treatment and underline the importance of biological controls to ensure the specificity of liposome uptake and depletion of the macrophage population.

## 5.2 Results

### 5.2.1 Effect of TNC knockdown in cancer cells on TME formation revisited

Tenascin-C (TNC) is a large extracellular matrix protein mostly absent in healthy adult tissues but upregulated during tissue injury, inflammation and pathological conditions such as rheumatoid arthritis[313,314] or cancer[221], where it is predominantly produced by stromal cells[315]. In cancer, TNC was found to be expressed by both stromal and cancer cells, with cancer-derived TNC being an important factor of lung colonisation during the establishment of metastatic breast cancer[222]. Furthermore, TNC is a known activator of TLR4 signalling, leading to proinflammatory macrophage polarisation[234]. TLR4-TNC signalling was associated with the promotion of metastatic niche by activation of perivascular macrophages in lungs[232], and in a primary model of breast cancer, only cancer-derived TNC and not host-derived TNC was proposed to polarise macrophages to a pro-tumorigenic M2-like state, enhancing the growth of NT193 TNC+ tumours[228]. Given that a) TNC polarises macrophages towards a more pro-tumorigenic phenotype in NT193 tumours[228], b) the unexpected finding of the tumour-associated eosinophils infiltration in NT193 tumours, described in Chapter 3, and c) the growing evidence of macrophage-eosinophil crosstalk during infection and cancer progression[170,316], I revisited the NT193 TNC-dependent breast cancer model to understand how and if the cancer-derived TNC shapes macrophage-eosinophil crosstalk in the tumour microenvironment (TME).

As previously described, the NT193 cell line was derived from a spontaneous tumour of a transgenic MMTV-NeuNT FVB mouse with an active form of ErbB2 (NeuNT) driving the tumorigenesis[317]. The NT193 cell line was genetically manipulated to downregulate TNC expression (shTNC/TNC-) by using shRNA interfering with *Tnc*. As a control, NT193 cells were transfected with a non-targeting shRNA, resulting in native levels of TNC expression (shCTL/TNC+)[231]. Both shTNC and shCTL NT193 cell lines were provided by Dr. Gertraud Orend. NT193 cells were orthotopically engrafted into the 4$^{th}$ mammary fat pad of wild-type

FVB female mice and tumours were analysed by flow cytometry and immunofluorescent imaging (Figure 5.1A). Prior to engraftment, downregulation of *Tnc* expression was confirmed by qPCR analysis of TNC+ and TNC- cancer cells (Figure 5.1B). Tumours were harvested on day 7 and day 18 and infiltration of eosinophils (CD11b+, Siglec-F+, Ly6G-), neutrophils (CD11b+, Siglec-F-, Ly6G+), monocytes (CD11b+, Siglec-F-, Ly6G-, Ly6C+), and macrophages (CD11b+, Siglec-F-, Ly6G-, Ly6C-) was assessed by flow cytometry (Figure 5.1C).

While no difference in TAMs infiltrating TNC+ and TNC- tumours was observed during early tumour development on day 7, TNC- tumours presented with increased macrophage levels on day 18 (Figure 5.1D). In contrast, monocytes were present in TNC+ tumours on day 7 significantly more, however, no difference in monocyte infiltration was observed on day 18 (Figure 5.1E). As the difference in macrophage infiltration during late tumour development was not previously reported, the macrophage phenotype was further investigated. TNC- TAMs were previously assigned a CD206+, $CD86^{low}$, $MHCI^{lo}$, $MHCII^{lo}$ phenotype[228]. I did not observe a statistically significant increase in MHC-II in TAMs infiltrating TNC- tumours, and increased expression of CD206 in TNC+ TAMs was observed in some but not all experimental repeats (Figure S8A). However, CD86 expression was consistently increased on TNC- TAMs across all experimental repeats, in agreement with the literature[228] (Figure S8B).

No statistically significant differences were observed when comparing neutrophil infiltration on either day 7 or day 18 post-engraftment in TNC+ and TNC- tumours (Figure 5.1F). As described in Chapter 3, CD45+ compartment of TNC+ tumours consisted of up to 30% of tumour-associated eosinophils on day 18, however, this was not observed in TNC- tumours, or in either of the phenotypes on day 7-post engraftment (Figure 5.1G). These results suggested that eosinophil infiltration is directly or indirectly supported by the TME formed during the late TNC+ tumour development.

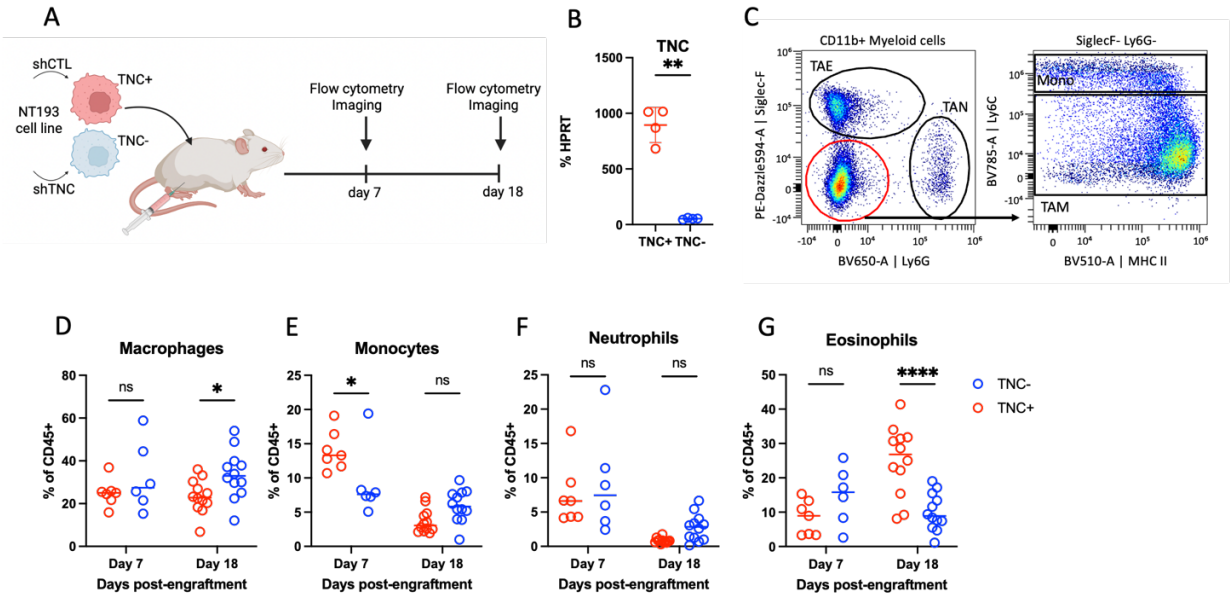


**Figure 5.1. Eosinophil infiltration in the NT193 model is reduced in shTNC tumours. (A)** Overview of the experimental set-up. The NT193 cancer cell line derived from spontaneous MMTV-NeuNT was transfected with shRNA interfering with *Tnc* expression (shTNC cells/ TNC-) or a control non-specific shRNA (shCTL cells/TNC+). TNC+ or TNC- NT193 cells were orthotopically grafted into immunocompetent FVB mice and tumours were analysed by imaging and flow cytometry on days 7 and 18 post-engraftment. **(B)** Relative *Tnc* expression in TNC+ and TNC- cancer cell lines, presented as percentage of *Hprt* expression ($n_{TNC+}$ = 4, $n_{TNC-}$ = 4). Data show individual values and mean ± SD, are pooled from 2 independent experiments, and were analysed by Student's t-test. **(C)** Representative gating strategy used for flow cytometry identification of tumour-associated eosinophils (TAE), tumour-associated neutrophils (TAN), monocytes (Mono), and tumour-associated macrophages (TAM). **(D-G)** Comparison of macrophages **(D),** monocytes **(E),** eosinophils **(F),** and neutrophils **(G)** on indicated days in TNC+ (red) and TNC- (blue) tumours, ($n_{TNC+,day7}$ = 7, $n_{TNC-,day7}$ = 6, $n_{TNC+,day18}$ = 12, $n_{TNC-,day18}$ = 12). Data show individual values and mean, day 7 data are pooled from 2 independent experiments, day 18 data are pooled from 4 independent experiments, each experiment containing 3 mice per group and all experiments showed the same trend. Data were analysed by a two-way ANOVA test using Šídák correction. Statistical significance is displayed on figures as follows: *p < 0.05, **p < 0.01, ***p<0.001, ****p<0.0001.

Previously, macrophage infiltration in NT193 TNC+ and TNC- tumours was investigated through F4/80 immunofluorescent staining, revealing no significant differences in macrophage distribution in treatment naïve mice[228]. Considering that eosinophils present a significant F4/80+ population, these findings were revisited. To understand if the temporal regulation of macrophages and eosinophils in TNC+ and TNC- tumours is associated with differences in spatial distribution, NT193 tumours were further characterised by anti-Siglec-F (eosinophil) and anti-CD68 (macrophage) immunofluorescent staining (Figure 5.2A) on day 7 and day 18. Interestingly, while both eosinophils and macrophages were mostly excluded towards the tumour edge during early tumour development (Figures 5.2B and C), eosinophils were found to be more evenly distributed in the TNC+ tumours on day 18 (Figure 5.2B). This was previously unreported and points to an interesting phenotype in which eosinophils are capable of penetrating the tumour core in TNC+ tumours.

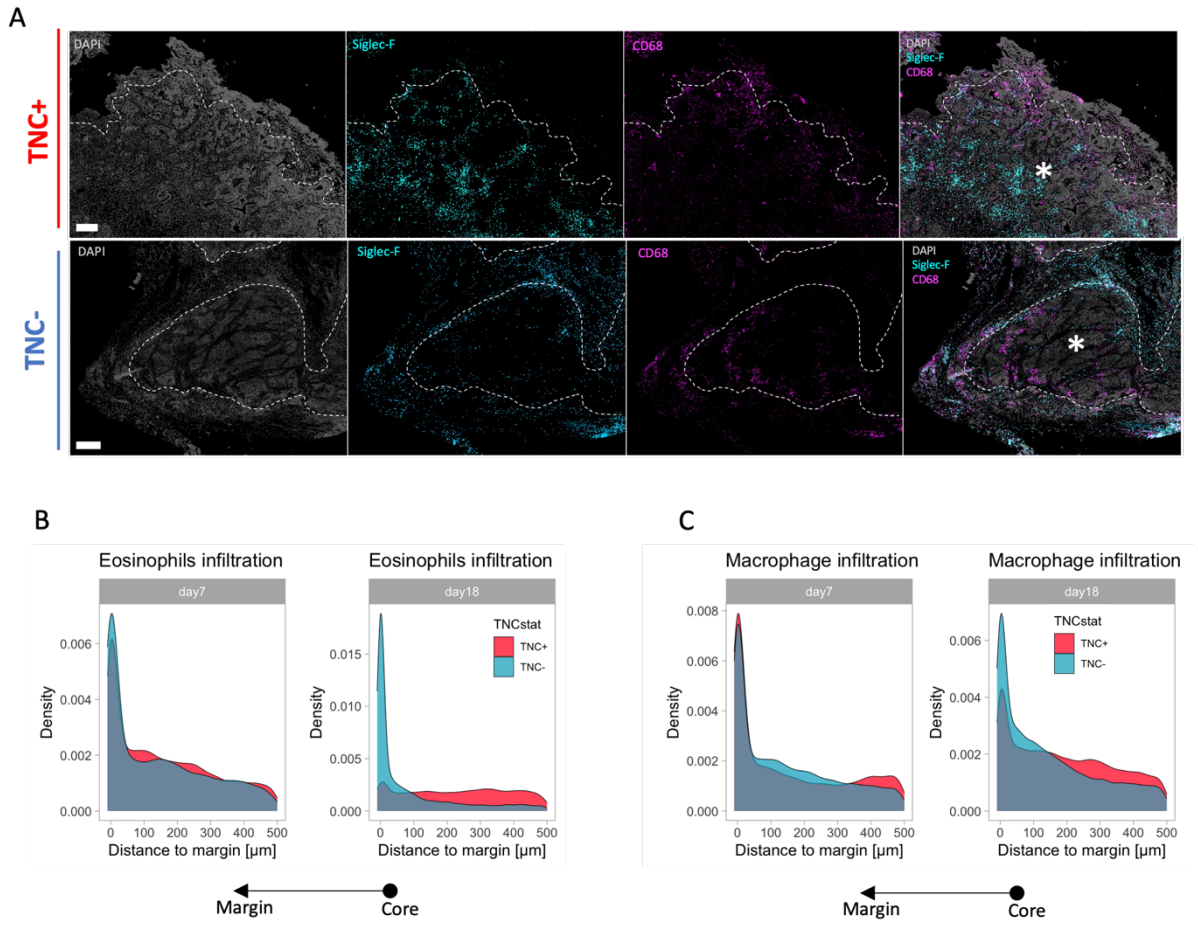


**Figure 5.2. Eosinophils are spatially excluded within shTNC NT193 tumours.** NT193 cancer cell line derived from spontaneous MMTV-NeuNT was transfected with shRNA interfering with *Tnc* expression (shTNC cells/ TNC-) or a control non-specific shRNA (shCTL cells/TNC+). TNC+ or TNC- NT193 cells were orthotopically grafted into immunocompetent FVB mice and tumours were analysed by immunofluorescent imaging on days 7 and 18 post-engraftment. Tumours were cryosectioned to 5µm thickness, stained with DAPI (nuclear stain), Siglec-F (eosinophils), and CD68 (macrophages) and imaged with Zeiss Axioscan7. All analysis was performed in QuPath software. **(A)** Representative image of TNC+ and TNC- tumour on day 18 post-engraftment. **(B)** Quantification of eosinophil distance from the tumour edge in TNC+ (red) and TNC- (blue) tumour on the indicated day. **(C)** Quantification of macrophage distance from the tumour edge in TNC+ (red) and TNC- (blue) tumour on the indicated day. Data representative of 3 tumours per each condition, plots (B) and (C) are representative of 3 pooled tumours per condition. Scale = 250µm.

Because of the increased eosinophil infiltration in TNC+ tumours (Figure 5.1G), their proposed anti-tumorigenic activity in NT193 TNC+ tumours (Figure 3.12), and the more even distribution of eosinophils at late stages of TNC+ tumour development, I next wanted to understand if this might be connected to the previously observed enhanced tumour growth of TNC+ tumours. Eight independent experiments focused on the comparison of TNC+ and TNC- tumour growth were performed. First, approximately 10 million NT193 cells in 50µl of PBS of either TNC+ or

TNC- phenotype were orthotopically grafted in FVB mice and no statistically significant difference in tumour volume at the final time point was observed (Figure 5.2A).

As this method was technically challenging, in the next set of experiments, 5 million NT193 cells in 100μl of PBS of either TNC+ or TNC- phenotype were orthotopically grafted in FVB mice. This approach resulted in similar findings, no statistically significant difference between tumours generated with TNC+ and TNC- NT193 cell line was observed (Figure 5.2B). It is important to note that only tumours that did not show signs of regression were included in this analysis, which resulted in a lower number of mice per cohort. Removal of regressing tumours was performed in all treatment naïve mice as both TNC+ and TNC- tumours were regressing at different rates depending on the experimental repeat (Figure S9). Importantly, on average, neither of the phenotypes was observed to regress more (Figure 5.3C).

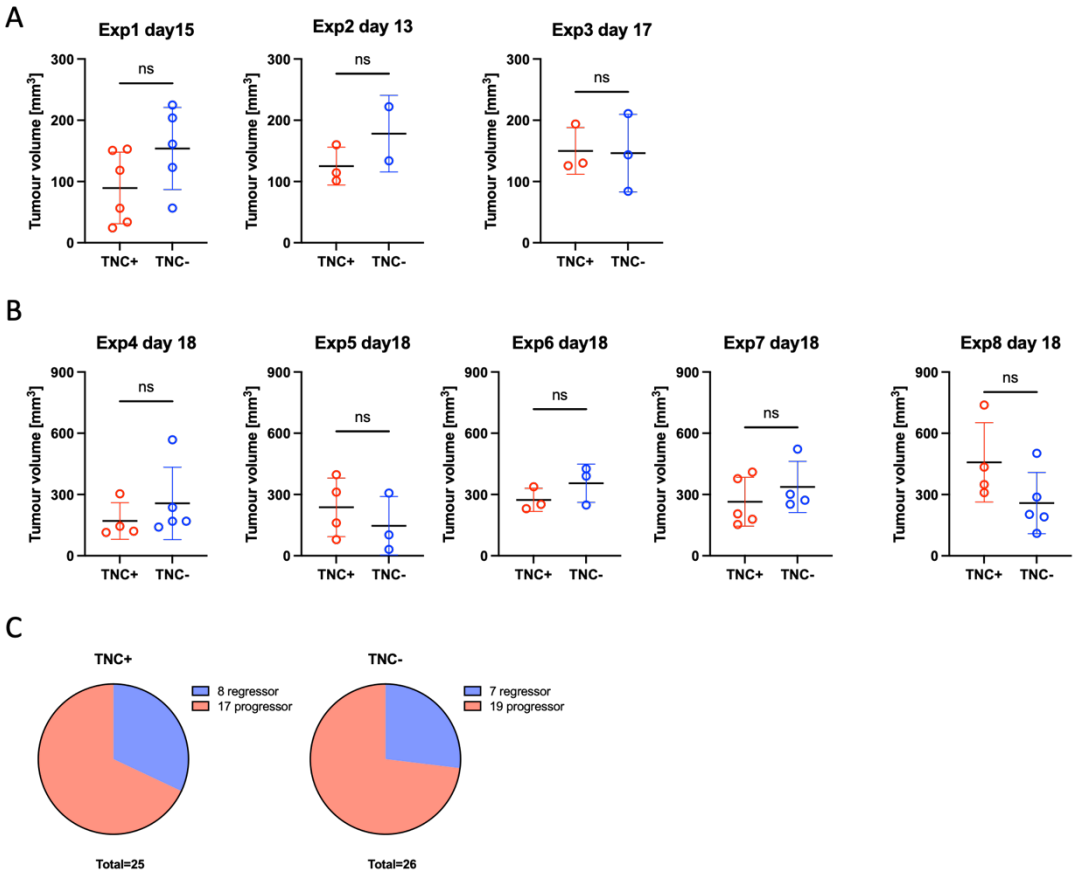


**Figure 5.3. Knockdown of TNC in cancer cells does not impact primary tumour growth.** The NT193 cancer cell line derived from spontaneous MMTV-NeuNT was transfected with shRNA interfering with *Tnc* expression (shTNC cells/ TNC-) or a control non-specific shRNA (shCTL cells/TNC+). TNC+ or TNC- NT193 cells were orthotopically grafted into immunocompetent FVB mice and tumours were

harvested on day when they reached a human endpoint. **(A)** Approximately 10 million of NT193 cells in 50μl was orthotopically engrafted. Comparison of tumour volume of TNC+ and TNC- at a final time point in all experimental repeats, as indicated ($n_{TNC+, exp1} = 6$, $n_{TNC-, exp1} = 5$; $n_{TNC+, exp2} = 3$, $n_{TNC-, exp2} = 2$, $n_{TNC+, exp3} = 3$, $n_{TNC-, exp3} = 3$). **(B)** 5 million NT193 cells in 100μl were orthotopically engrafted. Comparison of tumour volume of TNC+ and TNC- on day 18 in all experimental repeats, as indicated ($n_{TNC+, exp4} = 4$, $n_{TNC-, exp4} = 5$; $n_{TNC+, exp5} = 4$, $n_{TNC-, exp5} = 3$, $n_{TNC+, exp6} = 3$, $n_{TNC-, exp6} = 3$; $n_{TNC+, exp7} = 5$, $n_{TNC-, exp7} = 4$; $n_{TNC+, exp8} = 4$, $n_{TNC-, exp8} = 5$). **(C)** Summary of regressing TNC+ and TNC- tumours in experiments 4-8. Data show individual values and mean, and were analysed by Student's t-test. Statistical significance is displayed on figures as follows: ns = $p > 0.05$.

Overall, these results show that the formation of TME by the TNC+ NT193 cancer cells leads to increased levels of tumour-associated eosinophils that are able to penetrate through the tumour edge more efficiently compared to TNC- tumours. Furthermore, macrophage infiltration was also altered, with a slight, but statistically significant, increase observed in TNC- tumours, with TNC- macrophages being more CD86+. While I was not able to confirm the TNC-dependent growth, I have further used the NT193 model to better understand how eosinophils infiltrate orthoptic tumours.

### 5.2.2 Tumour-associated macrophages overexpress eotaxin-2 in TNC+ tumours

Because TNC is capable of macrophage activation in different disease contexts[232,234], polarisation of macrophages infiltrating TNC+ and TNC- tumours was further investigated in an unbiased manner. NT193 shCTL or shTNC cells were orthotopically engrafted in wild-type FVB female mice, and tumour-associated macrophages (CD11b+, F4/80+, Siglec-F-, Ly6G-, Ly6C-) were FACS sorted from both TNC+ and TNC- tumours and examined by bulk RNAseq (Figure 5.4A). Principal component analysis of the bulk RNAseq experiment revealed a clear separation between TNC+ and TNC- TAMs (Figure 4.1B). Furthermore, differential gene expression analysis (DESeq2) of the TNC+ and TNC- TAMs identified 361 differently expressed genes (DEGs) (logFC > 1, p-value < 0.05). Of these DEGs, 167 were downregulated and 194 were upregulated in TNC+ TAMs compared to TNC- TAMs (Figure 4.1C). Notably, the *Ccl24* gene transcript, encoding eotaxin-2, was among the most significantly upregulated genes in TNC+ TAMs. These results showed that macrophages present with a different phenotype in TNC+ and TNC- tumours, as confirmed by comparison of the top 40 DEGs (Figure S10A).

Further gene set enrichment analysis (GSEA) using the gene ontology (GO) resource revealed chemotaxis as the 4$^{th}$ most upregulated pathway in macrophages sorted from TNC+ tumours (Figure 5.4D), with a set of gene transcripts directly associated with granulocyte chemotaxis, including *Ccl24* (Figure 5.4E). Furthermore, normalised expression of *Ccl24* positively correlated with eosinophil infiltration in TNC+, but not in TNC- tumours (Figure 5.4F). These results collectively point at the possibility that macrophages in the TME containing cancer-derived TNC are capable of enhancing eosinophil infiltration.

Even though some of the chemokines regulated between TAM subsets are traditionally associated with neutrophil chemotaxis[318] (*Cxcl1, Cxcl2*), eosinophils were previously observed to migrate towards mKC (CXCL1) in vitro[108]. Therefore, differences in chemokine receptors on eosinophils infiltrating TNC+ and TNC- tumours were further explored to understand the capacity of eosinophils to sense these chemokines.

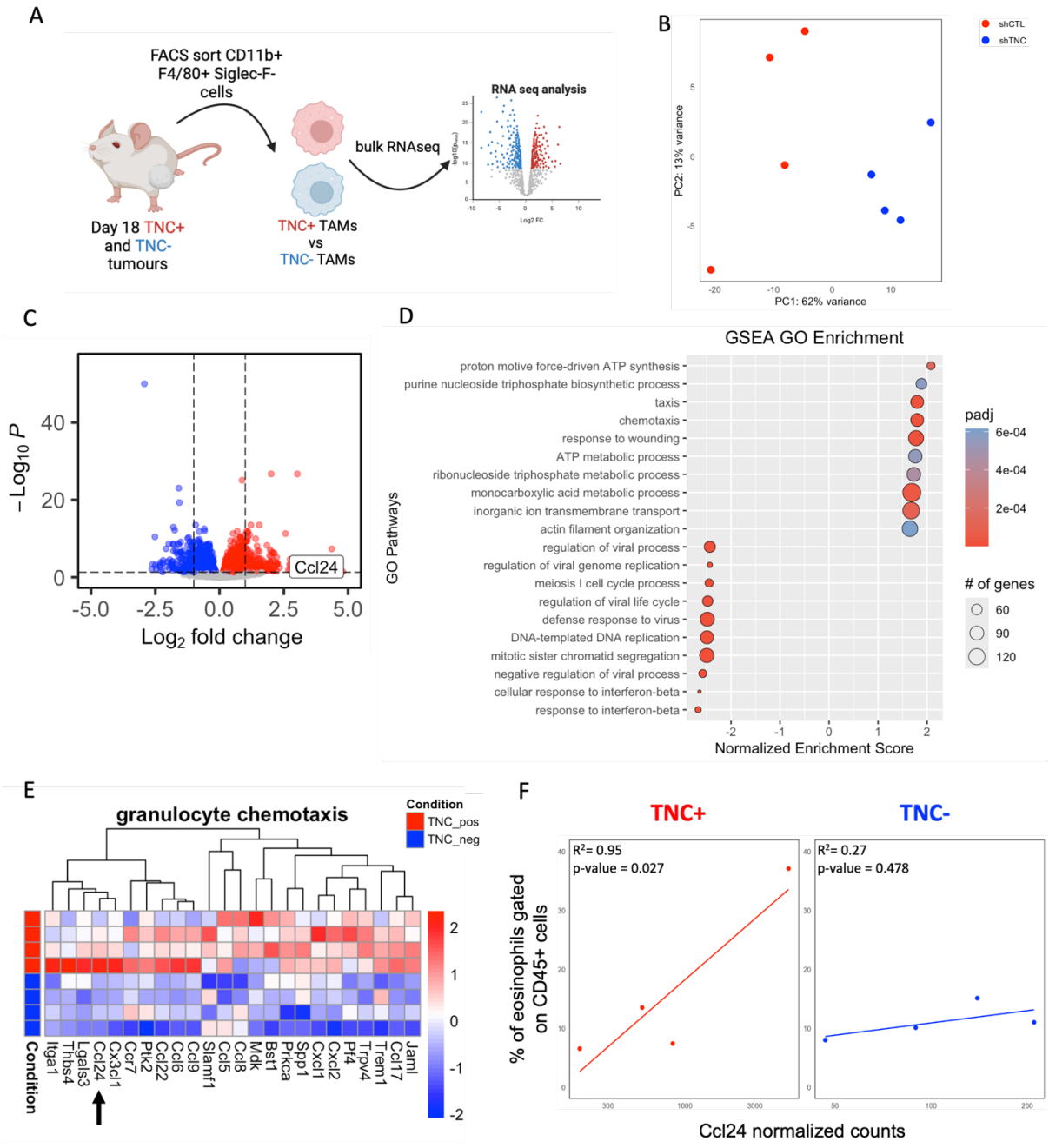


**Figure 5.4. Tumour-associated macrophages in shTNC tumours downregulate eotaxin-2. (A)** Overview of the experimental set-up. The NT193 cancer cell line derived from spontaneous MMTV-NeuNT was transfected with shRNA interfering with the *Tnc* expression (shTNC cells/ TNC-) or a control non-specific shRNA (shCTL cells/TNC+). TNC+ or TNC- NT193 cells were orthotopically grafted into immunocompetent FVB mice, tumours were harvested on day 18 post-engraftment, F4/80+, Siglec-F-, Ly6C- macrophages were FACS sorted and analysed by bulk RNAseq. **(B)** Visualisation of principal components (PC) 1 and 2 of PCA analysis performed on all sequenced samples after DESeq2 normalisation. Each point represents an individual sample, colour-coded by experimental condition as indicated - TNC+ (red) and TNC- (blue). **(C)** Volcano plot of differentially expressed genes between TNC+ associated macrophages and TNC- tumour-associated macrophages. Each point represents a gene; all genes are plotted by fold change ($log_2$) against statistical significance ($–log_{10}$ adjusted p-value). Significantly upregulated genes in TNC+ associated macrophages are marked in red, significantly downregulated genes are marked in blue. Eotaxin2 (Ccl24) is highlighted. **(D)** Gene Set Enrichment Analysis (GSEA) using the Gene Ontology (GO) database was performed using ranked gene expression data. Genes were ranked by differential expression and converted to Entrez IDs before enrichment testing across all GO categories (Biological process, Molecular function, and Cellular

component). Enriched pathways were identified based on normalised enrichment scores (NES) and adjusted p-values (adjusted p-value < 0.05). The dot plot displays the top significantly enriched GO terms for upregulated (NES>0) and downregulated (NES<0) gene sets in TNC+ TAMs, dot size represents the number of genes in each pathway and dot colour intensity indicates statistical significance (adjusted p-value). **(E)** Heatmap of normalised gene expression of genes associated with granulocyte chemotaxis in TNC+ (red) and TNC- (blue) associated macrophages. Rows represent individual samples and columns represent genes. Expression levels are colour-coded according to a custom palette. **(F)** Correlation of normalised Ccl24 expression by TNC+ (red) and TNC- (blue) associated macrophages and % of eosinophils in matched tumours analysed by flow cytometry. Data are analysed by simple linear regression.

As mentioned above, eosinophils were previously observed to migrate towards CXCL1 in vitro migration assays, and eosinophil migration is commonly regulated by CCL11 and CCL24[318]. Therefore, to test whether the increased expression of *Ccl24* and *Cxcl1* by TNC+ TAMs is matched with increased responsiveness of tumour-infiltrating eosinophils, expression of a) CCR3 receptor for eotaxins (CCL11, CCL24, and CCL26) and b) CXCR2 receptor for CXCL1 and CXCL2 chemokines, was compared on tumour-associated eosinophils infiltrating TNC+ and TNC- early and late tumours. Interestingly, no differences in CCR3 median fluorescence intensity were observed on day 7, however, TNC+ associated eosinophils overexpressed CCR3 on day 18, pointing to a possible increased responsiveness to CCL24+ macrophages (Figure 5.5A). This fits with the observation that eosinophils accumulate in the TNC+ tumours at late stages, while on day 7 no differences in eosinophil levels between TNC+ and TNC- tumours were observed (Figure 5.1G).

Analysis of CXCR2 expression did reveal possible overexpression on TNC+ associated eosinophils on day 18, however, the absolute values were very close to the fluorescence minus one (FMO) control for the CXCR2 antibody (Figure 5.5B). Therefore, CXCR2 expression was further investigated on TNC+ and TNC- tumour-infiltrating and compared to both FMO control and isotype control on both eosinophils and neutrophils (Figure 5.5C and D); neutrophils were chosen for comparison as they are known to express CXCR2 receptor[319]. These results suggested that the low levels of CXCR2 observed on eosinophils were most likely a technical artefact, as no clear CXCR2+ eosinophil population was observed on eosinophils compared to the isotype control (Figure 5.5C); however, neutrophils presented

with a clear expression of CXCR2 receptor compared to both FMO and isotype controls (Figure 5.5D).

These results show that the observed increase in tumour-infiltrating eosinophils in NT193 tumours might be partially supported by overexpression of the CCR3 receptor on TNC+ eosinophils, however, these eosinophils are unlikely to be migrating based on the CXCL1 or CXCL2 axis.

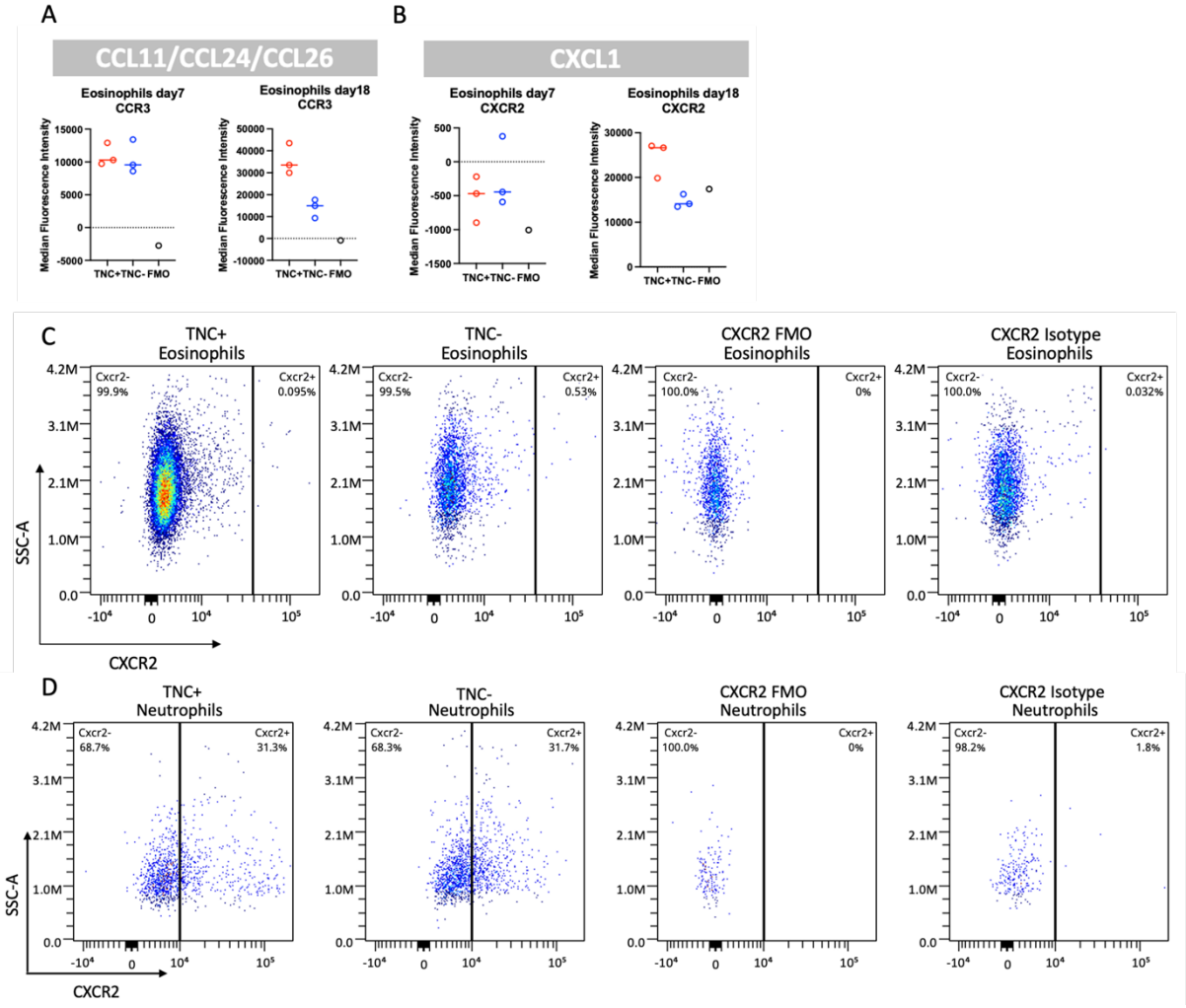


**Figure 5.5. Eosinophils overexpress CCR3 in TNC+ NT193 tumours.** The NT193 cancer cell line derived from spontaneous MMTV-NeuNT was transfected with shRNA interfering with *Tnc* expression (shTNC cells/ TNC-) or a control non-specific shRNA (shCTL cells/TNC+). TNC+ or TNC- NT193 cells were orthotopically grafted into immunocompetent FVB mice and tumours were analysed by flow cytometry on days 7 and 18 post-engraftment. **(A)** Comparison of CCR3 median fluorescence intensity on eosinophils infiltrating TNC+ and TNC- tumours on the indicated time points. **(B)** Comparison of CXCR2 median fluorescence intensity on eosinophils infiltrating TNC+ and TNC- tumours on the indicated time points. **(C)** Representative density plot of CXCR2 expression of eosinophils in TNC+ and TNC- tumours with 2 controls: fluorescence minus one (FMO) and CXCR2 isotype control. **(D)** Representative density plot of CXCR2 expression of neutrophils in TNC+ and TNC- tumours with 2 controls: fluorescence minus one (FMO) and CXCR2 isotype control.

To further investigate the potential macrophage-eosinophil crosstalk mediated by TNC activation, the spatial distribution of macrophages and eosinophils in relation to TNC tracks in both TNC+ and TNC- tumours on day 7 and day 18 was analysed by immunofluorescent imaging. These experiments revealed a co-localisation of macrophages and eosinophils in proximity to TNC tracks in both TNC+ and TNC- tumours (Figure 5.6A, B). Further analysis of eosinophil and macrophage distribution revealed that eosinophils in TNC+ tumours were more likely to reside on TNC track than in TNC- tumours by day 18 (Figure 5.6C), but no differences in macrophage-TNC distance were observed on either of the days (Figure 5.6D). However, most eosinophils in both tumour types were located in the tumour stroma, and therefore, the eosinophil-TNC distance analysis was influenced by the increased infiltration of eosinophils in the TNC+ tumour type, making them statistically more likely to reside closer to any type of matrix track.

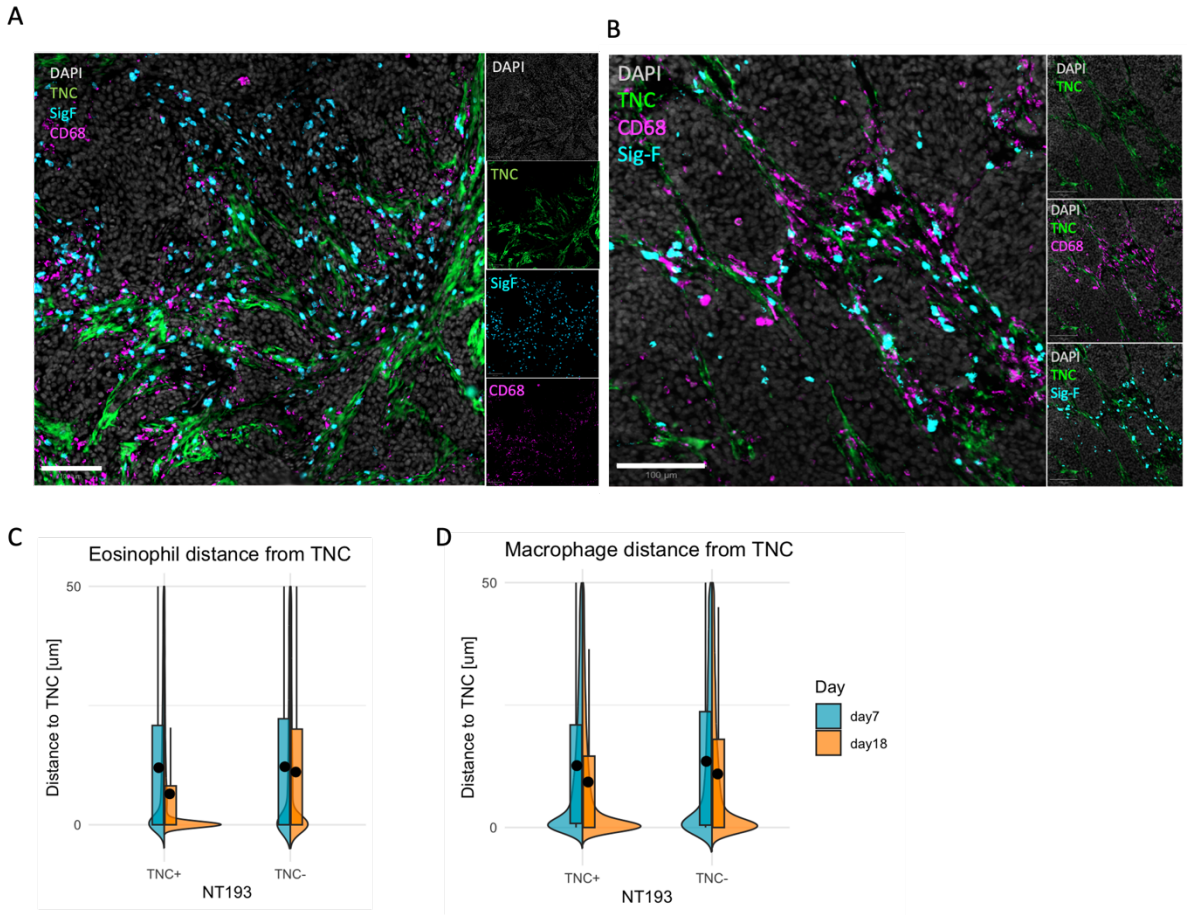


**Figure 5.6. Eosinophils co-localise with macrophages on TNC tracks.** The NT193 cancer cell line derived from spontaneous MMTV-NeuNT was transfected with shRNA interfering with *Tnc* expression (shTNC cells/ TNC-) or a control non-specific shRNA (shCTL cells/TNC+). TNC+ or TNC- NT193 cells were orthotopically grafted into immunocompetent FVB mice and tumours were analysed by

immunofluorescent imaging on days 7 and 18 post-engraftment. Tumours were cryosectioned to 5μm thickness, stained with DAPI (nuclear stain), Siglec-F (eosinophils), CD68 (macrophages), and tenascin-C (TNC) and imaged with Zeiss Axioscan7. All analysis was performed in QuPath software. **(A, B)** Representative images of TNC+ **(A)** and TNC- **(B)** tumour on day 18 post-engraftment. **(C, D)** Comparison of eosinophil **(C)** and macrophage **(D)** distance to the nearest TNC track on day 7 (blue) and day 18 (orange), in TNC+ and TNC- tumours. Data representative of 3 tumours per each condition, plot (B) summarises data of 3 pooled tumours per condition; all tumours were checked separately to ensure representativeness of the analysis. Scale = 100μm.

Overall, these results showed that macrophages in TNC+ tumours upregulate genes related to granulocyte chemotaxis, and *Ccl24*, eotaxin-2, is among the most upregulated genes compared to TNC- TAMs. Macrophages co-localise with eosinophils on TNC tracks in both tumours, however, only TNC+ tumours present with increased levels of infiltrating eosinophils. Therefore, I next wanted to understand if macrophages are directly polarised towards Ccl24+ phenotype by TNC, or the overall changes in the TME.

### 5.2.3 TNC-TLR4 interaction drives eotaxin production in macrophages

As previously reported, TNC stimulates expression of secreted cytokines, such as *Ccl3*, *Ccl4*, *Ccl5*, *Ccl24*, and *Cxcl1,* through TLR4 activation of macrophages. These findings originate from a study where unstimulated bone marrow-derived macrophages (BMDMs) were compared to TNC-activated BMDMs, and BMDMs treated with TLR4 inhibitor prior to TNC activation[232] (Figure 5.7A). This dataset was reanalysed to investigate if other cytokines supporting eosinophil chemotaxis, activation or survival are expressed following the TLR4 activation. Analysis confirmed overexpression of *Ccl3*, *Ccl4*, and *Ccl24* but showed no effect of TNC stimulation on eotaxin-1 (*Ccl11*) or *Il33,* whilst a slight but not significant increase in *Il5* was observed(Figure 5.7B).

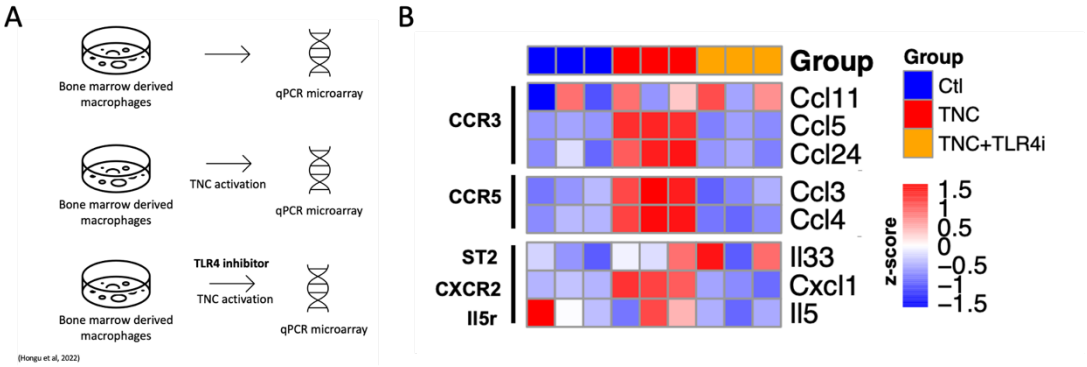


**Figure 5.7. Tenascin-c stimulates expression of eotaxin-2 in bone marrow-derived macrophages.** **(A)** Overview of the experimental set-up, as described by Hongu and colleagues. Bone marrow-derived

macrophages of Balb/c mice were stimulated with TNC for 6 hours, treated with TLR4 inhibitor for 1 hour prior to TNC stimulation, or left unstimulated (n=3, per condition). Microarray data were accessed using GSE156354. **(B)** Heatmap of normalized expression of selected CCR3 (*Ccl11, Ccl5, Ccl24*), CCR5 (*Ccl3, Ccl4*), ST2/Il33r (*Il33*), CXCR2 (*Cxcl1*), and IL5ra (*Il5*) ligands. Rows represent individual genes and columns represent samples. Expression levels are colour-coded according to a custom palette. Samples are colour-coded based on treatment as follows: untreated (Ctl, blue), TNC-stimulated (TNC, red), TNC-stimulation of TLR4-inhibited BMDMs (TNC+TLR4i, orange).

Next, I wanted to investigate if stimulation of bone marrow-derived macrophages (BMDMs) by TNC affects the migration of eosinophils in vitro. For this reason, the C-terminal domain of TNC, the fibrinogen-like globe (FBG) domain, known to activate TLR4 signalling in macrophages[234,320] was picked for BMDM activation. Supportive of the TNC-TLR4 activation dataset, FBG increased mRNA expression of Ccl5, Ccl24, and Ccl26 in human-derived macrophages (Figure 5.8A, data generated by A. Schwenzer). Therefore, BMDMs were serum starved overnight, stimulated with native FBG domain or heat-denatured FBG (dFBG) for 24 hours, and afterwards, conditioned media was used in a transwell migration assay with donor-matched bone marrow-derived eosinophils on day 14 (Figure 5.8B). This experiment revealed that FBG stimulation of BMDMs supports eosinophil migration in vitro, compared to dFBG (Figure 5.8C)

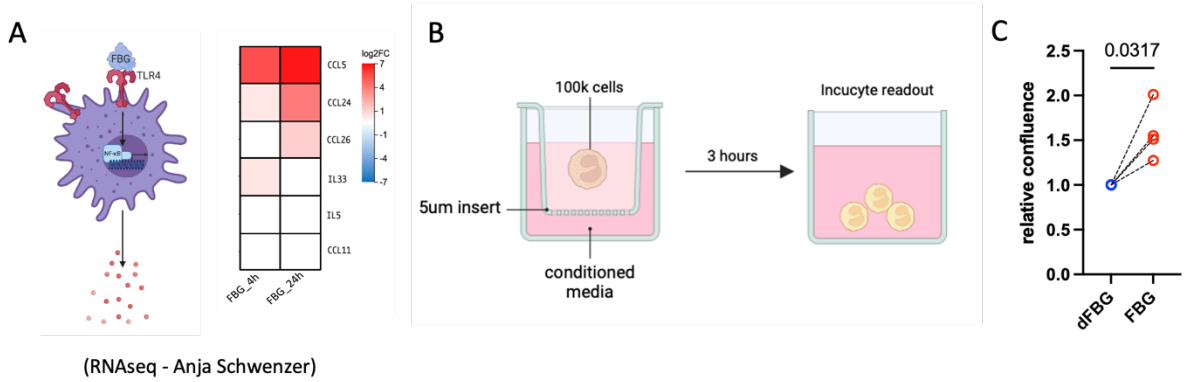


(RNAseq - Anja Schwenzer)

**Figure 5.8 FBG stimulation of bone marrow-derived macrophages enhances eosinophil migration. (A)** Data generated and analysed by Anja Schwenzer. PBMCs were isolated from 6 donors, differentiated into macrophages and afterwards stimulated with 1μM FBG domain activating TLR4 signalling for 4 and 24 hours. Log fold2 change difference of FBG stimulated to unstimulated controls were compared for *Ccl5, Ccl24, Ccl26, Il33, Il5,* and *Ccl11* gene transcripts. **(B)** Overview of experimental set-up. Bone marrow cells were isolated from C57/Bl6 mice (n = 4), and cells from each mouse were split into 2 cell culture experiments to generate donor-matched bone marrow-derived macrophages and eosinophils. Macrophages were serum starved overnight, stimulated with either FBG + polymyxin B (FBG) or heat-denatured FBG domain + polymyxin (dFBG) for 24 hours and the conditioned medium was collected. Conditioned media was added to the bottom well in a transwell migration assay with bone marrow-derived eosinophils added to the top well. Built-in Incucyte density analysis was used to compare the FBG and dFBG conditions. **(C)** Relative confluence of migrated eosinophils normalised to paired dFBG control. Data show individual values, are representative of 2 independent experiments and were analysed by a paired Student's t-test. Statistical significance is displayed in the form of a p-value above the data.

These experiments led to a hypothesis that TNC in the TME may directly polarise tumour-associated macrophages, which leads to increased expression of chemokines, such as *Ccl24*, and increased infiltration of eosinophils in TNC+ tumours. Therefore, further experiments were focused on testing this TNC-macrophage-eosinophil crosstalk in vivo.

### 5.2.4 Effects of early macrophage depletion in TNC+ NT193 model of breast cancer

Macrophages in TNC+ tumours were previously associated with a pro-tumorigenic phenotype, as clodronate liposome treatment effectively reduced the tumour growth[228]. Clodronate, a bisphosphonate, is a hydrophilic molecule that, when encapsulated in a liposome, can be selectively uptaken by phagocytic cells and causes apoptosis after being metabolised into a cytotoxic ATP analogue[321]. However, clodronate not encapsulated in a liposome is not cytotoxic and does not easily permeabilize membranes on its own; this proves the specificity of the clodronate liposome cytotoxicity exclusively towards phagocytic cells[322]. Therefore, NT193 tumours were treated with clodronate liposomes or control PBS liposomes, as previously described[228] (Figure 5.9A), to understand if macrophage depletion stops eosinophil infiltration.

In line with previous observations, clodronate liposome treatment significantly reduced the tumour growth compared to the PBS liposome-treated cohort (Figure 5.9B). Furthermore, clodronate treatment resulted in statistically significant eosinophil depletion on day 17, however, no reduction of macrophages was observed at day 17 of this first experiment (Figure 5.9C). Therefore, this experiment was repeated and the efficacy of clodronate treatment was investigated on day 9, one day after the last clodronate injection.

On day 9, macrophages presented 18% of all CD45+ tumour infiltrating lymphocytes (TILs) in PBS liposome-treated and 11.5% of all TILs in clodronate liposome-treated mice; representing a 36% decrease in TAM population in the clodronate-treated group (Figure 5.9D). No other myeloid population was observed to be affected on day 9 (Figure S11). While all macrophages

re-infiltrated the tumours by day 17, no difference in eosinophil infiltration was observed at the final time point (Figure 5.9E). Results of this experiment are, however, inconclusive as 3 mice had to be removed from both the PBS liposome and the clodronate liposome-treated groups due to tail necrosis. Therefore, these experiments were underpowered to study the effect of clodronate liposome treatment on eosinophil infiltration of NT193 tumours.

Despite the lack of complete macrophage depletion at day 9, clodronate effectively reduced tumour growth in both experimental repeats. Clodronate prevented splenomegaly associated with cancer onset on day 9, and spleens of clodronate-treated mice were visibly altered and appeared to be depleted of red blood cells on day 17 (Figure 5.9F). This raises a question of whether the TAM depletion or rather the systemic response of the organism to the clodronate treatment is responsible for the reduced tumour growth.

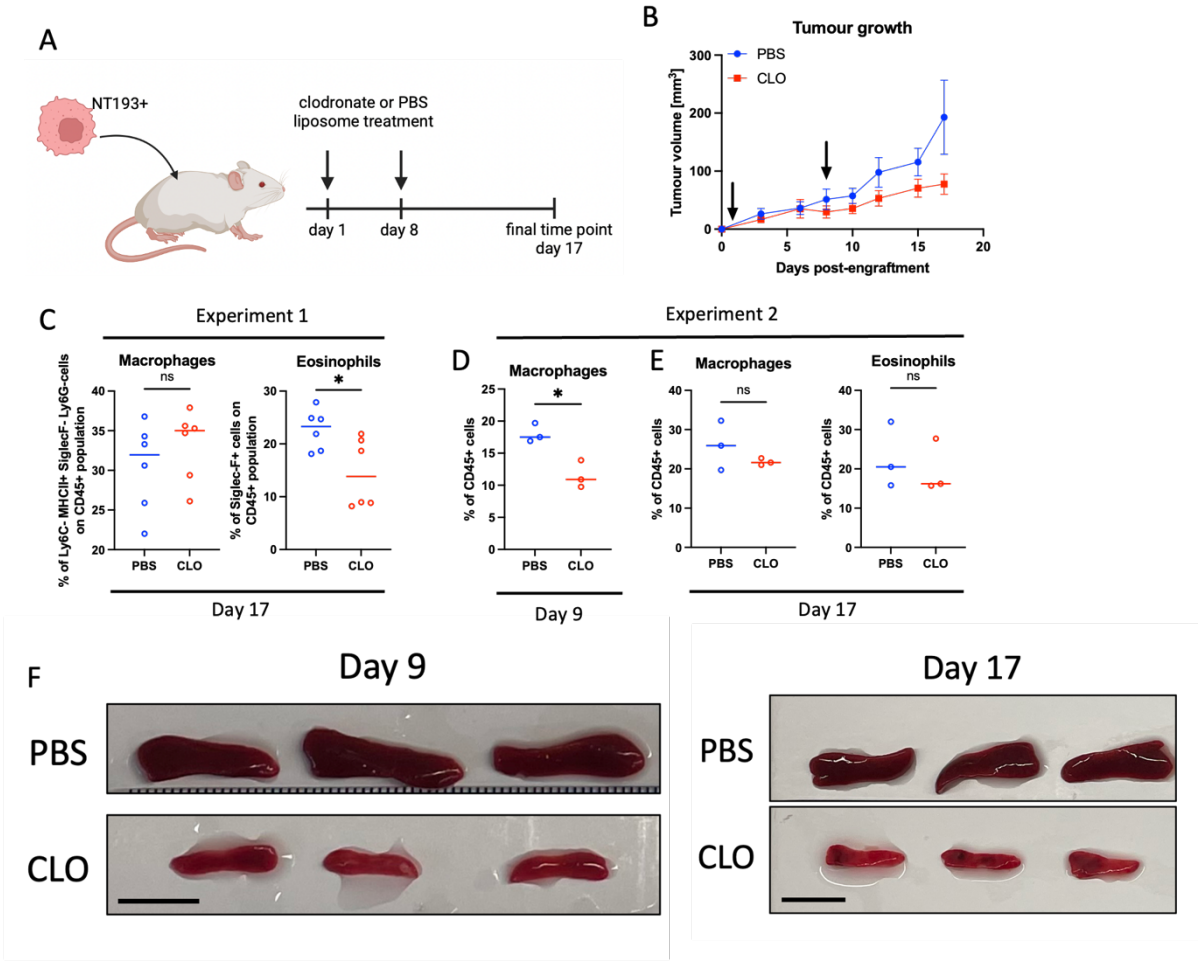


**Figure 5.9. Treatment with clodronate liposomes causes a minor reduction of macrophages. (A)** Overview of the experimental set-up. TNC+ NT193 cancer cells were orthotopically engrafted into immunocompetent wild-type FVB female mice. Tumours were treated with clodronate or PBS liposomes

on day 1 and day 8 post-engraftment, were harvested on day 17 and analysed by flow cytometry. **(B)** Tumour growth curve of mice treated with PBS or CLO liposomes. ($n_{TNC+,PBS}$ = 6, $n_{TNC+,\ CLO}$ = 6). Data are representative of 2 repeats. Arrows indicate the administration of liposomes. **(C-E)** Flow cytometry analysis of macrophage and eosinophil infiltration in two experimental repeats, on the indicated days. **(F)** Comparison of spleen size and general morphology between PBS and CLO treated mice on the indicated time point. Scale = 1cm. Data show individual values and mean, were analysed student t-test and statistical significance is displayed on figures as follows: *p < 0.05.

Because NT193 tumours were often spontaneously regressing, the clodronate treatment did not completely deplete macrophages, and had a systemic off-site effect on the spleen, these experiments were discontinued. Potential future avenues that could explore the macrophage-eosinophil crosstalk are discussed in section 5.3.1.

## 5.3 Technical discussion

### 5.3.1 Usage of clodronate liposomes for macrophage depletion

One of the aims of this chapter was to confirm that macrophages support eosinophil infiltration of TNC+ tumours. For this purpose, a protocol using clodronate liposome treatment was adapted[228], as the uptake of clodronate liposomes by phagocytic cells is a commonly used method for depletion of macrophages[321,322]. However, like every treatment, the usage of clodronate liposomes comes with several technical and biological challenges, as described more in more detail below.

First, macrophages are not the only phagocytic cells being depleted by clodronate liposomes, this includes monocytes and dendritic cells[323]. However, recently published data strongly suggest that even neutrophils are capable of engulfing the liposomes with high efficiency[323] (Figure 5.11). Second, liposomes are often administered systemically through intraperitoneal or intravenous injections, leading to depletion of phagocytic cells at distant sites, such as the bone marrow and spleen[324]. As tumours are known to affect distant organs during cancer progression, for example through emergent myelopoiesis[83], anti-tumorigenic effects of clodronate might not be directly associated with depletion of tumour-associated myeloid cells. Third, as macrophages are known to affect angiogenesis and the attraction of other cell types to the TME, the broad changes observed in the TME following the clodronate treatment are usually attributed to the absence of macrophages. However, some of these findings could be challenged, as more technical controls would be necessary to understand the extent of liposome uptake by individual cell types with individual protocols targeting different tissue resident/infiltrating macrophages. Finally, TAMs heterogeneity is well well-established phenomenon[247,248,325], with some studies suggesting that certain subsets of macrophages, such as Lyve1+ TAMs[325], are more efficient in phagocytosing liposomes than other TAMs. Overall, while clodronate is a broadly used treatment in a number of studies investigating the

role of macrophages, the effects observed during these experiments need to be carefully interpreted and presented with appropriate technical and biological controls.

The clodronate treatment regimen used in this chapter did affect NT193 TAMs levels only short term, as macrophages fully re-infiltrated tumours by day 17. If these experiments were repeated, more frequent, 3-times a week administration would be used to deplete macrophages with higher efficiency. Alternatively, macrophages could be more specifically targeted through anti-CSF-1R antibody treatment, previously observed to successfully deplete TAMs[326]. In contrast to clodronate liposome treatment, administration of anti-CSF-1R antibody was not observed to prolong overall survival[276] or impact the tumour growth of established tumours[327] in murine cancer models on its own. Therefore, it would be interesting to understand if anti-CSF-1R could have an impact on the TNC+ NT193 model with increased levels of eosinophils and macrophages polarised towards an M2-like phenotype.

### 5.3.2 Limitations of transwell migration assays

The transwell migration assay was used to investigate whether macrophage activation with TNC leads to increased eosinophil migration. While this mechanism is supported by a bulk RNAseq dataset[232], and the overall increased migration of eosinophils towards conditioned media of TNC-stimulated BMDMs, these experiments would benefit from several controls. First, protein levels of CCL11, CCL24 and CCL26 could be assessed in the macrophage conditioned media to confirm overexpression and secretion of these eotaxins upon TNC stimulation. Second, the fold change differences are statistically significant, however, the biological effect is less than 2-fold in most cases (Figure 5.8). Therefore, optimisation of the transwell migration assay in terms of incubation time and number of eosinophils in the upper chamber should be tested to confirm that the observed biological phenotype is relevant. Lastly, eosinophils used in these migration assays were cultured from bone marrow progenitors for 14 days, as described in Chapter 3. This means that the eosinophil population used in these experiments was heterogeneous in terms of Ly6C and CCR3 (eotaxin receptor) expression.

Preferably, these bone marrow-derived eosinophils would be FACS sorted and migration of individual populations would be tested, however, the sorting would affect the eosinophil viability and lower the total number of cells available for these assays, therefore eosinophils were used in bulk.

## 5.4 Biological discussion

### 5.4.1 How does clodronate liposome treatment reduce tumour burden?

Treatment of wild-type FVB tumour-bearing mice with clodronate liposomes during the early TME formation significantly reduced tumour burden, even though macrophages re-infiltrated the NT193 tumours of FVB mice by the final time point (Figures 5.9, 5.11). Similar results were observed in early experiments testing clodronate liposome effects[322], with 2 injections of clodronate liposomes at day 8 and 12 being able to reduce the tumour growth of murine F9 teratocarcinoma by day 14. While there is no doubt that macrophages are being depleted by clodronate liposomes when administered at high frequency[322], even clodronate liposome treatment that does not result in significant TAM depletion (Figure 5.9) or depletes only specific TAM populations[325] is capable of reducing the tumour burden.

Enlargement of the spleen, splenomegaly, is commonly observed during cancer progression[83,328]. In agreement with these findings, the NT193 tumour model induced splenomegaly in FVB during tumour progression (Figure S12A, B). The observed splenomegaly was reversed in mice treated with clodronate liposomes (Figures S12C, D). Moreover, clodronate treatment led to a gross difference in spleen morphology suggesting a reduction of red blood cells (Figure 5.9F). This is supported by reports showing that administration of clodronate liposomes led to reduced erythropoiesis in the spleen during 4T1 tumour progression, and both splenectomy and clodronate administration reduced 4T1 tumour burden[329]. While these effects were attributed to macrophage depletion, this publication does not include data on splenic macrophage levels in PBS or CLO treated tumours. However, in the murine model of encephalitis, intravenous administration of clodronate liposomes significantly reduced red blood cells and their proliferation in bone marrow[330], proving that clodronate treatment affects even non-phagocytic cells. Overall, this suggests that the tumour reduction observed in the NT193 model used in this chapter might be associated with the

profound effect of clodronate treatment on the spleen. To test if red blood cells in spleen and bone marrow in the NT193 model are getting similarly impacted as in previous reports[329,330], EdU proliferation assay together with Ter119 marker used to identify cells of erythroid lineage could be analysed by flow cytometry.

More importantly, as previously discussed, treatment of tumour-bearing mice with clodronate liposome to prove pro-tumorigenic properties of TAMs has to be accompanied by appropriate controls proving efficiency of TAM depletion with every tested protocol, as usage of clodronate liposomes results in tumour reduction even in the presence of TAMs and therefore can lead to misleading conclusions. In future experiments, fluorescently labelled DIL liposomes could be injected into a separate cohort of mice to identify the population of cells with the highest uptake of liposomes. This experiment could further lead to phenotypical characterization of the macrophage subset that is being depleted during the clodronate liposome treatment.

### 5.4.2 Impact of TNC on eosinophil biology

Results of this chapter build on the well-studied macrophage activation by TNC and further focus on how this interaction might support eosinophil migration. However, not only macrophages are being impacted by TNC in the tumours, but also eosinophils reside on the TNC matrix tracks (Figure 5.6). It was previously suggested that TNC blocks IL-5 driven maturation of bone marrow-derived eosinophils in vitro[331]. These co-culture experiments were performed with MAPTrix TNC peptide (M- VAEIDGIEL motif) that has specificity for binding of integrin α9β1. To test whether bone marrow-derived eosinophils respond to this peptide, a small pilot adhesion assay was performed, suggesting a minor but statistically not significant increase in adhesion of bone marrow-derived eosinophils towards MAPTrix protein compared to the BSA-blocked, TNC coated or FBG coated wells (Figure S13A). It would be therefore interesting to investigate if the MAPTrix peptide but also other functional domains of TNC are affecting either adhesion or the Ly6C-CCR3 eosinophil development in vitro. These

experiments might also help with understanding how eosinophils progress to the Ly6C- phenotype at late stages of tumour progression.

Furthermore, murine studies of lung development show that TNC deposition strongly corresponds with eosinophil accumulation during postnatal alveolar septation. Additionally, $TNC^{-/-}$ mice presented with significantly decreased eosinophil infiltration during lung development compared to their wild-type counterparts[127]. It is yet unclear how TNC impacts the eosinophil infiltration, however, bulk RNA sequencing together with flow cytometry analysis comparing a) naïve bone marrow-derived eosinophils with b) Matrigel stimulated and c) Matrigel enriched with TNC, pointed at TNC-enriched matrices enhancing eosinophil viability and regulation of immune responses[127]. To understand if tumour-associated eosinophils in the NT193 model are equipped to respond to TNC, set of TNC receptors previously reviewed by Midwood and colleagues[220], was extracted from the bulk RNAseq dataset of Ly6C+ and Ly6C- eosinophils. No differences between Ly6C+ and Ly6C- eosinophils were observed, however, CD44, integrin beta 1 and integrin beta 3, all involved in adhesion to TNC, were highly expressed based on their normalized count expression (baseMean > 5000) (Figure S13B). These data collectively imply that TNC-rich matrices can promote eosinophil survival and adhesion, fitting with the eosinophil localization on TNC tracks and the increased eosinophil levels in TNC+ tumours.

Investigating the TNC-eosinophil interaction was out of the scope of this thesis, however, future experiments targeting TNC in vivo could help with investigating how extracellular matrix contributes to eosinophil plasticity. For example, a recent study shows how matrix regulating motif-mimicking peptide blocks TNC pro-tumorigenic properties and leads to increased IFNγ signature and release of lymphocytes, such as F4/80+ cells, off the TNC tracks in the NT193 model[238]. As a significant part of this thesis discusses how F4/80+ eosinophils can be mistaken for F4/80+ macrophages, it would be interesting to know if eosinophil distribution is also being affected within this TNC-blocking experiment.

### 5.4.3 Macrophage-eosinophil or eosinophil-macrophage crosstalk?

Current literature describes the link between 1) TNC and macrophage activation[234,320], 2) TNC and eosinophil interaction[127,331], and 3) the macrophage-eosinophil crosstalk in different disease contexts[170,316], with a very recent study describing the anti-tumorigenic role of peritumoral macrophages by recruiting eosinophils in murine breast tumours[332]. However, how these interactions integrate within a complex TME remains unexplored. This chapter aims to connect these findings by describing how tumour-associated macrophages within TNC+ tumours acquire a CCL24+ phenotype that correlates with increased levels of tumour-infiltrating eosinophils. The functional axis between TNC, macrophages, and eosinophils is supported by an in vitro BMDM stimulation and eosinophil migration assay. However, macrophages in both TNC+ and TNC- tumours reside on TNC tracks in close proximity to eosinophils. This raises a key question: why do only TNC+ TAMs overexpress *Ccl24*, leading to increased eosinophil migration? One potential explanation could stem from the intrinsic properties of the NT193 cells that have a broadly altered cytokine profile following the TNC knockdown[92]. The importance of the cancer cell secreted factors on the set-up of the early TME was recently demonstrated, with the early TME being decisive for stromal and myeloid compartment polarisation at late stages of the tumour development[278]. Therefore, understanding this temporal and spatial dynamic in the broader context of cytokine differences could help clarify how matrix components like TNC regulate communication between macrophages and eosinophils in cancer.

In this chapter, I focused on how macrophages might be affecting eosinophils, however, it is also important to consider how eosinophils affect macrophages. Eosinophils infiltrating colorectal tumours were linked to decreased levels of pro-metastatic macrophages by inhibiting their differentiation into the Spp1+ subset[170]. Opposite to these finidngs, TNC+ macrophages presented with increased *Spp1* expression and a wound healing phenotype (Figures 5.4, S10) despite the accumulation of eosinophils. It would be interesting to know if

eosinophils in progressing TME adapt a more M2-like phenotype themselves and support macrophages in their wound healing response. Of particular interest could be the IL-4 axis, important for the maintenance of M2-like dermal macrophages[316]. To understand how eosinophils affect macrophages in TNC+ and TNC- tumours, TNC- infiltrating eosinophils could be sequenced similarly to TNC+ tumours infiltrating eosinophils in Chapter 3 and matched receptor-ligand analysis with tumour-associated macrophages could reveal how this communication is being shaped in distinct TMEs.

Despite the NT193 model being an interesting tool to study the eosinophil plasticity and macrophage-eosinophil crosstalk, the main disadvantage is that there is no difference in the tumour growth. Because TNC+ tumours are known to respond to immunotherapy (Chapter 4), it would also be interesting to know if TNC- tumours, which present with fewer Ly6C+ eosinophils at the final timepoint (Figure S14), also respond to ICB. Differences in treatment response of TNC+ and TNC- tumours could make the macrophage-eosinophil axis an interesting target.

## 5.5 Appendix

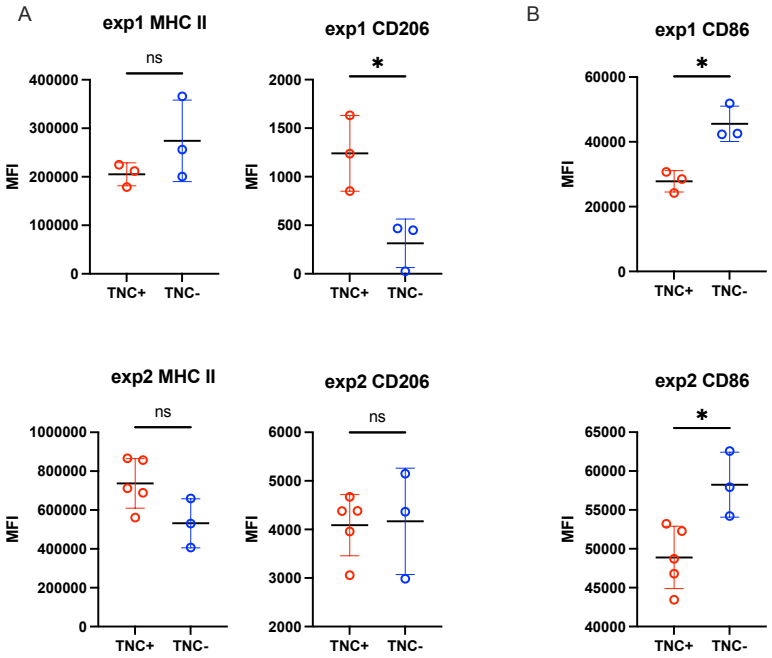


**Figure S8. Macrophage polarisation in TNC+ and TNC- NT193 tumours.** The NT193 cancer cell line derived from spontaneous MMTV-NeuNT was transfected with shRNA interfering with *Tnc* expression (shTNC cells/ TNC-) or a control non-specific shRNA (shCTL cells/TNC+). TNC+ or TNC- NT193 cells were orthotopically grafted into immunocompetent FVB mice and tumours were analysed by flow cytometry on day 18 post-engraftment. **(A)** Comparison of MHC-II AND CD206 median fluorescence intensity on eosinophils infiltrating TNC+ and TNC- tumours in two experimental repeats. **(B)** Comparison of CD86 median fluorescence intensity on eosinophils infiltrating TNC+ and TNC- tumours in two experimental repeats. Data show individual values, and were analysed by Student's t-test. Statistical significance is displayed on figures as follows: *p < 0.05.

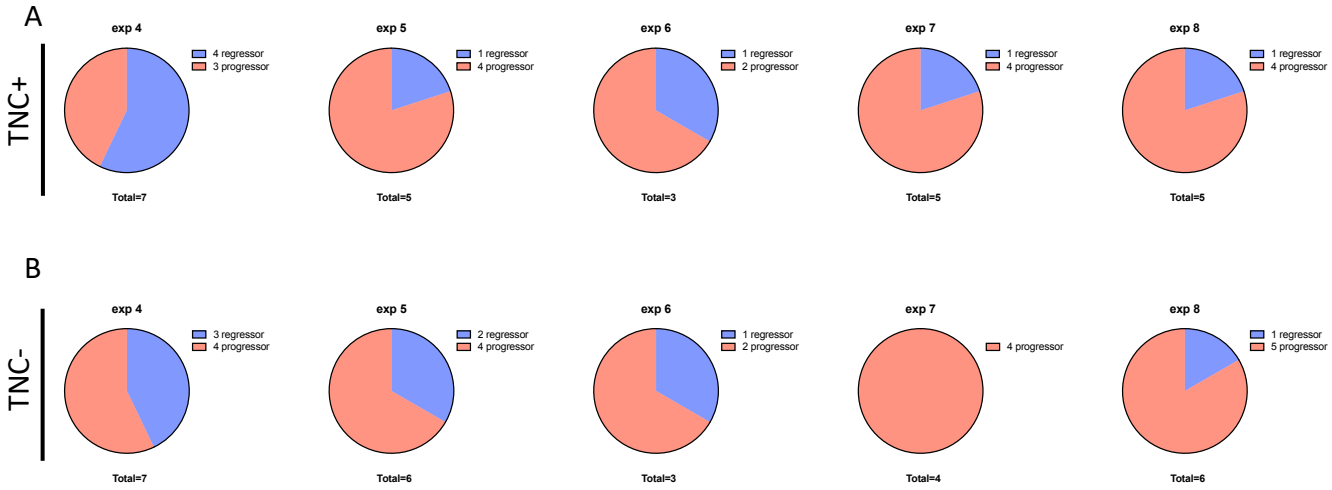


**Figure S9. NT193 TNC+ and TNC- tumours are prone to spontaneous regression.** The NT193 cancer cell line derived from spontaneous MMTV-NeuNT was transfected with shRNA interfering with *Tnc* expression (shTNC cells/ TNC-) or a control non-specific shRNA (shCTL cells/TNC+). TNC+ or TNC- NT193 cells were orthotopically grafted into immunocompetent FVB mice and tumours were monitored 3 times a week. **(A)** Comparison of the number of mice engrafted with TNC+ NT193 cells with progressing (red) and regressing (blue) tumour phenotype on day 18. **(B)** Comparison of the number

of mice engrafted with TNC- NT193 cells with progressing (red) and regressing (blue) tumour phenotype on day 18.

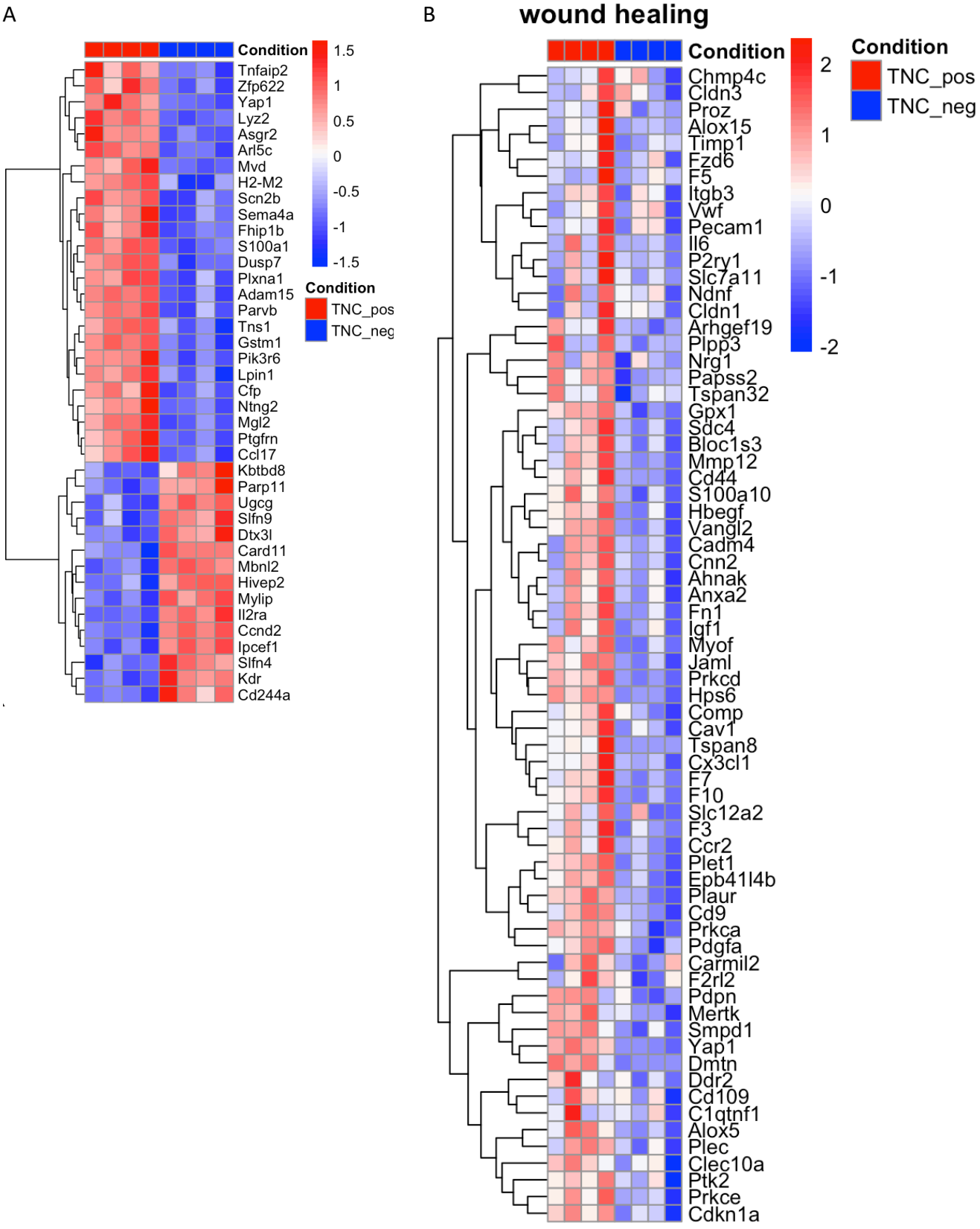


**Figure S10. Polarisation of tumour-associated macrophages in TNC+ and TNC- NT193 tumours.** The NT193 cancer cell line derived from spontaneous MMTV-NeuNT was transfected with shRNA

interfering with *Tnc* expression (shTNC cells/ TNC-) or a control non-specific shRNA (shCTL cells/TNC+). TNC+ or TNC- NT193 cells were orthotopically grafted into immunocompetent FVB mice, tumours were harvested on day 18 post-engraftment, F4/80+, Siglec-F-, Ly6C- macrophages were FACS sorted and analysed by bulk RNAseq. **(A)** Heatmap of normalised gene expression of top 40 most significantly differentially expressed genes in TNC+ (red, n = 3) and TNC- (blue, n = 3) associated macrophages. Rows represent individual genes and columns represent samples. Expression levels are colour-coded according to a custom palette. **(B)** Heatmap of normalised gene expression of genes associated with wound healing in TNC+ (red) and TNC- (blue) associated macrophages. Rows represent individual genes and columns represent samples. Expression levels are colour-coded according to a custom palette.

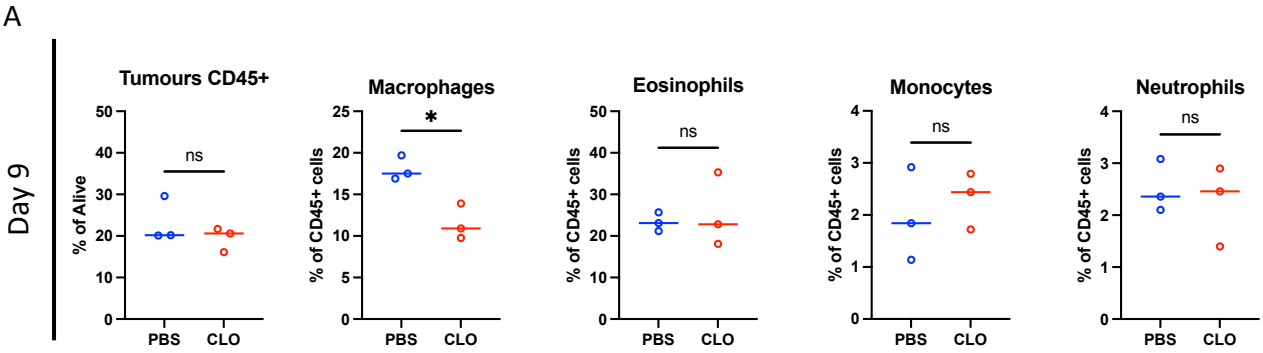


**Figure S11. Systemic clodronate treatment of NT193 mice causes spleen reduction on day 17.** TNC+ NT193 cancer cells were orthotopically engrafted into immunocompetent wild-type FVB female mice. Tumours were treated with clodronate (CLO) or PBS liposomes on day 1 and day 8 post-engraftment, were harvested on day 9 and analysed by flow cytometry. **(A)** Comparison of all CD45+ cells as gated on live cells, and macrophages, eosinophils, monocytes, and neutrophils as a proportion of the CD45+ compartment between PBS and CLO treated mice on day 9. Data show individual values, are representative of one experimental repeat and were analysed by Student's t-test. Statistical significance is displayed on figures as follows: *p < 0.05.

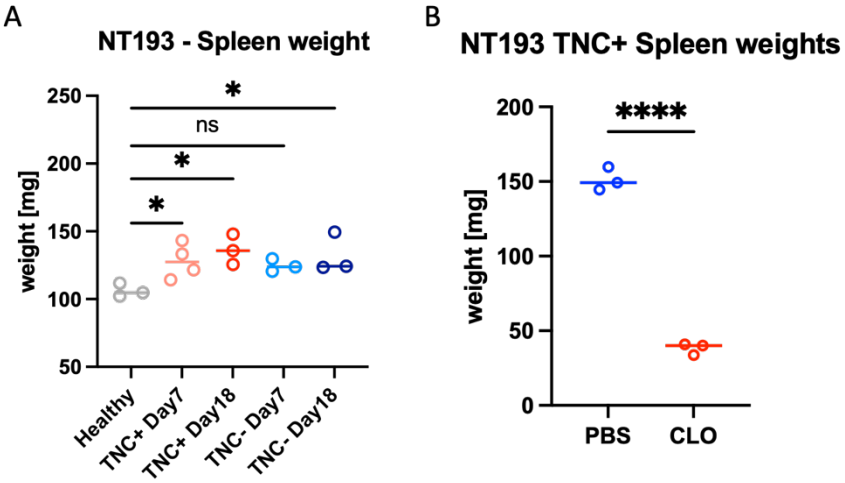


**Figure S12. Comparison of spleen weight during tumour progression and clodronate treatment.** **(A)** TNC+ or TNC- NT193 cancer cells were orthotopically engrafted into immunocompetent wild-type FVB mice. Tumour weights were compared on the indicated days. **(B)** TNC+ tumours were treated with clodronate (CLO) or PBS liposomes as described in Figures 5.9. Comparison of spleen weights of NT193 bearing mice. Data show individual values, are representative of one experimental repeat and were analysed by student t-test. Statistical significance is displayed on figures as follows: *p < 0.05, **p < 0.01, ***p<0.001, ****p<0.0001.

A

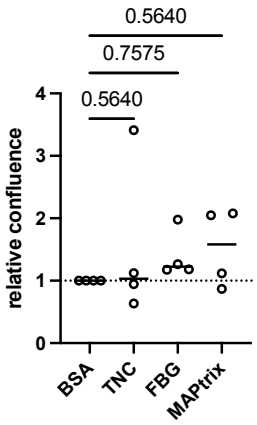


B

| gene name | gene | baseMean | log2FoldChange | padj |
|---|---|---|---|---|
| Hyaluronic acid receptor | Cd44 | 14778.4231 | -0.082423799 | 0.999856677 |
| Integrin beta 1 | Itgb1 | 11178.3797 | -0.135319389 | 0.999856677 |
| Integrin beta 3 | Itgb3 | 5123.6987 | -0.548155859 | 0.762176295 |
| Annexin A2 | Anxa2 | 5111.42239 | 0.200644627 | 0.999856677 |
| Syndecan 4 | Sdc4 | 2765.8211 | 0.550638348 | 0.999856677 |
| Integrin alpha V | Itgav | 1195.88936 | 0.162239002 | 0.999856677 |
| Integrin alpha IIb | Itga2b | 1126.784 | -0.082895295 | 0.999856677 |
| Glypican 1 | Gpc1 | 846.475226 | 0.107221284 | 0.999856677 |
| Toll-like receptor 4 | Tlr4 | 664.41677 | 0.080134255 | 0.999856677 |
| Integrin alpha 5 | Itga5 | 515.918245 | 0.51649543 | 0.999856677 |
| Integrin alpha 9 | Itga9 | 168.019687 | 1.427755434 | 0.675724317 |
| Integrin beta 6 | Itgb6 | 101.457247 | -0.45618899 | 0.999856677 |

**Figure S13. Eosinophil interactions with TNC. (A)** Comparison of adhesion of bone marrow-derived eosinophils on day 14 to different matrices (n =4). **(B)** The NT193 cancer cell line was grafted into the 4$^{th}$ mammary fat pad of FVB female mice, on day 18 tumours (n = 3) were harvested and Siglec-F+ CD11b+ eosinophils were sorted based on their expression of Ly6C receptor. Ly6C+ and Ly6C- sorted eosinophils were then processed and analysed by bulk RNA sequencing. The table summarises expression data of available eosinophil receptors interacting with TNC.

A

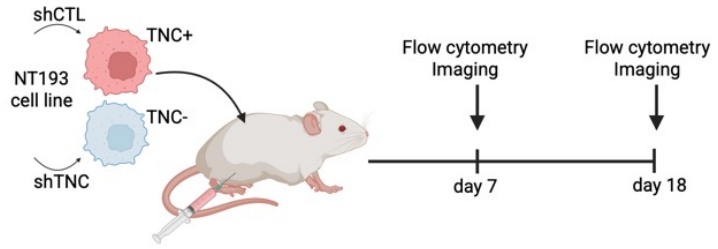


B

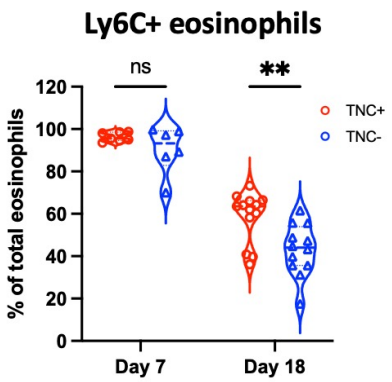


**Figure S14. Ly6C+ eosinophils in TNC+ and TNC- NT193 tumours. (A)** Overview of the experimental set-up. NT193 cancer cell line derived from spontaneous MMTV-NeuNT was transfected with shRNA interfering with *Tnc* expression (shTNC cells/ TNC-) or a control non-specific shRNA (shCTL cells/TNC+). TNC+ or TNC- NT193 cells were orthotopically grafted into immunocompetent FVB mice and tumours were analysed by flow cytometry on days 7 and 18 post-engraftment. **(B)** Comparison of Ly6C+ eosinophils between TNC+ and TNC- NT193 tumours on the indicated time points, ($n_{TNC+,day7}$ = 7, $n_{TNC-,day7}$ = 6, $n_{TNC+,day18}$ = 12, $n_{TNC-,day18}$ = 12). Data show individual values, are pooled from two experimental repeats and were analysed using two-way ANOVA. Statistical significance is displayed on figures as follows: *p < 0.05, **p < 0.01, ***p<0.001, ****p<0.0001.

# Chapter 6 | Final discussion

## 6.1 Conclusions

The tumour microenvironment (TME) is a complex ecosystem that plays a key role in shaping the behaviour and plasticity of immune cells. Among the many cells influenced by the TME, eosinophils have emerged as intriguing but understudied players; traditionally known for their role in allergy and helminth infections[117], yet increasingly linked to anti-tumour responses[102,166,167,171]. Notably, their presence was associated with a successful response to immune checkpoint blockade (ICB) therapy in both breast cancer patients and murine models of the disease[184]. However, their role in treatment-naïve breast cancer models is limited[184,188,199,240] compared to models of lung or colon cancer[102,166], pointing to their deactivation by the breast TME. Therefore, using the murine models of breast cancer, this work aimed to explore how progressing TME shapes eosinophil phenotypical and functional heterogeneity to evade their anti-tumorigenic properties.

### 6.1.1 Tumour microenvironment deactivates eosinophils to Ly6C- state

Spectral flow cytometry analysis of tumour-infiltrating eosinophils, detailed in Chapter 3, identified two tumour-associated eosinophil populations distinguished by expression of Ly6C receptor, with Ly6C- eosinophils appearing at late stages of tumour development. Because Ly6C+ eosinophils were 1) exclusively present in bone marrow and blood of naïve and tumour-bearing mice, 2) the first eosinophilic population to infiltrate tumours, and 3) had the potential to transition to the Ly6C- subset ex vivo, the Ly6C+ population was considered a root cluster for the Ly6C- subset.

In line with this conclusion, bone marrow-derived eosinophils mimicked the Ly6C+ to Ly6C- transition in the final stages of their development. It is important to note that the expression of both Ly6C and CCR3 receptors clearly defined 4 stages of eosinophil maturation ex vivo, presenting a novel model for studying eosinophils. Both tumour-associated and bone marrow-derived Ly6C+ eosinophils were more cytotoxic and degranulating than their Ly6C- counterparts. Furthermore, bulk RNA-seq of Ly6C+ and Ly6C- eosinophils revealed increased

responsiveness of Ly6C+ eosinophils to both IFNγ and IFNβ, while Ly6C- eosinophils overexpressed Wnt ligands and signalling. Given that a) systemic depletion of eosinophils during NT193 tumour development led to enhanced tumour growth, and b) 70% of eosinophils presented with a Ly6C+ more cytotoxic phenotype even at late stages of tumour development, this led to the conclusion that eosinophil infiltration in the NT193 tumour has an overall anti-tumorigenic role. While this is in contrast with eosinophil depletion not causing a significant difference in other orthotopic tumour models[188,189,199], it could be hypothesised that NT193 tumours with significantly elevated levels of eosinophils present a new model for studying eosinophil cytotoxicity at steady state. Collectively, these data provide evidence that the TME deactivates eosinophils towards a less active Ly6C- state in situ, without systemic reprogramming of bone marrow progenitors (Figure 6.1).

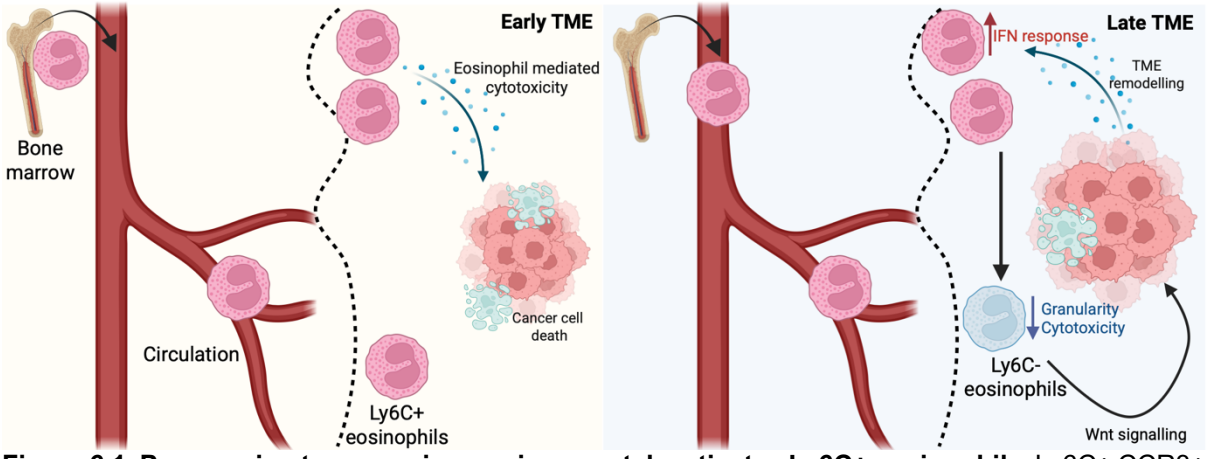


**Figure 6.1. Progressing tumour microenvironment deactivates Ly6C+ eosinophils.** Ly6C+ CCR3+ eosinophils emerge from bone marrow, infiltrate tumours through vasculature and present with a more cytotoxic phenotype at early stages of tumour development. While only Ly6C+ eosinophils are present in bone marrow and blood of tumour-bearing mice during late stages of tumour progression, the proportion of Ly6C+ IFN responsive population decreases under the influence of tumour microenvironment, giving rise to Ly6C- eosinophils with lower granularity, less cytotoxic potential ex vivo and upregulated expression of Wnt ligands, further supporting tumour growth and progression.

### 6.1.2 IFNs support eosinophil cytotoxicity

Bulk RNA-seq analysis in Chapter 4 showed that Ly6C+ eosinophils are more responsive to IFNγ and IFNβ, compared to Ly6C- eosinophils. Validation of these results ex vivo confirmed the increased responsiveness of Ly6C+ eosinophils in both tumour-associated and bone marrow-derived eosinophils. These results were of particular interest as a) IFNγ was shown to induce degranulation of active eosinophils[125], b) IFNγ stimulation leads to increased

cytotoxicity towards cancer cell lines[171], and c) eosinophils play an important role in mediating ICB response[184], but their phenotype during the ICB-induced regression is uncharacterized. Results in this thesis further prove that IFNγ and IFNβ stimulation of both Ly6C+ and Ly6C- eosinophils enhances their cytotoxic abilities. Furthermore, IFNs vastly increased the expression of major histocompatibility complexes I & II and PD-L1 expression, overall leading them towards a more activated phenotype. However, only Ly6C+ eosinophils significantly decrease their granularity upon IFNγ stimulation, and actively degranulate during ICB response. While IFNs have a major effect on eosinophil phenotype in vivo and ex vivo, the Ly6C+/Ly6C- ratio of tumour-infiltrating eosinophils is independent of IFN levels, as shown through IFN-blocking experiment or anti-PD-L1 treatment of NT193 tumours.

Together, these data create a more complex picture of eosinophil functional plasticity in the tumour microenvironment, where interferon-driven activation enhances cytotoxicity ex vivo and antigen presentation across both Ly6C+ and Ly6C- subsets both in vivo and ex vivo; yet only Ly6C+ eosinophils undergo significant phenotypic changes such as active degranulation in response to IFNγ and immune checkpoint blockade, further suggesting their role in an anti-tumorigenic response (Figure 6.2).

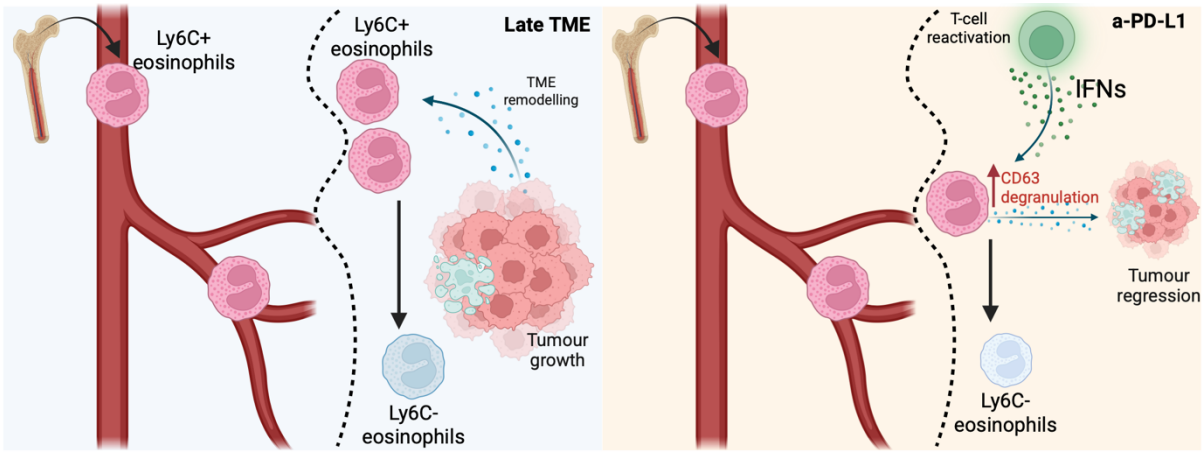


**Figure 6.2. Proposed effect of IFNs on eosinophil degranulation in vivo during anti-PD-L1 therapy.** Eosinophils emerge from the bone marrow, enter the circulation and infiltrate the tumour in their Ly6C+ state, however, they transition to Ly6C- state, marked with lesser responsiveness to IFNγ and IFNβ (IFNs), under the influence of progressing TME. During anti-PD-L1 treatment that reactivates T-cell responses and is in general, well known to lead to T-cell IFN expression[184], Ly6C+ eosinophils

actively degranulate. This leads to a hypothesis that due to the increased IFN responsiveness, Ly6C+ eosinophils actively degranulate during anti-PD-L1 response in response to IFN-enriched TME.

### 6.1.3 Can tumours hijack eosinophil cytotoxicity to form a pro-tumorigenic niche?

IFNγ has a profound effect on the eosinophil transcriptomic signature[125,180], however, these changes can be attenuated in the presence of apoptotic cells[179]. Furthermore, engulfment of apoptotic cells by non-stimulated eosinophils led to broad transcriptomic changes, enhancement of Th2 polarisation and upregulation of pathways involved in wound healing and cell migration. Even though previously unnoticed, *Ly6c2* is among the top 10 most highly expressed genes in unstimulated eosinophils, however, its expression decreased almost 6-fold following the apoptotic cell co-culture[179]. Considering the proposed increased cytotoxicity of Ly6C+ eosinophils and their elevated responsiveness to IFNs, it is possible that Ly6C+ cells reside in close proximity to apoptotic cells that might, in reverse, tune down the IFN response and enhance eosinophil transition into the Ly6C- subset. This could present a mechanism similar to the well-established polarisation of efferocytic macrophages to a more pro-resolving phenotype during inflammation[333], with very recent studies providing evidence on how efferocytosis reprograms tumour-associated macrophages to enhance cancer progression[334,335]. If this was the case for eosinophils, this would present an elegant positive feedback loop between Ly6C+ eosinophil-induced cytotoxicity and their transition to a less IFN-responsive Ly6C- state, enabling the tumour progression (Figure 6.3).

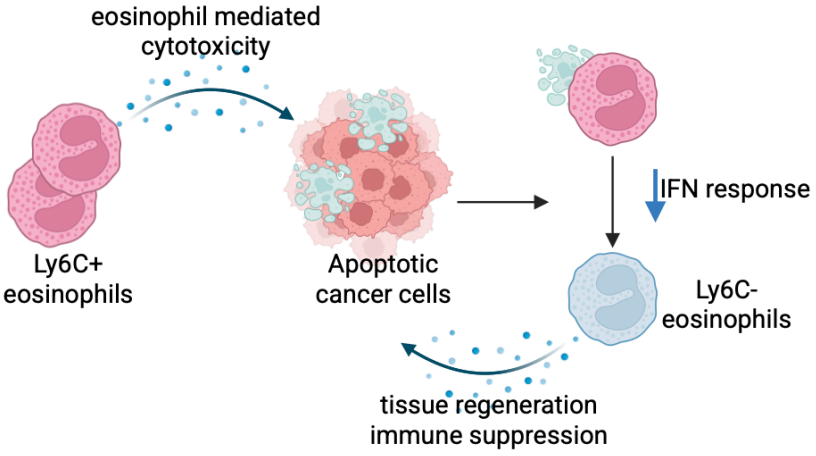


**Figure 6.3. Proposed model of apoptotic cells downregulating eosinophil IFN response.** Ly6C+ eosinophil-mediated cytotoxicity induces cancer apoptosis in their close spatial proximity. Eosinophils

might be sensing apoptotic cells in their local niche and this could lead to downregulation of their IFN responsiveness and possibly downregulation of the Ly6C receptor. It is important to note that down-tuning of IFN responsiveness and transition to Ly6C- phenotype might be in a correlative rather than a causative relationship in this apoptotic sensing hypothesis.

### 6.1.4 Tenascin-C–macrophage interaction supports eosinophil chemotaxis

Characterisation of the myeloid immune landscape of TME formed by a) wild-type NT193 cancer cells expressing tenascin-C (TNC+) compared to b) TNC-knockdown (TNC-) NT193 cell line, revealed increased infiltration of eosinophils in the TNC+ TME. Because TNC expression was previously associated with polarisation of tumour-associated macrophages (TAMs) in primary[228] and metastatic[232] breast cancer, TAMs of both TNC+ and TNC- tumours were further analysed by bulk RNA-sequencing. These results revealed eotaxin-2 (*Ccl24*) among the most overexpressed genes in TNC+ TAMs. Moreover, analysis of publicly available datasets and a dataset generated in the Midwood lab showed that TNC interaction with macrophages through Tlr4 receptor leads to increased *Ccl24* expression in a controlled setting. These results were complemented with a transwell migration assay, further demonstrating this functional link between TNC-macrophage interaction and increased migration of eosinophils towards TNC-stimulated macrophages.

Together, these data suggest that TNC-macrophage interaction enhances eosinophil infiltration in the TNC+ TME. As TNC is a known pro-tumorigenic factor in metastatic niche formation[222], knockdown of TNC reduced metastatic outgrowth[232] and blocking of TNC induced IFN signalling and immune reactivation[238], it would be intuitive to think that TNC-mediated macrophage-eosinophil crosstalk should be pro-tumorigenic. However, data in Chapter 5 are inconclusive in this sense and lead to open questions such as a) what is the role of macrophage-eosinophil crosstalk in the TME formation but also b) how does TNC shape eosinophil phenotype and activation (Figure 6.4). It could be hypothesised that while TNC-macrophage crosstalk has the well-described pro-tumorigenic effect, eosinophil infiltration at least partially compensates this effect during the early stages of TME development through direct cytotoxicity. Because TNC is a known modulator of the metastatic niche[222] and

eosinophils have an anti-tumorigenic role in metastatic models of breast cancer[166,167], it would be interesting to investigate if and how this interaction occurs during metastatic progression.

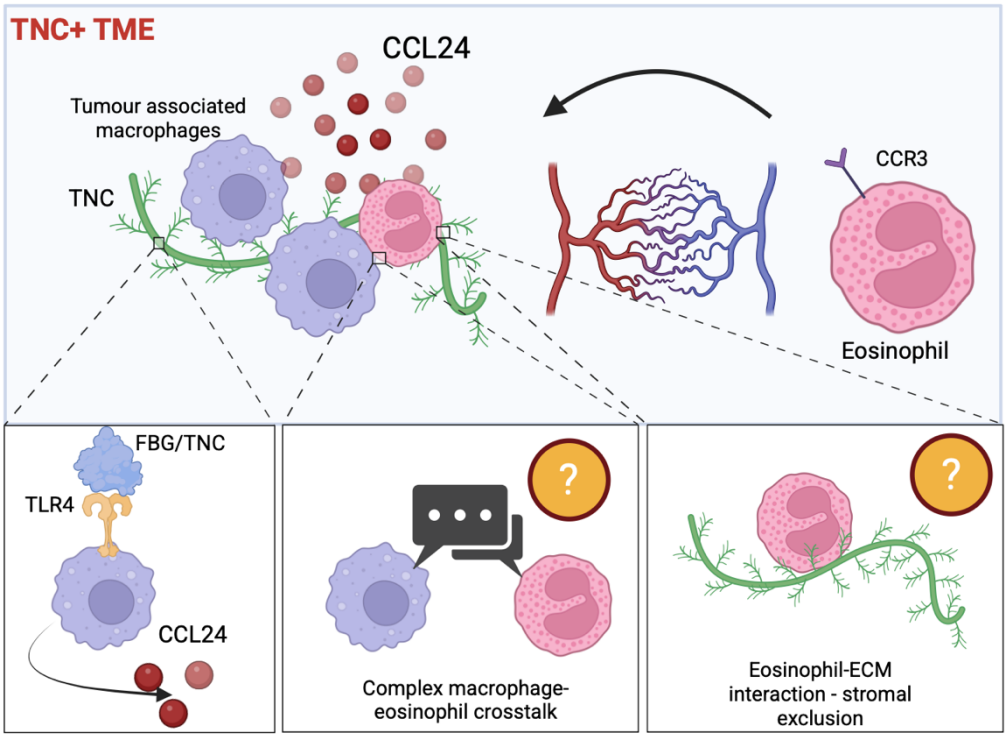


**Figure 6.4. Summary of TNC-macrophage-eosinophil crosstalk in TNC+ NT193 tumours.** Tumour-associated macrophages (TAMs) overexpress eotaxin-2 *Ccl24*, compared to TNC- TAMs. Overexpression of Ccl24 is associated with increased proportions of eosinophils in TNC+ tumours. Mechanistically, TNC or Tlr4-binding domains of TNC lead to overexpression of *Ccl24*, and enhanced migration of eosinophils in transwell assays. However, the complexity of macrophage-eosinophil communication or the direct impact of TNC on eosinophil phenotype and function remains elusive.

## 6.2 Clinical relevance

Eosinophils represent a minor myeloid population within most breast tumours, however, data in Chapter 4 reveal an increased eosinophil presence in patients with locally recurrent triple-negative breast cancer (TNBC). This observation might be of clinical relevance, as increased intratumoral eosinophil signature and elevated levels of circulating eosinophils were associated with improved responses to ICB therapy of metastatic TNBC patients[184]. While ICB in combination with chemotherapy is improving overall and event-free survival of early TNBC patients[336–339], there is an absence of biomarkers that would help predict treatment response and limit overtreatment. Because eosinophils were already linked with better patients' outcomes[184], and eosinophil staining in Chapter 4 suggests eosinophil exclusion to the tumour

periphery, it might be of interest to understand if a subgroup of recurrent TNBC patients might present with increased tumour-associated eosinophils at baseline, predicting their better response to ICB. Indeed, to confirm this hypothesis, it would require extensive confirmation of the very preliminary results presented in section 4.2.8. In case these results were confirmed, further patients' characterisation might reveal other clinical factors predisposing locally recurrent TNBC patients to increased eosinophil infiltration.

One of the major limitations of the work presented in this thesis is the translatability of the Ly6C+ and Ly6C- eosinophil subsets findings to human datasets, as the Ly6C protein is exclusively a murine marker. Notably, during the write-up of this thesis, Ly6C was proposed as a marker distinguishing two types of neutrophils; with Ly6C- neutrophils emerging later during tumour progression, restricted to the vasculature, and more efficiently causing neutrophil extracellular traps, causing downstream tumour necrosis[340]. As presented in this study[340], while Ly6C could not be used to validate these findings in humans, the transcriptomic signature of these neutrophils was matched to a specific subset of circulating neutrophils of TNBC patients. Because both Ly6C+ and Ly6C- eosinophil populations described in this thesis are tumour-associated, and there is currently no available single-cell transcriptomic dataset of eosinophils infiltrating breast tumours, this type of validation was not feasible. Nevertheless, if analogous eosinophil subsets can be identified in human breast tumours through transcriptomic or spatial profiling, this might have potentially prognostic or predictive value for breast cancer patients.

## 6.3 Future work

The work presented in Chapters 3 and 4 demonstrates that the TME progressively deactivates eosinophils by driving their transition from Ly6C+ to Ly6C- subset with reduced IFN responsiveness. Furthermore, IFN stimulation enhances eosinophil cytotoxicity, with preliminary data suggesting direct eosinophil degranulation in response to IFNγ and during ICB response. While these results provide novel insights into eosinophil plasticity, additional

experiments are required to elucidate the mechanism by which eosinophils transition to Ly6C- state and to validate the proposed eosinophil degranulation in response to IFNγ.

### 6.3.1 Ongoing and near future work

a) Transcription factor analysis of Ly6C+ and Ly6C- eosinophils

Transcription factor (TF) analysis will be inferred from the existing bulk RNA-seq dataset of tumour-associated Ly6C+ and Ly6C- eosinophils using the Discriminant Regulon Expression Analysis (DoRothEA) database, in combination with the Virtual Inference of Protein-activity by Enriched Regulon analysis (VIPER) algorithm, providing a list of differentially regulated TFs. Complementary to this analysis, bone marrow-derived CCR3+ eosinophils were FACS-sorted into Ly6C+, Ly6C$^{med}$, Ly6C- populations and sent off for bulk RNA-sequencing. These samples will undergo identical TF activity analysis to identify the most conserved regulatory patterns associated with the eosinophil transition to the Ly6C- state. Depending on the number of candidate TFs identified, the current literature on TF regulation of eosinophil maturation, and the availability of TFs small molecule inhibitors, a few of these candidates might be selected for further investigation.

b) Assessment of IFNγ and IFNβ concentration in progressing and ICB treated tumours

Eosinophil phenotype during ICB treatment mimicked the phenotype of eosinophils stimulated with IFNγ or IFNβ ex vivo. While this, in combination with the well-known ICB effects, was used as a proxy for concluding anti-PD-L1 treatment-induced IFN-rich environment, IFNγ and IFNβ levels should be directly assessed by analysing tumour supernatants collected during these experiments. Once these ELISA assays are optimised, it could also be informative to know whether IFN levels differ during early and late stages of NT193 development.

c) Confirmation of IFN-mediated degranulation

To validate that IFNγ stimulation leads to eosinophil degranulation, supernatant from eosinophil cultures after the stimulation should be collected, and eosinophil peroxidase or

major basic protein, two main eosinophil cationic granule proteins, could be assessed by commercially available ELISA kits. These results could be particularly valuable in validating the mechanism by which IFNs induce cytotoxicity.

### 6.3.2 Medium-term future work

In the medium term (3-6 months), sections of day 7 and day 18 NT193 tumours will be stained for signs of early and late apoptosis, through TUNEL assay, Caspase-3 or Annexin-V staining. These staining protocols, even though well published, might present a technical challenge in terms of optimal tissue fixation, biological and technical controls needed and staining protocol optimisation. If eosinophils localise within apoptotic niches, effects of apoptotic cancer cells will be tested in ex vivo assays by a) transition rate to Ly6C- state and b) IFN responsiveness. Furthermore, it was recently shown that macrophages adjust their response depending on the type of apoptotic cell they encounter[341]. It would therefore be interesting if eosinophils are capable of distinguishing between apoptotic cancer cells and possibly apoptotic immune cells, such as Ly6C- eosinophils with decreased viability.

Second, depending on the results of TF analysis, top candidates implicated in eosinophil transition might be tested through the use of small molecule inhibitors during ex vivo bone marrow development. This model is well equipped to enable us to robustly study how TF inhibitors added to the culture at different concentrations and at different exposure times affect the transition of Ly6C+ eosinophils to Ly6C- state. Depending on the TF candidates, results of these assays and availability of small molecule inhibitors, pilot in vivo experiments might be considered to attempt to stop the eosinophil transition in the NT193 tumours.

### 6.3.3 Long-term project outlooks

This project uncovered a well-conserved transition of Ly6C+ to Ly6C- eosinophils in the progressing TME, suggesting possible mechanisms of how eosinophils contribute to anti-tumorigenic response during ICB treatment, but also explored alternative ways of eosinophil

recruitment to tumours. These results, therefore, lead to several possible avenues that could be further investigated, such as:

- What guides eosinophil transition into the Ly6C-state? Could this transition be therapeutically targeted to maintain eosinophil activation?
- How do eosinophils contribute to and regulate their local niche in treatment naïve disease and during ICB response?
- How does different extracellular matrix composition regulate eosinophil functional and phenotypical heterogeneity?

## References


1. Hanahan, D. & Weinberg, R. A. The Hallmarks of Cancer Review. *Cell* **100**, 57–70 (2000).
2. White, M. C. *et al.* Age and Cancer Risk. *Am. J. Prev. Med.* **46**, S7–S15 (2014).
3. Sieweke, M. H., Thompson, N. L., Sporn, M. B. & Bissell, M. J. Mediation of Wound-Related Rous Sarcoma Virus Tumorigenesis by TGF-β. *Science* **248**, 1656–1660 (1990).
4. Moore, R. J. *et al.* Mice deficient in tumor necrosis factor-α are resistant to skin carcinogenesis. *Nat. Med.* **5**, 828–831 (1999).
5. M Suganuma *et al.* Essential role of tumor necrosis factor alpha (TNF-alpha) in tumor promotion as revealed by TNF-alpha-deficient mice. *Cancer Res.* **59**, 4516–8 (1999).
6. Hanahan, D. & Weinberg, R. A. Hallmarks of Cancer: The Next Generation. *Cell* **144**, 646–674 (2011).
7. Giraldo, N. A. *et al.* The clinical role of the TME in solid cancer. *Br. J. Cancer* **120**, 45–53 (2019).
8. De Visser, K. E. & Joyce, J. A. The evolving tumor microenvironment: From cancer initiation to metastatic outgrowth. *Cancer Cell* **41**, 374–403 (2023).
9. Galon, J. *et al.* Type, Density, and Location of Immune Cells Within Human Colorectal Tumors Predict Clinical Outcome. *Science* **313**, 1960–1964 (2006).
10. Gooden, M. J. M., De Bock, G. H., Leffers, N., Daemen, T. & Nijman, H. W. The prognostic influence of tumour-infiltrating lymphocytes in cancer: a systematic review with meta-analysis. *Br. J. Cancer* **105**, 93–103 (2011).
11. Thommen, D. S. & Schumacher, T. N. T Cell Dysfunction in Cancer. *Cancer Cell* **33**, 547–562 (2018).
12. Tay, R. E., Richardson, E. K. & Toh, H. C. Revisiting the role of CD4+ T cells in cancer immunotherapy—new insights into old paradigms. *Cancer Gene Ther.* **28**, 5–17 (2021).
13. DeNardo, D. G. *et al.* CD4+ T Cells Regulate Pulmonary Metastasis of Mammary Carcinomas by Enhancing Protumor Properties of Macrophages. *Cancer Cell* **16**, 91–102 (2009).
14. Togashi, Y., Shitara, K. & Nishikawa, H. Regulatory T cells in cancer immunosuppression — implications for anticancer therapy. *Nat. Rev. Clin. Oncol.* **16**, 356–371 (2019).
15. Saleh, R. & Elkord, E. FoxP3+ T regulatory cells in cancer: Prognostic biomarkers and therapeutic targets. *Cancer Lett.* **490**, 174–185 (2020).

16. Ribas, A. & Wolchok, J. D. Cancer immunotherapy using checkpoint blockade. *Science* **359**, 1350–1355 (2018).
17. Schumacher, T. N. & Thommen, D. S. Tertiary lymphoid structures in cancer. *Science* **375**, eabf9419 (2022).
18. Laumont, C. M., Banville, A. C., Gilardi, M., Hollern, D. P. & Nelson, B. H. Tumour-infiltrating B cells: immunological mechanisms, clinical impact and therapeutic opportunities. *Nat. Rev. Cancer* **22**, 414–430 (2022).
19. Franklin, R. A. & Li, M. O. Ontogeny of Tumor-Associated Macrophages and Its Implication in Cancer Regulation. *Trends Cancer* **2**, 20–34 (2016).
20. Azizi, E. *et al.* Single-Cell Map of Diverse Immune Phenotypes in the Breast Tumor Microenvironment. *Cell* **174**, 1293-1308.e36 (2018).
21. Martinez, F. O. & Gordon, S. The M1 and M2 paradigm of macrophage activation: time for reassessment. *F1000Prime Rep.* **6**, (2014).
22. Zhang, W. *et al.* Macrophage polarization in the tumor microenvironment: Emerging roles and therapeutic potentials. *Biomed. Pharmacother.* **177**, 116930 (2024).
23. Zhang, Q. *et al.* Prognostic Significance of Tumor-Associated Macrophages in Solid Tumor: A Meta-Analysis of the Literature. *PLoS ONE* **7**, e50946 (2012).
24. Cassetta, L. & Pollard, J. W. Targeting macrophages: therapeutic approaches in cancer. *Nat. Rev. Drug Discov.* **17**, 887–904 (2018).
25. Qian, B.-Z. *et al.* CCL2 recruits inflammatory monocytes to facilitate breast-tumour metastasis. *Nature* **475**, 222–225 (2011).
26. Olingy, C. E., Dinh, H. Q. & Hedrick, C. C. Monocyte heterogeneity and functions in cancer. *J. Leukoc. Biol.* **106**, 309–322 (2019).
27. Templeton, A. J. *et al.* Prognostic Role of Neutrophil-to-Lymphocyte Ratio in Solid Tumors: A Systematic Review and Meta-Analysis. *JNCI J. Natl. Cancer Inst.* **106**, dju124 (2014).
28. Hedrick, C. C. & Malanchi, I. Neutrophils in cancer: heterogeneous and multifaceted. *Nat. Rev. Immunol.* **22**, 173–187 (2022).
29. Fridlender, Z. G. *et al.* Polarization of Tumor-Associated Neutrophil Phenotype by TGF-β: "N1" versus "N2" TAN. *Cancer Cell* **16**, 183–194 (2009).
30. Coffelt, S. B. *et al.* IL-17-producing γδ T cells and neutrophils conspire to promote breast cancer metastasis. *Nature* **522**, 345–348 (2015).

31. Wculek, S. K. & Malanchi, I. Neutrophils support lung colonization of metastasis-initiating breast cancer cells. *Nature* **528**, 413–417 (2015).
32. Cools-Lartigue, J. *et al.* Neutrophil extracellular traps sequester circulating tumor cells and promote metastasis. *J. Clin. Invest.* **123**, 3446–3458 (2013).
33. Steele, C. W. *et al.* CXCR2 Inhibition Profoundly Suppresses Metastases and Augments Immunotherapy in Pancreatic Ductal Adenocarcinoma. *Cancer Cell* **29**, 832–845 (2016).
34. Yang, S. *et al.* Targeting neutrophils: Mechanism and advances in cancer therapy. *Clin. Transl. Med.* **14**, e1599 (2024).
35. Sahai, E. *et al.* A framework for advancing our understanding of cancer-associated fibroblasts. *Nat. Rev. Cancer* **20**, 174–186 (2020).
36. Özdemir, B. C. *et al.* Depletion of Carcinoma-Associated Fibroblasts and Fibrosis Induces Immunosuppression and Accelerates Pancreas Cancer with Reduced Survival. *Cancer Cell* **25**, 719–734 (2014).
37. Amersfoort, J., Eelen, G. & Carmeliet, P. Immunomodulation by endothelial cells — partnering up with the immune system? *Nat. Rev. Immunol.* **22**, 576–588 (2022).
38. Schaaf, M. B., Garg, A. D. & Agostinis, P. Defining the role of the tumor vasculature in antitumor immunity and immunotherapy. *Cell Death Dis.* **9**, 115 (2018).
39. Guelfi, S., Hodivala-Dilke, K. & Bergers, G. Targeting the tumour vasculature: from vessel destruction to promotion. *Nat. Rev. Cancer* **24**, 655–675 (2024).
40. Sung, H. *et al.* Global Cancer Statistics 2020: GLOBOCAN Estimates of Incidence and Mortality Worldwide for 36 Cancers in 185 Countries. *CA. Cancer J. Clin.* **71**, 209–249 (2021).
41. Bray, F. *et al.* Global cancer statistics 2022: GLOBOCAN estimates of incidence and mortality worldwide for 36 cancers in 185 countries. *CA. Cancer J. Clin.* **74**, 229–263 (2024).
42. Cristea, S. & Polyak, K. Dissecting the mammary gland one cell at a time. *Nat. Commun.* **9**, 2473 (2018).
43. Nolan, E., Lindeman, G. J. & Visvader, J. E. Deciphering breast cancer: from biology to the clinic. *Cell* **186**, 1708–1728 (2023).
44. Perou, C. M. *et al.* Molecular portraits of human breast tumours. *Nature* **406**, 747–752 (2000).

45. Sørlie, T. *et al.* Gene expression patterns of breast carcinomas distinguish tumor subclasses with clinical implications. *Proc. Natl. Acad. Sci.* **98**, 10869–10874 (2001).
46. Sørlie, T. *et al.* Repeated observation of breast tumor subtypes in independent gene expression data sets. *Proc. Natl. Acad. Sci.* **100**, 8418–8423 (2003).
47. Fan, C. *et al.* Concordance among Gene-Expression– Based Predictors for Breast Cancer. *N. Engl. J. Med.* **355**, 560–569 (2006).
48. Hu, Z. *et al.* The molecular portraits of breast tumors are conserved across microarray platforms. *BMC Genomics* **7**, 1–12 (2006).
49. Sørlie, T. *et al.* Distinct molecular mechanisms underlying clinically relevant subtypes of breast cancer: gene expression analyses across three different platforms. *BMC Genomics* **7**, (2006).
50. Vasconcelos, I. *et al.* The St. Gallen surrogate classification for breast cancer subtypes successfully predicts tumor presenting features, nodal involvement, recurrence patterns and disease free survival. *The Breast* **29**, 181–185 (2016).
51. Harbeck, N. *et al.* Breast cancer. *Nat. Rev. Dis. Primer* **5**, 66 (2019).
52. Early Breast Cancer Trialists' Collaborative Group. Tamoxifen for early breast cancer: an overview of the randomised trials. *The Lancet* **351**, 1451–1467 (1998).
53. Cameron, D. *et al.* 11 years' follow-up of trastuzumab after adjuvant chemotherapy in HER2-positive early breast cancer: final analysis of the HERceptin Adjuvant (HERA) trial. *The Lancet* **389**, 1195–1205 (2017).
54. Poggio, F. *et al.* Platinum-based neoadjuvant chemotherapy in triple-negative breast cancer: a systematic review and meta-analysis. *Ann. Oncol.* **29**, 1497–1508 (2018).
55. Robson, M. *et al.* Olaparib for Metastatic Breast Cancer in Patients with a Germline *BRCA* Mutation. *N. Engl. J. Med.* **377**, 523–533 (2017).
56. Turner, N. C. *et al.* Palbociclib in Hormone-Receptor–Positive Advanced Breast Cancer. *N. Engl. J. Med.* **373**, 209–219 (2015).
57. André, F. *et al.* Alpelisib for PIK3CA-Mutated, Hormone Receptor–Positive Advanced Breast Cancer. *N. Engl. J. Med.* **380**, 1929–1940 (2019).
58. Cortazar, P. *et al.* Pathological complete response and long-term clinical benefit in breast cancer: the CTNeoBC pooled analysis. *The Lancet* **384**, 164–172 (2014).
59. Wherry, E. J. & Kurachi, M. Molecular and cellular insights into T cell exhaustion. *Nat. Rev. Immunol.* **15**, 486–499 (2015).

60. Keren, L. *et al.* A Structured Tumor-Immune Microenvironment in Triple Negative Breast Cancer Revealed by Multiplexed Ion Beam Imaging. *Cell* **174**, 1373-1387.e19 (2018).
61. Reck, M. *et al.* Pembrolizumab versus Chemotherapy for PD-L1–Positive Non–Small-Cell Lung Cancer. *N. Engl. J. Med.* **375**, 1823–1833 (2016).
62. Robert, C. *et al.* Pembrolizumab versus Ipilimumab in Advanced Melanoma. *N. Engl. J. Med.* **372**, 2521–2532 (2015).
63. Sha, D. *et al.* Tumor Mutational Burden as a Predictive Biomarker in Solid Tumors. *Cancer Discov.* **10**, 1808–1825 (2020).
64. Chalmers, Z. R. *et al.* Analysis of 100,000 human cancer genomes reveals the landscape of tumor mutational burden. *Genome Med.* **9**, 34 (2017).
65. Thomas, A. *et al.* Tumor mutational burden is a determinant of immune-mediated survival in breast cancer. *OncoImmunology* **7**, e1490854 (2018).
66. Mittendorf, E. A. *et al.* PD-L1 Expression in Triple-Negative Breast Cancer. *Cancer Immunol. Res.* **2**, 361–370 (2014).
67. Cortes, J. *et al.* Pembrolizumab plus Chemotherapy in Advanced Triple-Negative Breast Cancer. *N. Engl. J. Med.* **387**, 217–226 (2022).
68. Schmid, P. *et al.* Overall Survival with Pembrolizumab in Early-Stage Triple-Negative Breast Cancer. *N. Engl. J. Med.* **391**, 1981–1991 (2024).
69. Huober, J. *et al.* Atezolizumab With Neoadjuvant Anti–Human Epidermal Growth Factor Receptor 2 Therapy and Chemotherapy in Human Epidermal Growth Factor Receptor 2–Positive Early Breast Cancer: Primary Results of the Randomized Phase III IMpassion050 Trial. *J. Clin. Oncol.* **40**, 2946–2956 (2022).
70. The Cancer Genome Atlas Network. Comprehensive molecular portraits of human breast tumours. *Nature* **490**, 61–70 (2012).
71. Thorsson, V. *et al.* The Immune Landscape of Cancer. *Immunity* **48**, 812-830.e14 (2018).
72. Ali, H. R., Chlon, L., Pharoah, P. D. P., Markowetz, F. & Caldas, C. Patterns of Immune Infiltration in Breast Cancer and Their Clinical Implications: A Gene-Expression-Based Retrospective Study. *PLOS Med.* **13**, e1002194 (2016).
73. Wagner, J. *et al.* A Single-Cell Atlas of the Tumor and Immune Ecosystem of Human Breast Cancer. *Cell* **177**, 1330-1345.e18 (2019).
74. Jackson, H. W. *et al.* The single-cell pathology landscape of breast cancer. *Nature* **578**, 615–620 (2020).

75. Wu, S. Z. *et al.* A single-cell and spatially resolved atlas of human breast cancers. *Nat. Genet.* **53**, 1334–1347 (2021).
76. Danenberg, E. *et al.* Breast tumor microenvironment structures are associated with genomic features and clinical outcome. *Nat. Genet.* **54**, 660–669 (2022).
77. Wang, X. Q. *et al.* Spatial predictors of immunotherapy response in triple-negative breast cancer. *Nature* **621**, 868–876 (2023).
78. Wang, X. *et al.* Spatial transcriptomics reveals substantial heterogeneity in triple-negative breast cancer with potential clinical implications. *Nat. Commun.* **15**, 10232 (2024).
79. Sachs, N. *et al.* A Living Biobank of Breast Cancer Organoids Captures Disease Heterogeneity. *Cell* **172**, 373-386.e10 (2018).
80. Prahallad, A. *et al.* Unresponsiveness of colon cancer to BRAF(V600E) inhibition through feedback activation of EGFR. *Nature* **483**, 100–103 (2012).
81. Wellenstein, M. D. *et al.* Loss of p53 triggers WNT-dependent systemic inflammation to drive breast cancer metastasis. *Nature* **572**, 538–542 (2019).
82. Ethier, J.-L., Desautels, D., Templeton, A., Shah, P. S. & Amir, E. Prognostic role of neutrophil-to-lymphocyte ratio in breast cancer: a systematic review and meta-analysis. *Breast Cancer Res.* **19**, 2 (2017).
83. Garner, H. *et al.* Understanding and reversing mammary tumor-driven reprogramming of myelopoiesis to reduce metastatic spread. *Cancer Cell* **43**, 1–17 (2025).
84. Sacks, D. & Noben-Trauth, N. The immunology of susceptibility and resistance to Leishmania major in mice. *Nat. Rev. Immunol.* **2**, 845–858 (2002).
85. Sellers, R. S., Clifford, C. B., Treuting, P. M. & Brayton, C. Immunological Variation Between Inbred Laboratory Mouse Strains: Points to Consider in Phenotyping Genetically Immunomodified Mice. *Vet. Pathol.* **49**, 32–43 (2012).
86. Piranlioglu, R. *et al.* Primary tumor-induced immunity eradicates disseminated tumor cells in syngeneic mouse model. *Nat. Commun.* **10**, 1430 (2019).
87. Cato, A. C., Henderson, D. & Ponta, H. The hormone response element of the mouse mammary tumour virus DNA mediates the progestin and androgen induction of transcription in the proviral long terminal repeat region. *EMBO J.* **6**, 363–368 (1987).
88. Ross, S. R. Mouse Mammary Tumor Virus Molecular Biology and Oncogenesis. *Viruses* **2**, 2000–2012 (2010).

89. Penuel, E., Akita, R. W. & Sliwkowski, M. X. Identification of a Region within the ErbB2/HER2 Intracellular Domain That Is Necessary for Ligand-independent Association. *J. Biol. Chem.* **277**, 28468–28473 (2002).
90. Muller, W. J., Sinn, E., Pattengale, P. K., Wallace, R. & Leder, P. Single-step induction of mammary adenocarcinoma in transgenic mice bearing the activated c-neu oncogene. *Cell* **54**, 105–115 (1988).
91. Chantale T. Guy, Robert D. Cardiff, & William J. Muller. Induction of Mammary Tumors by Expression of Polyomavirus Middle T Oncogene: A Transgenic Mouse Model for Metastatic Disease. *Mol. Cell. Biol.* **12**, 954–961 (1992).
92. Murdamoothoo, D. *et al.* Tenascin-C immobilizes infiltrating T lymphocytes through CXCL12 promoting breast cancer progression. *EMBO Mol. Med.* **13**, e13270 (2021).
93. Quesada, I. V. Elucidating novel molecular and cellular mechanisms in Tenascin-C dependent breast cancer aggressiveness. (Université de Strasbourg, 2015).
94. Arnold, I. C. & Munitz, A. Spatial adaptation of eosinophils and their emerging roles in homeostasis, infection and disease. *Nat. Rev. Immunol.* **24**, 858–877 (2024).
95. Drissen, R. *et al.* Distinct myeloid progenitor–differentiation pathways identified through single-cell RNA sequencing. *Nat. Immunol.* **17**, 666–676 (2016).
96. Tusi, B. K. *et al.* Population snapshots predict early haematopoietic and erythroid hierarchies. *Nature* **555**, 54–60 (2018).
97. Weinreb, C., Rodriguez-Fraticelli, A., Camargo, F. D. & Klein, A. M. Lineage tracing on transcriptional landscapes links state to fate during differentiation. *Science* **367**, eaaw3381 (2020).
98. Jorssen, J. *et al.* Single-cell proteomics and transcriptomics capture eosinophil development and identify the role of IL-5 in their lineage transit amplification. *Immunity* **57**, 1549-1566.e8 (2024).
99. Hall, L. R., Mehlotra, R. K., Higgins, A. W., Haxhiu, M. A. & Pearlman, E. An Essential Role for Interleukin-5 and Eosinophils in Helminth-Induced Airway Hyperresponsiveness. *Infect. Immun.* **66**, 4425–4430 (1998).
100. Kopf, M. *et al.* IL-5-Deficient Mice Have a Developmental Defect in CD5+ B-1 Cells and Lack Eosinophilia but Have Normal Antibody and Cytotoxic T Cell Responses. *Immunity* **4**, 15–24 (1996).

101. Kyriakopoulos, C. *et al.* Effectiveness of anti-IL-5/5Rα biologics in severe asthma in real-world studies: a systematic review and meta-analysis. *ERJ Open Res.* **11**, 00625–02024 (2025).
102. Arnold, I. C. *et al.* The GM-CSF–IRF5 signaling axis in eosinophils promotes antitumor immunity through activation of type 1 T cell responses. *J. Exp. Med.* **217**, e20190706 (2020).
103. Chojnacki, A. *et al.* Intravital imaging allows real-time characterization of tissue resident eosinophils. *Commun. Biol.* **2**, 181 (2019).
104. Lee, J. J. *et al.* Human versus mouse eosinophils: "That which we call an eosinophil, by any other name would stain as red". *J. Allergy Clin. Immunol.* **130**, 572–584 (2012).
105. Feng, Y. & Mao, H. Expression and preliminary functional analysis of Siglec-F on mouse macrophages. *J. Zhejiang Univ. Sci. B* **13**, 386–394 (2012).
106. Uguccioni, M. *et al.* High expression of the chemokine receptor CCR3 in human blood basophils. Role in activation by eotaxin, MCP-4, and other chemokines. *J. Clin. Invest.* **100**, 1137–1143 (1997).
107. Pope, S. M., Zimmermann, N., Stringer, K. F., Karow, M. L. & Rothenberg, M. E. The Eotaxin Chemokines and CCR3 Are Fundamental Regulators of Allergen-Induced Pulmonary Eosinophilia. *J. Immunol.* **175**, 5341–5350 (2005).
108. Borchers, M. T. *et al. In vitro* assessment of chemokine receptor-ligand interactions mediating mouse eosinophil migration. *J. Leukoc. Biol.* **71**, 1033–1041 (2002).
109. Yu, C. *et al.* Targeted Deletion of a High-Affinity GATA-binding Site in the GATA-1 Promoter Leads to Selective Loss of the Eosinophil Lineage In Vivo. *J. Exp. Med.* **195**, 1387–1395 (2002).
110. Lee, J. J. *et al.* Defining a Link with Asthma in Mice Congenitally Deficient in Eosinophils. *Science* **305**, 1773–1776 (2004).
111. Jacobsen, E. A. *et al.* Eosinophil activities modulate the immune/inflammatory character of allergic respiratory responses in mice. *Allergy* **69**, 315–327 (2014).
112. Yoshida, T. *et al.* Defective B-1 Cell Development and Impaired Immunity against *Angiostrongylus cantonensis* in IL-5Ra-Deficient Mice. *Immunity* **4**, 483–494 (1996).
113. Humbles, A. A. *et al.* The murine CCR3 receptor regulates both the role of eosinophils and mast cells in allergen-induced airway inflammation and hyperresponsiveness. *Proc. Natl. Acad. Sci.* **99**, 1479–1484 (2002).

114. Dent, L. A., Strath, M., Mellor, A. L. & Sanderson, C. J. Eosinophilia in transgenic mice expressing interleukin 5. *J. Exp. Med.* **172**, 1425–1431 (1990).
115. Doyle, A. D. *et al.* Homologous recombination into the eosinophil peroxidase locus generates a strain of mice expressing *Cre* recombinase exclusively in eosinophils. *J. Leukoc. Biol.* **94**, 17–24 (2013).
116. Wechsler, M. E. *et al.* Eosinophils in Health and Disease: A State-of-the-Art Review. *Mayo Clin. Proc.* **96**, 2694–2707 (2021).
117. Weller, P. F. & Spencer, L. A. Functions of tissue-resident eosinophils. *Nat. Rev. Immunol.* **17**, 746–760 (2017).
118. Steinbach, K. H. *et al.* Estimation of kinetic parameters of neutrophilic, eosinophilic, and basophilic granulocytes in human blood. *Blut* **39**, 27–38 (1979).
119. Lee, J. J., Jacobsen, E. A., McGarry, M. P., Schleimer, R. P. & Lee, N. A. Eosinophils in health and disease: the *LIAR* hypothesis. *Clin. Exp. Allergy* **40**, 563–575 (2010).
120. Arnold, I. C. *et al.* Eosinophils suppress Th1 responses and restrict bacterially induced gastrointestinal inflammation. *J. Exp. Med.* **215**, 2055–2072 (2018).
121. Chu, V. T. *et al.* Eosinophils Promote Generation and Maintenance of Immunoglobulin-A-Expressing Plasma Cells and Contribute to Gut Immune Homeostasis. *Immunity* **40**, 582–593 (2014).
122. Cao, Y. G. *et al. Faecalibaculum rodentium* remodels retinoic acid signaling to govern eosinophil-dependent intestinal epithelial homeostasis. *Cell Host Microbe* **30**, 1295-1310.e8 (2022).
123. Ignacio, A. *et al.* Small intestinal resident eosinophils maintain gut homeostasis following microbial colonization. *Immunity* **55**, 1250-1267.e12 (2022).
124. I. Kutyavin, V., Korn, L. L. & Medzhitov, R. Nutrient-derived signals regulate eosinophil adaptation to the small intestine. *Proc. Natl. Acad. Sci.* **121**, e2316446121 (2024).
125. Gurtner, A. *et al.* Active eosinophils regulate host defence and immune responses in colitis. *Nature* **615**, 151–157 (2023).
126. Borrelli, C., Gurtner, A., Arnold, I. C. & Moor, A. E. Stress-free single-cell transcriptomic profiling and functional genomics of murine eosinophils. *Nat. Protoc.* **19**, 1679–1709 (2024).
127. Loffredo, L. F. *et al.* Eosinophil accumulation in postnatal lung is specific to the primary septation phase of development. *Sci. Rep.* **10**, 4425 (2020).

128. Jackson, D. J. & Pavord, I. D. Living without eosinophils: evidence from mouse and man. *Eur. Respir. J.* **61**, 2201217 (2023).
129. Mesnil, C. *et al.* Lung-resident eosinophils represent a distinct regulatory eosinophil subset. *J. Clin. Invest.* **126**, 3279–3295 (2016).
130. Dolitzky, A. *et al.* Mouse resident lung eosinophils are dependent on IL-5. *Allergy* **77**, 2822–2825 (2022).
131. Gouon-Evans, V., Rothenberg, M. E. & Pollard, J. W. Postnatal mammary gland development requires macrophages and eosinophils. *Development* **127**, 2269–2282 (2000).
132. Tower, H. *et al.* Estrogen-induced immune changes within the normal mammary gland. *Sci. Rep.* **12**, 18986 (2022).
133. Gouon-Evans, V., Lin, E. Y. & Pollard, J. W. Requirement of macrophages and eosinophils and their cytokines/chemokines for mammary gland development. *Breast Cancer Res.* **4**, 155 (2002).
134. Cansever, D. *et al.* Lactation-associated macrophages exist in murine mammary tissue and human milk. *Nat. Immunol.* **24**, 1098–1109 (2023).
135. Artham, S. *et al.* Estrogen signaling suppresses tumor-associated tissue eosinophilia to promote breast tumor growth. *Sci. Adv.* **10**, eadp2442 (2024).
136. Fettrelet, T., Gigon, L., Karaulov, A., Yousefi, S. & Simon, H.-U. The Enigma of Eosinophil Degranulation. *Int. J. Mol. Sci.* **22**, 7091 (2021).
137. Melo, R. C. N., Perez, S. A. C., Spencer, L. A., Dvorak, A. M. & Weller, P. F. Intragranular Vesiculotubular Compartments are Involved in Piecemeal Degranulation by Activated Human Eosinophils. *Traffic* **6**, 866–879 (2005).
138. Carmo, L. A. S., Bonjour, K., Spencer, L. A., Weller, P. F. & Melo, R. C. N. Single-Cell Analyses of Human Eosinophils at High Resolution to Understand Compartmentalization and Vesicular Trafficking of Interferon-Gamma. *Front. Immunol.* **9**, 1542 (2018).
139. Spencer, L. A., Bonjour, K., Melo, R. C. N. & Weller, P. F. Eosinophil Secretion of Granule-Derived Cytokines. *Front. Immunol.* **5**, (2014).
140. Caruso, R., Irato, E. & Rigoli, L. Eosinophil exocytosis in a poorly differentiated tubular gastric adenocarcinoma: case report. *Ultrastruct. Pathol.* **46**, 139–146 (2022).
141. Yousefi, S. *et al.* Catapult-like release of mitochondrial DNA by eosinophils contributes to antibacterial defense. *Nat. Med.* **14**, 949–953 (2008).

142. Ueki, S. *et al.* Eosinophil extracellular DNA trap cell death mediates lytic release of free secretion-competent eosinophil granules in humans. *Blood* **121**, 2074–2083 (2013).
143. Hatano, Y. *et al.* Phagocytosis of heat-killed *Staphylococcus aureus* by eosinophils: comparison with neutrophils. *APMIS* **117**, 115–123 (2009).
144. Camuña Correa, J. *et al.* Yeast phagocytosis by eosinophils: a case of disseminated histoplasmosis diagnosed in a peripheral blood smear. *Lancet Infect. Dis.* **23**, e325 (2023).
145. Melo, R. C. N., Liu, L., Xenakis, J. J. & Spencer, L. A. Eosinophil-derived cytokines in health and disease: unraveling novel mechanisms of selective secretion. *Allergy* **68**, 274–284 (2013).
146. Voehringer, D., Shinkai, K. & Locksley, R. M. Type 2 Immunity Reflects Orchestrated Recruitment of Cells Committed to IL-4 Production. *Immunity* **20**, 267–277 (2004).
147. Nouri-Aria, K. T. *et al.* Cytokine expression during allergen-induced late nasal responses: IL-4 and IL-5 mRNA is expressed early (at 6 h) predominantly by eosinophils. *Clin. Exp. Allergy* **30**, 1709–1716 (2000).
148. Dent, L. A. *et al.* Interleukin-5 Transgenic Mice Show Enhanced Resistance to Primary Infections with *Nippostrongylus brasiliensis* but Not Primary Infections with *Toxocara canis*. *Infect. Immun.* **67**, 989–993 (1999).
149. Fabre, V. *et al.* Eosinophil Deficiency Compromises Parasite Survival in Chronic Nematode Infection. *J. Immunol.* **182**, 1577–1583 (2009).
150. Akuthota, P., Wang, H. & Weller, P. F. Eosinophils as antigen-presenting cells in allergic upper airway disease. *Curr. Opin. Allergy Clin. Immunol.* **10**, 14–19 (2010).
151. McBrien, C. N. & Menzies-Gow, A. The Biology of Eosinophils and Their Role in Asthma. *Front. Med.* **4**, 93 (2017).
152. Jean Bousquet *et al.* Eosinophilic Inflammation in Asthma. *N. Engl. J. Med.* **323**, 1033–1039 (1990).
153. Benson, V. S. *et al.* Blood eosinophil counts in the general population and airways disease: a comprehensive review and meta-analysis. *Eur. Respir. J.* **59**, 2004590 (2022).
154. Koshak, E. A. & Alamoudi, O. S. Do eosinophil counts correlate differently with asthma severity by symptoms versus peak flow rate? *Ann. Allergy. Asthma. Immunol.* **83**, 567–571 (1999).
155. Humbles, A. A. *et al.* A Critical Role for Eosinophils in Allergic Airways Remodeling. *Science* **305**, 1776–1779 (2004).

156. Balzar, S. *et al.* Increased TGF-β2 in severe asthma with eosinophilia. *J. Allergy Clin. Immunol.* **115**, 110–117 (2005).
157. Ortega, H. G. *et al.* Mepolizumab Treatment in Patients with Severe Eosinophilic Asthma. *N. Engl. J. Med.* **371**, 1198–1207 (2014).
158. FitzGerald, J. M. *et al.* Benralizumab, an anti-interleukin-5 receptor α monoclonal antibody, as add-on treatment for patients with severe, uncontrolled, eosinophilic asthma (CALIMA): a randomised, double-blind, placebo-controlled phase 3 trial. *The Lancet* **388**, 2128–2141 (2016).
159. Grisaru-Tal, S., Jacobsen, E. A. & Munitz, A. Evolving role for eosinophils in cancer: from bench to bedside. *Trends Cancer* **11**, S2405803325001311 (2025).
160. Varricchi, G. *et al.* Eosinophils: The unsung heroes in cancer? *OncoImmunology* **7**, e1393134 (2018).
161. Lotfi, R., Lee, J. J. & Lotze, M. T. Eosinophilic Granulocytes and Damage-associated Molecular Pattern Molecules (DAMPs): Role in the Inflammatory Response Within Tumors. *J. Immunother.* **30**, 16–28 (2007).
162. Grisaru-Tal, S. *et al.* Primary tumors from mucosal barrier organs drive unique eosinophil infiltration patterns and clinical associations. *OncoImmunology* **10**, 1859732 (2021).
163. Onesti, C. E. *et al.* Blood eosinophilic relative count is prognostic for breast cancer and associated with the presence of tumor at diagnosis and at time of relapse. *OncoImmunology* **9**, 1761176 (2020).
164. Onesti, C. E. *et al.* Predictive and prognostic role of peripheral blood eosinophil count in triple-negative and hormone receptor-negative/HER2-positive breast cancer patients undergoing neoadjuvant treatment. *Oncotarget* **9**, 33719–33733 (2018).
165. Ownby, H. E., Roi, L. D., Isenberg, R. R. & Brennan, M. J. Peripheral lymphocyte and eosinophil counts as indicators of prognosis in primary breast cancer. *Cancer* **52**, 126–130 (1983).
166. Grisaru-Tal, S. *et al.* Metastasis-Entrained Eosinophils Enhance Lymphocyte-Mediated Antitumor Immunity. *Cancer Res.* **81**, 5555–5571 (2021).
167. Cederberg, R. A. *et al.* Eosinophils Decrease Pulmonary Metastatic Mammary Tumor Growth. *Front. Oncol.* **12**, 841921 (2022).
168. Li, F. *et al.* Eosinophilic inflammation promotes CCL6-dependent metastatic tumor growth. *Sci. Adv.* **7**, eabb5943 (2021).

169. Zaynagetdinov, R. *et al.* Interleukin-5 Facilitates Lung Metastasis by Modulating the Immune Microenvironment. *Cancer Res.* **75**, 1624–1634 (2015).
170. Handler, K. *et al.* Eosinophils restrict CRC metastasis by inhibiting pro-tumorigenic SPP1+ macrophage differentiation. Preprint at https://doi.org/10.1101/2024.12.13.628333 (2024).
171. Reichman, H. *et al.* Activated Eosinophils Exert Antitumorigenic Activities in Colorectal Cancer. *Cancer Immunol. Res.* **7**, 388–400 (2019).
172. Mattes, J. *et al.* Immunotherapy of Cytotoxic T Cell–resistant Tumors by T Helper 2 Cells. *J. Exp. Med.* **197**, 387–393 (2003).
173. Simson, L. *et al.* Regulation of Carcinogenesis by IL-5 and CCL11: A Potential Role for Eosinophils in Tumor Immune Surveillance. *J. Immunol.* **178**, 4222–4229 (2007).
174. Kataoka, S., Konishi, Y., Nishio, Y., Fujikawa-Adachi, K. & Tominaga, A. Antitumor Activity of Eosinophils Activated by IL-5 and Eotaxin against Hepatocellular Carcinoma. *DNA CELL Biol.* **23**, 549–560 (2004).
175. Xing, Y. *et al.* CCL11-induced eosinophils inhibit the formation of blood vessels and cause tumor necrosis. *Genes Cells* **21**, 624–638 (2016).
176. Rivoltini, L. *et al.* In vitro anti-tumor activity of eosinophils from cancer patients treated with subcutaneous administration of interleukin 2. Role of interleukin 5. *Int. J. Cancer* **54**, 8–15 (1993).
177. Andreone, S. *et al.* IL-33 Promotes CD11b/CD18-Mediated Adhesion of Eosinophils to Cancer Cells and Synapse-Polarized Degranulation Leading to Tumor Cell Killing. *Cancers* **11**, 1664 (2019).
178. Lucarini, V. *et al.* IL-33 restricts tumor growth and inhibits pulmonary metastasis in melanoma-bearing mice through eosinophils. *OncoImmunology* **6**, e1317420 (2017).
179. Dolitzky, A. *et al.* Differential regulation of Type 1 and Type 2 mouse eosinophil activation by apoptotic cells. *Front. Immunol.* **13**, 1041660 (2022).
180. Dolitzky, A. *et al.* Transcriptional Profiling of Mouse Eosinophils Identifies Distinct Gene Signatures Following Cellular Activation. *Front. Immunol.* **12**, 802839 (2021).
181. Gatault, S. *et al.* IL-18 Is Involved in Eosinophil-Mediated Tumoricidal Activity against a Colon Carcinoma Cell Line by Upregulating LFA-1 and ICAM-1. *J. Immunol.* **195**, 2483–2492 (2015).

182. Kienzl, M. *et al.* IL-33 reduces tumor growth in models of colorectal cancer with the help of eosinophils. *OncoImmunology* **9**, 1776059 (2020).
183. Dyer, K. D., Percopo, C. M. & Rosenberg, H. F. IL-33 promotes eosinophilia in vivo and antagonizes IL-5-dependent eosinophil hematopoiesis ex vivo. *Immunol. Lett.* **150**, 41–47 (2013).
184. Blomberg, O. S. *et al.* IL-5-producing CD4+ T cells and eosinophils cooperate to enhance response to immune checkpoint blockade in breast cancer. *Cancer Cell* **41**, 106-123.e10 (2023).
185. Levi-Schaffer, F. *et al.* Human eosinophils regulate human lung- and skin-derived fibroblast properties *in vitro* : A role for transforming growth factor β (TGF-β). *Proc. Natl. Acad. Sci.* **96**, 9660–9665 (1999).
186. Bhattacharyya, S. *et al.* Autotaxin–lysolipid signaling suppresses a CCL11–eosinophil axis to promote pancreatic cancer progression. *Nat. Cancer* **5**, 283–298 (2024).
187. Hollande, C. *et al.* Inhibition of the dipeptidyl peptidase DPP4 (CD26) reveals IL-33-dependent eosinophil-mediated control of tumor growth. *Nat. Immunol.* **20**, 257–264 (2019).
188. Carretero, R. *et al.* Eosinophils orchestrate cancer rejection by normalizing tumor vessels and enhancing infiltration of CD8+ T cells. *Nat. Immunol.* **16**, 609–617 (2015).
189. Cheng, J.-N. *et al.* Radiation-induced eosinophils improve cytotoxic T lymphocyte recruitment and response to immunotherapy. *Sci. Adv.* **7**, eabc7609 (2021).
190. Delyon, J. *et al.* Experience in daily practice with ipilimumab for the treatment of patients with metastatic melanoma: an early increase in lymphocyte and eosinophil counts is associated with improved survival. *Ann. Oncol.* **24**, 1697–1703 (2013).
191. Martens, A. *et al.* Baseline Peripheral Blood Biomarkers Associated with Clinical Outcome of Advanced Melanoma Patients Treated with Ipilimumab. *Clin. Cancer Res.* **22**, 2908–2918 (2016).
192. Alvaro Moreira, Waltraud Leisgang, Gerold Schuler, & Lucie Heinzerling. Eosinophilic Count as a Biomarker for Prognosis of Melanoma Patients and Its Importance in The Response to Immunotherapy. *Immunotherapy* **9**, 115–121 (2017).
193. Caliman, E. *et al.* Absolute eosinophil count predicts clinical outcomes and toxicity in non-small cell lung cancer patients treated with immunotherapy. *Cancer Treat. Res. Commun.* **32**, 100603 (2022).

194. Yoshimura, A. *et al.* The prognostic impact of peripheral blood eosinophil counts in metastatic renal cell carcinoma patients treated with nivolumab. *Clin. Exp. Med.* **24**, 111 (2024).
195. Gambale, E. *et al.* Neutrophil-to-Eosinophil Ratio Predicts the Efficacy of Avelumab in Patients With Advanced Urothelial Carcinoma Enrolled in the MALVA Study (Meet-URO 25). *Clin. Genitourin. Cancer* **22**, 102099 (2024).
196. Ghebeh, H., Elshenawy, M. A., AlSayed, A. D. & Al-Tweigeri, T. Peripheral Blood Eosinophil Count is Associated with Response to Chemoimmunotherapy in Metastatic Triple-Negative Breast Cancer. *Immunotherapy* **14**, 189–199 (2022).
197. Qin, Y. *et al.* Peripheral eosinophils and immunotherapy response in patients with recurrent or metastatic HNSCC. *Sci. Rep.* **15**, 17351 (2025).
198. Yoshihiko Tasaki *et al.* Eosinophil is a predictor of severe immune-related adverse events induced by ipilimumab plus nivolumab therapy in patients with renal cell carcinoma: a retrospective multicenter cohort study. *Front. Immunol.* **15**, 1483956 (2025).
199. Zheng, X. *et al.* CTLA4 blockade promotes vessel normalization in breast tumors *via* the accumulation of eosinophils. *Int. J. Cancer* **146**, 1730–1740 (2020).
200. Sleeboom, J. J. F. *et al.* The extracellular matrix as hallmark of cancer and metastasis: From biomechanics to therapeutic targets. *Sci. Transl. Med.* **16**, eadg3840 (2024).
201. Shao, X., Taha, I. N., Clauser, K. R., Gao, Y. (Tom) & Naba, A. MatrisomeDB: the ECM-protein knowledge database. *Nucleic Acids Res.* **48**, D1136–D1144 (2020).
202. Hynes, R. O. & Naba, A. Overview of the Matrisome--An Inventory of Extracellular Matrix Constituents and Functions. *Cold Spring Harb. Perspect. Biol.* **4**, a004903–a004903 (2012).
203. Bonnans, C., Chou, J. & Werb, Z. Remodelling the extracellular matrix in development and disease. *Nat. Rev. Mol. Cell Biol.* **15**, 786–801 (2014).
204. Wynn, T. A. & Ramalingam, T. R. Mechanisms of fibrosis: therapeutic translation for fibrotic disease. *Nat. Med.* **18**, 1028–1040 (2012).
205. Harold F. Dvorak. Tumors: Wounds That Do Not Heal. *N. Engl. J. Med.* **315**, 1650–1659 (1986).
206. Sainio, A. & Järveläinen, H. Extracellular matrix-cell interactions: Focus on therapeutic applications. *Cell. Signal.* **66**, 109487 (2020).

207. Winkler, J., Abisoye-Ogunniyan, A., Metcalf, K. J. & Werb, Z. Concepts of extracellular matrix remodelling in tumour progression and metastasis. *Nat. Commun.* **11**, 5120 (2020).
208. Prakash, J. & Shaked, Y. The Interplay between Extracellular Matrix Remodeling and Cancer Therapeutics. *Cancer Discov.* **14**, 1375–1388 (2024).
209. Sutherland, T. E., Dyer, D. P. & Allen, J. E. The extracellular matrix and the immune system: A mutually dependent relationship. *Science* **379**, eabp8964 (2023).
210. Chauhan, V. P. *et al.* Angiotensin inhibition enhances drug delivery and potentiates chemotherapy by decompressing tumour blood vessels. *Nat. Commun.* **4**, 2516 (2013).
211. Peng, D. H. *et al.* Collagen promotes anti-PD-1/PD-L1 resistance in cancer through LAIR1-dependent CD8+ T cell exhaustion. *Nat. Commun.* **11**, 4520 (2020).
212. Chitty, J. L. *et al.* A first-in-class pan-lysyl oxidase inhibitor impairs stromal remodeling and enhances gemcitabine response and survival in pancreatic cancer. *Nat. Cancer* **4**, 1326–1344 (2023).
213. Sun, X. *et al.* Tumour DDR1 promotes collagen fibre alignment to instigate immune exclusion. *Nature* **599**, 673–678 (2021).
214. Du, W., Xia, X., Hu, F. & Yu, J. Extracellular matrix remodeling in the tumor immunity. *Front. Immunol.* **14**, 1340634 (2024).
215. Evans, A. *et al.* Pre-operative stromal stiffness measured by shear wave elastography is independently associated with breast cancer-specific survival. *Breast Cancer Res. Treat.* **171**, 383–389 (2018).
216. Shi, S. *et al.* The Strain Ratio as Obtained by Endoscopic Ultrasonography Elastography Correlates With the Stroma Proportion and the Prognosis of Local Pancreatic Cancer. *Ann. Surg.* **271**, 559–565 (2020).
217. Kim, J. Y. *et al.* Tumor stiffness measured by shear-wave elastography: association with disease-free survival in women with early-stage breast cancer. *Br. J. Radiol.* **94**, 20210584 (2021).
218. Abe, H. *et al.* Tumor stiffness measurement using magnetic resonance elastography can predict recurrence and survival after curative resection of hepatocellular carcinoma. *Surgery* **173**, 450–456 (2023).
219. Yuzhalin, A. E., Urbonas, T., Silva, M. A., Muschel, R. J. & Gordon-Weeks, A. N. A core matrisome gene signature predicts cancer outcome. *Br. J. Cancer* **118**, 435–440 (2018).

220. Midwood, K. S., Chiquet, M., Tucker, R. P. & Orend, G. Tenascin-C at a glance. *J. Cell Sci.* **129**, 4321–4327 (2016).
221. Midwood, K. S. & Orend, G. The role of tenascin-C in tissue injury and tumorigenesis. *J. Cell Commun. Signal.* **3**, 287–310 (2009).
222. Oskarsson, T. *et al.* Breast cancer cells produce tenascin C as a metastatic niche component to colonize the lungs. *Nat. Med.* **17**, 867–875 (2011).
223. Jahkolal, T., Toivonen, T., Virtanen, I. & Blomqvist, C. Tenascin-C expression in invasion border of early breast cancer: a predictor of local and distant recurrence. *Br. J. Cancer* **11**, 1507–1513 (1998).
224. Yang, Z.-T. *et al.* Tenascin-C, a Prognostic Determinant of Esophageal Squamous Cell Carcinoma. *PLOS ONE* **11**, e0145807 (2016).
225. Gocheva, V. *et al.* Quantitative proteomics identify Tenascin-C as a promoter of lung cancer progression and contributor to a signature prognostic of patient survival. *Proc. Natl. Acad. Sci.* **114**, E5625–E5634 (2017).
226. Yang, Z. *et al.* Tenascin-C predicts poor outcomes for patients with colorectal cancer and drives cancer stemness via Hedgehog signaling pathway. *Cancer Cell Int.* **20**, 122 (2020).
227. Schlensog, M. *et al.* Tenascin-C affects invasiveness of EGFR-mutated lung adenocarcinoma through a putative paracrine loop. *Biochim. Biophys. Acta BBA - Mol. Basis Dis.* **1869**, 166684 (2023).
228. Deligne, C. *et al.* Matrix-Targeting Immunotherapy Controls Tumor Growth and Spread by Switching Macrophage Phenotype. *Cancer Immunol. Res.* **8**, 368–382 (2020).
229. Gschwandtner, M. *et al.* Investigating Chemokine-Matrix Networks in Breast Cancer: Tenascin-C Sets the Tone for CCL2. *Int. J. Mol. Sci.* **24**, 8365 (2023).
230. Murdamoothoo, Devadarssen. Immuno-modulatory functions of tenascin-C in a tumor progression model. (Université de Strasbourg, 2018).
231. Sun, Z. *et al.* Tenascin-C increases lung metastasis by impacting blood vessel invasions. *Matrix Biol.* **83**, 26.47 (2019).
232. Hongu, T. *et al.* Perivascular tenascin C triggers sequential activation of macrophages and endothelial cells to generate a pro-metastatic vascular niche in the lungs. *Nat. Cancer* **3**, 486–504 (2022).
233. Ombrato, L. *et al.* Metastatic-niche labelling reveals parenchymal cells with stem features. *Nature* **572**, 603–608 (2019).

234. Midwood, K. *et al.* Tenascin-C is an endogenous activator of Toll-like receptor 4 that is essential for maintaining inflammation in arthritic joint disease. *Nat. Med.* **15**, 774–780 (2009).
235. Shimojo, N. *et al.* Tenascin-C May Accelerate Cardiac Fibrosis by Activating Macrophages via the Integrin αVβ3/Nuclear Factor–κB/Interleukin-6 Axis. *Hypertension* **66**, 757–766 (2015).
236. Domaingo, A. *et al.* Chemokine Binding to Tenascin-C Influences Chemokine-Induced Immune Cell Migration. *Int. J. Mol. Sci.* **24**, 14694 (2023).
237. Kimura, T. *et al.* Tenascin-C accelerates adverse ventricular remodelling after myocardial infarction by modulating macrophage polarization. *Cardiovasc. Res.* **115**, 614–624 (2019).
238. Li, C. *et al.* Targeting the MAtrix REgulating MOtif abolishes several hallmarks of cancer, triggering antitumor immunity. *Proc. Natl. Acad. Sci.* **121**, e2404485121 (2024).
239. Chen, W. *et al.* Clinical advances in TNC delivery vectors and their conjugate agents. *Pharmacol. Ther.* **253**, 108577 (2024).
240. Spisak, L. & Hülsken, J. The role of eosinophils in breast cancer. (EPFL, Lausanne, 2022).
241. Ombrato, L. *et al.* Generation of neighbor-labeling cells to study intercellular interactions in vivo. *Nat. Protoc.* **16**, 872–892 (2021).
242. Schmidt, E. K., Clavarino, G., Ceppi, M. & Pierre, P. SUnSET, a nonradioactive method to monitor protein synthesis. *Nat. Methods* **6**, 275–277 (2009).
243. Hidalgo San Jose, L. & Signer, R. A. J. Cell-type-specific quantification of protein synthesis in vivo. *Nat. Protoc.* **14**, 441–460 (2019).
244. Wang, G. G. *et al.* Quantitative production of macrophages or neutrophils ex vivo using conditional Hoxb8. *Nat. Methods* **3**, 287–293 (2006).
245. Dyer, K. D. *et al.* Functionally Competent Eosinophils Differentiated Ex Vivo in High Purity from Normal Mouse Bone Marrow. *J. Immunol.* **181**, 4004–4009 (2008).
246. *Eosinophils: Methods and Protocols*. vol. 2241 (Springer US, New York, NY, 2021).
247. Laviron, M. *et al.* Tumor-associated macrophage heterogeneity is driven by tissue territories in breast cancer. *Cell Rep.* **39**, 110865 (2022).
248. Cassetta, L. *et al.* Human Tumor-Associated Macrophage and Monocyte Transcriptional Landscapes Reveal Cancer-Specific Reprogramming, Biomarkers, and Therapeutic Targets. *Cancer Cell* **35**, 588-602.e10 (2019).

249. Piccirillo, C. A., Bjur, E., Topisirovic, I., Sonenberg, N. & Larsson, O. Translational control of immune responses: from transcripts to translatomes. *Nat. Immunol.* **15**, 503–511 (2014).
250. Bartish, M. *et al.* MNK2 governs the macrophage antiinflammatory phenotype. *Proc. Natl. Acad. Sci.* **117**, 27556–27565 (2020).
251. Belkina, A. C. *et al.* Automated optimized parameters for T-distributed stochastic neighbor embedding improve visualization and analysis of large datasets. *Nat. Commun.* **10**, 5415 (2019).
252. Le Naour, A., Rossary, A. & Vasson, M. EO771, is it a well-characterized cell line for mouse mammary cancer model? Limit and uncertainty. *Cancer Med.* **9**, 8074–8085 (2020).
253. Snipstad, S., Bremnes, F., Dehli Haugum, M. & Sulheim, E. Characterization of immune cell populations in syngeneic murine tumor models. *Cancer Med.* **12**, 11589–11601 (2023).
254. Kukan, E. N., Fabiano, G. L. & Cobb, B. A. Siglecs as modulators of macrophage phenotype and function. *Semin. Immunol.* **73**, 101887 (2024).
255. Pfirschke, C. *et al.* Tumor-Promoting Ly-6G+ SiglecFhigh Cells Are Mature and Long-Lived Neutrophils. *Cell Rep.* **32**, 108164 (2020).
256. Kikuchi, Y., Yasue, T., Miyake, K., Kimoto, M. & Takatsu, K. CD38 ligation induces tyrosine phosphorylation of Bruton tyrosine kinase and enhanced expression of interleukin 5-receptor alpha chain: synergistic effects with interleukin 5. *Proc. Natl. Acad. Sci.* **92**, 11814–11818 (1995).
257. Sallusto, F., Mackay, C. R. & Lanzavecchia, A. Selective Expression of the Eotaxin Receptor CCR3 by Human T Helper 2 Cells. *Science* **207**, 2005–2007 (1997).
258. Willems, L. I. & IJzerman, A. P. Small molecule antagonists for chemokine CCR3 receptors. *Med. Res. Rev.* **30**, 778–817 (2010).
259. Rose, C. E. *et al.* Murine lung eosinophil activation and chemokine production in allergic airway inflammation. *Cell. Mol. Immunol.* **7**, 361–374 (2010).
260. Leiferman, K. M. & Gleich, G. J. The true extent of eosinophil involvement in disease is unrecognized: the secret life of dead eosinophils. *J. Leukoc. Biol.* **116**, 271–287 (2024).
261. Massara, M. *et al.* Investigation of a fluorescent reporter microenvironment niche labeling strategy in experimental brain metastasis. *iScience* **27**, 110284 (2024).

262. Zimmermann, N., Conkright, J. J. & Rothenberg, M. E. CC Chemokine Receptor-3 Undergoes Prolonged Ligand-induced Internalization. *J. Biol. Chem.* **274**, 12611–12618 (1999).
263. Zimmermann, N. & Rothenberg, M. E. Receptor internalization is required for eotaxin-induced responses in human eosinophils. *J. Allergy Clin. Immunol.* **111**, 97–105 (2003).
264. Malactou, C. *et al.* Eosinophils and bioactive lipid mediators regulate skin inflammation and cancer growth. *J. Invest. Dermatol.* **0**, (2025).
265. Sferruzzi-Perri, A. N., Robertson, S. A. & Dent, L. A. Interleukin-5 Transgene Expression and Eosinophilia Are Associated with Retarded Mammary Gland Development in Mice1. *Biol. Reprod.* **69**, 224–233 (2003).
266. Voehringer, D., Van Rooijen, N. & Locksley, R. M. Eosinophils develop in distinct stages and are recruited to peripheral sites by alternatively activated macrophages. *J. Leukoc. Biol.* **81**, 1434–1444 (2007).
267. Kouro, T. & Takatsu, K. IL-5- and eosinophil-mediated inflammation: from discovery to therapy. *Int. Immunol.* **21**, 1303–1309 (2009).
268. Grisaru-Tal, S., Itan, M., Klion, A. D. & Munitz, A. A new dawn for eosinophils in the tumour microenvironment. *Nat. Rev. Cancer* **20**, 594–607 (2020).
269. Kurashima K *et al.* The role of vacuolar H(+)-ATPase in the control of intragranular pH and exocytosis in eosinophils. *J. Tech. Methods Pathol.* **75**, 689–698 (1996).
270. Rahman, A. H., Tordesillas, L. & Berin, M. C. Heparin reduces nonspecific eosinophil staining artifacts in mass cytometry experiments. *Cytometry A* **89**, 601–607 (2016).
271. Carpen, L. *et al.* A single-cell transcriptomic landscape of innate and adaptive intratumoral immunity in triple negative breast cancer during chemo- and immunotherapies. *Cell Death Discov.* **8**, 106 (2022).
272. Hurskainen, M. *et al.* Single cell transcriptomic analysis of murine lung development on hyperoxia-induced damage. *Nat. Commun.* **12**, 1565 (2021).
273. Doherty, G. P., Bailey, K. & Lewis, P. J. Stage-specific fluorescence intensity of GFP and mCherry during sporulation In Bacillus Subtilis. *BMC Res. Notes* **3**, 303 (2010).
274. Knuplez, E. *et al.* Superior mouse eosinophil depletion in vivo targeting transgenic Siglec-8 instead of endogenous Siglec-F: Mechanisms and pitfalls. *J. Leukoc. Biol.* **108**, 43–58 (2020).

275. Jacobsen, E. A. *et al.* Eosinophil Knockout Humans: Uncovering the Role of Eosinophils Through Eosinophil-Directed Biological Therapies. *Annu. Rev. Immunol.* **39**, 719–757 (2021).
276. Salvagno, C. *et al.* Therapeutic targeting of macrophages enhances chemotherapy efficacy by unleashing type I interferon response. *Nat. Cell Biol.* **21**, 511–521 (2019).
277. Hirano, R. *et al.* Tissue-resident macrophages are major tumor-associated macrophage resources, contributing to early TNBC development, recurrence, and metastases. *Commun. Biol.* **6**, 144 (2023).
278. Perdrix Rosell, A. *et al.* Early functional mismatch between breast cancer cells and their tumour microenvironment suppresses long term growth. *Cancer Lett.* **544**, 215800 (2022).
279. Loughner, C. L. *et al.* Organization, evolution and functions of the human and mouse Ly6/uPAR family genes. *Hum. Genomics* **10**, 10 (2016).
280. DeLong, J. H. *et al.* Cytokine- and TCR-Mediated Regulation of T Cell Expression of Ly6C and Sca-1. *J. Immunol.* **200**, 1761–1770 (2018).
281. Grace, J. O. *et al.* Reuse of public, genome-wide, murine eosinophil expression data for hypotheses development. *J. Leukoc. Biol.* **104**, 185–193 (2018).
282. Wen, T., Besse, J. A., Mingler, M. K., Fulkerson, P. C. & Rothenberg, M. E. Eosinophil adoptive transfer system to directly evaluate pulmonary eosinophil trafficking in vivo. *Proc. Natl. Acad. Sci.* **110**, 6067–6072 (2013).
283. Michael Dougan, Glenn Dranoff, & Stephanie K. Dougan4. GM-CSF, IL-3, and IL-5 Family of Cytokines: Regulators of Inflammation. *Immunity* **50**, 796–811 (2019).
284. Netali Ben Baruch-Morgenstern *et al.* Paired immunoglobulin-like receptor A is an intrinsic, self-limiting suppressor of IL-5–induced eosinophil development. *Nat. Immunol.* **15**, 36–44 (2014).
285. Sturm, E. M., Dyer, K. D., Percopo, C. M., Heinemann, A. & Rosenberg, H. F. Chemotaxis of bone marrow derived eosinophils in vivo: A novel method to explore receptor-dependent trafficking in the mouse. *Eur. J. Immunol.* **43**, 2217–2228 (2013).
286. Grasso, C. S. *et al.* Conserved Interferon-γ Signaling Drives Clinical Response to Immune Checkpoint Blockade Therapy in Melanoma. *Cancer Cell* **38**, 500-515.e3 (2020).
287. Rothenberg, M. E. & Hogan, S. P. The Eosinophil. *Annu. Rev. Immunol.* **24**, 147–174 (2006).

288. Garcia-Diaz, A. *et al.* Interferon Receptor Signaling Pathways Regulating PD-L1 and PD-L2 Expression. *Cell Rep.* **19**, 1189–1201 (2017).
289. Carmo, L. A. S. *et al.* CD63 is tightly associated with intracellular, secretory events chaperoning piecemeal degranulation and compound exocytosis in human eosinophils. *J. Leukoc. Biol.* **100**, 391–401 (2016).
290. Lamkhioued, B. *et al.* The CCR3 Receptor Is Involved in Eosinophil Differentiation and Is Up-Regulated by Th2 Cytokines in CD34+ Progenitor Cells. *J. Immunol.* **170**, 537–547 (2003).
291. Steimle, V., Siegrist, C.-A., Mottet, A., Lisowska-Grospierre, B. & Mach, B. Regulation of MHC Class II Expression by Interferon-γ Mediated by the Transactivator Gene CIITA. *Science* **265**, 106–109 (1994).
292. Chan, W. K. *et al.* MHC expression kinetics and immunogenicity of mesenchymal stromal cells after short-term IFN-γ challenge. *Exp. Hematol.* **36**, 1545–1555 (2008).
293. Quezada, S. A. *et al.* Tumor-reactive CD4+ T cells develop cytotoxic activity and eradicate large established melanoma after transfer into lymphopenic hosts. *J. Exp. Med.* **207**, 637–650 (2010).
294. Kaplan, D. H. *et al.* Demonstration of an interferon γ-dependent tumor surveillance system in immunocompetent mice. *Proc. Natl. Acad. Sci.* **95**, 7556–7561 (1998).
295. Irie-Sasaki, J. *et al.* CD45 is a JAK phosphatase and negatively regulates cytokine receptor signalling. *Nature* **409**, 349–354 (2001).
296. Newman, A. M. *et al.* Robust enumeration of cell subsets from tissue expression profiles. *Nat. Methods* **12**, 453–457 (2015).
297. Wall, L., Burke, F., Barton, C., Smyth, J. & Balkwill, F. IFN- Induces Apoptosis in Ovarian Cancer Cells in Vivo and in Vitro. *Clin. Cancer Res.* **9**, 2487–2496 (2003).
298. Song, M. *et al.* Low-Dose IFNγ Induces Tumor Cell Stemness in Tumor Microenvironment of Non–Small Cell Lung Cancer. *Cancer Res.* **79**, 3737–3748 (2019).
299. Peng, Q. *et al.* PD-L1 on dendritic cells attenuates T cell activation and regulates response to immune checkpoint blockade. *Nat. Commun.* **11**, 4835 (2020).
300. Zhou, F. Molecular Mechanisms of IFN-γ to Up-Regulate MHC Class I Antigen Processing and Presentation. *Int. Rev. Immunol.* **28**, 239–260 (2009).
301. Lim, J. *et al.* Type I interferon signaling regulates myeloid and T cell crosstalk in the glioblastoma tumor microenvironment. *iScience* **27**, 110810 (2024).

302. Shankaran, V. *et al.* IFNg and lymphocytes prevent primary tumour development and shape tumour immunogenicity. *Nature* **410**, 1107–1111 (2001).
303. Wizenty, J. *et al.* Autofluorescence: A potential pitfall in immunofluorescence-based inflammation grading. *J. Immunol. Methods* **456**, 28–37 (2018).
304. Navarro, A., Anand-Apte, B., Tanabe, Y., Feldman, G. & Larner, A. C. A PI-3 kinase-dependent, Stat1-independent signaling pathway regulates interferon-stimulated monocyte adhesion. *J. Leukoc. Biol.* **73**, 540–545 (2003).
305. Crocker, P. R., Paulson, J. C. & Varki, A. Siglecs and their roles in the immune system. *Nat. Rev. Immunol.* **7**, 255–266 (2007).
306. Zhang, M. *et al.* Defining the in vivo function of Siglec-F, a CD33-related Siglec expressed on mouse eosinophils. *Blood* **109**, 4280–4287 (2007).
307. Kanehisa, M., Furumichi, M., Sato, Y., Matsuura, Y. & Ishiguro-Watanabe, M. KEGG: biological systems database as a model of the real world. *Nucleic Acids Res.* **53**, D672–D677 (2025).
308. Reya, T. & Clevers, H. Wnt signalling in stem cells and cancer. *Nature* **434**, 843–850 (2005).
309. Ouko, L., Ziegler, T. R., Gu, L. H., Eisenberg, L. M. & Yang, V. W. Wnt11 Signaling Promotes Proliferation, Transformation, and Migration of IEC6 Intestinal Epithelial Cells. *J. Biol. Chem.* **279**, 26707–26715 (2004).
310. Jiang, W. *et al.* WNT11 Promotes immune evasion and resistance to Anti-PD-1 therapy in liver metastasis. *Nat. Commun.* **16**, 1429 (2025).
311. Amini, R.-M. *et al.* Mast cells and eosinophils in invasive breast carcinoma. *BMC Cancer* **7**, (2007).
312. Simon, S. C. S. *et al.* Eosinophil accumulation predicts response to melanoma treatment with immune checkpoint inhibitors. *OncoImmunology* **9**, 1727116 (2020).
313. Hasegawa, M. *et al.* Expression of large tenascin-C splice variants in synovial fluid of patients with rheumatoid arthritis. *J. Orthop. Res.* **25**, 563–568 (2007).
314. Salter, D. M. Tenascin is increased in cartilage and synovium from arthritic knees. *Br. J. Rheumatol.* **32**, 780–786 (1993).
315. Goh, F. G., Piccinini, A. M., Krausgruber, T., Udalova, I. A. & Midwood, K. S. Transcriptional Regulation of the Endogenous Danger Signal Tenascin-C: A Novel Autocrine Loop in Inflammation. *J. Immunol.* **184**, 2655–2662 (2010).

316. Lee, S. H. *et al.* M2-like, dermal macrophages are maintained via IL-4/CCL24–mediated cooperative interaction with eosinophils in cutaneous leishmaniasis. *Sci. Immunol.* **5**, eaaz4415 (2020).
317. Arpel, A. *et al.* Transmembrane Domain Targeting Peptide Antagonizing ErbB2/Neu Inhibits Breast Tumor Growth and Metastasis. *Cell Rep.* **8**, 1714–1721 (2014).
318. Zlotnik, A. & Yoshie, O. The Chemokine Superfamily Revisited. *Immunity* **36**, 705–716 (2012).
319. Delobel, P., Ginter, B., Rubio, E., Balabanian, K. & Lazennec, G. CXCR2 intrinsically drives the maturation and function of neutrophils in mice. *Front. Immunol.* **13**, 1005551 (2022).
320. Piccinini, A. M., Zuliani-Alvarez, L., Lim, J. M. P. & Midwood, K. S. Distinct microenvironmental cues stimulate divergent TLR4-mediated signaling pathways in macrophages. *Sci. Signal.* **9**, ra86 (2016).
321. Van Rooijen, Nico & Sanders, Annemarie. Liposome mediated depletion of macrophages mechanism of action, preparation of liposomes and applications. *J. Immunol. Methods* **174**, 83–93 (1994).
322. Zeisberger, SM, Odermatt, B, Zehnder-Fjallman, AHM, Ballmer-Hofer, K, & Schwendener, RA. Clodronate-liposome-mediated depletion of tumour-associated macrophages: a new and highly effective antiangiogenic therapy approach. *Br. J. Cancer* **95**, 272–281 (2006).
323. Culemann, S. *et al.* Stunning of neutrophils accounts for the anti-inflammatory effects of clodronate liposomes. *J. Exp. Med.* **220**, e20220525 (2023).
324. Depleting Macrophages In Vivo with Clodronate-Liposomes. in *Methods in Molecular Biology* vol. 1784 259–262 (Springer New York, New York, NY, 2018).
325. Opzoomer, J. W. *et al.* Macrophages orchestrate the expansion of a proangiogenic perivascular niche during cancer progression. *Sci. Adv.* **7**, 1–15 (2021).
326. Ries, C. H. *et al.* Targeting Tumor-Associated Macrophages with Anti-CSF-1R Antibody Reveals a Strategy for Cancer Therapy. *Cancer Cell* **25**, 846–859 (2014).
327. O'Brien, S. A. *et al.* Activity of tumor-associated macrophage depletion by CSF1R blockade is highly dependent on the tumor model and timing of treatment. *Cancer Immunol. Immunother.* **70**, 2401–2410 (2021).
328. Alshetaiwi, H. *et al.* Defining the emergence of myeloid-derived suppressor cells in breast cancer using single-cell transcriptomics. *Sci. Immunol.* **5**, eaay6017 (2020).

329. Liu, M. *et al.* Macrophages Support Splenic Erythropoiesis in 4T1 Tumor-Bearing Mice. *PLOS ONE* **10**, e0121921 (2015).

330. Spiteri, A. G., Van Vreden, C., Ashhurst, T. M., Niewold, P. & King, N. J. C. Clodronate is not protective in lethal viral encephalitis despite substantially reducing inflammatory monocyte infiltration in the CNS. *Front. Immunol.* **14**, 1203561 (2023).

331. Doan, T. C. *et al.* Matrix protein tenascin-C expands and reversibly blocks maturation of murine eosinophil progenitors. *J. Allergy Clin. Immunol.* **142**, 695-698.e4 (2018).

332. Saglimbeni, J. *et al.* Peritumoral macrophages recruit eosinophils to promote antitumor immune responses in breast cancer. *Proc. Natl. Acad. Sci.* **122**, e2504645122 (2025).

333. Korns, D., Frasch, S. C., Fernandez-Boyanapalli, R., Henson, P. M. & Bratton, D. L. Modulation of Macrophage Efferocytosis in Inflammation. *Front. Immunol.* **2**, 1664 (2011).

334. Astuti, Y. *et al.* Efferocytosis reprograms the tumor microenvironment to promote pancreatic cancer liver metastasis. *Nat. Cancer* **5**, 774–790 (2024).

335. Cheng, M. *et al.* CD276-dependent efferocytosis by tumor-associated macrophages promotes immune evasion in bladder cancer. *Nat. Commun.* **15**, 2818 (2024).

336. Loibl, S. *et al.* A randomised phase II study investigating durvalumab in addition to an anthracycline taxane-based neoadjuvant therapy in early triple-negative breast cancer: clinical results and biomarker analysis of GeparNuevo study. *Ann. Oncol.* **30**, 1279–1288 (2019).

337. Mittendorf, E. A. *et al.* Neoadjuvant atezolizumab in combination with sequential nab-paclitaxel and anthracycline-based chemotherapy versus placebo and chemotherapy in patients with early-stage triple-negative breast cancer (IMpassion031): a randomised, double-blind, phase 3 trial. *The Lancet* **396**, 1090–1100 (2020).

338. Schmid, P. *et al.* Pembrolizumab for Early Triple-Negative Breast Cancer. *N. Engl. J. Med.* **382**, 810–821 (2020).

339. Schmid, P. *et al.* Event-free Survival with Pembrolizumab in Early Triple-Negative Breast Cancer. *N. Engl. J. Med.* **386**, 556–567 (2022).

340. Adrover, J. M. *et al.* Neutrophils drive vascular occlusion, tumour necrosis and metastasis. *Nature* **645**, 484–495 (2025).

341. Liebold, I. *et al.* Apoptotic cell identity induces distinct functional responses to IL-4 in efferocytic macrophages. *Science* **384**, eabo7027 (2024).